

Department of Biochemistry

University of Oxford

Somerville College

Control of the mitotic spindle by dynein light chain 1 complexes.

Anja Katrin Dunsch

DPhil Thesis in Biochemistry

Supervisor: Prof. Francis Barr, Laboratory of Cell and Chromosome Biology

Co-Supervisor: Dr. Ulrike Grüneberg, Sir William Dunn School of Pathology, Oxford

Abstract

Robust control mechanisms ensure faithful inheritance of an intact genome through the processes of mitosis and cytokinesis. Different populations of the cytoplasmic dynein motor defined by specific dynein adaptor complexes are required for the formation of a stable bipolar mitotic spindle. This study analysed how different dynein subcomplexes contribute to spindle formation and orientation. Various dynein subpopulations were identified by mass spectrometry. I have shown that the dynein light chain 1 (DYNLL1) directly interacts with the kinetochore localised Astrin-Kinastrin complex as well as the spindle microtubule associated complex formed by CHICA and HMMR. I have characterised both complexes and identified unique functions in chromosome alignment and mitotic spindle orientation, respectively.

I have found that Kinastrin (C15orf23) is the major Astrin-interacting protein in mitotic cells and is required for Astrin targeting to microtubule plus ends proximal to the plus tip tracking protein EB1. Fixed cell microscopy revealed that cells over-expressing or depleted of Kinastrin mislocalise Astrin. Additionally, depletion of the Astrin-Kinastrin complex delays chromosome alignment and causes the loss of normal spindle architecture and sister chromatid cohesion before anaphase onset (Dunsch *et al.*, 2011).

Using immunoprecipitation and microtubule binding assays, I have shown that CHICA and HMMR interact with one another, and target to the spindle by a microtubule-binding site in the amino-terminal region of HMMR. CHICA interacts with DYNLL1 by a series of conserved TQT motifs in the carboxy-terminal region. Depletion of DYNLL1, CHICA or HMMR causes a slight increase in mitotic index but has little effect on spindle formation or checkpoint function. Fixed and live cell microscopy reveal, however, that the asymmetric distribution of cortical dynein is lost and the spindle in these cells fails to orient correctly in relation to the culture surface (Dunsch *et al.*, 2012).

These findings presented here suggest that the Astrin-Kinastrin complex is required for normal spindle architecture and chromosome alignment, and that perturbations of this pathway result in delayed mitosis and non-physiological separase activation, whereas HMMR and CHICA act as part of a dynein-DYNLL1 complex with a specific function defining or controlling spindle orientation.

Acknowledgements

I would like to thank everyone who supported me and this DPhil work. In particular,

- I am very grateful towards Prof. Francis Barr for giving me the opportunity to work in his laboratory and for the great supervision.
- I would like to thank Dr. Ulrike Grüneberg for discussions and helpful advices throughout this project.
- I also want to thank the Boehringer Ingelheim Fonds, who funded my DPhil work and my attendance at various conferences. I am also grateful to Cancer Research UK for covering the laboratory research costs.
- Thank you to Dr. Lothar Schermelleh for his help with the 3D super-resolution structural illumination OMX microscopy.
- I also want to express my gratitude to Dr. Dean Hammond for assistance with the analysis of my samples by mass spectrometry and Jennifer Lloyd for providing me with antibodies to HMMR, CHICA and HURP.
- Another thank you goes to Emily Linnane, who established the GFP-DYNLL1 cell line and conducted some repeat experiments regarding sister chromatid separation.
- Thanks also to Dr. Andrea Linford for supporting me and for comments on this manuscript.
- Furthermore, I want to say thank you to Dr. Matt Higgins, who supported the completion of this thesis.
- A very special thank you goes to my best friend Kira Fischer, who was there for me throughout this project and far beyond.
- Last not least, many thanks to my parents Katrin and Michael Dunsch, who always supported me during my studies and encouraged me to pursue my objectives.

List of Abbreviations

aa amino acid
APC/C anaphase promoting complex/cyclosome
ATP adenosine triphosphate
BSA bovine serum albumin
CCAN constitutive centromere-associated network
Cdks cyclin-dependent kinases
CPC chromosomal passenger complex
DAPI diamidino-phenylindole
DMEM Dulbecco's modified Eagle's medium
DNA deoxyribonucleic acid
EB end binding
ECM extracellular matrix
E. coli *Escherichia coli*
EDTA ethylene diamine tetraacetic acid
EGTA ethylene glycol tetraacetic acid
FBS fetal-bovine serum
FRT Flp recombination target
GAP GTPase activating protein
GEF guanine nucleotide exchange factor
GST glutathione-S-transferase
HEK293T human embryonic kidney cells (transformed with SV40 large T-antigen)
HRP horseradish-peroxidase
IPTG isopropyl-thiogalactopyranoside
kb kilobase
kD kilodalton
KMN Knl1, Mis12, Ndc80
KLH keyhole limpet hemocyanin
LB Luria Bertani
MAP microtubule associated protein
MCC mitotic checkpoint complex
MD megadalton
MTOC microtubule organising centres
MW molecular weight
NE nuclear envelope
NEBD nuclear envelope breakdown
NTA nitrilotriacetic acid

NPC nuclear pore complex
NuMA nuclear mitotic apparatus
PAGE polyacrylamide gel electrophoresis
PBS phosphate-buffered saline
PCM pericentriolar matrix
PCR polymerase chain reaction
PFA paraformaldehyde
PIPES piperazine-bis(ethanesulphonic acid)
PTEMF PIPES, Triton X-100, EGTA, $MgCl_2$, formaldehyde
RNA ribonucleic acid
RT room temperature
SAC spindle assembly checkpoint
SDS sodium dodecyl sulphate
STLC S-trityl-L-cysteine
TBS tris-buffered saline
γ-TuRC γ-tubulin ring complex
WB Western blot

Contents

1. Introduction **9**

1.1. Eukaryotic cell cycle 9

1.2. Mitotic spindle formation and centrosomes 13

1.2.1. Spindle poles 13

1.2.2. Microtubule nucleation 15

1.2.3. Microtubule attachments at kinetochores 17

1.3. Sister chromatid cohesion 19

1.4. The spindle assembly checkpoint 21

1.5. Mitotic spindle positioning and orientation 24

1.6. Cytoplasmic dynein 28

1.7. Aims and course of action 32

2. Results **33**

2.1. DYNLL 1 interacts with a subset of mitotic spindle proteins 33

2.2. Analysis of the Astrin-Kinastrin complex 39

2.3. The Astrin-Kinastrin complex is required for faithful chromosome alignment 45

2.4. Astrin localisation to the spindle and kinetochores is required for normal mitotic progression 50

2.5. The Astrin-Kinastrin complex localises to microtubule plus ends and promotes stable kinetochore attachments 60

2.6. Kinetochore and spindle targeting of DYNLL1 69

2.7. HMMR targets CHICA to the mitotic spindle 72

2.8. Mitotic progression is delayed in the absence of the DYNLL1- CHICA-HMMR complex 79

2.9. Loss of the DYNLL1-CHICA-HMMR complex results in spindle misorientation 84
2.10. CHICA binds DYNLL1 via three TQT motifs in its C-terminus 92
2.11. Asymmetric localisation of cortical dynein requires the DYNLL1-CHICA-HMMR complex 95
2.12. Loss of retraction fibres in CHICA-HMMR-depleted cells 99

3. Discussion **103**
3.1. Formation of stable microtubule-kinetochore attachments by the Astrin-Kinastrin complex 105
3.2. Plus end tracking behaviour of the Astrin-Kinastrin complex 107
3.3. Loss of the Astrin-Kinastrin complex induces untimely separase activation 109
3.4. DYNLL1 is recruited to the spindle by the CHICA-HMMR complex . . . 114
3.5. DYNLL1-CHICA-HMMR complexes promote correct spindle orientation 115

4. Materials and Methods **120**
4.1. Reagents 120
4.2. Equipment 120
4.3. Solutions and buffers 121
4.4. Molecular cloning 123
4.4.1. Gene amplification by nested PCR and cloning into pCR2.1-TOPO-vector 123
4.4.2. Amplification and preparation of plasmid DNA 126
4.4.3. Restriction enzyme digests 127
4.4.4. Ligation and transformation 127
4.4.5. Site-directed mutagenesis 128
4.5. Recombinant protein purification from *Escherichia coli* (*E. coli*) 129
4.6. Antibody production 132

4.7. Mammalian cell culture and cell synchronisation . . . 133
4.8. Transfection of mammalian cells . . . 133
4.8.1. Transient transfection . . . 134
4.8.2. Stable transfection . . . 134
4.8.3. siRNA-mediated depletion . . . 135
4.9. Immunofluorescence procedure . . . 136
4.10. Mitotic chromosome spreads . . . 136
4.11. Image acquisition and time-lapse microscopy . . . 137
4.12. SDS-polyacrylamide gel electrophoresis and Western blotting . . . 138
4.13. Isolation of protein complexes . . . 139
4.14. Co-immunoprecipitation assays . . . 140
4.15. Mass spectrometry of protein complexes . . . 140
4.16. *In vitro* translation . . . 141
4.17. Microtubule spin down assay . . . 142
4.18. Microtubule polymerisation assay . . . 143
4.19. Gel filtration . . . 143

5. References **144**

A. Appendix **155**
A.1. Cell lines . . . 155
A.2. Plasmids . . . 155
A.3. Primers . . . 157
A.4. siRNA target sequences . . . 159
A.5. Antibodies . . . 159
A.6. Publications . . . 162
A.6.1. Publication 1 . . . 162
A.6.2. Publication 2 . . . 173

1. Introduction

The cell is the fundamental unit of life. In the seventeenth century, Hooke and van Leeuwenhoek discovered that organisms are composed of building blocks, which they called cells. In multicellular organisms, cells are differentiated to fulfil discrete functions in a cell community. However, a common feature of all cells is the ability to grow and divide via the cell cycle in order to keep the organism viable.

1.1. Eukaryotic cell cycle

The eukaryotic cell cycle is the sequence of events that results in the division of a cell into two daughter cells. The cell cycle program ensures that the genetic material and other components are duplicated and faithfully distributed to provide both daughter cells with complete sets of chromosomes.

The mammalian cell cycle is comprised of four distinct stages (Figure 1.1, page 10) (Mitchison, 1971). The G_1 phase is the major growth and biosynthesis period. Cells integrate information from their environment in order to decide whether to undergo cell proliferation or to enter a state of quiescence, the G_0 phase. If cells proliferate, the DNA of the dividing cell is replicated in the following synthesis (S) phase generating chromosomes comprising two identical sister chromatids that are linked together. The centrosomes, cellular structures required for faithful segregation of these replicated chromosomes, are duplicated, but remain tightly associated until they are separated in mitosis. The G_2 phase is an additional period of cell growth and protein synthesis before cells progress into the mitotic (M) phase. The G phases are referred to as gap (G) phases, since they were first observed as a gap between mitosis and the beginning of DNA replication (G_1) and the gap between the completion of DNA replication and the start of mitosis (G_2). The following M phase comprises two steps, nuclear division (mitosis) and cellular division (cytokinesis). Cells in phases G_1, S and G_2 are often col-

lectively referred to as interphase cells to distinguish them from mitotic cells (Morgan, 2007).

M phase is characterised by the segregation of the duplicated chromosomes followed by the division of the cell (cytokinesis). While the complete cell cycle takes around 24 hours in a cultured adult mammalian cell, the process of mitosis, which involves major morphological changes of the cell, occurs within approximately only 1 hour (Cooper, 2000).

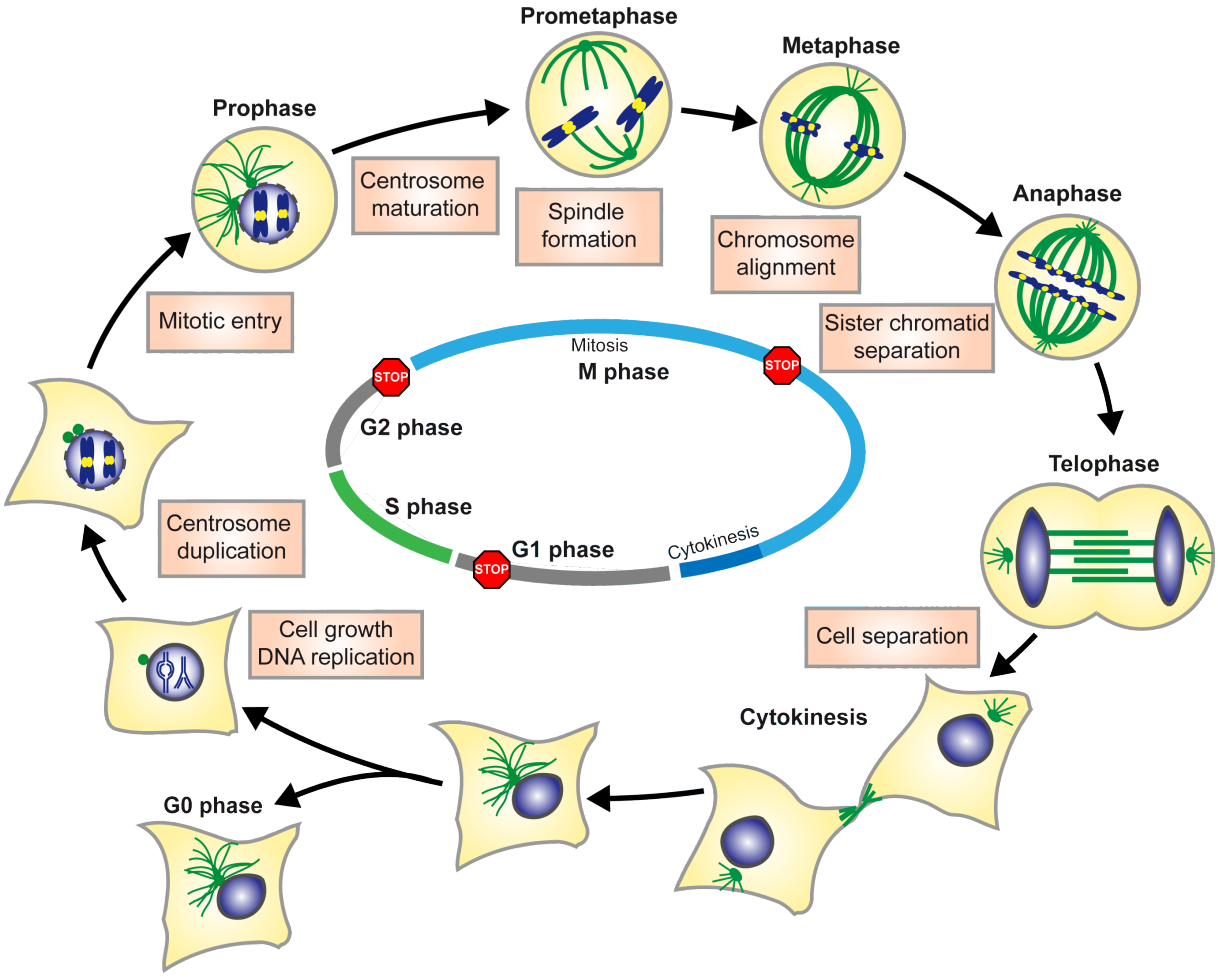


Figure 1.1: The events of the eukaryotic cell cycle. Interphase comprises the G_1 phase, S (synthesis) phase and G_2 phase. The M phase is divided into mitosis and cytokinesis. A schematic of the major morphological changes of the cell throughout the cell cycle is shown. Centromeres are visualised in yellow and centrosomes are depicted as green dots. Cell cycle checkpoints in G_1 phase, at the G_2/M and the metaphase to anaphase transition are represented by stop signs.

The key players regulating timely cell cycle progression are cyclin-dependent kinases (Cdks), that are activated upon association with regulatory subunits called cyclins (Murray *et al.*, 1989). Whereas Cdks are constitutively expressed throughout the cell cycle and their protein levels do not change, their activity depends on the oscillatory expression of cyclins at particular cell cycle stages. The mitotic cyclin B, whose expression is induced in G_2 phase, binds and activates Cdk1, which promotes entry into mitosis. In addition to its association with cyclin B, Cdk1 activity is controlled by its phosphorylation state. Phosphorylation at threonine 14 and tyrosine 15 by Wee1 and Myt1 kinases inhibits Cdk1 activity in interphase, whereas dephosphorylation of these residues by Cdc25 phosphatase activates Cdk1 in mitosis (Lew and Kornbluth, 1996). The activity of Wee1 and Myt1 is controlled by DNA damage response proteins, which delay entry into mitosis in the presence of damaged DNA (Margolis *et al.*, 2006), while Cdc25 is kept inactive in interphase by association with 14-3-3 protein and PP2A-B56δ and is phosphorylated and activated at the entry of mitosis by polo-like kinase 1 (Plk1) (Kumagai *et al.*, 1998; Kumagai and Dunphy, 1996; Liu *et al.*, 2004).

Mitosis is subdivided into five major phases: prophase, prometaphase, metaphase, anaphase and telophase (Figure 1.1, page 10). At mitotic entry, the DNA condenses into chromosomes. In prophase, the two replicated centrosomes separate from each other, migrate to opposite sites of the nucleus and start nucleating radial microtubules (asters). In prometaphase, the nuclear envelope disassembles and the bipolar mitotic spindle is nucleated from the two centrosomes, 'searching' for the chromosomes, which are made up of two duplicated sister chromatids linked together by cohesin, a protein complex described in more detail in section 1.3. The chromosomes are 'captured' by the spindle microtubules and are moved to the equatorial region of the cell, defining metaphase (Kirschner and Mitchison, 1986). Faithful alignment of all chromosomes at the metaphase plate triggers anaphase initiation. Then, the E3 ubiquitin-ligase

anaphase promoting complex/cyclosome (APC/C) associates with its activator subunit Cdc20 (Figure 1.5, page 22). Active APC/C promotes degradation of securin and cyclin B, thereby inactivating Cdk1 and allowing mitotic exit. Securin acts as an inhibitor of the protease separase and upon its destruction, active separase is released, which then cleaves the cohesin component Scc1. Thereby, sister chromatid cohesion is simultaneously lost at the onset of anaphase. The sister chromatids are pulled towards the two opposing poles of the cell by shortening of the attached microtubules and by subsequent elongation of the spindle. Mitosis is completed in telophase by the invagination of the cell membrane around the spindle midzone (cleavage furrow formation) and disassembly of the mitotic spindle. During the subsequent stage of cytokinesis, an actomyosin-based contractile ring, which gradually contracts and finally separates the cell into two daughter cells, is formed from actin filaments around the central spindle (Cao and Wang, 1990).

The progression from one stage of the cell cycle to the next one is controlled by checkpoints, which are regulatory mechanisms that can arrest the cell within the cell cycle to prevent unfaithful or abnormal cell proliferation (Figure 1.1, page 10). The checkpoint machinery monitors whether one event of the cell cycle has successfully occurred before the following is initiated and also limits each duplication and segregation process to one per cell cycle. The G_1 checkpoint senses if all requirements are fulfilled to undergo cell proliferation. When the conditions are satisfactory, cell cycle entry and expression of the G_1 phase cyclin D is induced. After duplication of the chromosomes in S phase, the G_2/M transition checkpoint controls whether DNA replication has been completed correctly, before promoting mitotic entry. Mitosis is controlled at the metaphase to anaphase transition by the spindle assembly checkpoint (SAC), discussed in section 1.4.

1.2. Mitotic spindle formation and centrosomes

The assembled bipolar spindle is a highly dynamic macromolecular complex consisting of bundled microtubules, microtubule motor proteins and microtubule associated proteins (MAPs). The spindle microtubules are organised in two antiparallel arrays, which are used as tracks for chromosome movement in mitosis. Motor proteins assist in arranging the microtubules in this antiparallel, bipolar fashion. The kinesin superfamily of motors promotes both plus and minus end directed movement, while cytoplasmic dynein moves its cargo towards minus ends only. There are three different kinds of spindle microtubules: astral microtubules, which originate from the poles and attach the spindle to the cell cortex, kinetochore fibres (K-fibres), that link chromosomes to the spindle, and finally microtubules nucleating from centrosomes and overlapping in an antiparallel way at the spindle equator. While interphase microtubules have a half-life in order of minutes to hours, spindle microtubules are very dynamic and the half-life is reduced to a minute or less. These microtubule dynamics as well as spindle length are regulated by stabilising MAPs like CLASP, MAP4 or ch-TOG, and microtubule-destabilising or -severing proteins such as stathmin or katanin (Akhmanova *et al.*, 2001; Gavet *et al.*, 1998; McNally and Thomas, 1998; Tournebize *et al.*, 2000). In mitosis, microtubules nucleating from the spindle poles search and capture chromosomes with their plus ends and become stabilised upon attachment (see section 1.4), whereas unattached microtubules rapidly depolymerise again (Kirschner and Mitchison, 1986; Mitchison and Kirschner, 1984).

1.2.1. Spindle poles

The microtubule organising centres (MTOC) of human cells are the centrosomes, which are composed of a pair of orthogonally arranged cylindrical centrioles and the surrounding electron-dense pericentriolar matrix (PCM) (Bornens and Piel, 2002). In G_1,

the cell contains one centrosome, which is duplicated in S phase in a semiconservative manner. New centrioles grow perpendicular to the two existing centrioles and connect to each other (centriole engagement). They are closely tethered to the nucleus by the motor protein dynein-dynactin, which is recruited to the nuclear envelope via the dynein-adaptor BicD2 and the nuclear pore complex (NPC) component RanBP2 (Splinter *et al.*, 2010). Both centrosomes start nucleating microtubules, which is the basis for the formation of a bipolar spindle. The centrosome movement to opposite poles is mediated by the plus end directed microtubule motor Eg5 and the minus end directed motor dynein (Sawin *et al.*, 1992; Raaijmakers *et al.*, 2012). Eg5 is a tetramer that crosslinks microtubules and slides them apart, thereby pushing the centrosomes along the nuclear envelope (Blangy *et al.*, 1995). Additional pulling forces are applied onto the centrosomes by a pool of dynein associated with the nuclear envelope (Vaisberg *et al.*, 1993; Raaijmakers *et al.*, 2012; Splinter *et al.*, 2010). This centrosome splitting is controlled by the Nek2 protein kinase and the opposing phosphatase PP1α (Mi *et al.*, 2007). The coiled-coil protein C-Nap1, which is required for centrosome cohesion, is phosphorylated by Nek2 at the G_2/M transition thereby displacing C-Nap1 from the centrioles and dissolving the centrosome tethering structure (Fry *et al.*, 1998; Mayor *et al.*, 2000; Faragher and Fry, 2003). The formation of stable spindle poles requires the recruitment of structural proteins like pericentrin, TACCs, TPX2 or NuMA (nuclear mitotic apparatus) by the dynein-dynactin motor complex (Gergely *et al.*, 2000; Gaglio *et al.*, 1996; Merdes *et al.*, 2000). The PCM contains γ-tubulin ring complexes (γ-TuRCs), which form a structural template for the microtubule minus ends. The γ-TuRC is targeted to the centrosomes by Nedd1, which directly interacts with the γ-TuRC subunit γ-tubulin (Haren *et al.*, 2006). Whilst NuMA crosslinks these microtubule minus ends and forms a focused spindle pole, TPX2 regulates the density of microtubules and the spindle pole structure (Merdes *et al.*, 1996; Wittmann *et al.*, 2000). During anaphase, the two centrioles of each centrosome are separated (centriole disengagement) and

thus licensed for duplication in the next cell cycle (Tsou and Stearns, 2006). This disengagement depends on the activity of the mitotic kinase Plk1 and separase, a protease which also resolves the sister chromatid cohesion in anaphase (see section 1.3) (Tsou *et al.*, 2009; Schöckel *et al.*, 2011). A recent model suggests that the Akt kinase-interacting protein 1 (Aki1) recruits the cohesin subunit Scc1 to the centrosomes, where it mediates centriole cohesion until cleavage by separase (Nakamura *et al.*, 2009). By this timely regulated centriole engagement and disengagement, centrosome duplication is precisely limited to one duplication per cell cycle and is coupled to cell cycle regulation, which is essential to prevent formation of multipolar spindles as a result of centrosome splitting or multiple duplications.

1.2.2. Microtubule nucleation

While centrosomes are the primary site for microtubule nucleation, microtubule polymerisation in mitotic mammalian cells has also been shown to be initiated in the vicinity of the chromosomes or along existing spindle microtubules suggesting that centrosomes are not essential for mitotic spindle assembly (Khodjakov *et al.*, 2000; Lüders and Stearns, 2007; Mahoney *et al.*, 2006). This idea is supported by the finding that *Drosophila* mutants that have lost their centrioles are able to develop into morphologically normal adult flies (Basto *et al.*, 2006). Moreover, cultured cells whose centrosomes were removed by laser ablation or microsurgery could still form bipolar spindles (Hinchcliffe *et al.*, 2001; Khodjakov *et al.*, 2000). Microtubules are nucleated from mitotic chromosomes or from existing microtubules and tethered into the PCM to form a bipolar spindle. This tethering is promoted by cytoplasmic dynein, which crosslinks microtubules to focus their minus ends into spindle poles (Gadde and Heald, 2004).

De novo microtubule nucleation at chromosomes is regulated by the small GTPase Ran, which is active when bound to GTP and inactive in its GDP-bound form (Wilde and Zheng, 1999). In mitosis the Ran guanine nucleotide exchange factor (GEF) factor RCC1 associates with chromatin, whereas the RanGTPase activating protein (GAP) is cytoplasmic (Figure 1.2, page 16). This difference in localisation generates a gradient of Ran in its active form Ran·GTP, with the highest concentration at the chromatin (Kalab *et al.*, 2002; Kaláb *et al.*, 2006).

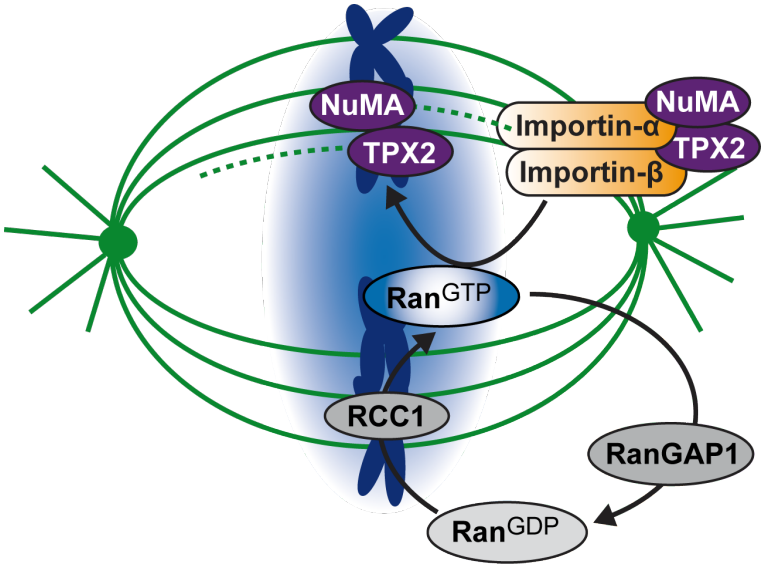


Figure 1.2: *De novo* microtubule nucleation in the vicinity of chromosomes. Chromosome-bound RCC1 promotes association of Ran with GTP, while cytoplasmic RanGAP1 induces GTP hydrolysis to GDP. This generates a gradient of active Ran (shown in light blue) with its highest concentration at chromatin, where it releases spindle-assembly factors, such as NuMA and TPX2, from the importin-α/β carrier.

Ran·GTP controls the release and activity of spindle assembly factors (SAFs) from importin-α/β complexes (Carazo-Salas *et al.*, 1999; Clarke and Zhang, 2008; Nachury *et al.*, 2001). One of these factors is TPX2, which activates Aurora A (Gruss *et al.*, 2001, 2002). This kinase then in turn phosphorylates the γ-TuRC recruiting factor Nedd1 and triggers microtubule nucleation in the vicinity of chromosomes (Pinyol *et al.*, 2012). A complex of dynein/dynactin, Eg5, KIF4 and NuMA then slides these micro-

tubules, subsequently focussing the microtubule minus ends into defined spindle poles as well as tethering existing centrosomes into the spindle body (Sawin *et al.*, 1992; Vernos *et al.*, 1995; Merdes *et al.*, 1996; Compton, 1998).

A second pathway for microtubule nucleation, which is independent of centrosomes, involves the Augmin complex. This protein complex promotes microtubule nucleation on existing microtubules by targeting the γ-TuRC via γ-tubulin to spindle microtubules (Goshima *et al.*, 2007, 2008). Ran·GTP and TPX2 then induce the branching microtubule nucleation (Petry *et al.*, 2013). These daughter microtubules grow at a low angle towards the mother microtubules and with the same polarity, thereby providing ideal structures for generating parallel microtubule bundles.

1.2.3. Microtubule attachments at kinetochores

Spindle microtubules nucleated from the spindle poles exhibit a search-and-capture behaviour and initially encounter the kinetochores of chromosomes by chance. The kinetochore is a large proteinaceous structure consisting of more than 80 components, that is formed in mitosis to physically connect chromosomes to the plus ends of spindle microtubules. It forms a trilaminar plate comprising an inner, a middle and an outer layer with a fibrous corona extending from the outer plate (Santaguida and Musacchio, 2009). In mammalian cells the inner plate is composed of specialised chromatin, repetitive centromeric DNA with the histone H3 variant CenpA (Figure 1.3, page 18). Some of its components, such as CenpA, CenpB, and the constitutive centromere-associated network (CCAN) proteins are constitutively bound to the chromatin throughout the cell cycle. The outer kinetochore comprises the stable components of the KMN network (Knl1, Mis12 and Ndc80 complex) and the Ska complex, as well as the microtubule motors CenpE and dynein, and spindle checkpoint proteins (Cheeseman *et al.*, 2006; Burke and Stukenberg, 2008; Welburn *et al.*, 2009; Weaver *et al.*, 2003). CLIP-

associated proteins (CLASPs) are outer kinetochore proteins that interact with and regulate the dynamics of microtubule plus ends (Maffini *et al.*, 2009; Akhmanova *et al.*, 2001; Maiato *et al.*, 2003).

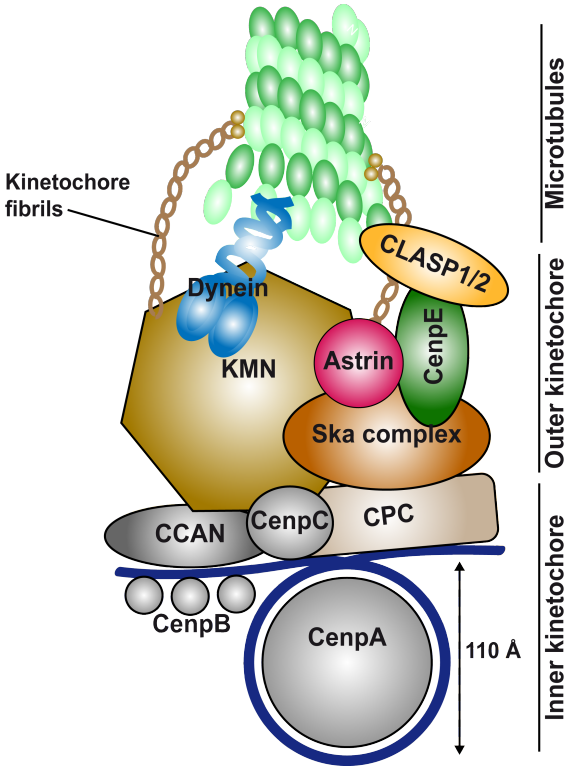


Figure 1.3: Schematic of the kinetochore structure. The KMN complex comprises the three subcomplexes Knl1 (Knl1, Zwint), Mis12 (Mis12, Dsn1, Nnf1, Nsl1) and Ndc80 (Ndc80/Hec1, Nuf2, Spc24 and Spc25). The CPC is composed of Aurora B kinase, INCENP, survivin and borealin. CCAN are proteins of the Constitutive Centromere-Associated Network (McAinsh and Meraldi, 2011). Model modified from Santaguida and Musacchio, 2009.

In animal cells one kinetochore is captured by a bundle of approximately 20-40 microtubules, referred to as kinetochore fibres (K-fibres) (McEwen *et al.*, 1997; Morgan, 2007). These microtubules bind in both, end-on and side-on arrangements (Dong *et al.*, 2007). The major site of microtubule polymerisation and depolymerisation are the plus ends at the kinetochore (Maiato *et al.*, 2004). Thus, the kinetochore assembly is highly dynamic in order to maintain attachment of the kinetochores to growing and shrinking microtubules. The KMN network directly associates with microtubules by means of Ndc80 binding to tubulin every 4 nm, the spacing of tubulin monomers (Cheeseman *et al.*, 2006; Alushin *et al.*, 2010). The Ska complex also promotes stable microtubule-kinetochore attachments by binding to these dynamic microtubules (Welburn *et al.*,

2009). A ring structure formed by the full Ska complex was proposed to encircle the microtubule plus ends and generate attachment by several weak bonds between Ska1 and microtubules (Welburn *et al.*, 2009; Santaguida and Musacchio, 2009). In an alternative theoretical model, it was suggested that microtubules insert into a sleeve formed by the kinetochore and multiple weak interactions between the tubulin subunits of the microtubules and the sleeve walls promote the attachment. Movement of the chromosomes is facilitated by polymerisation at the plus ends within the sleeve and depolymerisation at the minus ends at the poles (Maiato *et al.*, 2004; Santaguida and Musacchio, 2009). In yet another model, it has been proposed that kinetochore-microtubule attachments are established by fibril-like structures emanating from the kinetochore and contacting the microtubule protofilaments (McIntosh *et al.*, 2008).

1.3. Sister chromatid cohesion

In mitosis, the duplicated genetic material is faithfully distributed between two daughter cells, so that each daughter inherits a complete set of chromosomes. To allow the precise separation, the duplicated chromatids need to be tightly linked to one another from the point of duplication until their migration to opposite poles in anaphase. This strong association is achieved by the cohesin complex, which is loaded onto the DNA before replication in S-phase and that maintains this tight association in the following phases, when chromosomes are subjected to considerable physical pushing and pulling forces (Ciosk *et al.*, 2000; Haering *et al.*, 2002; Uhlmann and Nasmyth, 1998). The cohesin complex comprising the subunits SMC1, SMC3, Scc1 and SA1 or SA2 forms a ring capable of surrounding and entrapping the two DNA strands of a chromosome (Haering *et al.*, 2002). Faithful cohesion is important to oppose the pulling forces of the mitotic spindle microtubules, which generates tension sensed by the SAC, described in section 1.4. In mitosis, the cohesin complex is removed from the chromosomes

in two steps: firstly, cohesin is released from the chromosome arms in the 'prophase pathway', whereas the centromeric cohesin is removed at the onset of anaphase by cleavage of Scc1(Figure 1.4, page 20) (Waizenegger *et al.*, 2000; Gandhi *et al.*, 2006).

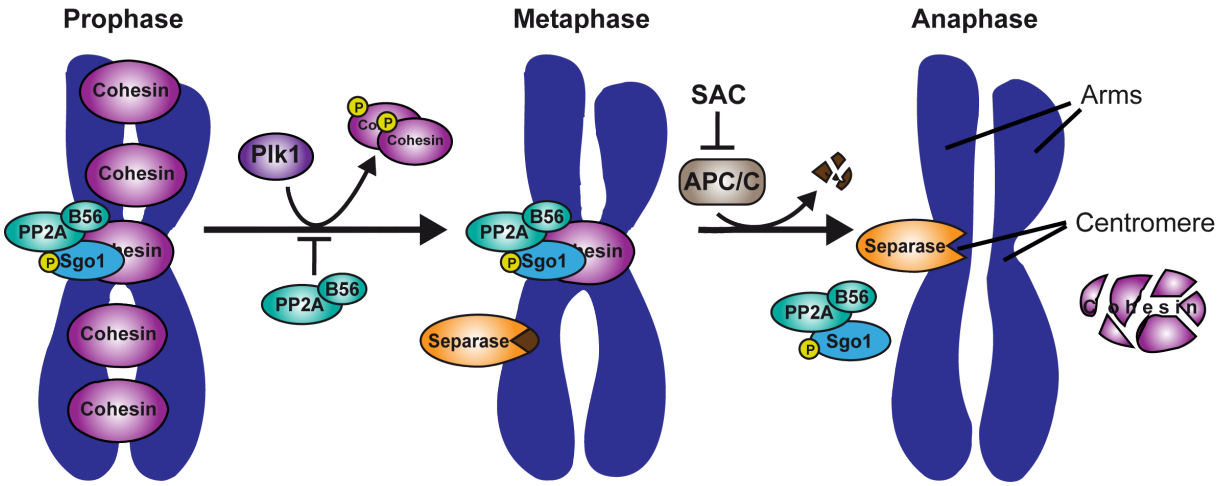


Figure 1.4: Cohesin removal pathways. Cohesin is removed from the chromosomes in two steps. In prophase, cohesin is removed from the chromosome arms upon phosphorylation by Plk1, while centromeric cohesin is protected by Sgo1 and PP2A. In anaphase, activation of separase upon SAC silencing cleaves and releases cohesin from centromeric DNA and allows the separation of the sister chromatids.

In prophase, phosphorylation of the SA1/2 subunit by Plk1 triggers the removal of cohesin from chromosome arms (Hauf *et al.*, 2005; Sumara *et al.*, 2002). Centromeric cohesin is protected by the 'guardian spirit' protein shugoshin (Katis *et al.*, 2004; Kitajima *et al.*, 2004). The two mammalian shugoshin proteins, Sgo1 and Sgo2, play divergent roles in mitosis. Sgo1 is required for protecting the centromeric cohesin (McGuinness *et al.*, 2005), while Sgo2 is thought to load the protein MCAK onto centromeres, which participates in the correction of attachment errors (see section 1.4) (Huang *et al.*, 2007; Tanno *et al.*, 2010). The protection of centromeric cohesion in the prophase pathway is achieved by the interaction of Sgo1 with the phosphatase PP2A·B56, which presumably counteracts the Plk1-mediated phosphorylation of the SA1/2 subunit (McGuinness *et al.*, 2005; Kitajima *et al.*, 2006). Moreover, a recent study has proposed that a splice

variant of Sgo1 also protects centriole pairs from disengagement in prophase (Wang *et al.*, 2008). As described earlier, centromeric cohesion is lost upon cleavage of Scc1 by the protease separase. Separase is kept inactive before anaphase by at least two independent regulatory mechanisms. In vertebrates the proteolytic activity is inhibited by binding of the chaperone securin as well as stable binding of cyclin B·Cdk1 upon Cdk1-mediated phosphorylation (Funabiki *et al.*, 1996; Holland and Taylor, 2006; Stemmann *et al.*, 2001; Gorr *et al.*, 2005). Silencing of the SAC in anaphase results in an activation of the E3 ligase APC/C, which in turn ubiquitinates securin and cyclin B. Subsequently, separase is activated upon destruction of both, securin and cyclin B. Active separase then not only cleaves the remaining Scc1 at the centromeres, but also itself. It has been suggested that autocleavage of separase releases separase-bound PP2A·B56, liberating this phosphatase for its functions in mitotic exit (Holland *et al.*, 2007).

1.4. The spindle assembly checkpoint

The spindle assembly checkpoint (SAC) is a control mechanism that monitors kinetochore attachments and tension of chromatids. It prevents chromosome segregation defects by inhibiting metaphase to anaphase transition until all sister chromatids are attached to kinetochore fibres from opposing poles and sufficient tension is sensed across the kinetochore (Musacchio and Salmon, 2007). Initially, the chromosomes will be captured by microtubules from one pole only and become mono-oriented. These mono-oriented chromosomes generate a spindle checkpoint signal, which delays the onset of anaphase, until all kinetochores show bi-oriented, amphitelic attachments. Bi-orientation and amphitely are defined by attachment of one sister chromatid to microtubules solely from one pole and attachment of the corresponding sister chromatid to microtubules solely from the other pole (Rieder and Salmon, 1998). Due to the cohe-

sion between both chromatids, bi-oriented sister chromatids are under tension across the sister kinetochores.

Unattached kinetochores recruit a complex consisting of the checkpoint proteins Bub3, BubR1, Mad2 and Cdc20 (comprising the mitotic checkpoint complex (MCC)) as well as other proteins Mad1, Bub1, Spindly, Aurora B and Mps1, which halts cell cycle progression (Figure 1.5, page 22) (Sudakin *et al.*, 2001; Abrieu *et al.*, 2001; Griffis *et al.*, 2007; Nilsson *et al.*, 2008).

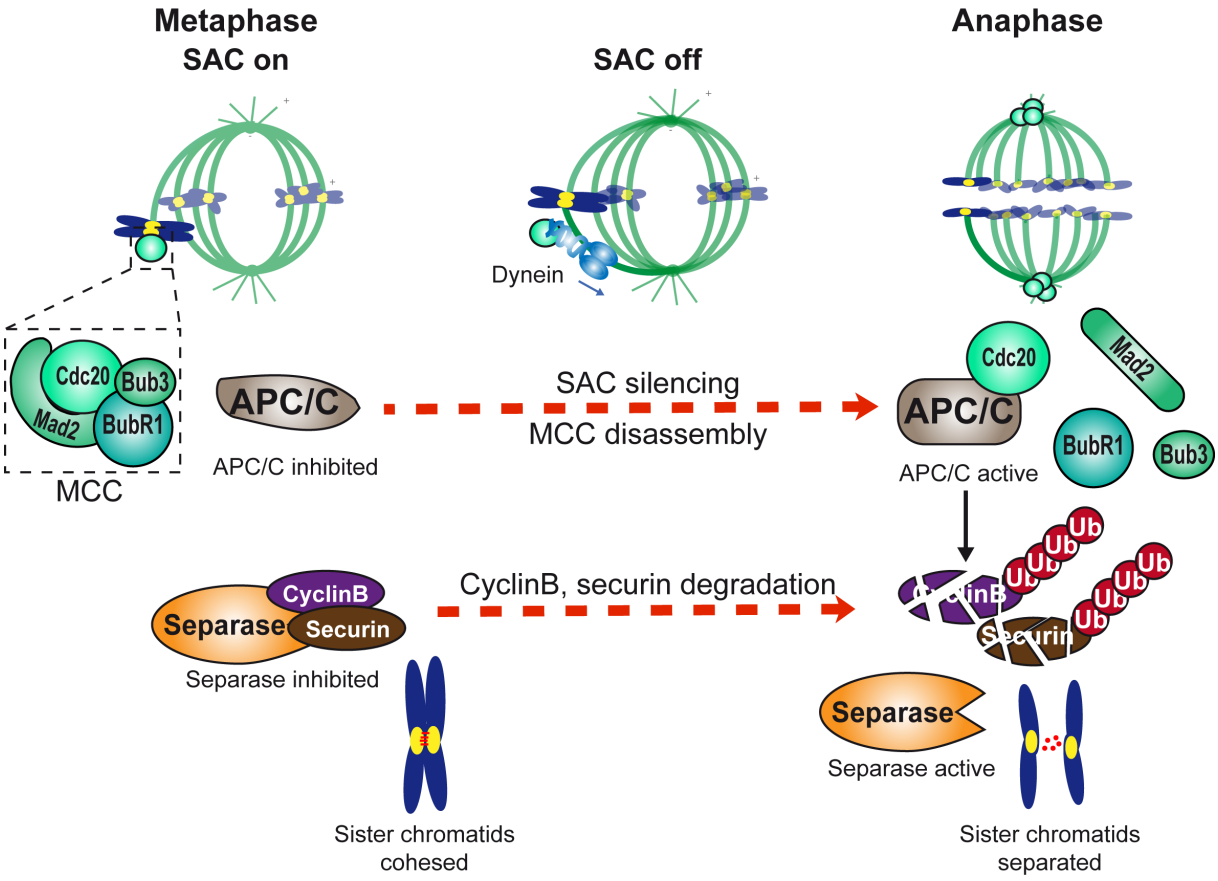


Figure 1.5: Spindle assembly checkpoint function. The MCC comprising Mad2, BubR1 and Bub3 recognises and binds to unattached kinetochores thereby tethering the APC/C activator Cdc20. Upon attachment of all kinetochores, dynein strips the MCC off the kinetochore, the MCC disassembles and Cdc20 activates APC/C. This activated E3-ligase then marks cyclin B and securin for degradation enabling separase activation and sister chromatid separation.

The assembly of the mitotic checkpoint complex at the unattached kinetochore is dependent on the kinase activity of the monopolar spindle protein 1 (Mps1) (Abrieu *et al.*, 2001). Mps1 is required for the recruitment of Bub1, BubR1 and CenpE (Abrieu *et al.*, 2001; Vigneron *et al.*, 2004; Zhao and Chen, 2006). Bub1 and BubR1 in turn recruit Mad1 and Mad2 to the kinetochore, which enables binding of Mad2 to Cdc20. Mad2 acts as a dimer, with each of the monomers adopting one of two conformations, a closed conformation (C-Mad2) when bound to Mad1 or Cdc20, and the open conformation (O-Mad2) when free of ligands (Luo *et al.*, 2004). The kinetochore-localised Mad1·C-Mad2 complex recruits free O-Mad2 thereby converting it into C-Mad2 that competes with the APC/C for the binding site on Cdc20 (DeAntoni *et al.*, 2005; Izawa and Pines, 2012). Sequestration of the APC/C co-activator Cdc20 into the MCC inhibits the activation of APC/C. Unattached kinetochores therefore drive MCC formation, and thus prevent premature anaphase onset. One unattached kinetochore can delay mitotic progression for hours (Rieder *et al.*, 1995).

Attachment of both sister chromatids to one pole only (syntelic attachment) and thereby insufficient tension across the kinetochore is sensed by Aurora B kinase, which is embedded in the centromere. Aurora B phosphorylates the Ndc80 complex subunit Hec1 and the Ska complex decreasing its affinity to microtubules and therefore abolishing the attachment, generating unattached kinetochores that are sensed by the SAC and allowing another opportunity for microtubule interaction (Cheeseman *et al.*, 2006; Chan *et al.*, 2012). Upon amphitelic attachment, the sister chromatids are under tension, inducing both, a centromeric and intrakinetochore stretch, which prevents destabilisation of the attachment by Aurora B (Maresca and Salmon, 2009; Uchida *et al.*, 2009). According to the prevailing model, kinetochore stretching reduces the ability of Aurora B to reach its substrate Hec1 in the outer kinetochore, while a kinetochore localised phosphatase counteracts the Aurora B-mediated phosphorylations (Liu *et al.*, 2009). Initially

this function was attributed to PP1, however recent work suggests that PP2A-B56 stabilises kinetochore-microtubule attachments (Liu *et al.*, 2010; Foley *et al.*, 2011). It has been suggested that PP2A-B56 is directly recruited to improperly attached kinetochores by interaction with BubR1 (Kruse *et al.*, 2013).

Once all chromosomes show amphitelic attachments and all MCC assembly sites are occupied, the SAC is satisfied. The checkpoint proteins disassemble and are transported away from the kinetochores to the centrosomes by the minus end directed motor protein dynein, which is recruited onto the kinetochore via Spindly (Howell *et al.*, 2001; Griffis *et al.*, 2007; Gassmann *et al.*, 2010). The MCC component Mad2 in its Cdc20-bound conformation is bound by activated p31^{COMET}, which folds into a structural mimic of Mad2 thereby binding to the Mad2 dimerisation interface (Xia *et al.*, 2004; Yang *et al.*, 2007). This binding of p31^{COMET} to Mad2 disassembles the MCC releasing Cdc20 (Westhorpe *et al.*, 2011). The ubiquitin-ligase APC/C is phosphorylated by active Cdks allowing the association with its activator subunit Cdc20. Active APC/C promotes degradation of the separase inhibitor securin and of cyclin B, thereby inactivating Cdk1. Upon destruction of securin, active separase is released, which cleaves the cohesin component Scc1 and sister chromatid cohesion is simultaneously lost at the onset of anaphase (Figure 1.5, page 22).

1.5. Mitotic spindle positioning and orientation

In addition to capturing and aligning the chromosomes, the position and orientation of the mitotic spindle within the cell is critical to define the cleavage plane in telophase (Rappaport, 1971; Bringmann and Hyman, 2005). Placing the spindle in the centre of the cell will cause a symmetrical division, which is critical for the clonal expansion of cells and the generation of identical daughter cells of equal size. Positioning the

spindle asymmetrically results in asymmetric division and in daughter cells of different sizes. Asymmetric cell divisions play an important role in stem cells, in order to maintain the self-renewal and differentiation properties of these cells by asymmetric segregation of cell fate determinants, protein or RNA molecules that determine distinct cell fates (Inaba and Yamashita, 2012). Therefore, correct spindle positioning is an essential process in development, tissue morphogenesis and the generation of cellular diversity.

Studies in budding yeast have been influential for identifying and understanding the spindle positioning machinery. In *Saccharomyces cerevisiae*, a daughter cell (bud) is formed on the mother cell and the spindle is positioned along the mother-bud axis to distribute the genetic material between mother and daughter cell. At least two distinct pathways, one dependent on Kar9p, the other on dynein, are regulating the position of the mitotic spindle in these cells. Kar9p accumulates at one spindle pole, where it tracks the plus ends of emanating astral microtubules and guides those into the daughter cell by associating with the bud neck (Merlini and Piatti, 2011) (Figure 1.6, page 26). Dynein also localises asymmetrically to the spindle pole that is closer to the bud neck and moves along the astral microtubules nucleating from that pole. It slides these astral microtubules along the bud cortex, so that the spindle is finally pulled across the bud neck (Merlini and Piatti, 2011). In budding yeast mitosis, this correct spindle orientation and position is controlled by the mechanisms of a spindle-positioning and orientation checkpoint (SPOC), which delays mitotic exit and cytokinesis until the spindle is properly positioned and oriented (Muhua *et al.*, 1998; Merlini and Piatti, 2011).

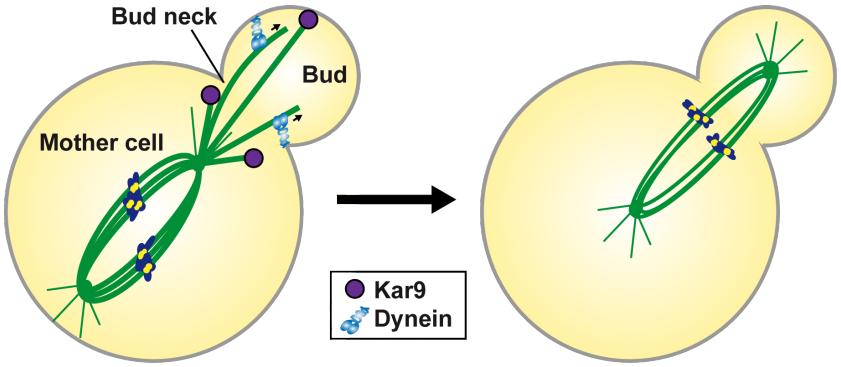


Figure 1.6: Spindle positioning in *Saccharomyces cerevisiae* In budding yeast the mitotic spindle aligns with the mother cell-daughter cell axis. Kar9p directs astral microtubules into the bud, where dynein slides these microtubules along the bud cortex thereby pulling the spindle into the bud.

However, it is currently unknown whether such a checkpoint also exists in metazoans.

In yeast as well as in mammalian cells, the establishment of a defined orientation axis requires the interaction of astral microtubules with motors and other proteins at the cell cortex. Astral microtubules have their minus ends embedded in the spindle poles, while their plus ends are growing towards the cell cortex. It has been suggested that the spindle in mammalian cells is positioned by a balance of forces generated by growing astral microtubules that are pushing against the cell cortex and by cortically localised dynein-dynactin, which is pulling on these astral microtubules, a mechanism termed 'cortical pulling' (Dujardin and Vallee, 2002). It has been shown that growing microtubules rapidly switch into a depolymerising state upon touching the cortex. Dynein attaches to these depolymerising microtubules thereby generating the pulling forces (Kozlowski *et al.*, 2007). The cell cortex is physically supported by an underlying actin mesh scaffold (Alberts *et al.*, 2004; Morone *et al.*, 2006). This cortex rigidity opposes the pulling forces created by dynein to avoid membrane invaginations and instead promote spindle movement (Redemann *et al.*, 2010). Thus, the position of the mitotic spindle ultimately is dictated by the localisation of dynein at the cortex.

In mammalian mitosis, orientation and position of the mitotic spindle are controlled by a combination of extrinsic factors, intrinsic cues and physical constraints, all of which result in the polarisation of the cell cortex and thereby influence cortical dynein accumulation. Extrinsic factors are transmitting information about neighbouring cells and the cell matrix to the dividing cell in order to coordinate the division plane with tissue architecture. The extracellular matrix (ECM) influences the distribution of cortical cues in interphase. These dynamic actin cues are maintained in mitosis and associate with retraction fibres, extensions of the plasma membrane that adhere the rounded mitotic cells to their surrounding tissue (Figure 1.7, page 27) (Théry *et al.*, 2005; Fink *et al.*, 2011). The plasma-membrane associated Gα protein then transmits information to the mitotic spindle via a set of TPR-GoLoco proteins such as LGN. These proteins have an Gα-binding 'GoLoco' domain and a tetratricopeptide repeat (TPR) domain, and directly bind to microtubule-associated proteins (NuMA in human cells), which then in turn recruit dynein (Kotak *et al.*, 2012). Asymmetric localisation of the TPR-GoLoco protein or asymmetric recruitment of dynein then provides pulling forces from a specific site at the cortex (Gotta *et al.*, 2003; Colombo *et al.*, 2003; Schaefer *et al.*, 2000).

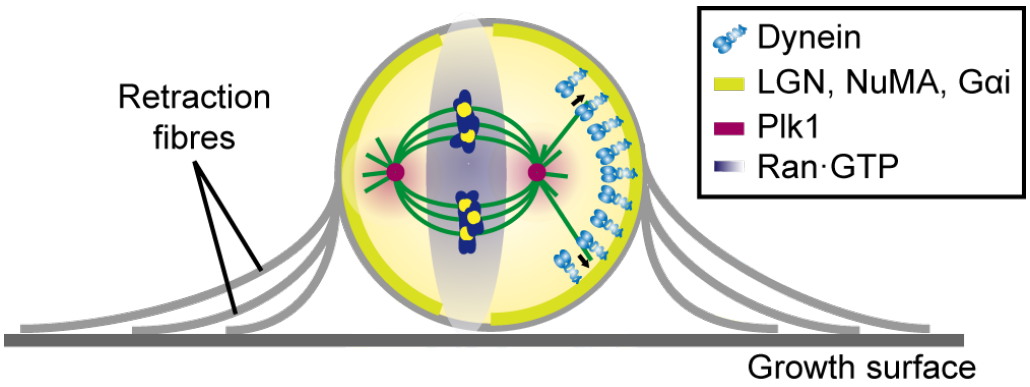


Figure 1.7: Symmetric cell division of human cells. Plk1 and Ran·GTP restrict dynein to a defined region at the cell cortex. Dynein exerts pulling forces on astral microtubules, thereby positioning the mitotic spindle within the plane of cortical dynein.

It has recently been shown that in addition to such extrinsic influences, factors intrinsic to the mitotic spindle and the chromosomes control the spindle position and orienta-

tion of mammalian cells (Kiyomitsu and Cheeseman, 2012). In symmetric divisions of human cells, the spindles align parallel to the substratum (planar orientation), which is sensed by the aforementioned retraction fibres. Thereby the geometry of the adhesion pattern dictates the orientation of the mitotic spindle (Théry *et al.*, 2005). As described before, the microtubule motor protein dynein is targeted to the cell cortex upon interaction with LGN, NuMA and Gα (Figure 1.7, page 27) (Dujardin and Vallee, 2002). Kiyomitsu *et al.* hypothesised that spindle pole localised polo-like kinase 1 (Plk1) emits a short-range inhibitory signal, which disrupts the dynein-LGN-NuMA interaction thereby removing cortical dynein/dynactin from the nearby cell cortex (Kiyomitsu and Cheeseman, 2012). Concomitantly, a chromosome-derived concentration gradient of Ran·GTP locally decreases the ability of LGN-NuMA to interact with the membrane near the chromosomes. This results in an asymmetric distribution of the motor protein dynein. Consequently, the spindle oscillates between the cell poles until the balance of forces aligns the spindle in the centre of the cell (Kiyomitsu and Cheeseman, 2012).

1.6. Cytoplasmic dynein

The multisubunit adenosine triphosphate (ATP)-driven, minus end directed motor protein dynein plays important roles in the transport of cargo at distinct localisations in cellular compartments including the cell cortex, intracellular vesicles, microtubule plus ends and the nuclear envelope (NE) (Kardon and Vale, 2009; Tanenbaum *et al.*, 2010). In order to couple to its diverse range of cargo and to carry out its various transport functions, dynein associates with several adaptor or regulator proteins, such as dynactin, LIS1, NudE, Rod-Zw10-Zwilch (RZZ) and Bicaudal D (Kardon and Vale, 2009). Dynein in association with its activator dynactin participates in the microtubule-based retrograde transport of vesicles and organelles, as well as the transport of proteins, such as Spindly, from the kinetochores to the spindle poles in the process of silencing

the SAC (see section 1.4) (Karki and Holzbaur, 1999; Howell *et al.*, 2001; Gassmann *et al.*, 2010). Additionally, dynein-dynactin is involved in focusing the spindle poles by transporting structural factors such as TPX2 and NuMA to the minus ends (Wittmann and Hyman, 1999). Dynactin facilitates these dynein functions by targeting dynein to the microtubule plus ends by directly interacting with microtubule plus end binding proteins via its $p150^{Glued}$ subunit, linking dynein to its cargo and increasing the processivity of the motor (Kardon and Vale, 2009). Furthermore, dynactin also interacts with the plus end directed motors kinesin 5 and kinesin 2 and thus was suggested to coordinate the bidirectional transport of certain dynein cargo (Kim *et al.*, 2007).

The interaction of dynein with its adaptors LIS1, NudE and NudE-like is essential for the positioning of the nucleus and the centrosomes during the polarisation of cells in asymmetric cell divisions or cell migration (Shu *et al.*, 2004; Tanaka *et al.*, 2004; Tsai *et al.*, 2007). The LIS1-NudE and the LIS1-NudE-like complexes are also important for the recruitment of dynein to the cell cortex (Faulkner *et al.*, 2000). Cortical dynein regulates spindle positioning and orientation by interacting with astral microtubules (see section 1.5). Dynein captures dynamic microtubule plus ends in an 'end on' configuration, inhibits their growth and promotes microtubule catastrophe (Laan *et al.*, 2012). This microtubule shrinkage then generates a pulling force on the mitotic spindle, which drives spindle positioning.

The adaptors Rod-ZW10-Zwilch and Spindly recruit dynein to the kinetochore (Kops *et al.*, 2005; Chan *et al.*, 2009), where it plays an important role in microtubule capturing and chromosome congression in prometaphase (Santaguida and Musacchio, 2009). Upon bi-orientation of the chromosomes and increased interkinetochore tension, kinetochore-localised dynein switches from ZW10 to dynactin binding to fulfil its function in the transport of MCC proteins in order to silence the SAC (Kardon and Vale, 2009).

Dynein-mediated transport of mRNA or Golgi vesicles is promoted by interaction with

the adaptor Bicaudal D (BicD), which links dynein to its cargo (Dienstbier *et al.*, 2009; Matanis *et al.*, 2002). Moreover, BicD recruits dynein to the nuclear envelope to pull the centrosomes along the NE during bipolar spindle formation (see section 1.2) (Splinter *et al.*, 2010; Raaijmakers *et al.*, 2012).

The cytoplasmic dynein 1 motor is a large complex of around 1.4 megadalton (MD) and consists of two homodimers of heavy chains (≈530 kD), which are required to associate with multiple intermediate chain (≈75 kD), light intermediate chain (50-60 kD) and light chain (10-13 kD) subunits for correct complex formation (Figure 1.8, page 30) (Pfister *et al.*, 2006; Trokter *et al.*, 2012). The C-termini of the heavy chains form the motor domains consisting of a six-membered AAA ATPase ring and an additional region that interacts with the ring (Kon *et al.*, 2012). Most adaptor proteins associate with dynein via its intermediate chains (Pfister *et al.*, 2006).

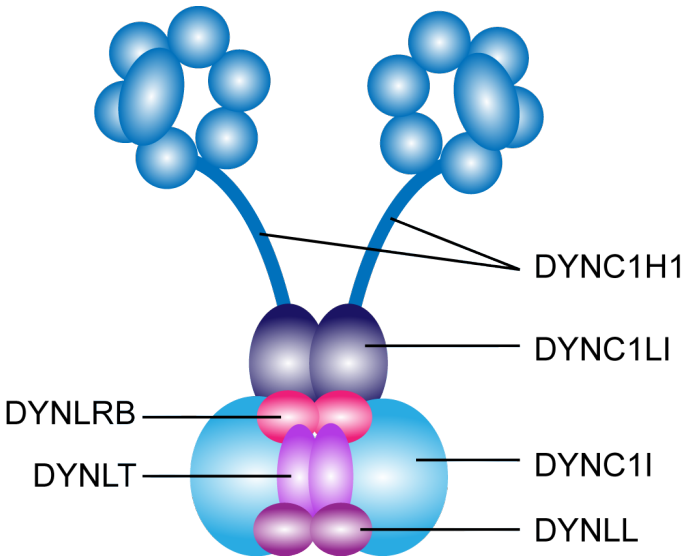


Figure 1.8: Structure of cytoplasmic dynein 1 complexes. Two homodimers of dynein heavy chain (DYNC1H1), which form the motor domain, associate with two intermediate chain (DYNC1I) and two light intermediate chain (DYNC1LI) subunits. Dynein light chain dimers of the t-complex-associated family (DYNLT), the Roadblock family (DYNLRB) and the LC8 family (DYNLL) interact with the DYNC1I subunits. Adapted from Pfister *et al.*, 2006 and Trokter *et al.*, 2012

The dynein light chains can be subdivided into three gene families: the t-complex-associated family (DYNLT), the Roadblock family (DYNLRB) and the LC8 family. All of them associate with cytoplasmic dynein via binding to dynein intermediate chains. Two monomers form a dimer with two symmetrical grooves, which act as binding sites for two dynein intermediate chain polypeptides (Wu and King, 2003).

The highly conserved dynein light chains of the LC8 family are regulatory hub proteins, that interact with a large number of proteins involved in diverse biological processes, independent of complex formation with dynein (Barbar, 2008; Pfister *et al.*, 2006). In vertebrates, two LC8 family members, DYNLL1 and DYNLL2, which differ in only 6 out of 89 residues, are present. As described, dynein light chains form homodimers thereby often promoting the dimerisation of their binding partners (Rapali *et al.*, 2011b). Rapali *et al.* have identified the DYNLL binding motif $[D/S]_{-4}K_{-3}X_{-2}[T/V/I]_{-1}Q_0[T/V]_1[D/E]_2$ and predicted a large number of DYNLL-interaction proteins based on this pattern, amongst them the spindle proteins Nek9, p53, Astrin and FAM83D/CHICA (Rapali *et al.*, 2011a).

1.7. Aims and course of action

- The aim of this study was to obtain valuable insights into how Plk1 controls the formation of the mitotic spindle and chromosome capture by identifying a complete set of substrates of Plk1 in metaphase.
- Astrin was identified as a Plk1 interaction partner and substrate. Phosphorylation sites were mapped, however analysis of Astrin phospho-mutants was inconclusive.
- Reciprocal immunoprecipitation demonstrated that the previously uncharacterised protein C15orf23 (Kinastrin) is the major binding partner of Astrin. Therefore, the role of the Astrin-Kinastrin complex in mitosis was investigated further.
- The Astrin-Kinastrin complex was shown to track microtubule plus ends and promote stable spindle formation and chromosome attachments.
- DYNLL1 has been identified as a minor interactor of the Astrin-Kinastrin complex. Thus, I wanted to investigate the role of DYNLL1 as a novel adaptor and regulator accessory protein for the dynein complex.
- Mass spectrometry of DYNLL1 complexes demonstrated that DYNLL1 defines two subcomplexes in metaphase, the Astrin-Kinastrin complex, and the CHICA-HMMR complex.
- The novel CHICA-HMMR complex was then analysed further and its function in mitosis was investigated.
- It was shown that the CHICA-HMMR-DYNLL1 plays a role in spindle orientation by regulating dynein localisation at the cell cortex.

2. Results

2.1. DYNLL 1 interacts with a subset of mitotic spindle proteins

To understand the function of DYNLL1 at the mitotic spindle, HeLa cells stably expressing GFP-DYNLL1 were used to identify DYNLL1 interaction partners. The cells were arrested in mitosis, lysed and cell lysates were incubated with GFP antibodies to immunoprecipitate GFP-DYNLL1 complexes. The samples were size-separated by SDS-PAGE. Staining of proteins with Colloidal Coomassie Blue revealed the presence of specific protein bands in GFP immunoprecipitations, that were absent from the control precipitates obtained with an antibody against mCherry (Figure 2.1, page 33).

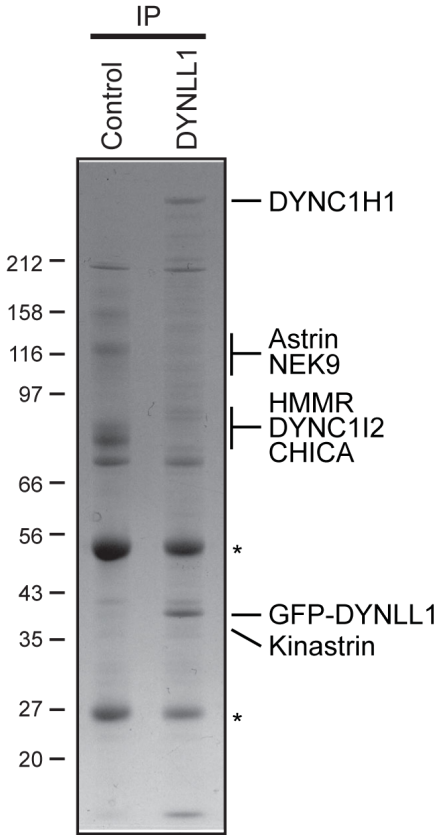


Figure 2.1: Purification of DYNLL1 complexes. DYNLL1 complexes were purified from a HeLa cell line stably expressing GFP-DYNLL1, previously generated by Emily Linnane, using GFP antibodies with mCherry antibodies serving as a negative control. Cells were arrested in mitosis using 100 ng/ml nocodazole for 18 hours and released into fresh growth medium for 20 min prior to cell lysis. The complexes were analysed by SDS-PAGE and the major proteins identified by mass spectrometry are marked. Asterisks mark the antibody heavy and light chains.

Analysis of these complexes by mass spectrometry revealed the presence of dynein heavy, intermediate, light intermediate, and the specific DYNLL1 light chain, indicating that the complete dynein motor protein had been precipitated (Table 2.1, page 34). For protein identification by mass spectrometry, proteins are digested into peptides, which are ionised, separated according to their mass to charge ratio, and subsequently detected producing a spectrum of peaks of a certain mass to charge ratio. The number of peptides detected for each protein and their intensity, which is the integrated area under these peaks, are both ultimately dependent on the size of the protein. Larger proteins are digested into more peptides resulting in a higher intensity. To obtain an indication about the amount of a protein within a complex, the relative intensity was calculated as the intensity to size ratio.

Table 2.1: DYNLL1-interacting proteins identified by mass spectrometry.

Gene symbol	Protein name	Size (kD)	Peptides	Intensity	Rel. intensity
DYNLL1	Dynein light chain 1	10.4	2	12,885,000	1,238,942
HMMR	Hyaluronan-mediated motility receptor	84.2	28	24,338,000	289,049
CHICA	CHICA; Isoform 2 of FAM83D	67.7	9	5,117,900	75,597
DYNC1H1	Dynein 1 heavy chain 1	532.4	59	31,966,000	60,041
DYNC1I2	Dynein 1 intermediate chain 2	71.5	7	2,798,600	39,141
SPAG5	Astrin; Sperm-associated antigen 5	134.4	14	5,129,400	38,165
C15ORF23	Kinastrin; SKAP	35.4	2	935,910	26,438
DYNC1LI1	Dynein 1 light intermediate chain 1	56.6	3	751,930	13,285
NEK9	Nek9 protein kinase	107.2	3	536,300	5,003

This analysis shows, that in addition to these dynein subunits a subset of mitotic spindle proteins, namely HMMR, FAM83D/CHICA, Astrin, C15orf23 (Kinastrin), and the kinase Nek9, were identified (Table 2.1, page 34 and Figure 2.1, page 33). Western blotting of the immunoprecipitation samples confirmed the presence of the different dynein subunits and additional proteins Astrin, Kinastrin, HMMR and CHICA in DYNLL1 complexes (Figure 2.2, page 35). It also showed that these complexes do not contain detectable levels of tubulin, or other spindle and spindle pole proteins Eg5, HURP, and NuMA, or the $p150^{Glued}$ subunit of dynactin. Therefore DYNLL1 defines specific

subcomplexes at the mitotic spindle, which are discrete from those formed by dynactin.

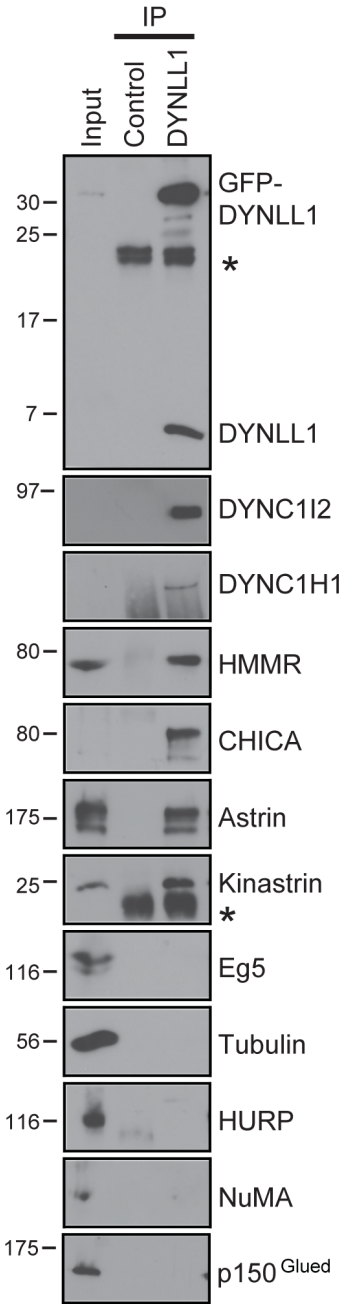


Figure 2.2: DYNLL1-dynein interacts with several spindle proteins in mitosis. DYNLL1 complexes were purified using GFP or mCherry (control) antibodies from a GFP-DYNLL1 cell line. Cells were arrested in mitosis using 100 ng/ml nocodazole for 18 hours and released into fresh growth medium for 20 min prior to cell lysis. Control and DYNLL1 complexes were analysed by Western blotting using the specific antibodies shown in the figure. No size standard exists for the range of dynein heavy chain 1, which has a predicted MW of 532 kD. Asterisks mark the antibody light chains.

Interestingly, both GFP-tagged and endogenous DYNLL1 were found in the GFP immune precipitates, indicating that DYNLL1 either forms oligomers or that these complexes contain DYNLL1 bound at multiple sites within the complex (Figure 2.2, page 35). To analyse the interaction of DYNLL1 with the identified spindle proteins, recip-

rocal immunoprecipitations were performed. Specific antibodies against HMMR and CHICA were raised in sheep, and affinity purified to permit characterisation of these two proteins (Figure 2.3, page 36). Western blotting showed that HMMR antibodies detected a single protein of the expected size of approximately 80 kilodalton (kD), and that this was depleted by two different siRNA duplexes targeting HMMR (Figure 2.3 A, page 36).

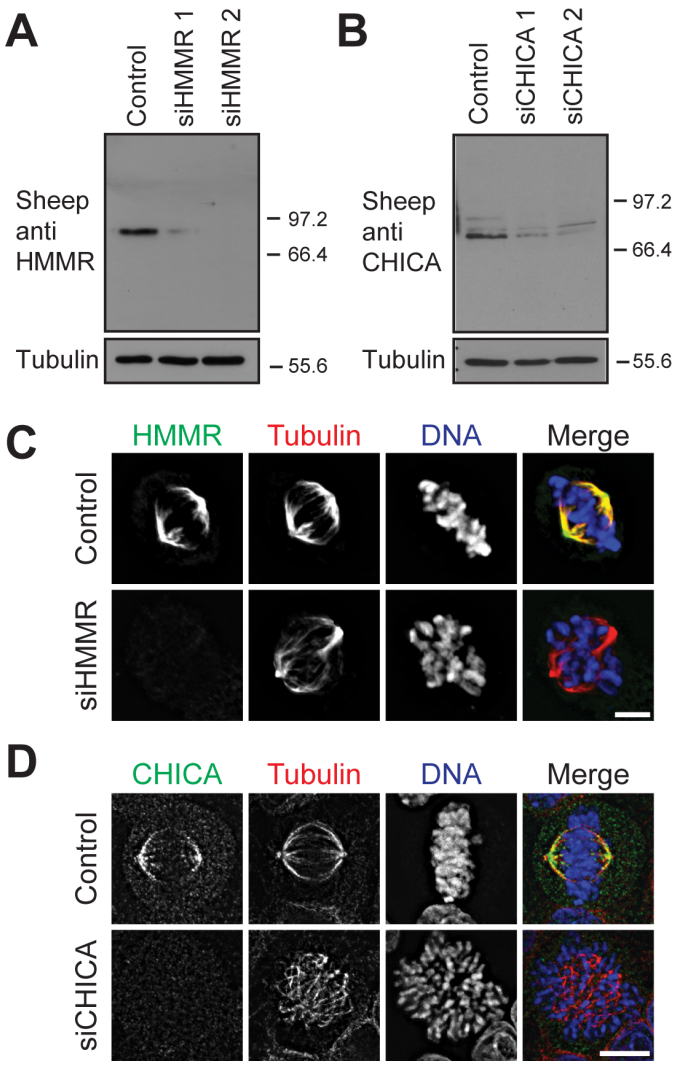


Figure 2.3: Antibody characterisation (A) Extracts of control or HMMR-depleted cells were Western blotted with affinity-purified sheep anti-HMMR antibodies. (B) Extracts of control or cells treated with two different CHICA siRNA duplexes were Western blotted with affinity-purified sheep anti-CHICA antibodies. (C) HeLa cells were treated with HMMR siRNA for 72 h and stained with antibodies to HMMR and tubulin. (D) HeLa cells were treated with CHICA siRNA for 72 h and stained with antibodies to CHICA and tubulin. DNA was stained with DAPI. Scale bar, 10 μm.

Similarly, CHICA antibodies detected a single protein of the expected size of 68 kD, and again this was depleted by two different siRNA duplexes directed towards CHICA (Figure 2.3 B, page 36). These HMMR and CHICA antibodies gave similar staining of

the mitotic spindle, and in both cases this was lost in cells treated with specific siRNA duplexes (Figure 2.3 C and D, page 36). Subsequently, these antibodies and specific antibodies to Astrin and Kinastrin were used for immunoprecipitations to test if Astrin, Kinastrin, HMMR and CHICA form one complex or independent subcomplexes with DYNLL1. Astrin or Kinastrin complexes and CHICA or HMMR complexes were isolated from mitotically arrested cells. Western blot analysis showed that Astrin and Kinastrin co-precipitated with DYNLL1 and with the minor interactors Plk1 and Sgo2 (Figure 2.4 A, page 37).

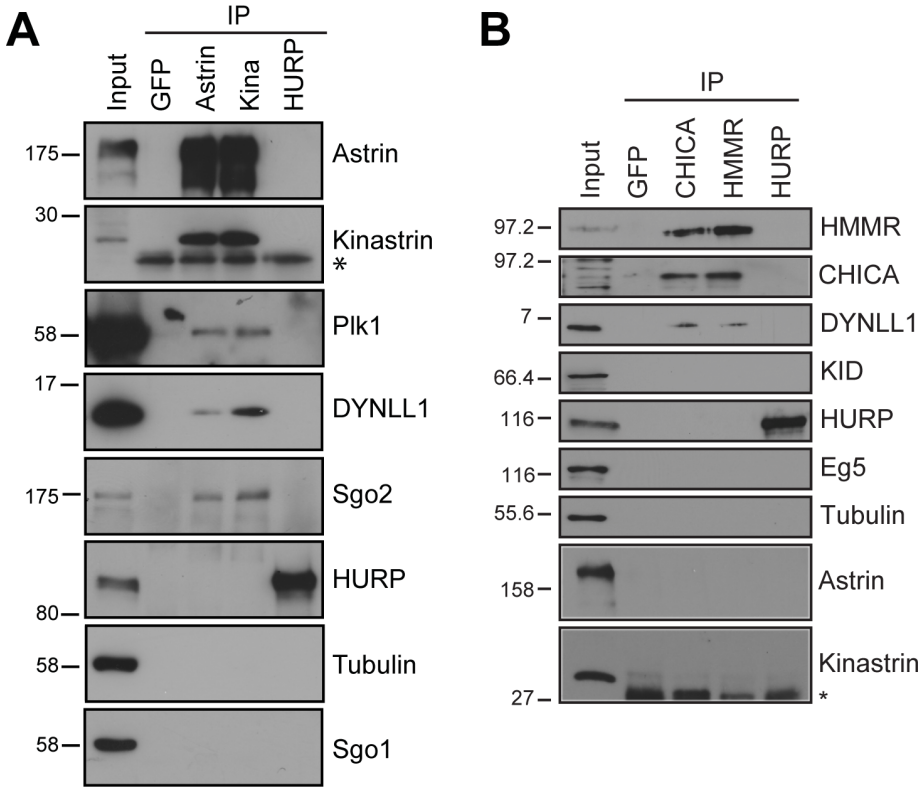


Figure 2.4: DYNLL1 associates with two defined spindle complexes in mitosis, the Astrin-Kinastrin and the CHICA-HMMR complex. (A) Astrin, Kinastrin, HURP, or GFP (control) immunoprecipitates from mitotic HeLa S3 extracts were Western blotted as indicated. (B) HMMR, CHICA, HURP, or GFP (control) complexes were immune precipitated using specific antibodies from HeLa cells arrested in mitosis using 200 ng/ml nocodazole for 18 hours prior to cell lysis. The immune precipitates were Western blotted using the antibodies shown in the figure. The asterisk indicates the antibody light chain.

Astrin, Kinastrin, DYNLL1, Plk1 and Sgo2 were not present in control or immune precipitations of the spindle and kinetochore fibre protein HURP. Further analysis of these complexes by quantitative mass spectrometry revealed that two molecules of Kinastrin interact with one molecule of Astrin, and confirmed that DYNLL1, Plk1 and Sgo2 are minor interaction partners of the Astrin-Kinastrin complex (Table 2.2, page 38).

Table 2.2: Proteins identified in Astrin-Kinastrin complexes.

Gene symbol	Protein name	Size (kD)	Peptides	Intensity	Stoichiometry
Astrin IP					
SPAG5	Astrin; Sperm-associated antigen 5	134.4	51	97,854,000	1
C15ORF23	Kinastrin; SKAP	35.4	19	48,654,000	1.9
DYNLL1	Dynein light chain 1	10.4	3	2,129,000	0.28
PLK1	Serine/threonine kinase Plk1	68.3	1	64,272	0.001
Kinastrin IP					
SPAG5	Astrin; Sperm-associated antigen 5	134.4	62	179,030,000	1
C15ORF23	Kinastrin; SKAP	35.4	19	96,467,000	2.0
DYNLL1	Dynein light chain 1	10.4	3	1,988,200	0.14
SGOL2	Shugoshin-like 2	144.7	2	366,340	0.002
PLK1	Serine/threonine kinase Plk1	68.3	1	126,960	0.001

Western blotting (Figure 2.4 B, page 37) and mass spectrometry (Table 2.3, page 38) of CHICA and HMMR immune precipitations showed that CHICA and HMMR co-precipitate consistent with the idea that the two proteins form a complex. Three molecules of HMMR are interacting with one molecule of CHICA.

Table 2.3: Proteins identified in CHICA-HMMR complexes.

Gene symbol	Protein name	Size (kD)	Peptides	Intensity	Stoichiometry
HMMR IP					
HMMR	Hyaluronan-mediated motility receptor	84.2	16	42,468,000	1
CHICA	CHICA; Isoform 2 of FAM83D	67.6	3	10,339,000	0.3
DYNLL1	Dynein light chain 1	10.4	2	8,286,000	1.58
CHICA IP					
HMMR	Hyaluronan-mediated motility receptor	84.2	23	32,887,000	1
CHICA	CHICA; Isoform 2 of FAM83D	67.6	7	6,699,200	0.3

In addition, DYNLL1, but not Astrin or Kinastrin, were present in both CHICA and HMMR immune precipitates (Figure 2.4 B, page 37). CHICA, HMMR, and DYNLL1 were not present in control or immune precipitations of the unrelated spindle protein HURP. Thus, DYNLL1 exists in at least two major subcomplexes in mitotic cells, the Astrin-Kinastrin and the CHICA-HMMR complex, both of which were analysed in detail in the present study.

2.2. Analysis of the Astrin-Kinastrin complex

The human protein Astrin was originally identified as a microtubule-associated protein in a mass spectrometry-based analysis (Mack and Compton, 2001). In initial studies by Mack *et al.*, microtubule-associated proteins were isolated from spindle preparations of cell-free mitotic extracts, in which over 90% of microtubules formed astral arrays. Under these *in vitro* conditions, the protein appeared to associate with astral microtubules and was therefore referred to as Astrin. However, *in vivo*, Astrin is associated with the mitotic spindle and outer kinetochores (Mack and Compton, 2001). In interphase cells, Astrin is diffuse in the cytoplasm. With the onset of mitosis, it localises at the pericentriolar material and developing spindle poles (Thein *et al.*, 2007). Astrin is found at the mitotic spindle throughout prometaphase, metaphase and anaphase and it targets to midbody microtubules during telophase and cytokinesis (Mack and Compton, 2001; Thein *et al.*, 2007). Moreover, Astrin also associates with the outer kinetochore of attached chromosomes and was suggested as a marker for intact kinetochore-microtubule attachments (Thein *et al.*, 2007; Mack and Compton, 2001). Astrin is required for the maintenance of spindle bipolarity and for faithful chromosome segregation and has been reported to prevent premature sister chromatid separation and centriole disengagement presumably by restraining separase activation (Thein *et al.*, 2007).

The previously uncharacterised protein C15orf23 was specifically identified in Astrin

immunoprecipitations. During metaphase and anaphase, it is found at the mitotic spindle and kinetochores of attached chromosomes. In response to the localisation at the KINetochore and binding to ASTRIN, C15orf23 was subsequently referred to as Kinastrin (Dunsch, 2010).

To analyse the expression profile of Astrin and Kinastrin, cells were synchronised in S-phase and then released into mitosis. Western blotting of samples of these synchronised cell extracts showed that both, Astrin and Kinastrin, are cell cycle regulated proteins with increased protein levels in mitosis (Figure 2.5 A, page 40). Astrin appears to be post-translationally modified in mitosis indicated by the slight mobility shift. Astrin is phosphorylated by Plk1 *in vitro*, however analysis of Astrin phospho-mutants was inconclusive. As expected, a similar expression profile is observed for the kinetochore fibre protein HURP.

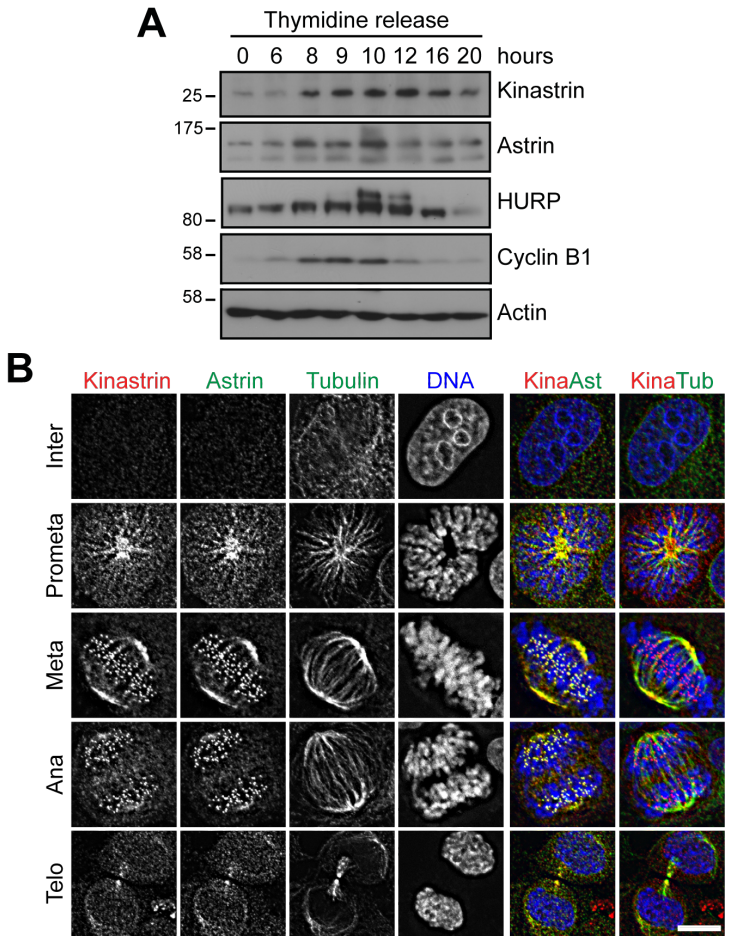


Figure 2.5: Astrin and Kinastrin localise to the mitotic spindle. (A) HeLa S3 cells were synchronised with a double thymidine release protocol. Samples taken at the indicated time points were kindly provided by Dr. Kang Zeng and 20 μg of cell lysate were loaded and Western blotted as shown. (B) HeLa S3 cells were stained with antibodies to Kinastrin, Astrin and tubulin. DNA was stained with DAPI. Scale bar, 10 μm

The mitotic cyclin B is induced in G_2 phase, its accumulation promotes mitotic entry, and finally cyclin B is rapidly degraded at the onset of anaphase. Blotting of cyclin B therefore provided a good marker of mitotic entry (8h) and metaphase to anaphase transition (between 10 and 12h). Moreover, co-staining of HeLa S3 cells with antibodies against Astrin and Kinastrin showed both proteins have a similar localisation throughout mitosis, in agreement with the finding that Astrin and Kinastrin exist in a complex (Figure 2.5 B, page 40). In interphase, both proteins are diffusely localised throughout the cytoplasm, but as cells enter mitosis the complex targeted to the spindle poles. Both proteins localised to the mitotic spindle and kinetochores in metaphase and anaphase, and were detected in the vicinity of the midbody in telophase. Astrin immune precipitates from interphase or mitotic cell lysates revealed that Astrin and Kinastrin exist in a complex, both in interphase and in mitosis, independently of the Astrin phosphorylation status (Figure 2.6 A, page 41).

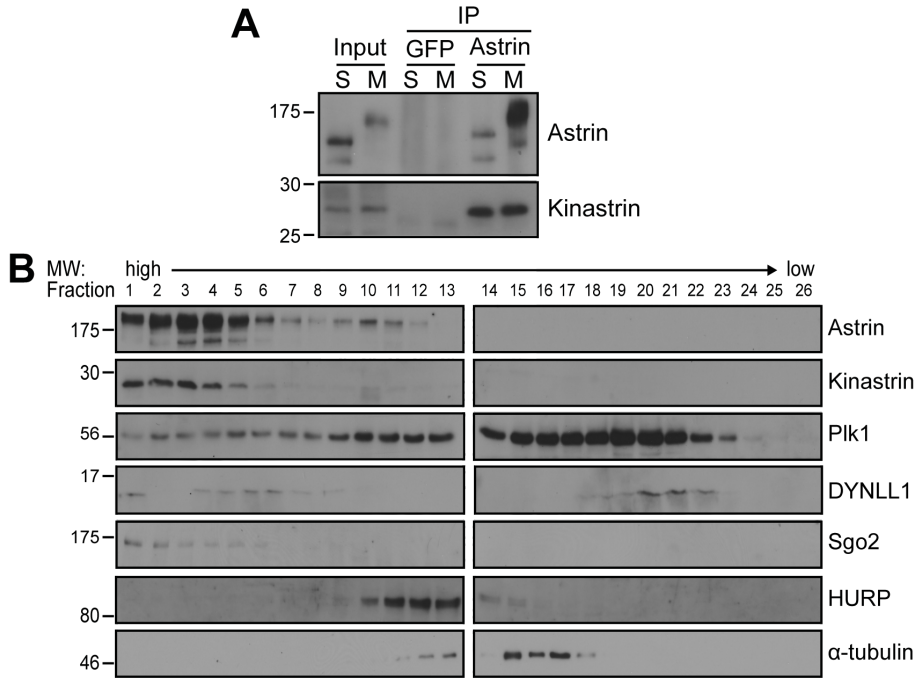


Figure 2.6: Kinastrin is a novel Astrin interaction partner. (A) Astrin immune precipitates from HeLa S3 cells arrested in interphase (S) or mitosis (M) were Western blotted with Astrin and Kinastrin antibodies. (B) Samples of mitotic cell extracts size-separated under native conditions using a Superose 6 10/300 GL column were kindly provided by Dr. Ricardo Nunes Bastos and were Western blotted as shown.

To investigate the size of the complex formed by Astrin, Kinastrin and the minor interaction partners, DYNLL1, Plk1 and Sgo2, mitotic cell lysates were size-separated by gel exclusion chromatography under native conditions. Western blotting of these samples further demonstrated that Astrin, Kinastrin and the minor interaction partners are found in the same high molecular weight fractions (Figure 2.6 B, page 41). This indicates that these proteins are components of one large protein complex.

Both Astrin and Kinastrin contain coiled-coil structures, but no other predicted domains. Therefore, the regions within the proteins required for spindle localisation and for the interaction between both proteins were investigated. To this end, Myc-Astrin fragments were transfected into HeLa S3 cells and the localisation of the transgene was determined (Figure 2.7, page 43). This analysis revealed that full-length Astrin and Astrin fragments comprising the amino acid (aa) 482-1193 and 482-850, respectively, are localising to the mitotic spindle, while other transfected fragments were cytoplasmic. Thus, amino acids 482-850 comprise the minimal region required for Astrin targeting to the mitotic spindle. To identify the Kinastrin binding domain within Astrin, Myc-Astrin fragments were transfected into HEK 293T cells in conjunction with full-length Kinastrin and immunoprecipitations were performed. Kinastrin was found in precipitations of full-length Astrin, and of the fragments aa 482-1193 and aa 482-850. Therefore, the same amino acids 482-850 within Astrin are required for binding to Kinastrin as well as for spindle targeting (Figure 2.7, page 43).

A reciprocal analysis for Kinastrin showed that full-length Kinastrin and Kinastrin fragments aa 79-317 and aa 159-317 localised to the mitotic spindle (Figure 2.8, page 44). Immune precipitations of Myc-Kinastrin fragments revealed that Kinastrin binds to Astrin via its C-terminal aa 159-317 (Figure 2.8, page 44).

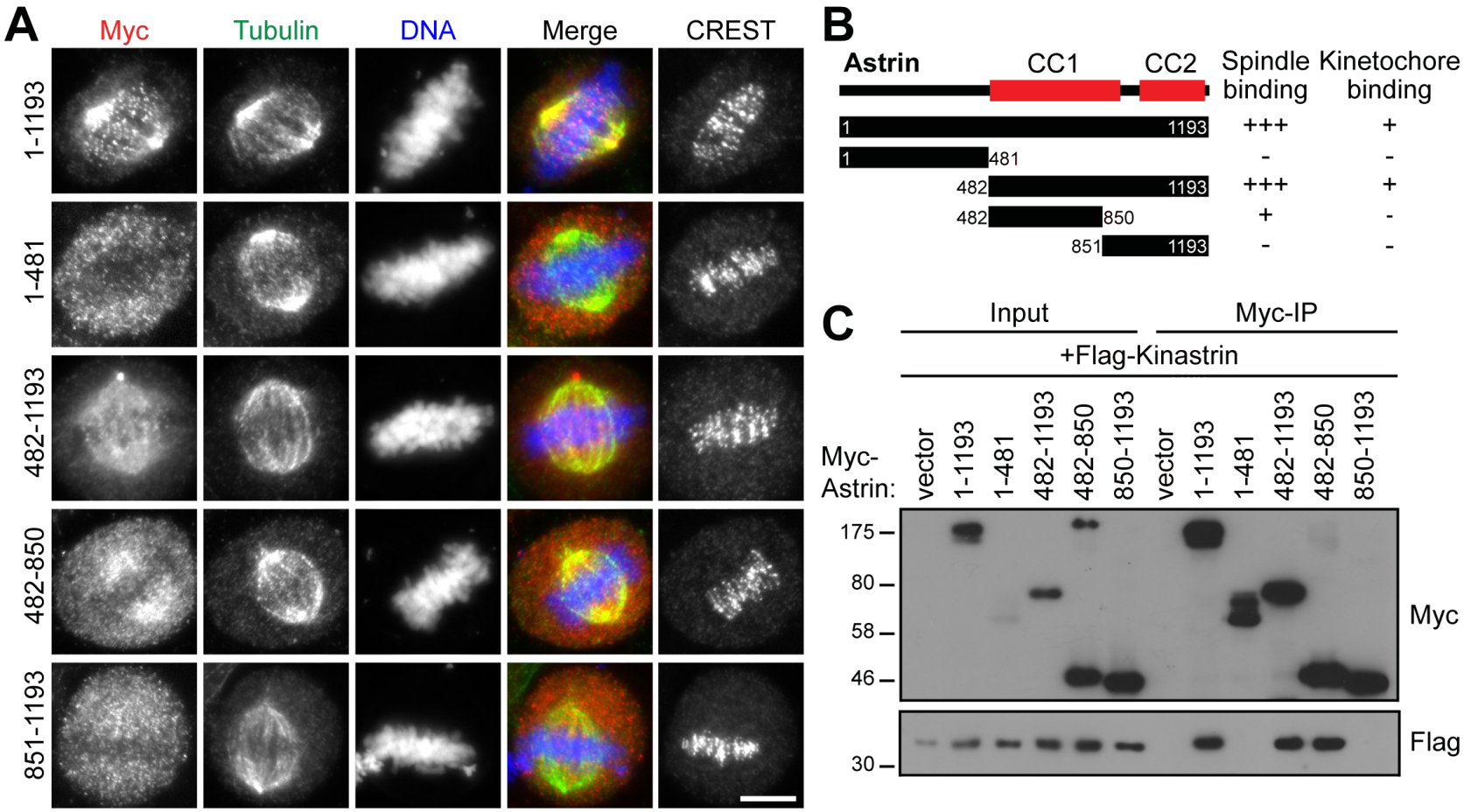


Figure 2.7: Astrin interacts with Kinastrin and localises to the mitotic spindle via its C-terminus. (A) Myc-Astrin fragments were transiently transfected into HeLa S3 cells for immunofluorescence analysis. Cells were fixed and stained with antibodies towards Myc, tubulin and CREST. DNA was stained with DAPI. Scale bar, 10 μm. (B) Schematic representing Astrin fragments and binding domains. CC, coiled coil domains (C) Myc-Astrin fragments in conjunction with Flag-Kinastrin were transiently transfected into HEK 293T cells for immunoprecipitation. Cells were synchronised in mitosis by addition of 10 μM STLC for 14 h after 24 h of transfection. The cells were then harvested and lysed, and anti-Myc immunoprecipitations were performed. Western blots were probed with antibodies against Myc and Flag.

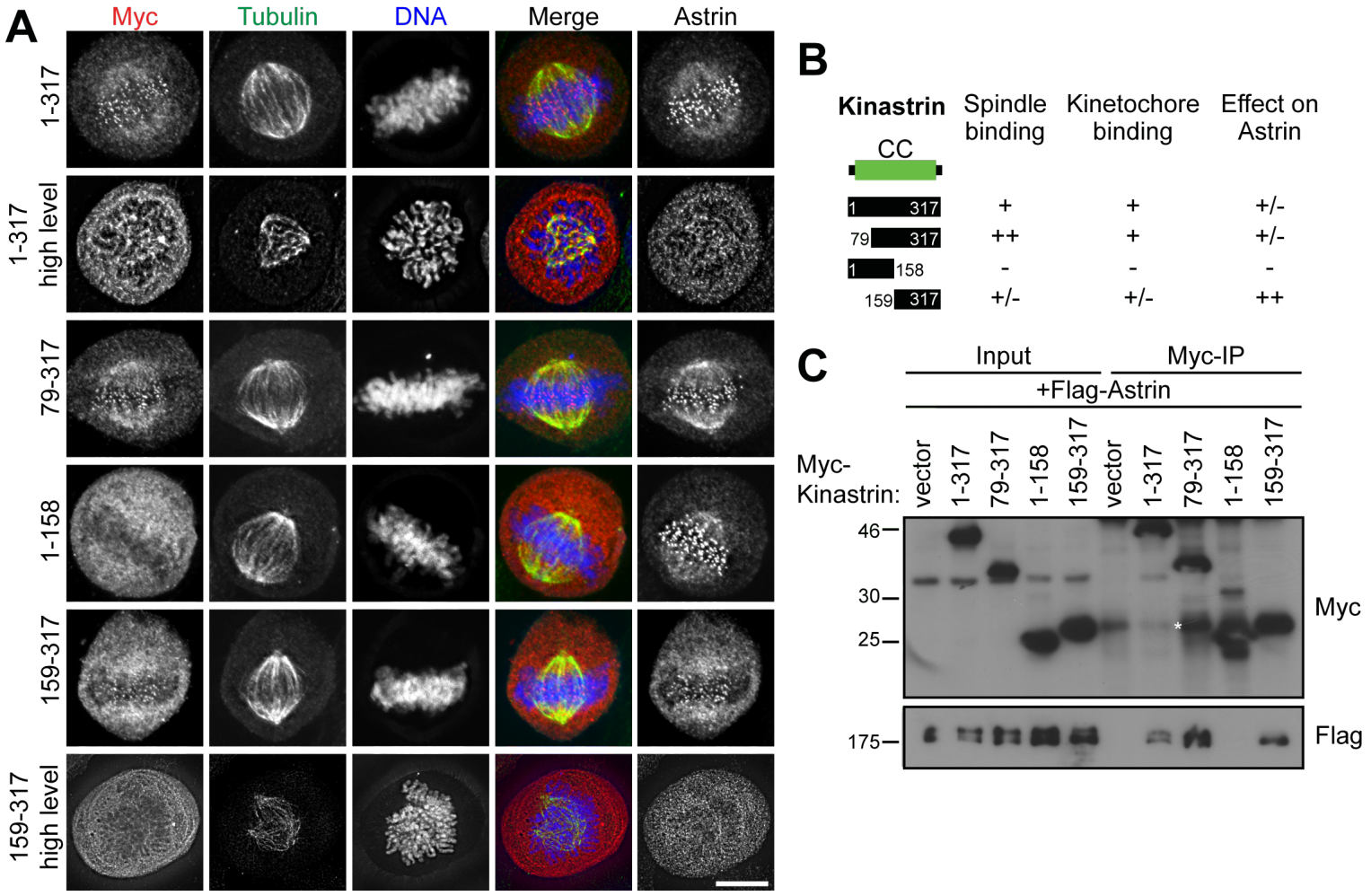


Figure 2.8: Kinastrin mediates Astrin-targeting to the spindle via its C-terminus. (A) Myc-Kinastrin fragments were transiently transfected into HeLa S3 cells for immunofluorescence analysis. Cells were fixed and stained with antibodies towards Myc, tubulin and CREST. DNA was stained with DAPI. Scale bar, 10 μm. (B) Schematic representing Kinastrin fragments and binding domains. CC, coiled coil domain (C) Myc-Kinastrin fragments in conjunction with Flag-Astrin were transiently transfected into HEK 293T cells for immunoprecipitation. Cells were synchronised in mitosis by addition of 10 μM STLC for 14 h after 24 h of transfection. The cells were then harvested and lysed, and anti-Myc immunoprecipitations were performed. Western blots were probed with antibodies against Myc and Flag. The asterisk indicates the antibody light chain.

Thus, amino acids 159-317 of Kinastrin comprise both the Astrin binding domain and the spindle targeting domain. Interestingly, it was observed that cells expressing Myc-Kinastrin at a high level showed abnormal spindle structures and Astrin was displaced from the spindle in these cells (Figure 2.8, page 44). This was found upon expression of both full-length Kinastrin as well as the fragment aa 159-317 capable of interacting with Astrin. This finding suggests that high levels of Kinastrin titrate Astrin into the cytoplasm, which causes impaired spindle formation.

2.3. The Astrin-Kinastrin complex is required for faithful chromosome alignment

To investigate the molecular function of the Astrin-Kinastrin complex, HeLa S3 cells were treated with siRNA duplexes targeting Astrin or Kinastrin. It was found that cells depleted of Astrin or Kinastrin exhibit striking phenotypes with multipolar spindles and disorganised chromosome structures (Figure 2.9, page 45).

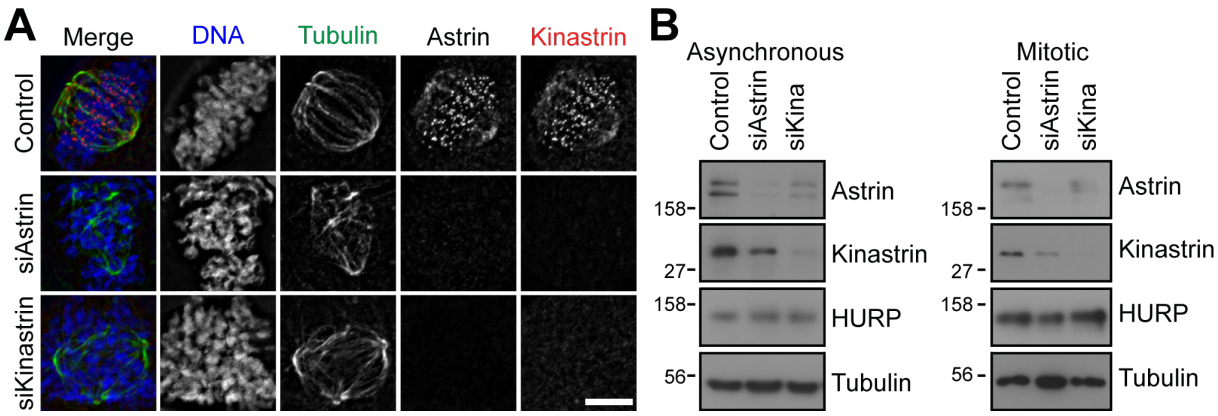


Figure 2.9: Complex formation between Astrin and Kinastrin is required to stabilise both proteins. (A) HeLa S3 cells were treated with the indicated siRNAs (Astrin for 48 h, Kinastrin for 72 h), fixed with PTEMF, which removes the cytoplasmic protein pool, and stained with antibodies to Kinastrin, Astrin and tubulin, DNA was stained with DAPI. Scale bar, 10 μm.(B) HeLa S3 cells were treated as in A). Cell extracts were prepared from total cells or mitotic shake-offs and Western blotted with the indicated antibodies.

Several different Kinastrin siRNA duplexes all efficiently reduced Kinastrin levels causing the described phenotype (Figure 2.10, page 46). For further analysis of Kinastrin, siRNA duplex 5 was used.

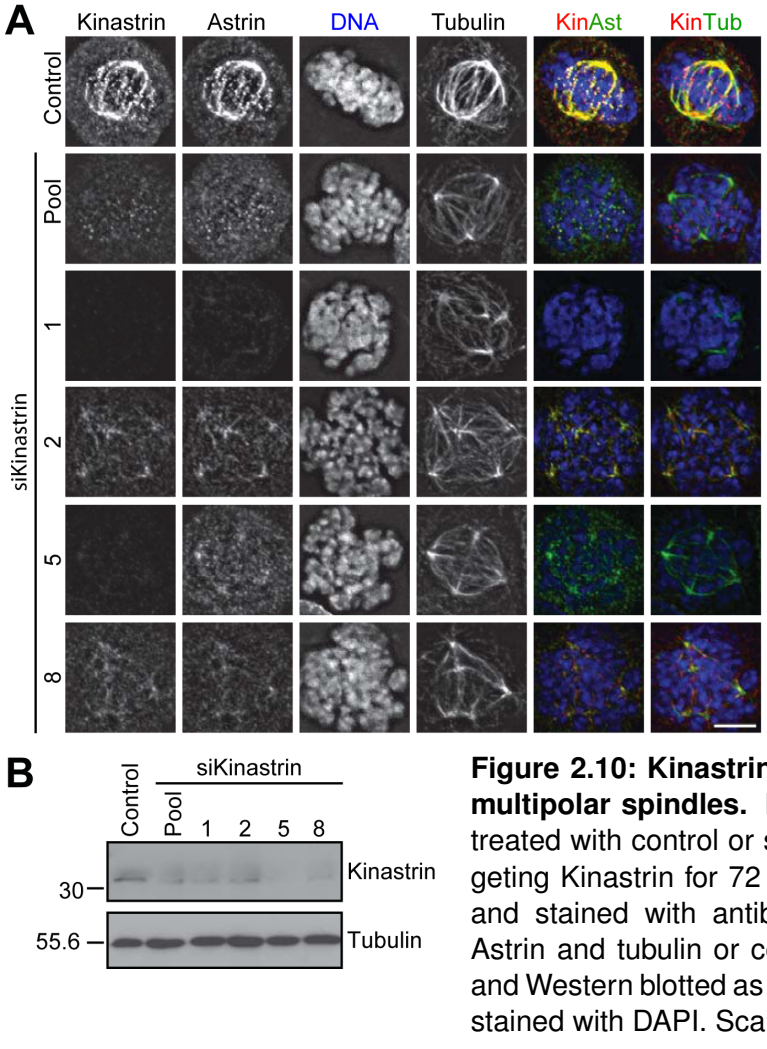


Figure 2.10: Kinastrin depletion causes multipolar spindles. HeLa S3 cells were treated with control or siRNA duplexes targeting Kinastrin for 72 h. Cells were fixed and stained with antibodies to Kinastrin, Astrin and tubulin or cells were harvested and Western blotted as indicated. DNA was stained with DAPI. Scale bar, 10 μm.

Interestingly, in all cases, depletion of Kinastrin resulted in a decrease in Astrin levels and *vice versa*, both in mitosis and in interphase, indicating that complex formation between Astrin and Kinastrin is required to stabilise both proteins (Figure 2.9, page 45). Next, HeLa S3 cells stably expressing mCherry-histone H2B and GFP-tubulin depleted of Astrin or Kinastrin were imaged for 12 h (Figure 2.11, page 47). This cell line permits visualisation of both the mitotic spindle and chromosome structures in living cells and could therefore be used to analyse the development of the phenotype.

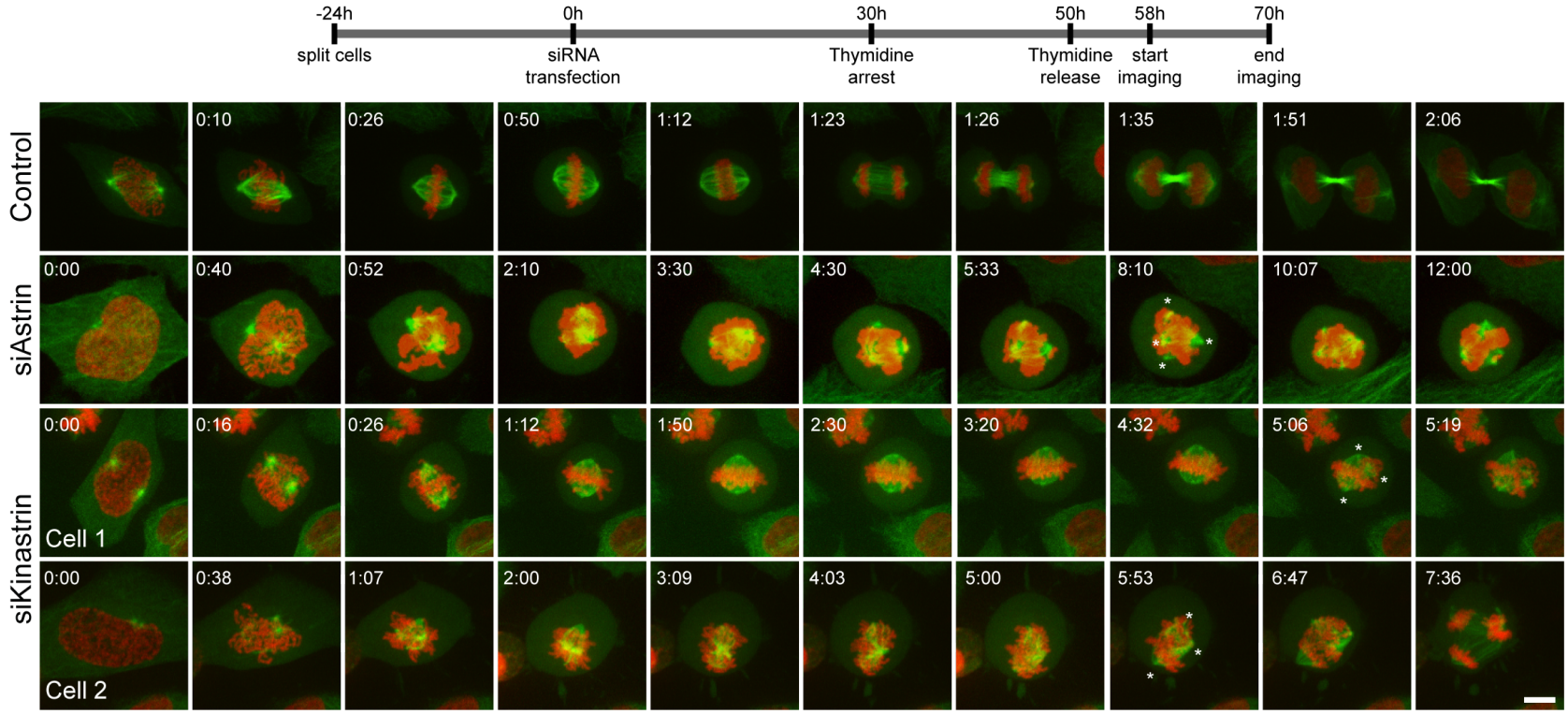


Figure 2.11: The Astrin-Kinastrin complex is required for efficient chromosome alignment and segregation. HeLa cells stably expressing mCherry-histone H2B and GFP-tubulin were treated with control, Astrin, or Kinastrin siRNA duplexes and synchronised with 2.5 mM thymidine 30 h after siRNA addition. After 20 h, the cells were released, incubated for 8 h at 37°C, and then filmed for 12 h. Images were captured every minute. Asterisks indicate multiple spindle poles. Scale bar, 10 μm.

This analysis confirmed that depletion of Kinastrin caused the same phenotype as loss of Astrin, specifically arrest in mitosis as well as spindle formation and chromosome congression defects. While control cells formed a stable bipolar spindle and showed chromosome alignment in a metaphase plate after approximately half an hour (Figure 2.11, top panel, page 47), Astrin- or Kinastrin-depleted cells were unable to achieve either the formation of a bipolar spindle or alignment of their chromosomes. These cells either remained in mitosis until the end of the experiment (Figure 2.11, middle panels, page 47) or did undergo anaphase and divided into more than two daughter cells (Figure 2.11, bottom panel, page 47). Measurements of the time required from nuclear envelope breakdown to the onset of anaphase revealed that 50% of Astrin- or Kinastrin-depleted cells took longer than 1000 min to achieve metaphase alignment, with the majority of cells remaining arrested in mitosis (Figure 2.12, page 48).

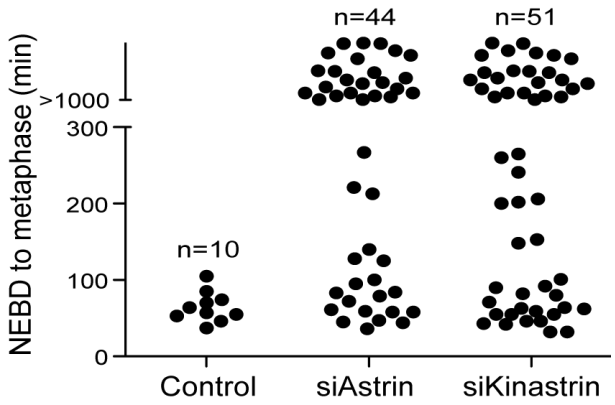


Figure 2.12: Astrin- or Kinastrin-depleted cells arrest in mitosis. HeLa cells stably expressing mCherry-histone H2B and GFP-tubulin were treated with control, Astrin, or Kinastrin siRNA duplexes and synchronised with 2.5 mM thymidine 30 h after siRNA addition. After 20 h, the cells were released, incubated for 8 h at 37°C, and then filmed for 12 h with images being acquired every minute. The time required from nuclear envelope breakdown (NEBD) to metaphase alignment was plotted for control, Astrin-, and Kinastrin-depleted cells.

Next the role of the spindle assembly checkpoint (SAC) in this arrest phenotype was investigated. To this end, Astrin- or Kinastrin-depleted cells were stained with antibodies to SAC components. This analysis showed that these cells contained spindles with high levels of BubR1 and Bub1 present at unattached kinetochores (Figure 2.13 A, page 49). Measurements of the signal intensities confirmed that BubR1 and Bub1 levels in Astrin- or Kinastrin-depleted cells were comparable to levels in control cells in

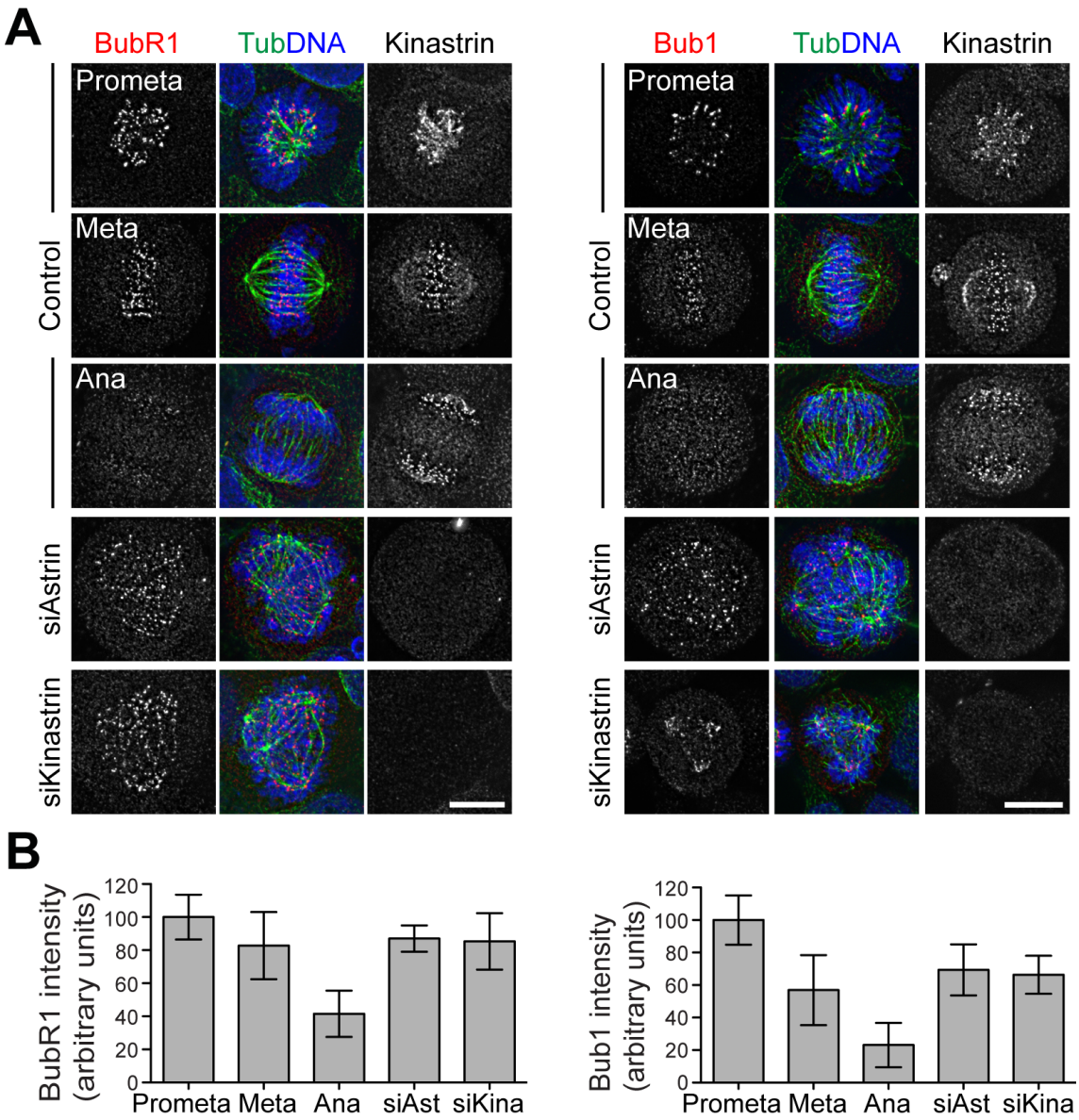


Figure 2.13: Astrin- or Kinastrin-depleted cells are spindle checkpoint arrested. (A) Control, Astrin-, or Kinastrin-depleted HeLa cells were fixed and stained with antibodies against Kinastrin and BubR1 (left) or Bub1 (right). DNA was stained with DAPI. Scale bars, 10 μm (B) The staining intensity was quantified and plotted. Error bars indicate the standard error of the mean.

prometaphase or metaphase, i.e. cells that have not satisfied the SAC (Figure 2.13 B, page 49). These findings suggest that the depletion phenotype of impaired chromosome alignment and spindle formation is sensed by components of the SAC inducing a halt in mitotic progression.

2.4. Astrin localisation to the spindle and kinetochores is required for normal mitotic progression

Kinastrin overexpression interferes with Astrin targeting to the spindle (Figure 2.8, page 44). To analyse the effect of this loss of Astrin localisation further, HeLa FlpIn cell lines inducibly expressing Myc-Kinastrin or Myc-Astrin were generated. The C15ORF23 gene contains two start codons at nucleotide position 1 and 237. Both resulting proteins are able to target the mitotic spindle and interact with Astrin (Figure 2.8, page 44). For the generation of the inducibly expressing Myc-Kinastrin cell line, the longest splice variant of C15ORF23 was chosen. Intriguingly, high expression levels of Myc-Kinastrin resulted in a striking mitotic arrest with multipolar spindles and unaligned chromosomes (Figure 2.14, page 50) recapitulating the phenotype observed upon transient transfection of Kinastrin fragments.

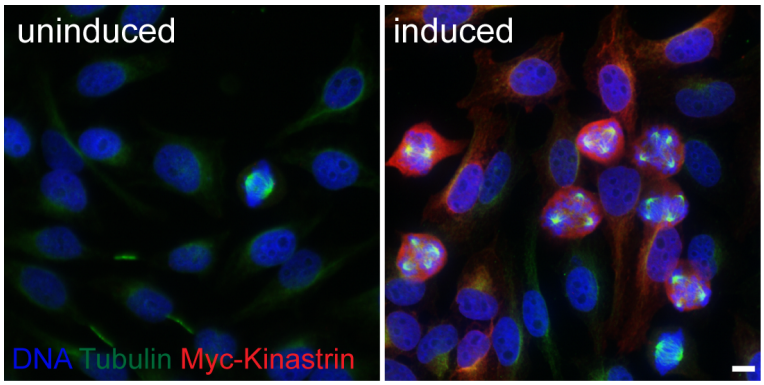


Figure 2.14: Kinastrin overexpression causes mitotic arrest and cells with multipolar spindles. HeLa FlpIn Myc-Kinastrin cells were mock-treated or expression of Myc-Kinastrin was induced for 24 h. The cells were then stained for Myc and tubulin. DNA was stained with DAPI. Scale bar, 10 μm. Image kindly provided by Dr. Ulrike Grüneberg.

Comparison of the mobility shift of endogenous and Myc-tagged Kinastrin indicates that endogenous Kinastrin conforms to the short splice variant of C15ORF23. Closer examination of Myc-Kinastrin overexpressing cells revealed that Astrin was mislocalised from the spindle and displaced into the cytoplasm (Figure 2.15 A, page 51). Astrin overexpression, on the other hand, recruited more Kinastrin onto the spindle, particularly the spindle poles (Figure 2.15 A, page 51).

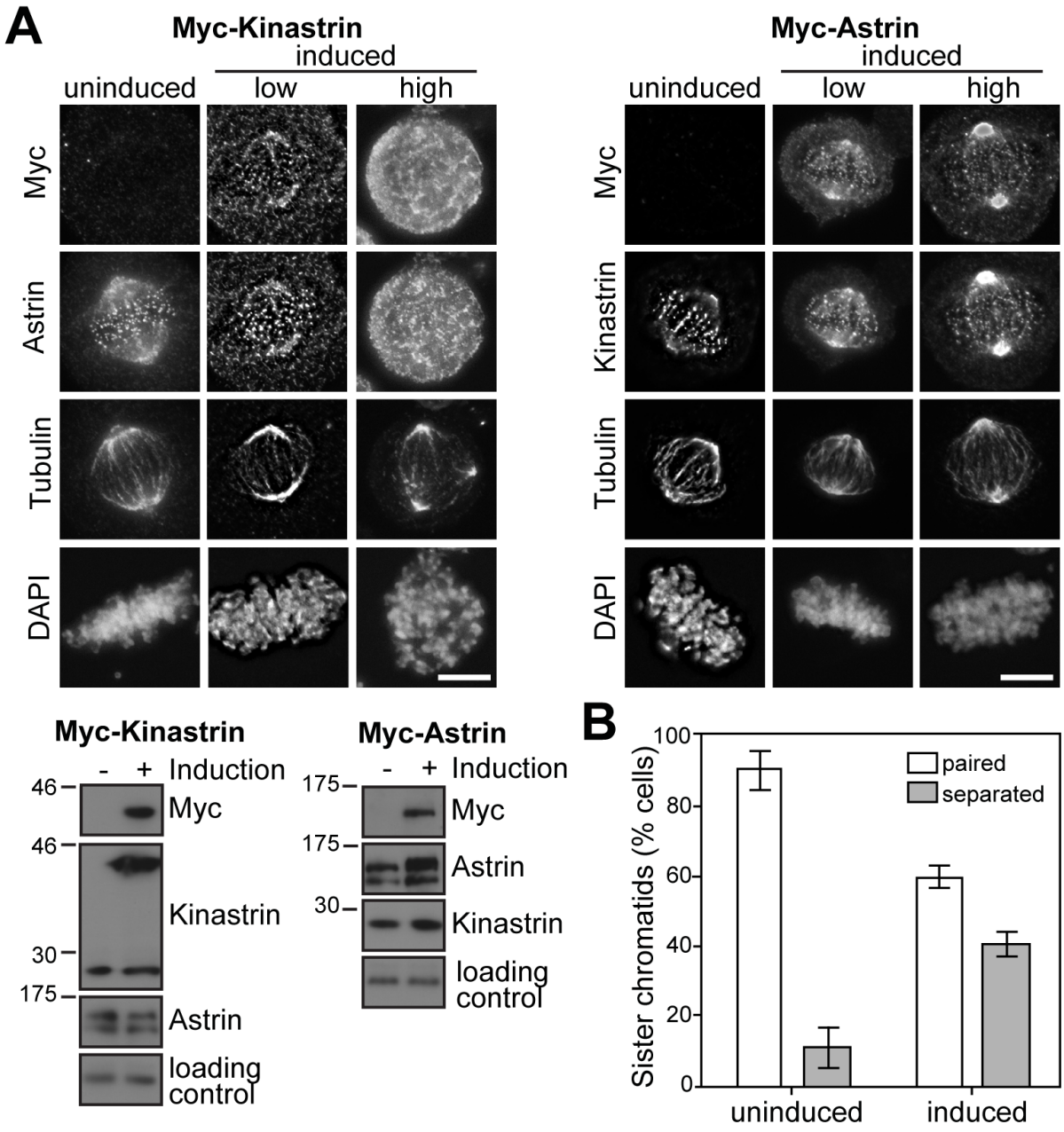


Figure 2.15: Overexpression of Kinastrin displaces Astrin from the spindle.
(A) HeLa FlpIn Myc-Kinastrin and HeLa FlpIn Myc-Astrin cells were mock treated or treated with 1 μg/ml doxycycline for 24 h to induce the expression of the transgene. The cells were then stained for Myc, Astrin, Kinastrin and tubulin, or Western blotted with the indicated antibodies. A non-specific band detected with the Astrin antibody was used as a loading control. DNA was stained with DAPI. Cells with different expression levels of Myc-Kinastrin or Myc-Astrin, respectively, are shown. Scale bar, 10 μm. (B) HeLa FlpIn Myc-Kinastrin cells were mock treated and mitotically arrested with 100 ng/ml nocodazole for 14 h or Myc-Kinastrin expression was induced for 24 h. Chromosome spreads were prepared and the percentage of cells with separated sister chromatids was assessed.

Together, these data indicate that Kinastrin targets the complex to the mitotic spindle, while Astrin is the limiting factor for complex formation. Kinastrin overexpressing cells showed multipolar spindles and disorganised chromosome structures reminiscent of the Astrin or Kinastrin depletion phenotype. Astrin depletion was previously reported to induce premature sister chromatid separation (Thein *et al.*, 2007). Chromosome spreads of Kinastrin-depleted cells showed that loss of Kinastrin induced the same phenotype with approximately 60% of cells containing single sister chromatids (Figure 2.16, page 52).

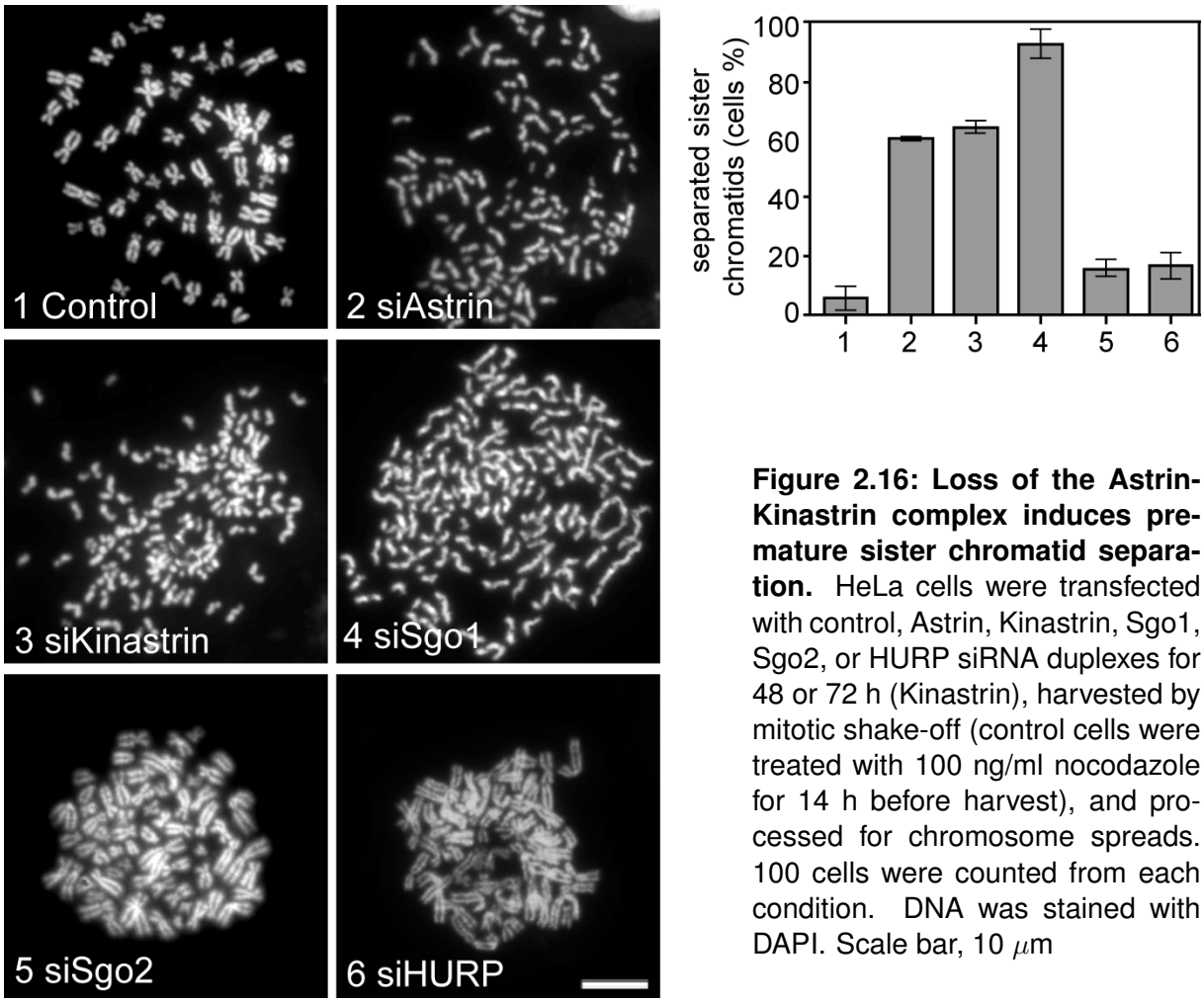


Figure 2.16: Loss of the Astrin-Kinastrin complex induces premature sister chromatid separation. HeLa cells were transfected with control, Astrin, Kinastrin, Sgo1, Sgo2, or HURP siRNA duplexes for 48 or 72 h (Kinastrin), harvested by mitotic shake-off (control cells were treated with 100 ng/ml nocodazole for 14 h before harvest), and processed for chromosome spreads. 100 cells were counted from each condition. DNA was stained with DAPI. Scale bar, 10 μm

Within one depleted cell the sister chromatid cohesion is lost between all chromosomes (Figure 2.16, page 52). This highly penetrant phenotype is specific for the loss of the Astrin-Kinastrin complex and depletion of the kinetochore fibre microtubule associated protein (MAP) HURP had only a minor effect on sister chromatid cohesion (Figure 2.16, page 52). As expected, depletion of Sgo1, which protects centromeric cohesin, also caused a significant loss of sister chromatid cohesion observed in almost 100% of cells. Interestingly, loss of Sgo2 did not cause sister chromatid separation, supporting the notion that the shugoshin proteins play divergent roles (McGuinness *et al.*, 2005; Huang *et al.*, 2007).

Next, it was investigated whether premature sister chromatid separation is also caused by Kinastrin overexpression. To this end, chromosome spreads were prepared from cells overexpressing Myc-Kinastrin. Indeed, about 40% of these cells showed prematurely separated sister chromatids (Figure 2.15 B, page 51).

Another key feature of Astrin-depleted cells is the premature disengagement of centrioles giving rise to multipolar spindles (Thein *et al.*, 2007). Again, it was analysed whether this aspect is shared by Kinastrin overexpressing cells. Thus, centrioles were imaged in Astrin- or Kinastrin-depleted and Myc-Kinastrin overexpressing cells. While control cells contained two poles with two centrioles each, more than 60% of spindle poles in cells depleted of Astrin or Kinastrin contained no centrioles or only one centriole (Figure 2.17, page 54). An additional 10% of spindle poles contained two centrioles, that were markedly separated from each other (Figure 2.17, page 54).

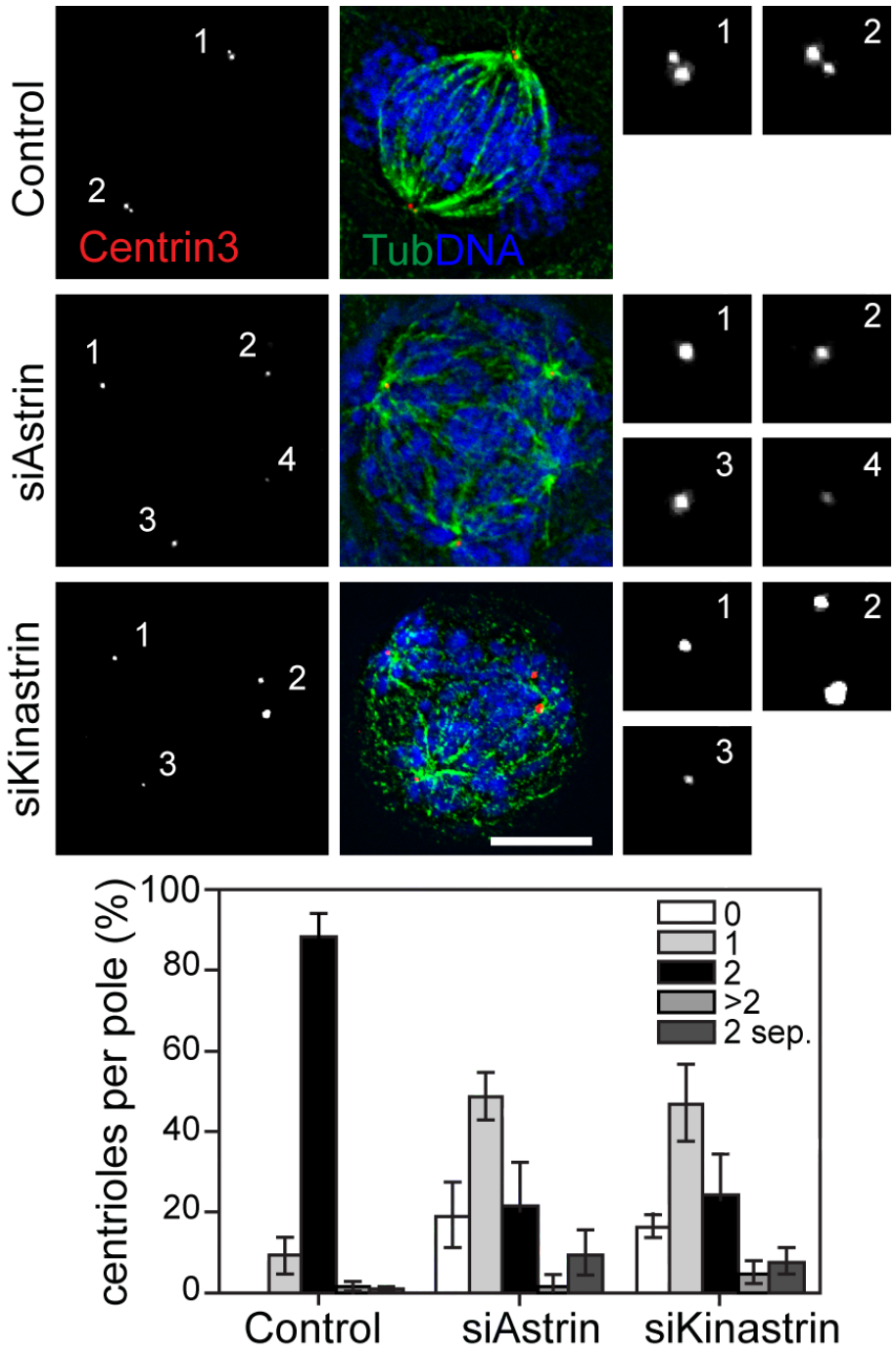


Figure 2.17: Loss of the Astrin-Kinastrin complex results in premature centriole disengagement. HeLa S3 cells treated with control, Astrin, or Kinastrin siRNA duplexes for 48 or 72 h (Kinastrin) were stained for centrin-3 and tubulin. The percentages of spindle poles with zero, one, two, more than two, or markedly separated centrioles are plotted in the bar graph. DNA was stained with DAPI. Scale bar, 10 μm

Similar results were obtained upon overexpression of Myc-Kinastrin (Figure 2.18, page 55). Around 90% of control spindles had two poles with two centrioles each. In Myc-Kinastrin overexpressing cells however over 60% of spindle poles contained fewer than two centrioles.

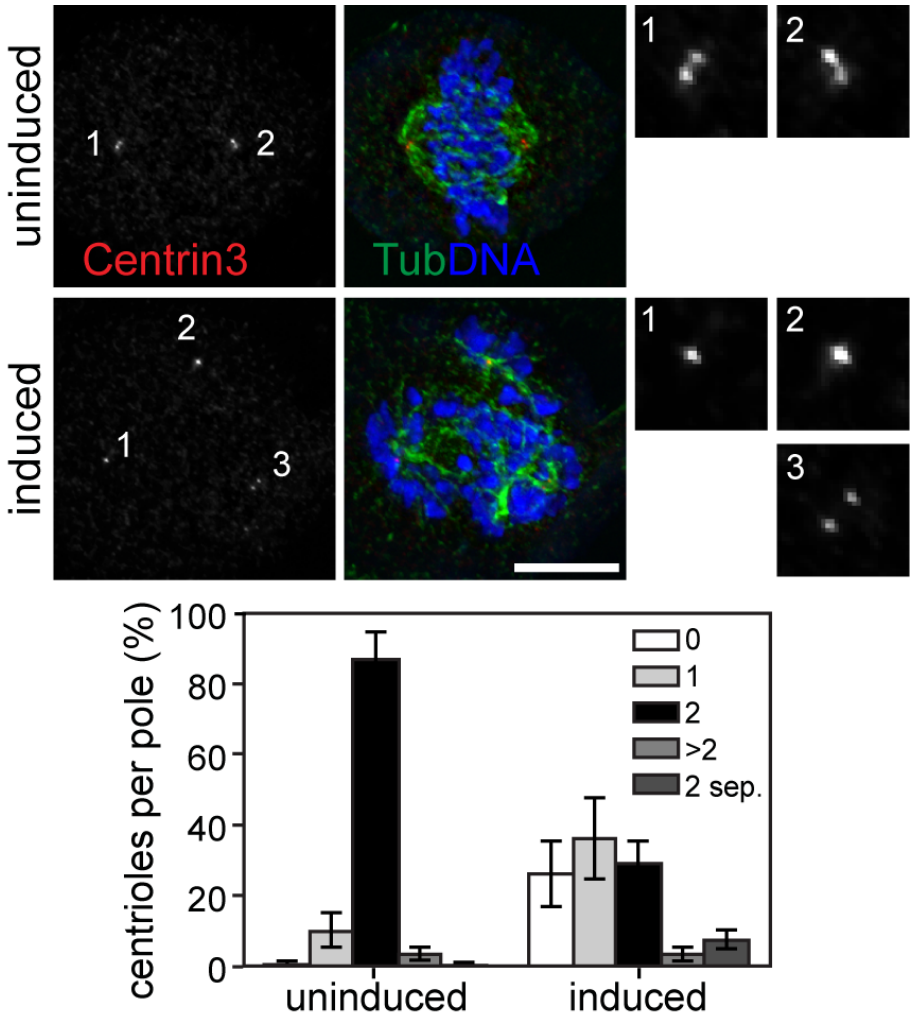


Figure 2.18: Kinastrin overexpression induced multipolar spindles by premature centriole disengagement. HeLa FlpIn Myc-Kinastrin cells were mock treated or expression of Myc-Kinastrin was induced with 1 μg/ml doxycycline for 24 h. Cells were stained for centrin-3 and tubulin. Centriole numbers at the spindle poles are plotted in the bar graph. DNA was stained with DAPI. Scale bar, 10 μm

Collectively, these findings confirm that overexpression of Kinastrin recapitulates the key features of Astrin depletion. Thus, Astrin displacement from the spindle induced by

Kinastrin overexpression and entire loss of Astrin function caused by siRNA-mediated depletion result in the same phenotype. Proper localisation of Astrin to the spindle is therefore crucial for Astrin function.

The underlying molecular defects causing premature sister chromatid separation in the absence of Astrin or Kinastrin function were investigated next. Centromeric cohesion is protected from removal via the 'prophase pathway' by Sgo proteins, which localise to the centromere and recruit the phosphatase PP2A·B56. This phosphatase then opposes Plk1-mediated phosphorylations on cohesin and thereby protects centromeric cohesion. Loss of the protective function by Sgo proteins could therefore explain the premature sister chromatid separation. Sgo2 and Plk1 were both found as minor interaction partners of the Astrin-Kinastrin complex (Figure 2.4 A, page 37 and Table 2.2, page 2.2) and suggested a functional link between Astrin and Sgo proteins. Therefore, the localisation of Sgo1, Sgo2 and the phosphatase subunit B56α in Astrin- or Kinastrin-depleted cells was investigated. This analysis revealed that Sgo1, Sgo2 and B56α targeted to centromeres in control as well as in Astrin- and Kinastrin-depleted cells (Figure 2.19, page 57). Premature sister chromatid separation is therefore unlikely to be due to a loss of centromeric protection by this pathway.

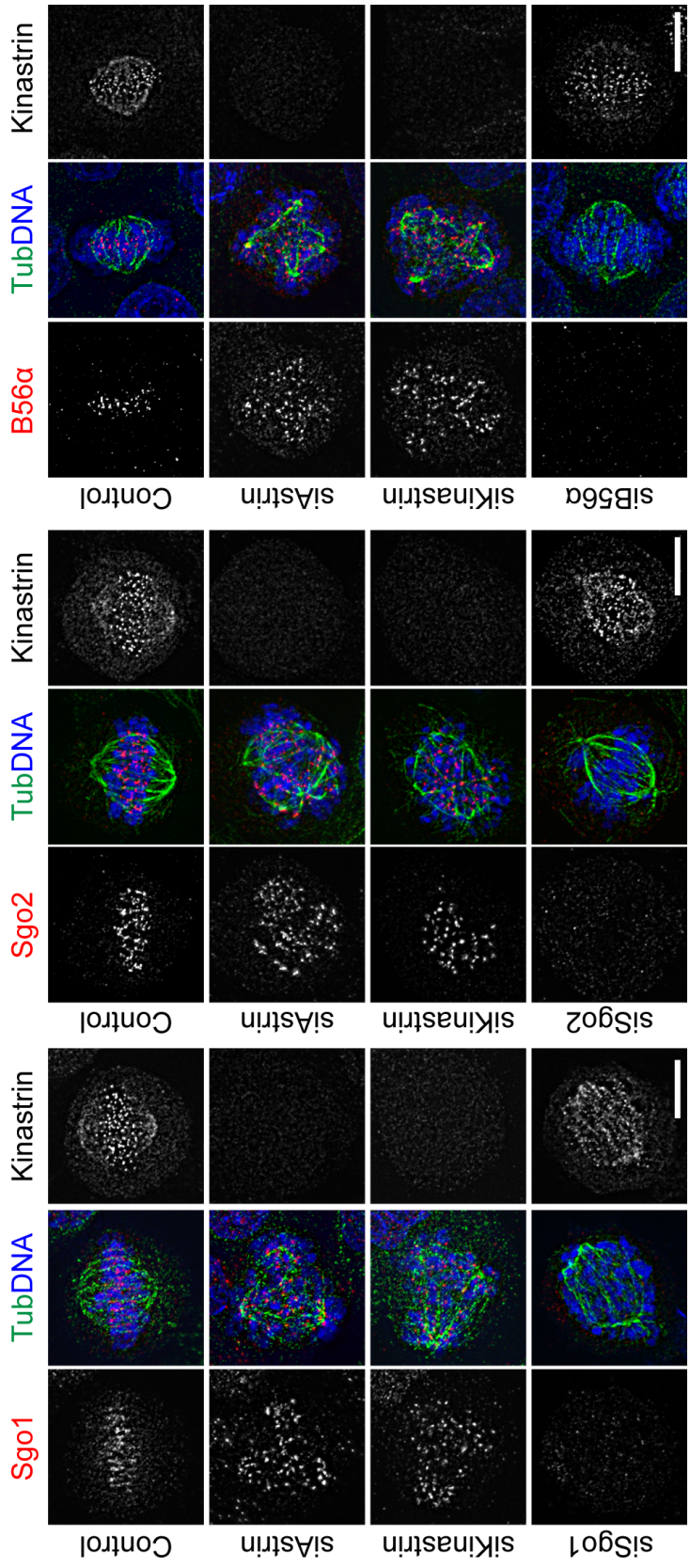


Figure 2.19: Localisation of the cohesion regulators Sgo1, Sgo2 and B56α is unaltered in Astrin- or Kinastrin-depleted cells. HeLa S3 cells treated with control, Astrin, Kinastrin or Sgo1, Sgo2 or B56α siRNA duplexes for 48 or 72 h (Kinastrin) were stained for tubulin, Kinastrin and Sgo1, Sgo2 and B56α, respectively. DNA was stained with DAPI. Scale bars, 10 μm

Another possible explanation for both aspects of the Astrin and Kinastrin depletion phenotype, premature centriole disengagement and chromatid separation, is the untimely activation of the protease separase. Separase is kept inactive in metaphase by association with its inhibitors securin and cyclin B (Holland and Taylor, 2006; Stemmann *et al.*, 2001). Upon satisfaction of the SAC, the E3 ubiquitin ligase APC/C becomes active and targets securin and cyclin B for degradation. Active separase then initiates anaphase by cleaving the cohesion between both sister chromatids allowing them to migrate to the opposing poles of the spindle. At the same time, the two centrioles of each centrosome are disengaged by the proteolytic activity of separase to license them for duplication in the next cell cycle (Tsou and Stearns, 2006; Tsou *et al.*, 2009). Thus, untimely separase activation could account for both features of the Astrin-Kinastrin-depletion phenotype. This idea is supported by the finding, that co-depletion of Astrin or Kinastrin and separase reduced the amount of separated sister chromatids (Figure 2.20 A, page 58).

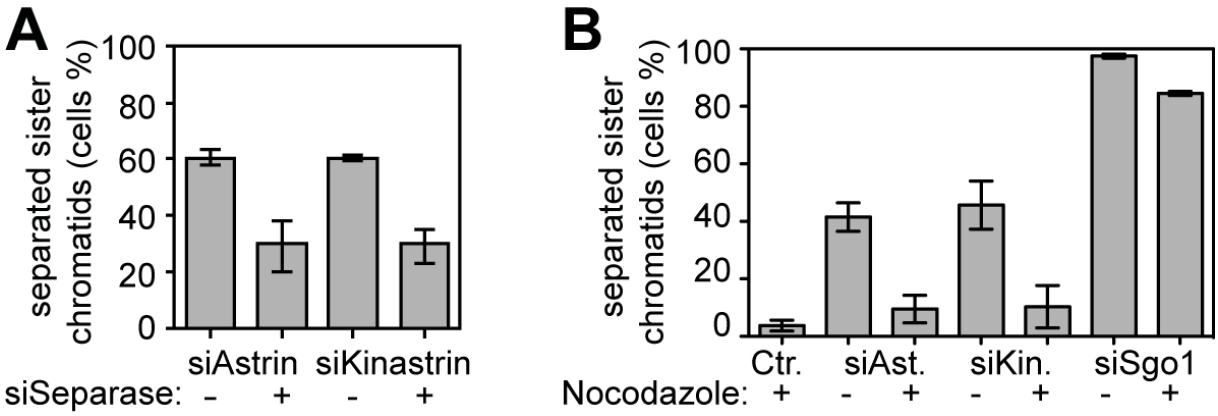


Figure 2.20: Premature sister chromatid separation in Astrin- or Kinastrin-depleted cells is dependent on separase. HeLa cells were transfected with control, Astrin, or Kinastrin siRNA duplexes for 48 or 72 h (Kinastrin), harvested by mitotic shake-off (control cells were treated with 100 ng/ml nocodazole for 14 h before harvest), and processed for chromosome spreads. 100 cells were counted from each condition. (A) Depletion of separase in addition to Astrin or Kinastrin or (B) the addition of nocodazole to Astrin- or Kinastrin-depleted cells released from a thymidine block significantly reduced the amount of premature loss of sister chromatid cohesion. Each graph represents the mean of three independent experiments, one of which was conducted by Emily Linnane. Error bars indicate the standard error of the mean.

Additionally, chromosome attachments to the spindle might be required for this premature chromatid separation, since addition of nocodazole to Astrin- or Kinastrin-depleted cells rescued the separation phenotype (Figure 2.20 B, page 58). Separase activation is accompanied by auto-cleavage. This separase auto-cleavage product was found in extracts prepared from anaphase or Kinastrin-depleted cells indicating that separase is activated in Kinastrin-depleted cells, although the SAC is still active (Figure 2.13, page 49) and cyclin B levels are still high (Figure 2.21 A, page 59).

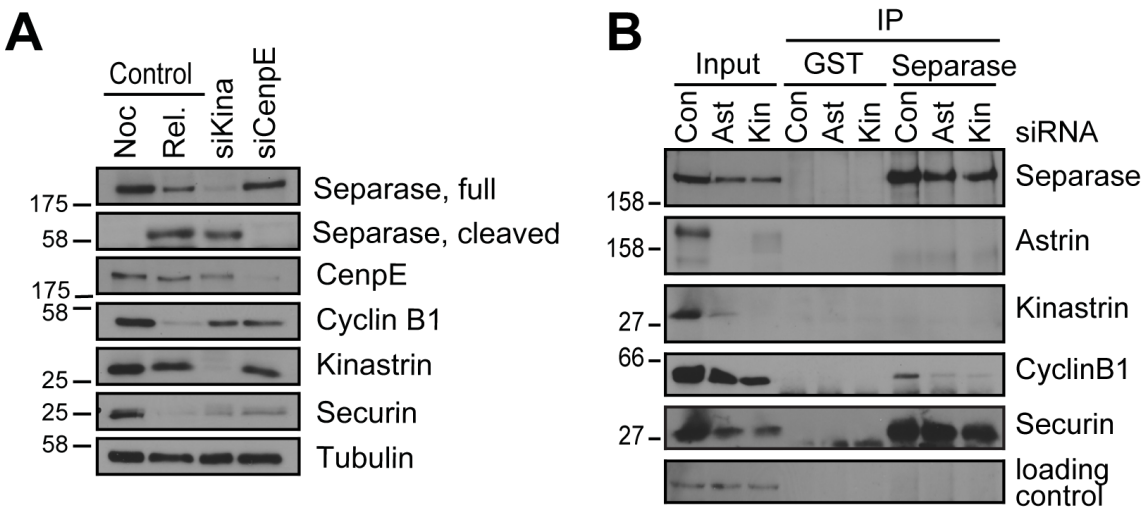


Figure 2.21: A fraction of separase is prematurely activated in Astrin- or Kinastrin-depleted cells. (A) HeLa cells arrested in mitosis with nocodazole for 14 h, released from the mitotic block, or treated with siRNAs targeting CenpE (48 h) or Kinastrin (72 h) were harvested by mitotic shake-off, then lysed and Western blotted with the indicated antibodies. (B) Separase immunoprecipitations from HeLa cells depleted of Astrin or Kinastrin for 48 or 72 h were blotted as indicated. A non-specific band detected with the separase antibody was used as a loading control.

Next, it was analysed if separase was still associated with its inhibitors securin or cyclin B in Astrin- or Kinastrin-depleted cells. This showed that separase precipitated from cells depleted of Astrin or Kinastrin existed in a complex with securin, however cyclin B levels associated with separase were drastically reduced (Figure 2.21 B, page 59). Therefore, in Astrin- or Kinastrin-depleted cells, a fraction of separase is activated, presumably due to a loss of inhibition by cyclin B, which facilitates sister chromatid sep-

aration and centriole disengagement. However, it remains currently unclear how the Astrin-Kinastrin complex prevents separase activation before the onset on anaphase. The Astrin-Kinastrin complex targets to spindle microtubules and kinetochores of attached chromosomes and it is conceivable that local changes in microtubule dynamics induced by the Astrin-Kinastrin complex promote the interaction between cyclin B and separase. Thus, the molecular function of the Astrin-Kinastrin complex at microtubules and its effect on spindle microtubule dynamics was investigated next.

2.5. The Astrin-Kinastrin complex localises to microtubule plus ends and promotes stable kinetochore attachments

HeLa S3 cells stably expressing GFP-Astrin were used for live-cell analysis of Astrin dynamics. These cells expressed GFP-tagged Astrin at an approximately fivefold higher level than endogenous protein (Figure 2.22 A, page 60). Nonetheless, Astrin localisation was not disturbed and the ectopically expressed protein targeted to the mitotic spindle and kinetochores (Figure 2.22 B, page 60).

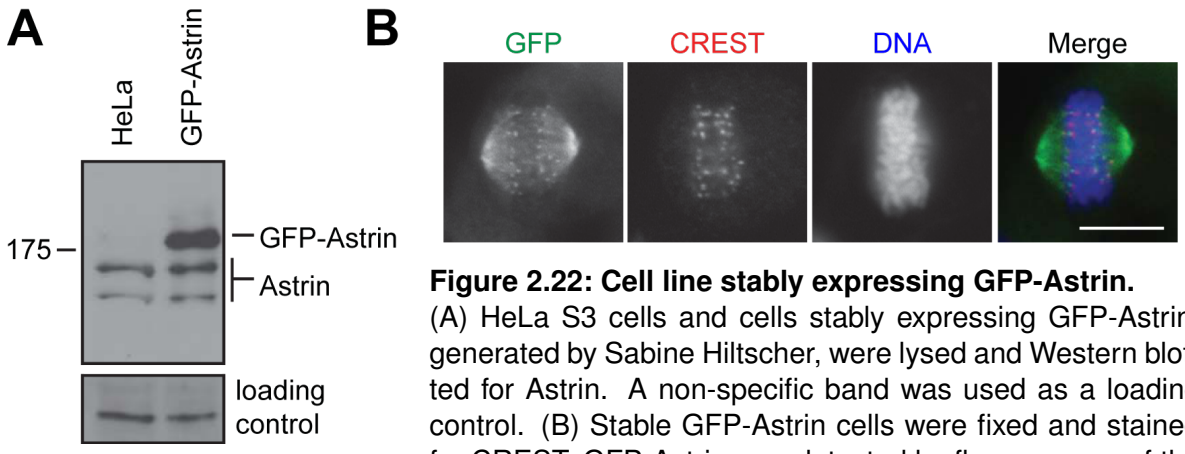


Figure 2.22: Cell line stably expressing GFP-Astrin. (A) HeLa S3 cells and cells stably expressing GFP-Astrin, generated by Sabine Hiltscher, were lysed and Western blotted for Astrin. A non-specific band was used as a loading control. (B) Stable GFP-Astrin cells were fixed and stained for CREST. GFP-Astrin was detected by fluorescence of the GFP tag. DNA was visualised with DAPI. Scale bar, 10 μm.

Imaging of these cells revealed comet-like structures of GFP-Astrin that were moving towards the periphery of the cell with a velocity of 0.43 $\pm$ 0.05 μm/s (Figure 2.23, page 61).

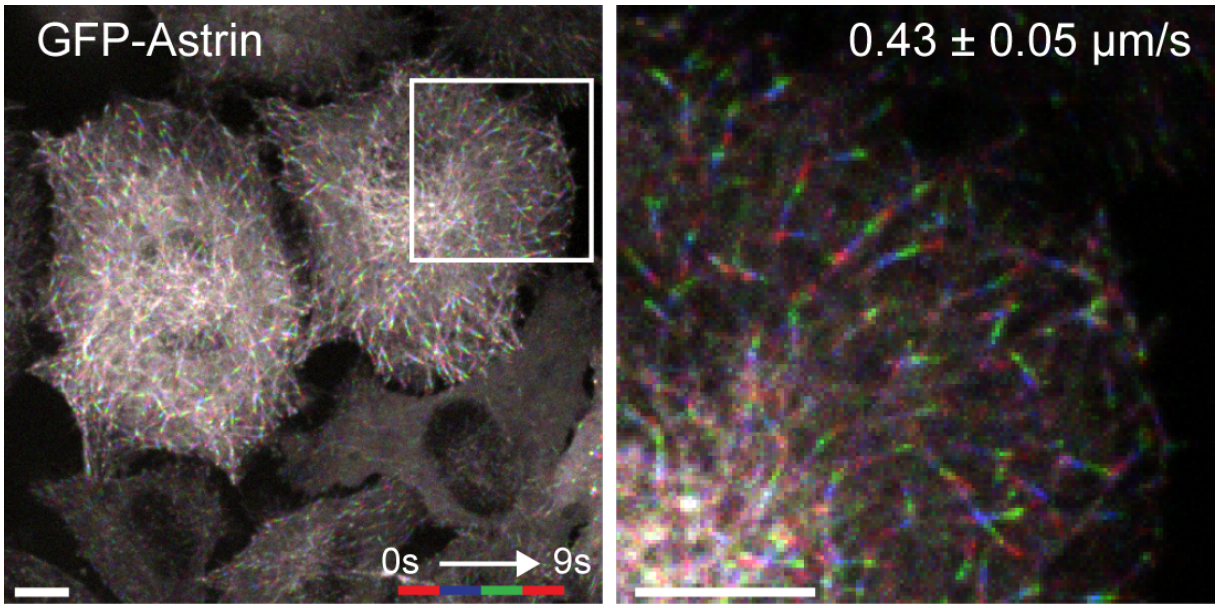


Figure 2.23: The Astrin-Kinastrin complex localises to growing microtubule plus ends. GFP-Astrin cells were imaged every 1.25 s. The first, third, fifth, and seventh frames were projected into one image using different colours as indicated. Scale bar, 10 μm

This movement resembled the dynamics of growing microtubule plus ends. To confirm this idea, the known microtubule plus end tracking protein EB1 was used as a marker. Indeed, transfection of these cells with mCherry-tagged EB1 as well as staining with EB1 antibodies demonstrated that GFP-Astrin tracks microtubule plus ends and moves with the same velocity as EB1 (Movie, Figure 2.24, page 62 and Figure 2.25 A, page 63).

Open file in Adobe Reader to view movie

Similar results were obtained by co-staining HeLa S3 cells with antibodies to Astrin and EB1 (Figure 2.25 B, page 63). In both interphase and mitotic cells, Astrin and EB1 were seen on the same microtubule tip, with EB1 closest to the plus tip followed by Astrin.

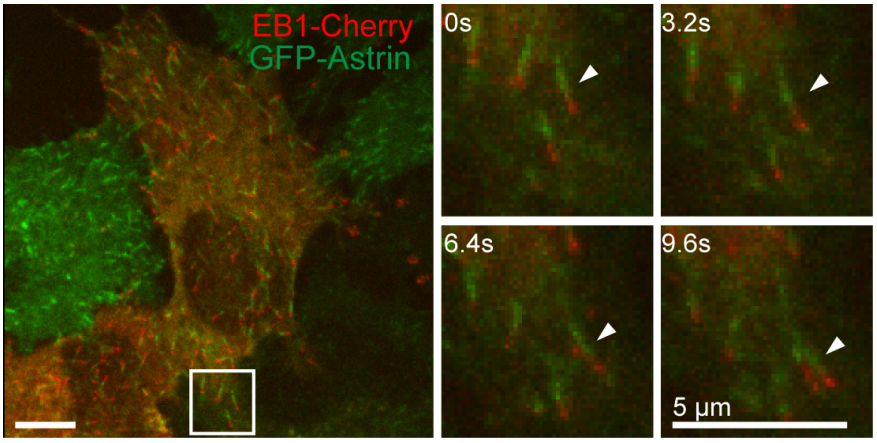


Figure 2.24: The Astrin-Kinastrin complex tracks microtubule plus tips proximal to EB1. GFP-Astrin cells transiently expressing EB1-mCherry were imaged every 3.2 s. The arrowheads indicate one growing microtubule plus end that can be followed through the different frames of the movie. Scale bar, 10 μm unless otherwise indicated.

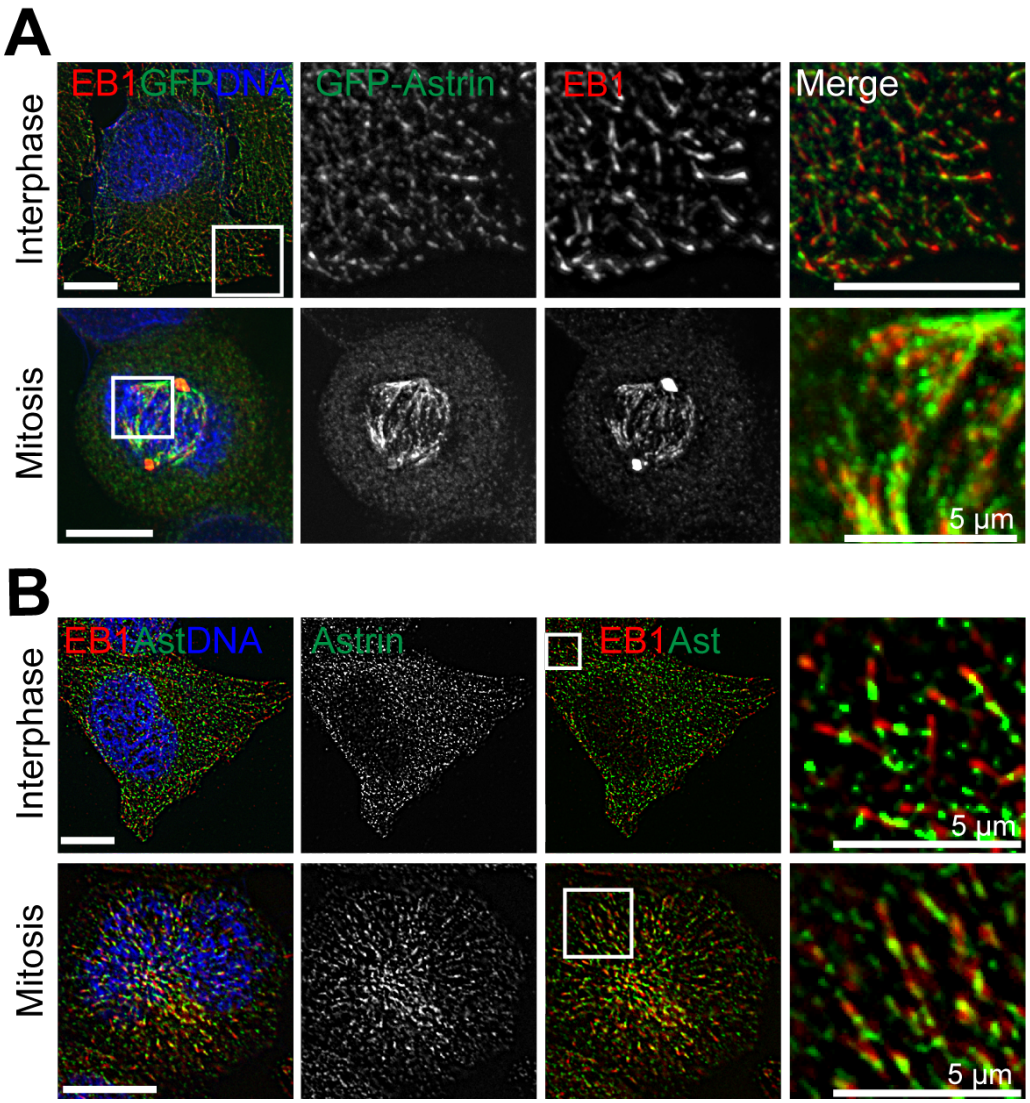


Figure 2.25: The Astrin-Kinastrin complex localises to microtubule plus tips proximal to EB1. (A) Methanol-fixed GFP-Astrin cells were stained for EB1. (B) Methanol-fixed HeLa cells were stained for Astrin and EB1. Single focal planes are shown. Scale bars, 10 μm unless otherwise indicated.

As expected for microtubule-associated staining, both GFP-Astrin and EB1 localisation were lost upon treatment with the microtubule destabilising drug nocodazole (Figure 2.26 A, page 64). Consistent with my finding that Kinastrin targets Astrin to the microtubules, GFP-Astrin comets were lost in Kinastrin-depleted cells (Figure 2.26 B, page 64). These findings show that the Astrin-Kinastrin complex tracks growing microtubule plus ends.

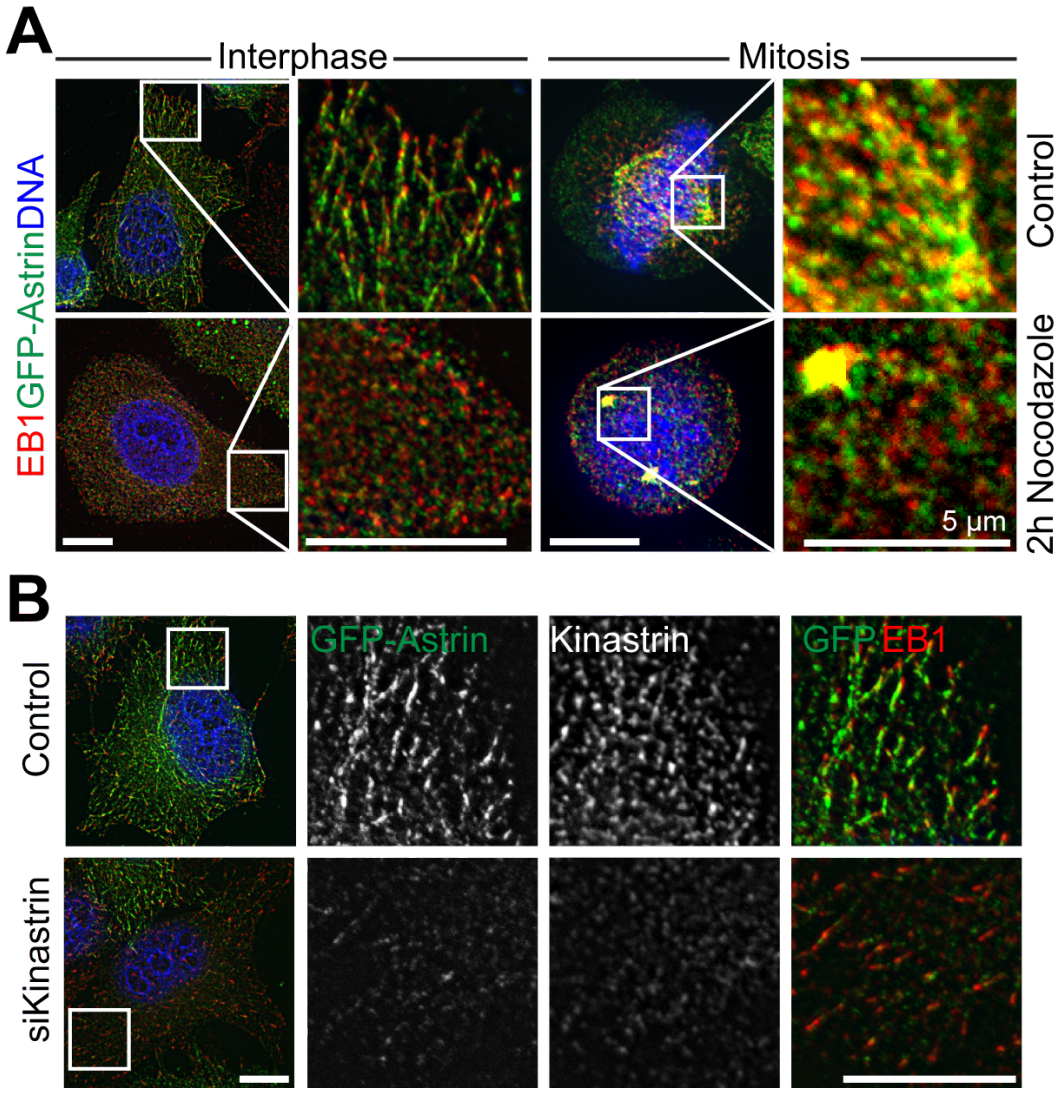


Figure 2.26: Kinastrin recruits Astrin onto microtubule tips. (A) GFP-Astrin cells were mock-treated or treated with 100 ng/ml nocodazole for 2 h, then stained for EB1. (B) GFP-Astrin cells were treated with control or Kinastrin siRNA for 72 h and stained for EB1 and Kinastrin. Boxed regions are shown enlarged on the right. Astrin was visualised by GFP fluorescence. Scale bars, 10 μm unless otherwise indicated.

To test if the Astrin-Kinastrin complex exerts a direct effect on the properties of these microtubules themselves, *in vitro* polymerisation assays were performed. Purified tubulin was incubated at 37°C to allow its polymerisation into microtubules. Because of the incorporation of a fluorescent dye into the tubulin polymer, microtubule polymerisation could be measured over time using a fluorimeter. As expected, addition of

glutathione-S-transferase (GST) had no effect on microtubule polymerisation (Figure 2.27, page 65). However, titration of recombinant Kinastrin into these assays resulted in an increased tubulin polymerisation, which suggested Kinastrin may act in stabilising microtubule plus ends (Figure 2.27, page 65). The effect of Astrin on microtubule polymerisation could not be determined due to difficulties in expressing the full length protein.

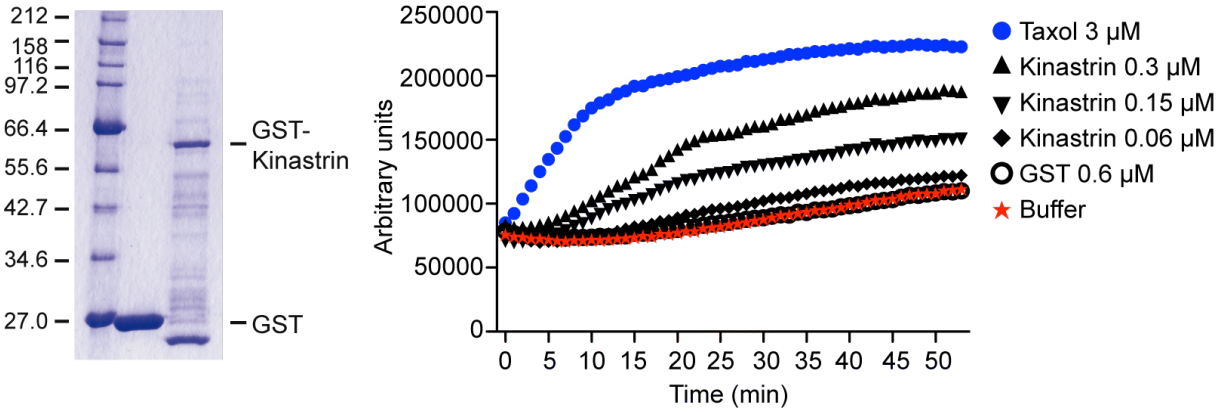


Figure 2.27: Kinastrin promotes microtubule polymerisation in a concentration dependent manner. Microtubule polymerisation in the presence of buffer, taxol, GST, or GST-Kinastrin at the indicated concentrations was followed in a fluorimeter. Each curve is representative of three independent experiments.

To test the idea that Kinastrin stabilises microtubules during kinetochore capture, its role in bipolar spindle formation was analysed. Cells were treated with the Eg5 inhibitor monastrol to interfere with centrosome separation and arrest them in a prophase-like state. After subsequent cold treatment to disassemble all unattached microtubules, cells were transferred to inhibitor-free medium at 37°C to allow the reformation of a bipolar spindle. In line with a microtubule stabilising function of Kinastrin, Kinastrin-depleted cells were impaired in their ability to reform robust bipolar spindles (Figure 2.28 A, page 66).

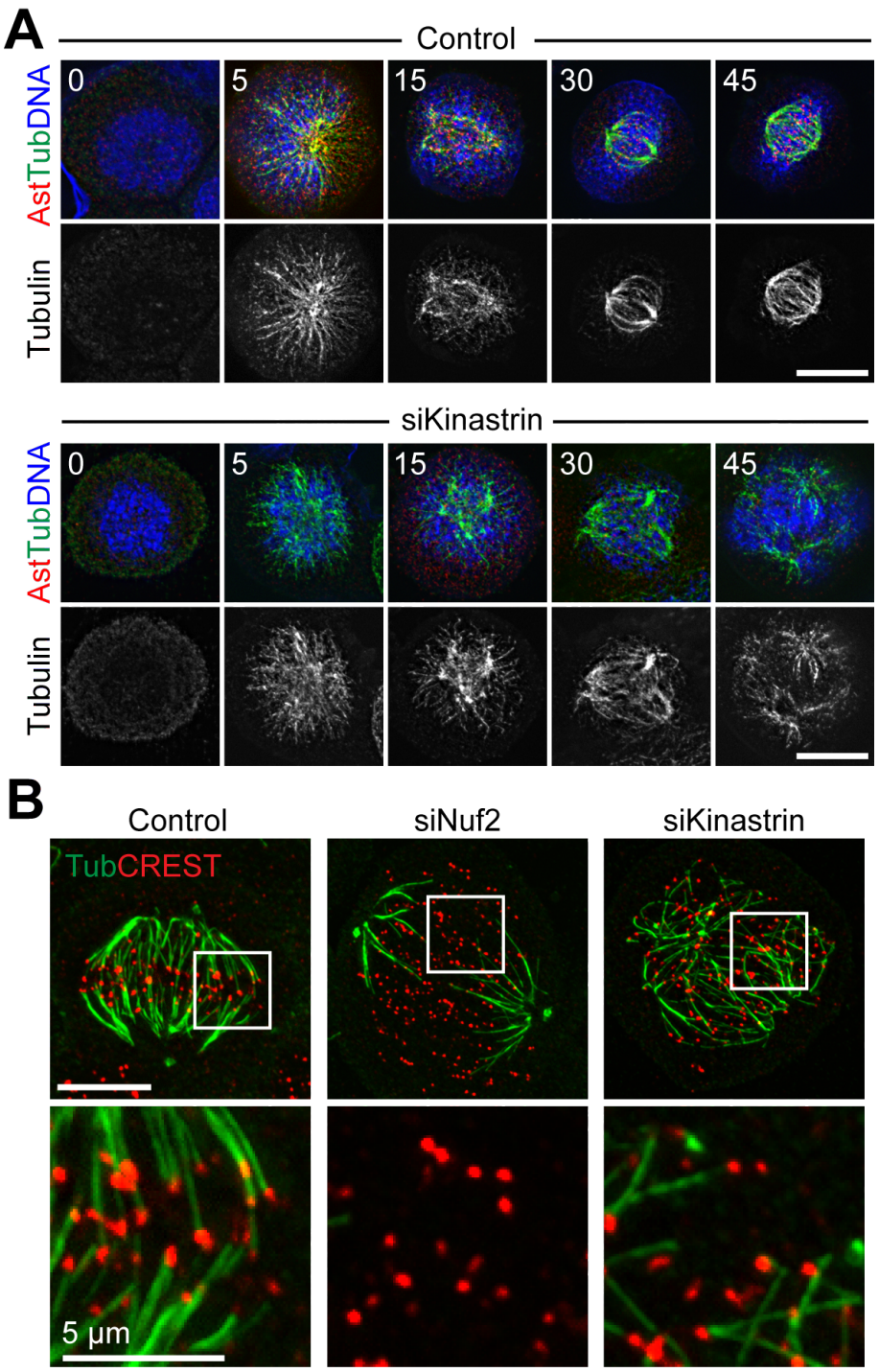


Figure 2.28: The Astrin-Kinastrin complex promotes stabilisation of microtubule attachments. (A) HeLa cells were treated for 18 h with 200 μM monastrol followed by 1 h cold treatment on ice. Microtubule regrowth was initiated by the addition of fresh 37°C medium, then monitored for 45 min by staining for Astrin, tubulin, and DNA. (B) HeLa cells treated with control, Nuf2, or Kinastrin siRNA duplexes for 72 h were cold treated for 10 min to visualise stable kinetochore fibres. The bottom row shows enlarged views of the boxed regions. Scale bars, 10 μm unless otherwise indicated.

While control cells showed stable bipolar spindles with aligned chromosomes after 30 min, Kinastrin-depleted cells assembled multipolar spindles and were unable to achieve chromosome alignment in a metaphase plate.

Moreover, kinetochore fibres formed in the absence of Kinastrin were disorganised, stained less intensely for tubulin compared to control cells, and were less resistant to cold treatment in Kinastrin-depleted cells (Figure 2.28 B, page 66). Additionally, a high proportion of unattached kinetochores was observed upon Kinastrin depletion. However, this phenotype is in contrast to depletion of Nuf2, which resulted in the loss of all kinetochore fibres and chromosome attachments.

Interestingly, Kinastrin contains a hydrophobic (S/T)xLP sequence motif, a common motif in EB-binding proteins (Kumar and Wittmann, 2012). To analyse whether this motif indeed mediates the interaction of Kinastrin with EB proteins, the serine and isoleucine residues were mutated to alanine residues and mutant Kinastrin complexes were purified. Western blotting of these samples revealed that Kinastrin interacts specifically with EB1 and this interaction is lost upon mutation of the SLLP motif (Figure 2.29, page 68).

As expected, Astrin was found in both wild-type and mutant Kinastrin precipitates and the interaction was not dependent on the (S/T)xLP motif.

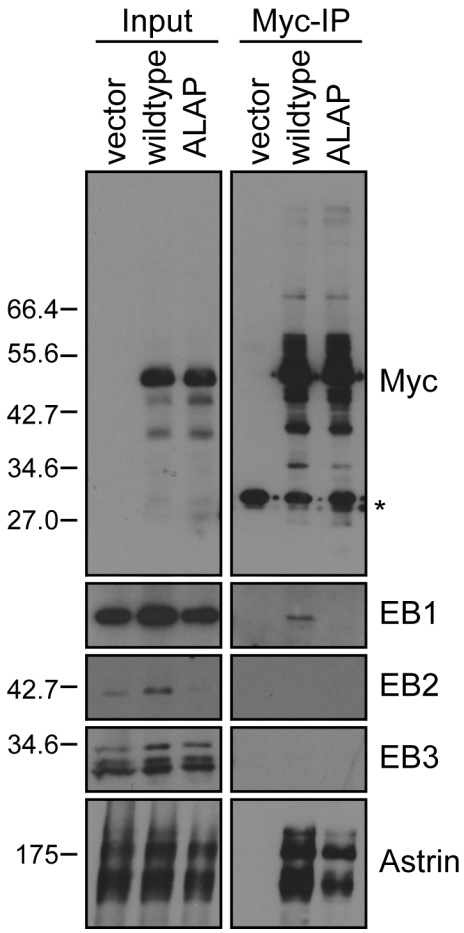


Figure 2.29: Kinastrin interacts specifically with EB1 via its SxLP motif. Myc-Kinastrin wild-type or SLLP (ALAP) mutant constructs were transiently transfected into HEK 293T cells for immune precipitations and Western blotting. Cells were synchronised in mitosis by addition of 10 μM STLC for 16 h after 24 h of transfection. The cells were then harvested and lysed, and anti-Myc immunoprecipitations were performed. Western blots were probed with the antibodies against Myc, EB1, EB2, EB3 and Astrin. The asterisk marks the Ig light chain.

Next, cell lines stably expressing GFP-tagged wild-type and SLLP mutant Kinastrin were generated to analyse the molecular function of the interaction with EB1. Preliminary experiments showed that spindle targeting of Kinastrin is reduced in Kinastrin SLLP mutant cells (Figure 2.30, page 69). Moreover, spindles of these cells appeared smaller and number and length of astral microtubules were reduced. However, further analysis of these Kinastrin mutant cells is required to reliably determine the role of the interaction between EB1 and Kinastrin.

Collectively, these results suggest that the Astrin-Kinastrin complex tracks and stabilises microtubule plus ends, which is required for stable microtubule kinetochore attachments and the formation of a proper mitotic spindle.

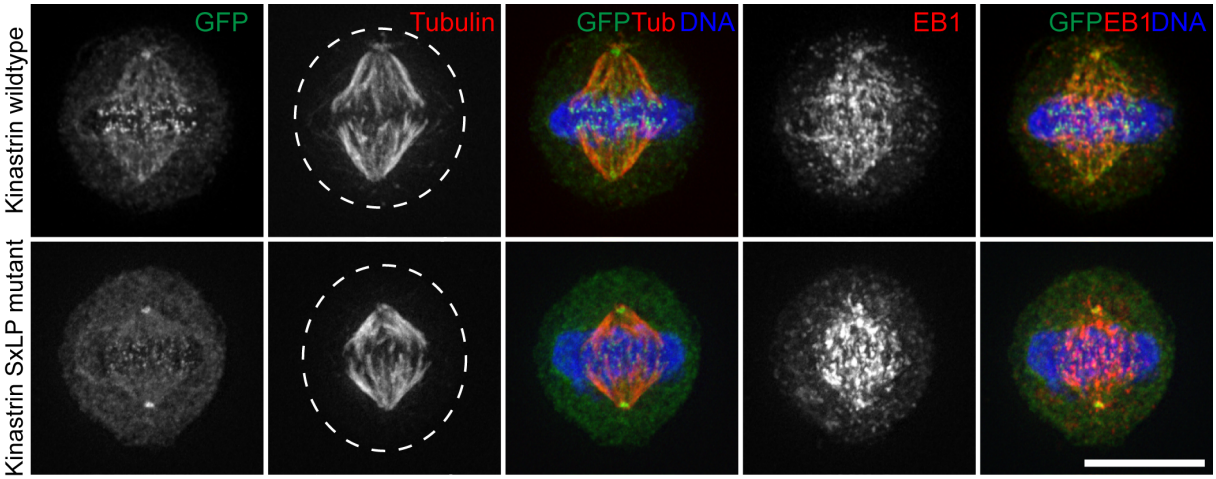


Figure 2.30: Expression of SxLP mutant Kinastrin causes smaller mitotic spindles. HeLa FlpIn cells stably expressing GFP-tagged wild-type or SxLP mutant Kinastrin were induced with 1 μg/ml doxycycline for 18 h, fixed and stained with antibodies to tubulin and EB1. Kinastrin was visualised by GFP fluorescence. DNA was stained with DAPI. Scale bar, 10 μm

2.6. Kinetochore and spindle targeting of DYNLL1

The initial mass spectrometry of immuno-isolated complexes showed that DYNLL1 forms two subcomplexes in mitosis, the Astrin-Kinastrin and CHICA-HMMR complex. Therefore, the requirement of these complexes for proper DYNLL1 localisation was investigated. HeLa cells stably expressing GFP-DYNLL1 were fixed, stained and DYNLL1 localisation was observed by GFP fluorescence. In metaphase, DYNLL1 targets to the spindle microtubules, the centrosomes and the kinetochores (control cells in Figure 2.31, page 70). Depletion of either HMMR or CHICA, but not two other spindle proteins HURP or TACC3, resulted in a loss of DYNLL1 from the mitotic spindle microtubules (Figure 2.31, page 70). Kinetochore or centrosome targeting was not affected.

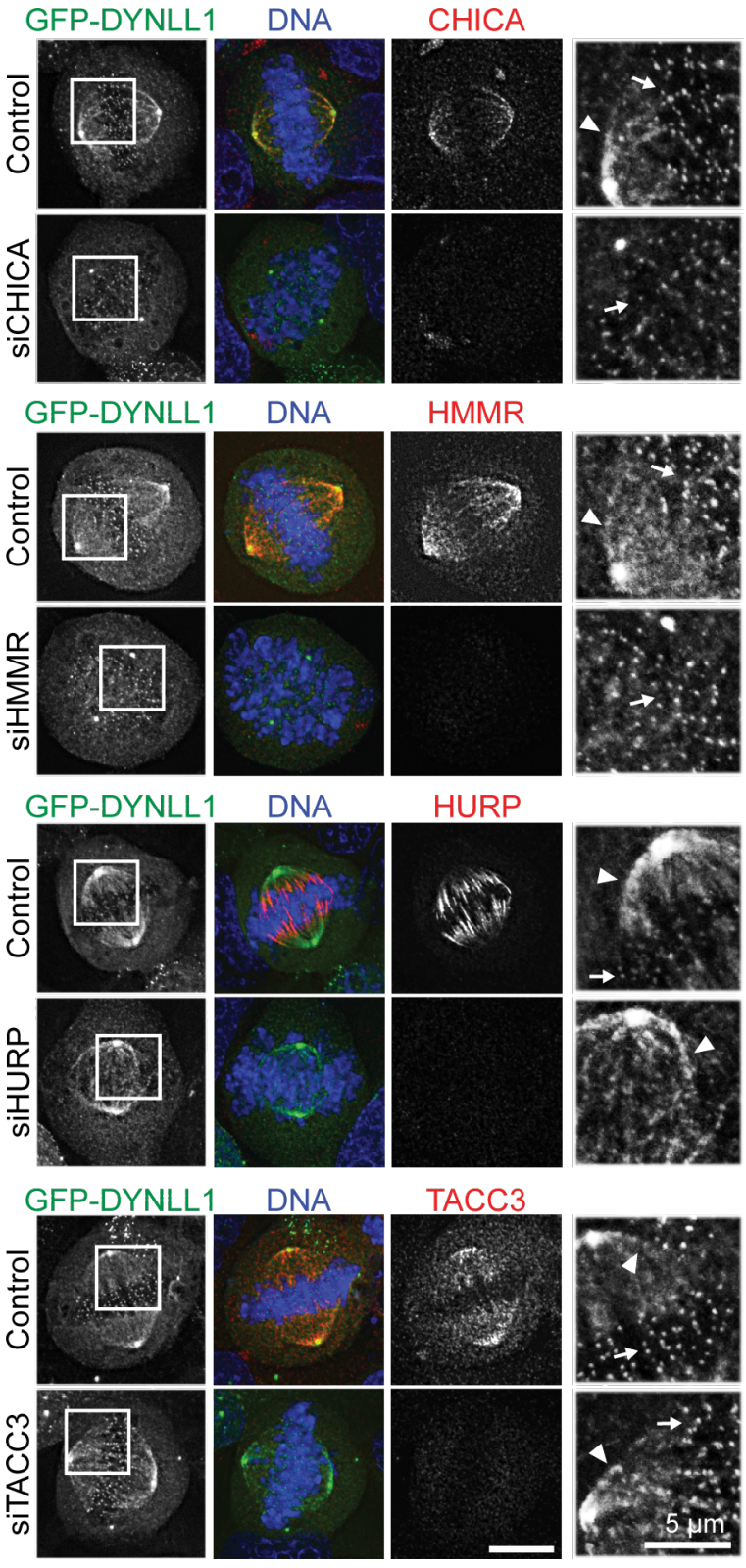


Figure 2.31: DYNLL1 localisation at spindle microtubules requires association with the CHICA-HMMR complex. HeLa cells stably expressing GFP-DYNLL1 were transfected with control, CHICA, HMMR (72 h), HURP, or TACC3 (48 h) siRNA duplexes. The cells were fixed, and then stained for CHICA, HMMR, HURP, or TACC3 as appropriate and DAPI to detect DNA. Right panel shows enlargement of the boxed region. Arrows indicate kinetochore-localised DYNLL1, arrowheads mark DYNLL1 at spindle microtubules. Scale bar is 10 μm unless otherwise indicated.

By contrast, depletion of the other DYNLL1 associated proteins Astrin or Kinastrin did not result in loss of DYNLL1 from the spindle microtubules (Figure 2.32, page 71), although spindles were highly disorganised as expected.

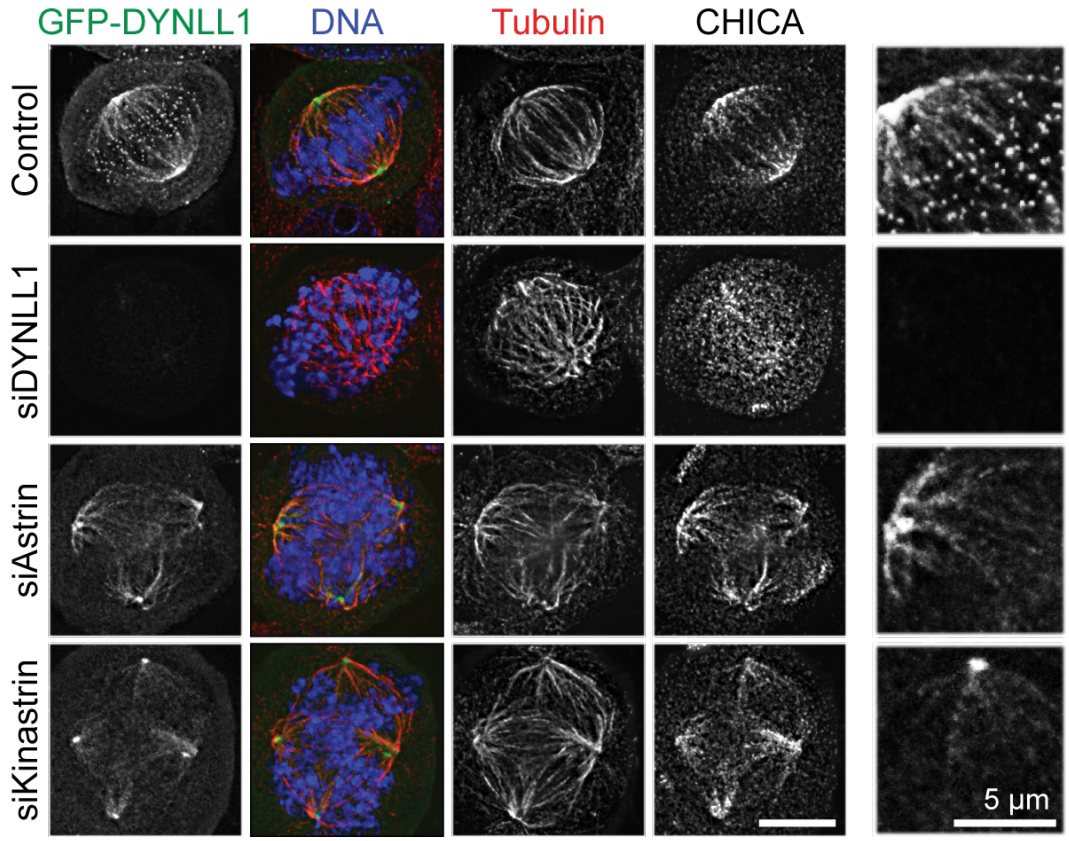


Figure 2.32: DYNLL1 is recruited to kinetochores by the Astrin-Kinastrin complex. HeLa cells stably expressing GFP-DYNLL1 were transfected with control, DYNLL1, Astrin (48 h), or Kinastrin siRNA duplexes for 72 hours. The cells were fixed, and then stained for tubulin, CHICA, and DAPI to detect DNA. DYNLL1 was visualised using GFP fluorescence. Scale bar is 10 μm unless otherwise indicated.

Careful examination of Astrin- and Kinastrin-depleted cells revealed that DYNLL1 was lost from kinetochores of these multipolar spindles.

Together, these findings support the idea that DYNLL1 is present in two discrete complexes at the mitotic spindle: one containing Astrin and Kinastrin at kinetochores, and a second novel spindle-associated complex containing HMMR and CHICA.

2.7. HMMR targets CHICA to the mitotic spindle

In the second part of this work the function of the novel DYNLL1-interacting CHICA-HMMR complex was investigated. The hyaluronan-mediated motility receptor protein, HMMR, was first described as an extracellular cell surface receptor mediating cell motility (Turley *et al.*, 1991). However, the HMMR protein sequence does not contain a signal sequence typical for extracellular proteins, making an extracellular function of HMMR rather unlikely. Consistent with data on HMMR localisation (Figure 2.31, page 70) and the idea of an intracellular function, later studies have shown that HMMR is a microtubule-associated protein, that localises to the mitotic spindle and interacts with TPX2 and γ-tubulin (Assmann *et al.*, 1999; Groen *et al.*, 2004). Moreover, HMMR was thought to modify microtubule stability by targeting MEK/ERK1/2 kinase to microtubules (Tolg *et al.*, 2010) and was suggested to play a role in focusing the spindle poles in the Ran-dependent, chromatin-driven microtubule nucleation pathway by restricting TPX2 activity to the poles (Groen *et al.*, 2004). It is highly overexpressed in many cancer types and has been proposed to regulate ras signalling (Wang *et al.*, 1998). An interaction between HMMR and dynein intermediate chain has been shown previously by Maxwell *et al.* (Maxwell *et al.*, 2003).

The other partner of the complex, CHICA (FAM83D), was previously identified as a binding partner for KID (CHICA, Spanish for "girl"), a chromokinesin that is required for the congression of chromosome arms to the spindle equator in metaphase (Santamaria *et al.*, 2008; Funabiki and Murray, 2000). In line with my localisation data (Figure 2.31, page 70), CHICA was shown to localise to the mitotic spindle, preferentially non-kinetochore fibres, and to directly bind to microtubules (Santamaria *et al.*, 2008). In this study depletion of CHICA resulted in apparently shorter spindles with misaligned metaphase chromosomes and an increase in mitotic index consistent with a slightly de-

layed progression from nuclear envelope breakdown to anaphase (Santamaria *et al.*, 2008).

Firstly, the localisation of HMMR and CHICA as cells passed through mitosis was investigated. This revealed that both proteins localise to the spindle poles in prophase and prometaphase, and then spread out along the mitotic spindle in metaphase and anaphase and dissociate from the spindle in telophase (Figure 2.33, page 73).

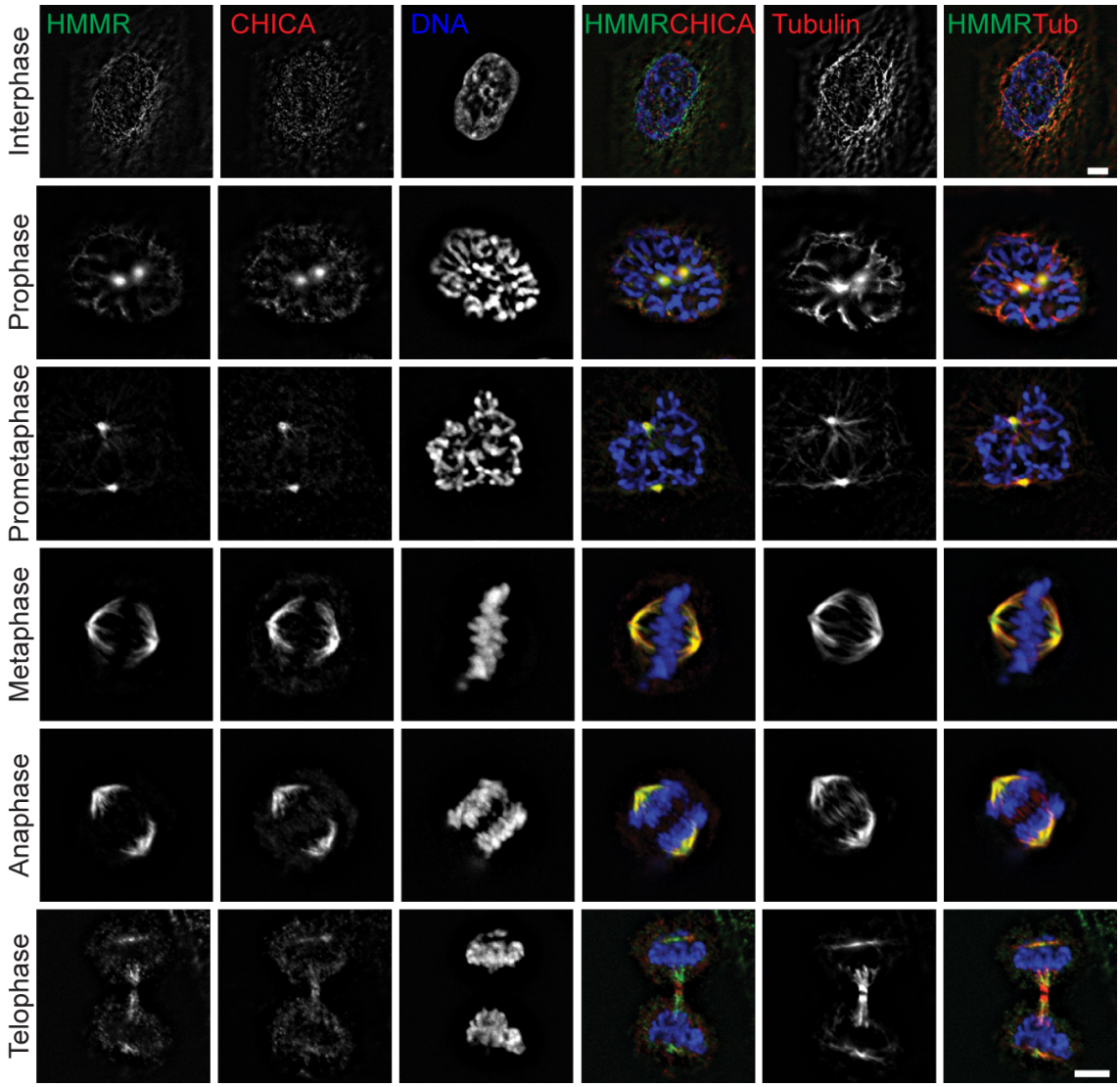


Figure 2.33: CHICA and HMMR localise to the mitotic spindle. HeLa S3 cells were fixed with PTEMF to remove the cytoplasmic pool of proteins and stained for HMMR, CHICA and tubulin. DNA was stained with DAPI. Scale bar, 10 μm

Expression of the GFP-tagged chromokinesin KID and staining with antibodies against CHICA and HMMR revealed that CHICA and KID localise to different mitotic structures (Figure 2.34, page 74).

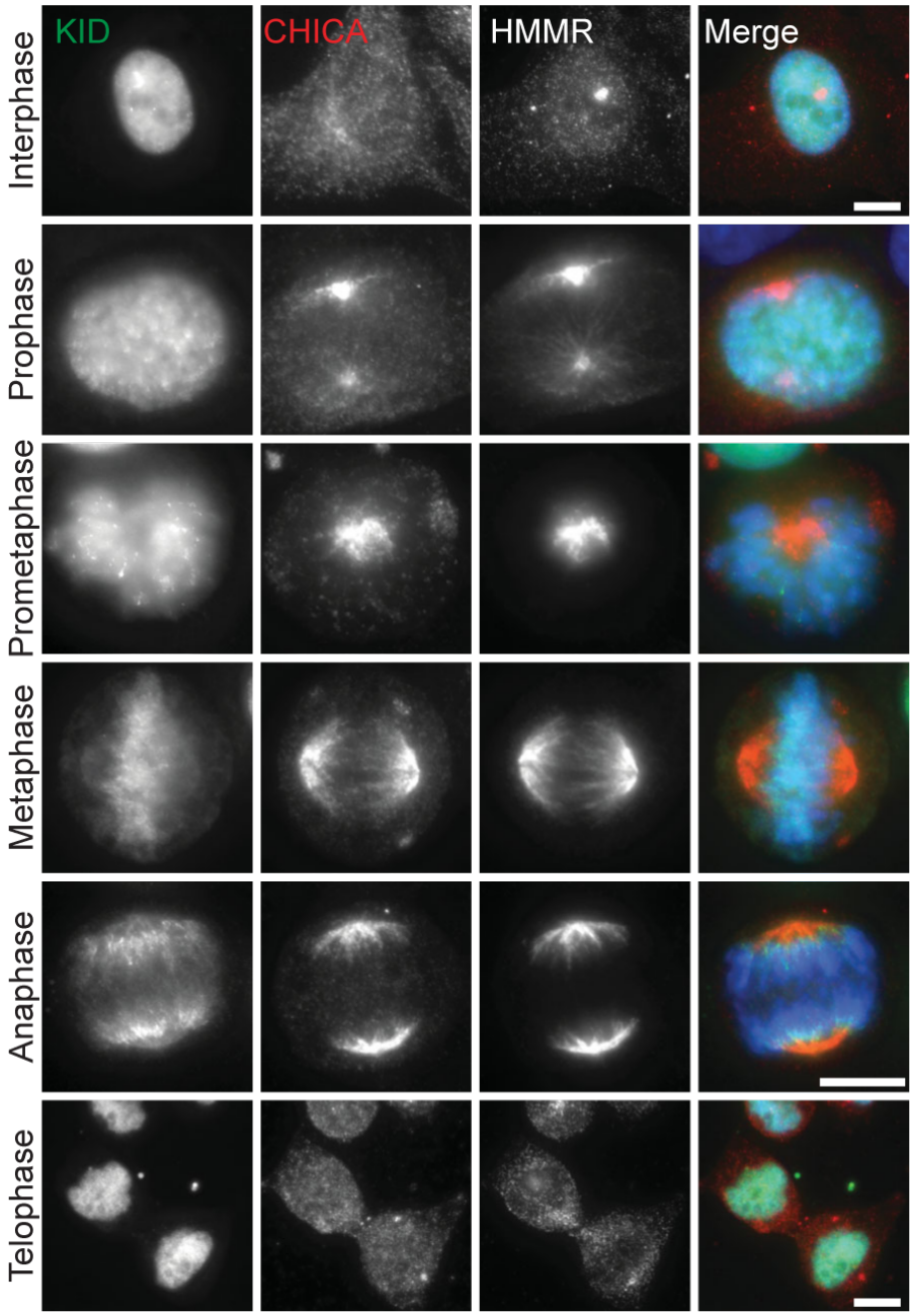


Figure 2.34: KID localises to mitotic chromatin structures. HeLa cells stably expressing GFP-KID were fixed and stained with antibodies against CHICA and HMMR. KID was visualised using GFP fluorescence. DNA was stained with DAPI. Scale bars, 10 μm

In fact, KID showed nuclear localisation and was found at the chromatin in inter- and prophase cells consistent with its function as a chromokinesin. It remained localised at the chromosomes in metaphase and stained the chromosome arms in anaphase. By contrast CHICA and HMMR co-localised at the mitotic spindle throughout mitosis. These findings suggest that CHICA exists in a complex with HMMR, rather than KID, which is in agreement with the proteins identified in CHICA complexes (Table 2.3, page 38) and with the absence of KID in CHICA precipitations (Figure 2.4 B, page 37).

Depletion of HMMR, CHICA or DYNLL1 resulted in apparently abnormal spindles with scattered chromatin (Figure 2.35, page 75). Intriguingly, CHICA localisation was lost in HMMR-depleted cells, indicating that HMMR is likely to be required for CHICA targeting to the spindle.

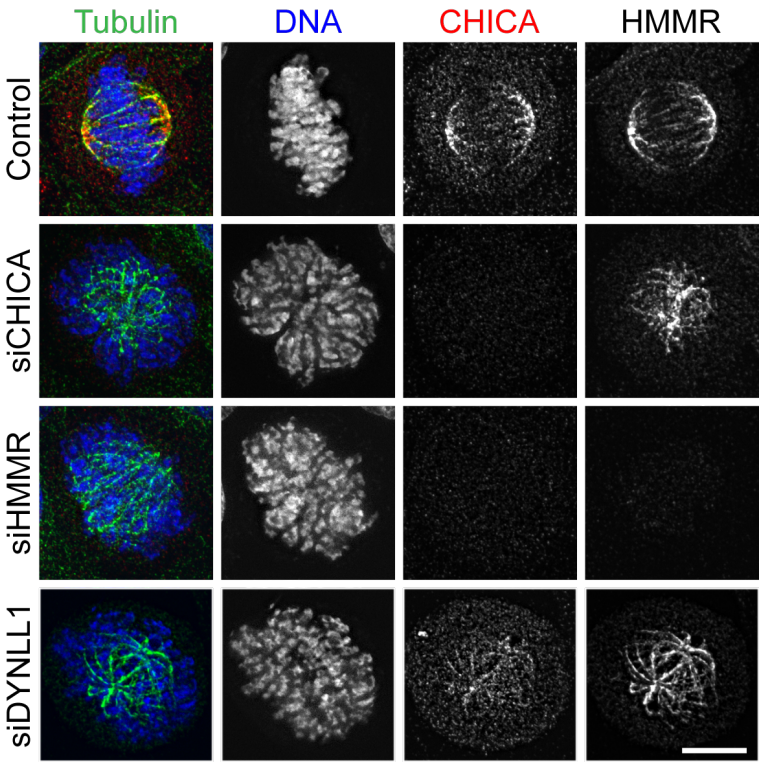


Figure 2.35: CHICA localisation to the spindle depends on HMMR. HeLa S3 cells were treated with control, HMMR, CHICA or DYNLL1 siRNA for 72 h and stained for tubulin, CHICA and HMMR. DNA was stained with DAPI. Scale bar, 10 μm

To test this idea, the interaction domains in both HMMR and CHICA as well as regions required for microtubule binding were mapped. Transfection of HeLa S3 cells with HMMR fragments revealed that the N-terminus of HMMR is required for spindle and interphase microtubule localisation (Figure 2.36, page 76).

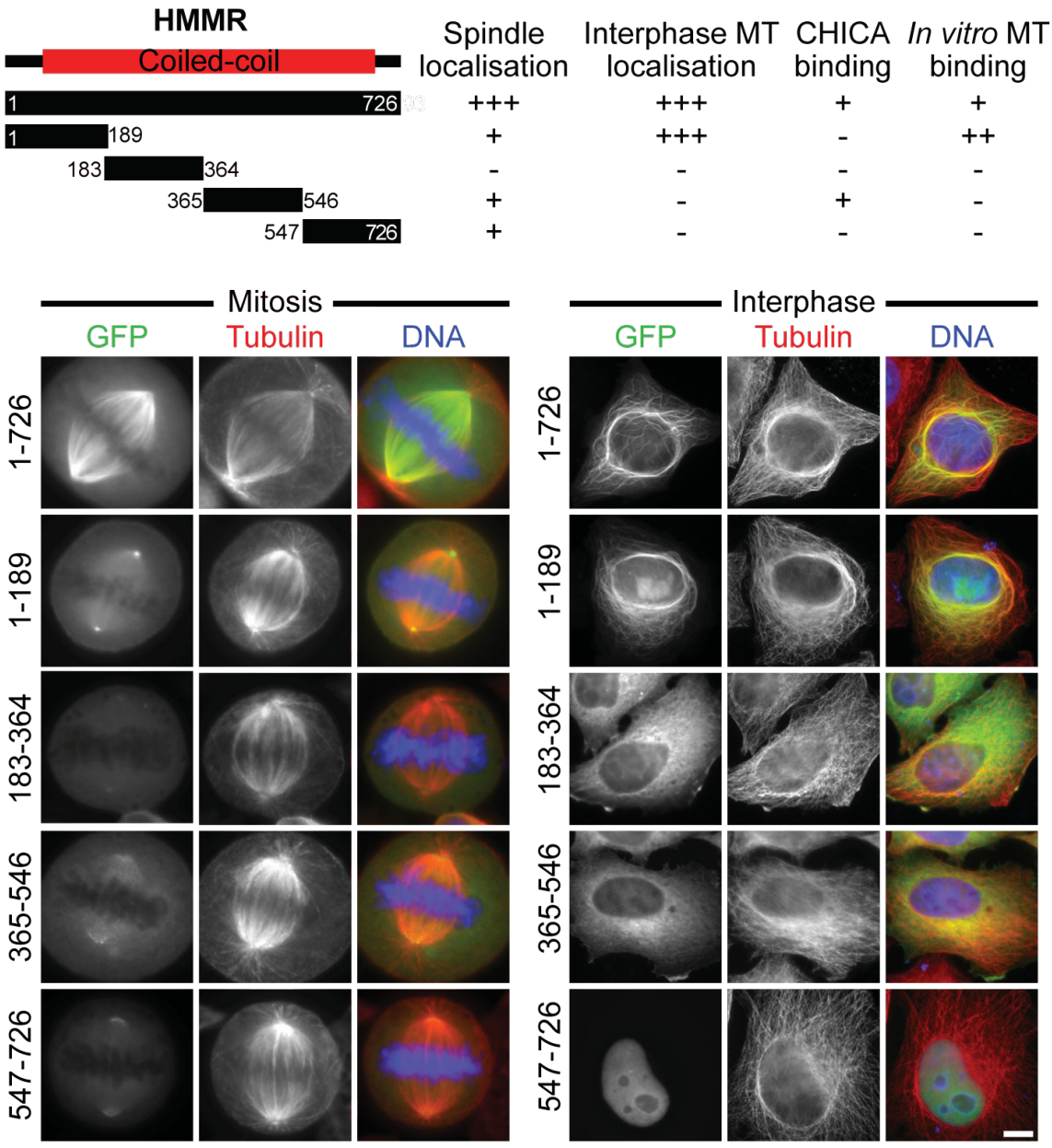


Figure 2.36: HMMR targets to microtubules via its N-terminus.
HeLa S3 cells were transfected with full-length GFP-HMMR or fragment constructs as outlined in the schematic. After 24 h cells were fixed and stained for tubulin and DAPI. HMMR was visualised using GFP fluorescence. Scale bar represents 10 μm.

However, spindle targeting of this HMMR fragment aa 1-189 is reduced compared to transfection with full-length HMMR. Additionally, fragments aa 365-546 and aa 547-726 were recruited to the spindle poles. Thus, while fragment aa 1-189 is required for mitotic spindle targeting of HMMR, it is not sufficient and other domains within the protein are necessary for the robust spindle localisation as seen for full-length HMMR. Consistent with the requirement of the N-terminus for microtubule targeting, *in vitro* microtubule pelleting assays showed that HMMR fragment aa 1-189 can directly bind to microtubules (Figure 2.37 A, page 77).

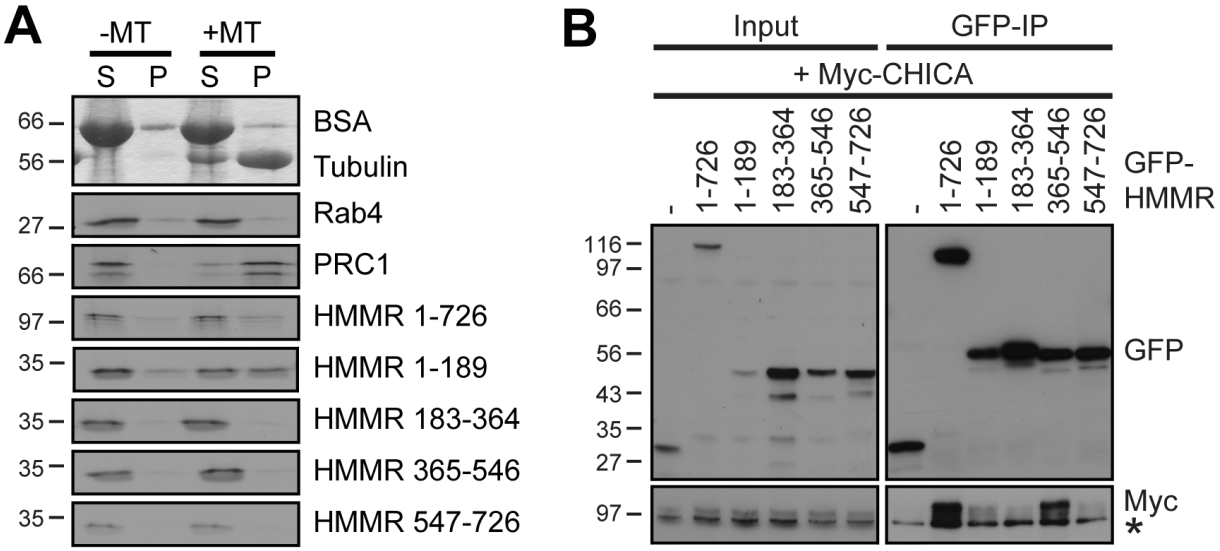


Figure 2.37: HMMR is a microtubule-binding protein.
(A) Microtubule-binding assays were performed with *in vitro*-translated full-length HMMR and HMMR fragments. The central spindle protein PRC1 and the GTPase Rab4 were used as a positive and negative control, respectively. (B) HEK 293T cells were co-transfected with full-length GFP-HMMR and HMMR fragments in conjunction with full-length Myc-CHICA for 40 h. Cells were arrested in mitosis for 16 h, harvested, lysed and GFP immunoprecipitations were performed and Western blotted with antibodies against GFP and Myc. The asterisk marks a non-specific band in the Myc blot.

Co-transfection of HEK 293T cells with HMMR fragments and full-length CHICA revealed that HMMR binds to CHICA through the amino acids 365-546 (Figure 2.37 B, page 77). In conclusion, HMMR binds directly to microtubules via its N-terminus and recruits CHICA to the spindle via its C-terminal half.

To investigate whether CHICA can also directly bind to microtubules and to identify the regions required for HMMR interaction and spindle binding, a reciprocal analysis was performed using CHICA fragments. This analysis revealed that the C-terminus of CHICA is responsible for spindle localisation (Figure 2.38, page 78). Both full-length CHICA or aa 383-615 showed mitotic spindle localisation and targeted interphase microtubules.

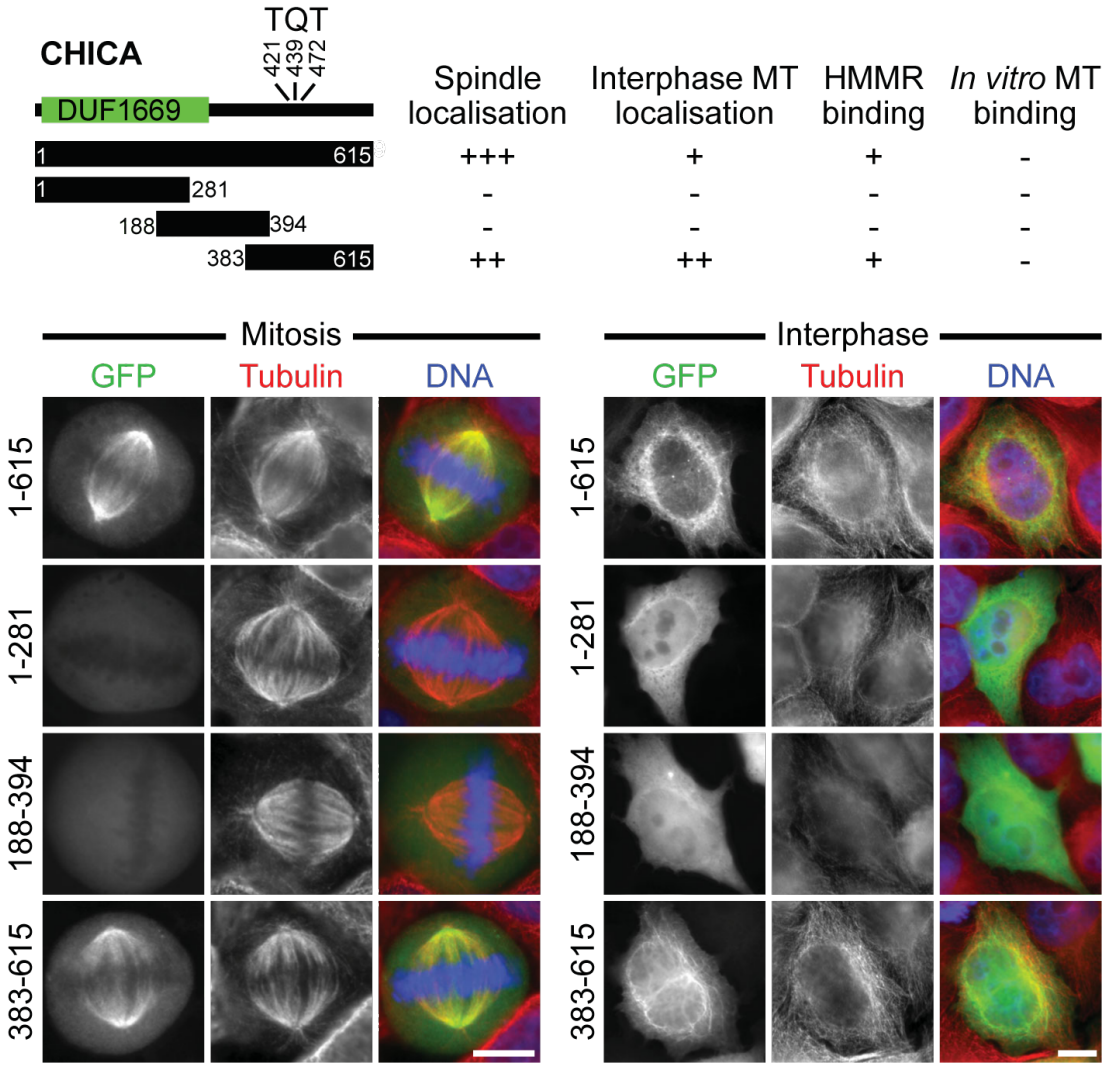


Figure 2.38: CHICA targets to the mitotic spindle via its C-terminus.
HeLa S3 cells were transfected with full-length GFP-CHICA or fragment constructs as outlined in the schematic. After 24 h cells were fixed and stained for tubulin and DAPI. CHICA was visualised using GFP fluorescence. Scale bar represents 10 μm.

Consistent with the results presented in Figure 2.35 (page 75), this spindle binding is likely mediated by HMMR, since CHICA was unable to bind to microtubules directly (Figure 2.39 A, page 79). Additionally, immune precipitations of CHICA fragments revealed that the C-terminus, which is required for spindle targeting, also represents the region mediating the interaction with HMMR (Figure 2.39 B, page 79).

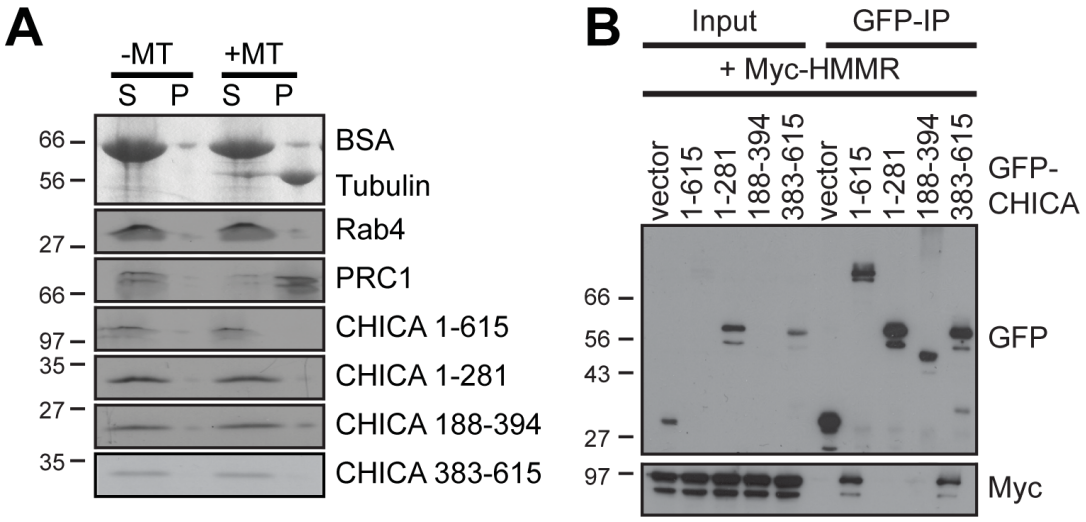


Figure 2.39: Spindle-targeting of CHICA is mediated through the HMMR-binding domain. (A) Microtubule-binding assays were performed with *in vitro*-translated full-length CHICA and CHICA fragments. The central spindle protein PRC1 and the GTPase Rab4 were used as a positive and negative control, respectively. (B) HEK 293T cells were co-transfected with full-length GFP-CHICA and CHICA fragments in conjunction with full-length Myc-HMMR for 40 h. Cells were arrested in mitosis for 16 h, harvested, lysed and GFP immunoprecipitations were performed and Western blotted with antibodies against GFP and Myc.

2.8. Mitotic progression is delayed in the absence of the DYNLL1-CHICA-HMMR complex

Having analysed the interaction between CHICA and HMMR as well as the spindle targeting properties of the complex, the function of the DYNLL1-CHICA-HMMR complex was then investigated. To this end, HeLa cells were depleted of HMMR, CHICA, or DYNLL1. A small increase in mitotic index relative to the control was observed for all CHICA, HMMR, and DYNLL1 duplexes tested (Figure 2.40 A, page 80), consistent with the idea that these proteins have a function in mitosis.

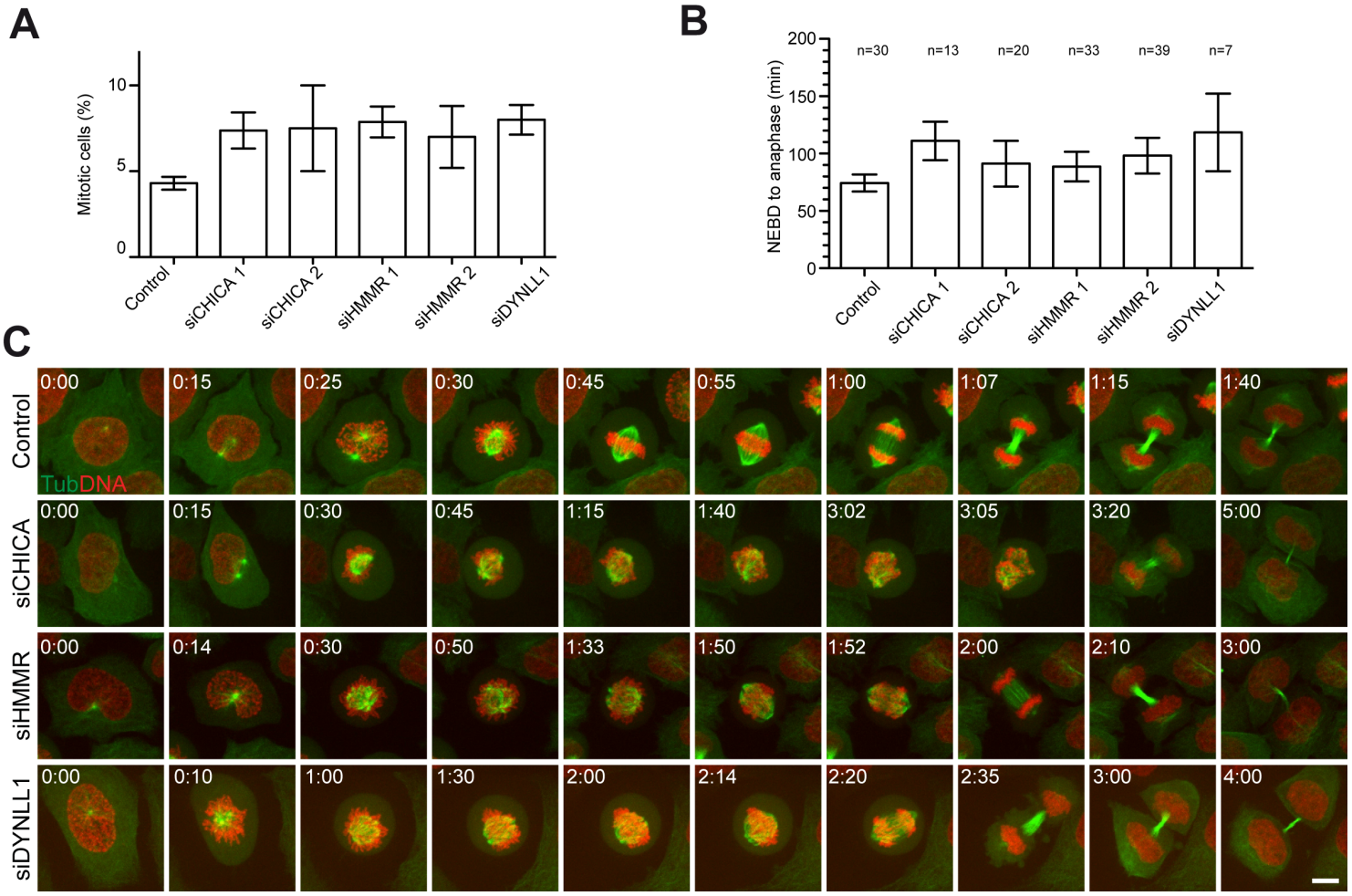


Figure 2.40: CHICA-, HMMR- or DYNLL1-depleted cells are delayed in mitosis.
(A) HeLa cells were treated with control, CHICA, HMMR or DYNLL1 siRNA duplexes for 72 h and mitotic cell numbers were determined. 100 cells were counted from each condition (n=3). (B and C) HeLa cells stably expressing mCherry-histone H2B and GFP-tubulin were treated as in A) and synchronised with 2.5 mM thymidine 30 h after siRNA addition for 20 h. Cells were released, incubated for 8 h at 37°C, and then filmed for 12 h. Images were acquired every minute. The time required from NEBD to onset of anaphase was plotted (B). Scale bar, 10 μm. Error bars represent the standard error of the mean.

Live cell imaging of cells expressing GFP-tubulin and mCherry-histone H2B showed that depletion of HMMR, CHICA, or DYNLL1 resulted in an increase in the time taken from nuclear envelope breakdown to the onset of anaphase from 70 minutes in control cells to 110 minutes (Figure 2.40 B, page 80). Although chromosomes and microtubules appeared disordered during spindle formation in each of these conditions, there was no obvious effect on chromosome segregation in anaphase (Figure 2.40 C, page 80).

Subsequently, it was analysed whether the abnormal spindle structures were caused by impaired kinetochore fibre formation. Microtubule depolymerisation induced by cold treatment revealed that cells depleted of CHICA, HMMR or DYNLL1, like control cells, form stable kinetochore fibres, which are resistant to cold (Figure 2.41 A, page 82). Cells depleted of the essential kinetochore fibre proteins Nuf2 and HURP showed reduced levels and thinner kinetochore fibres accompanied by a high number of unattached kinetochores. Analysis of HMMR, CHICA and DYNLL1 localisation upon cold treatment of cells showed that the DYNLL1-CHICA-HMMR complex targets to cold-sensitive microtubules (Figure 2.41 B, page 82). Under these conditions the kinetochore fibre MAP HURP remained associated with the spindle (Figure 2.41 B, page 82). Thus, the DYNLL1-CHICA-HMMR complex does not target to kinetochore fibres and is not required for their stabilisation. Therefore, impairment of kinetochore fibre stability was unlikely to explain the spindle formation defects observed upon depletion of DYNLL1, CHICA or HMMR.

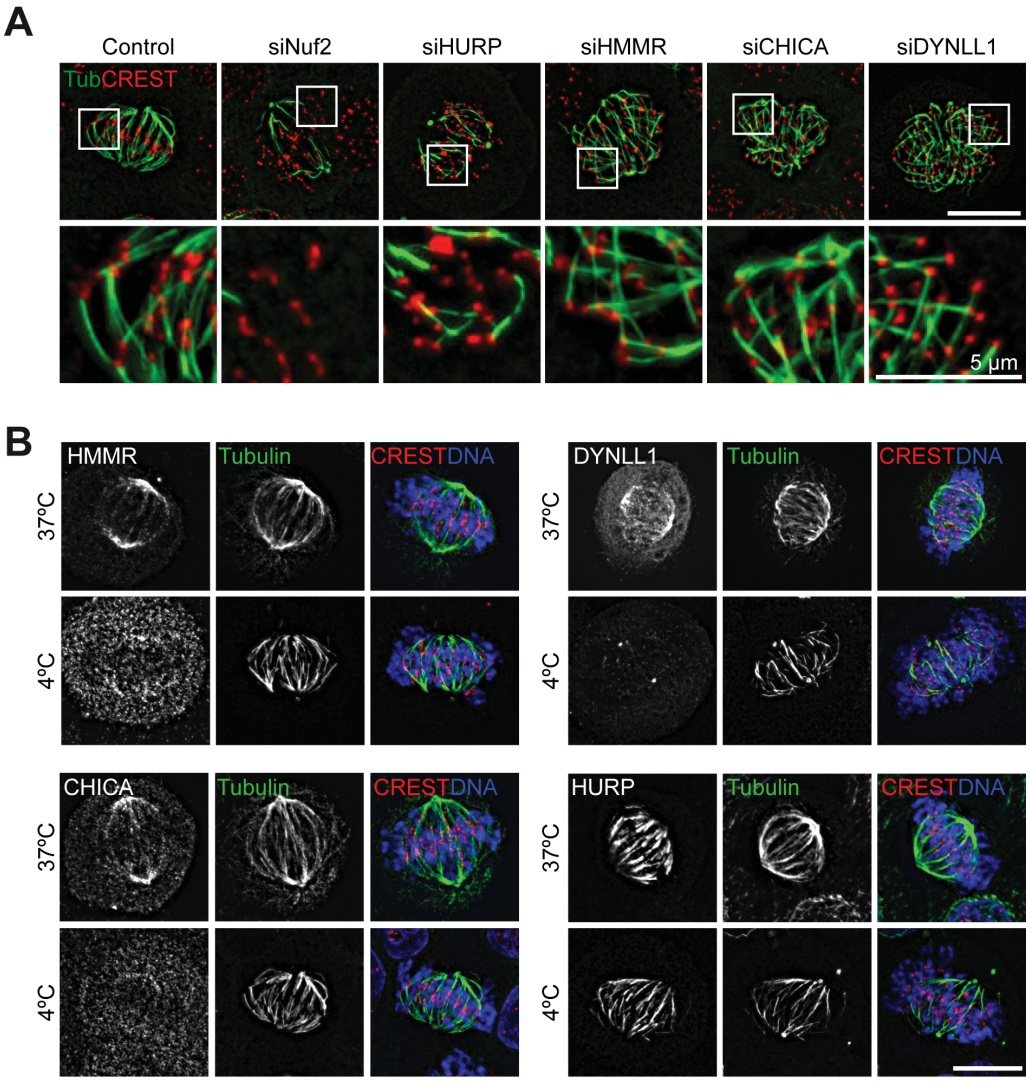


Figure 2.41: The DYNLL1-CHICA-HMMR complex is not required for stable kinetochore fibre formation and localises to cold-sensitive microtubules. (A) HeLa S3 cells were treated with siRNA duplexes targeting Nuf2 (48 h), HURP, HMMR, CHICA or DYNLL1, respectively, for 72 h. Subsequently, cells were incubated on ice for 10 min to depolymerise unattached microtubules, fixed and stained with antibodies towards tubulin and CREST. (B) HeLa S3 cells were mock treated (37°C) or incubated on ice for 10 min, fixed and stained with antibodies against tubulin, CREST and HMMR, CHICA, DYNNL1 or HURP, respectively. DNA was visualised with DAPI. Scale bars, 10 μm unless otherwise indicated

The localisation of the spindle checkpoint protein Bub1 in CHICA- and HMMR-depleted cells was then analysed to investigate whether SAC activation was altered in these cells. In control cells, CHICA-, and HMMR-depleted cells, Bub1 showed a strong kinetochore signal at unattached chromosomes (Figure 2.42 A, page 83).

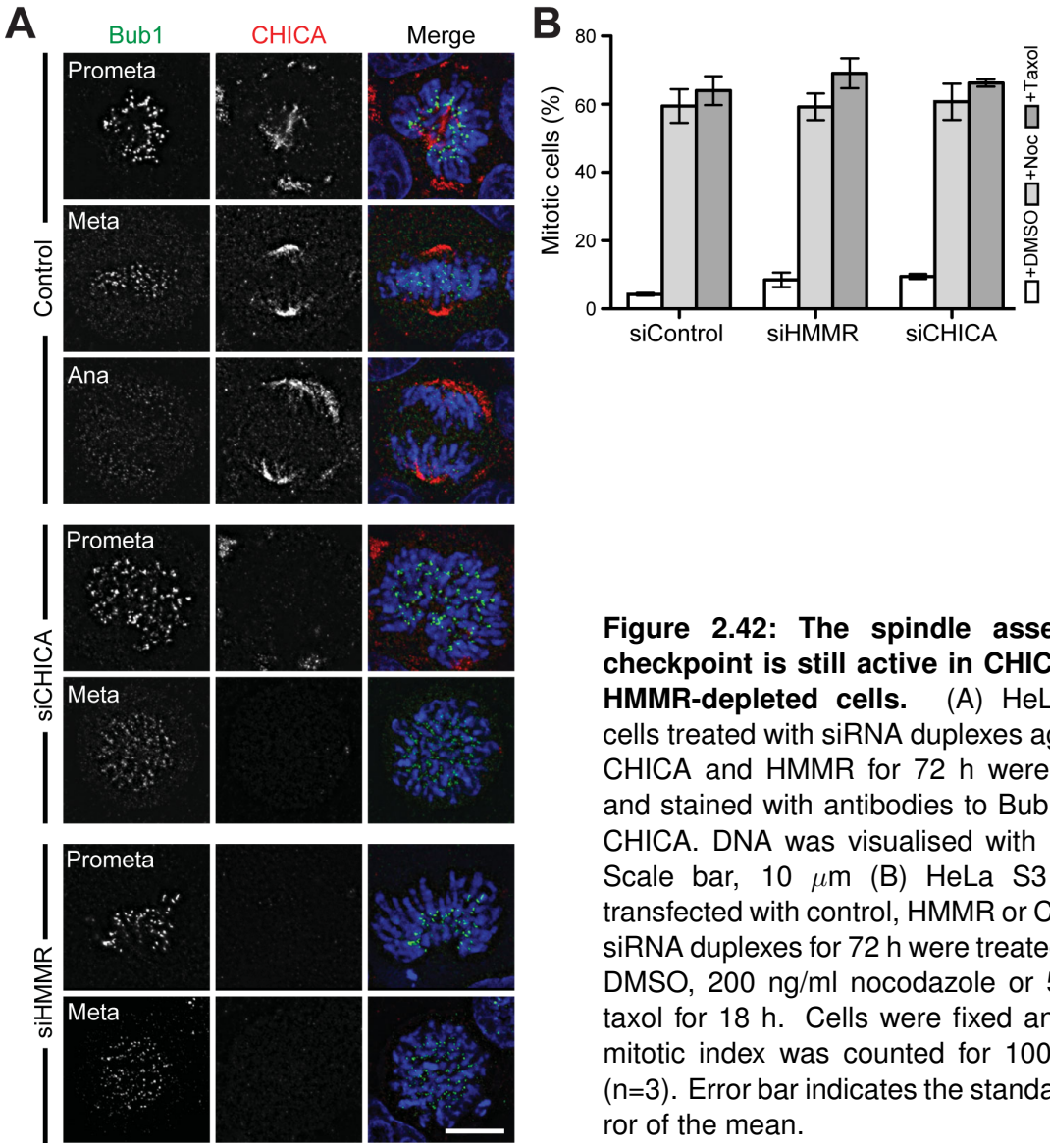


Figure 2.42: The spindle assembly checkpoint is still active in CHICA- or HMMR-depleted cells. (A) HeLa S3 cells treated with siRNA duplexes against CHICA and HMMR for 72 h were fixed and stained with antibodies to Bub1 and CHICA. DNA was visualised with DAPI. Scale bar, 10 μm (B) HeLa S3 cells transfected with control, HMMR or CHICA siRNA duplexes for 72 h were treated with DMSO, 200 ng/ml nocodazole or 5 mM taxol for 18 h. Cells were fixed and the mitotic index was counted for 100 cells (n=3). Error bar indicates the standard error of the mean.

In metaphase, as kinetochores become attached, less Bub1 is recruited and the signal is reduced. In anaphase and upon SAC satisfaction, no Bub1 staining is observed (Figure 2.42 A, page 83). This finding indicates that the SAC signalling is unaltered in CHICA- or HMMR-depleted cells. To further test whether the SAC is intact in CHICA- and HMMR-depleted cells, cells were either mock treated or treated with the microtubule depolymerising drug nocodazole or the microtubule stabiliser taxol, respectively. Because altered microtubule dynamics prevent the formation of a proper mitotic spindle, both treatments strongly activate the SAC and therefore induce a cell arrest in

normal cells (Figure 2.42 B, page 83). The same increase in mitotically arrested cells was found upon depletion of HMMR or CHICA, again confirming the idea that SAC activation is unaltered in these cells.

2.9. Loss of the DYNLL1-CHICA-HMMR complex results in spindle misorientation

The abnormal spindle structures observed upon loss of CHICA, HMMR or DYNLL1 were unlikely caused by altered kinetochore fibre stability and did not evoke a strong SAC response. Therefore, other explanations for the apparent defects in spindle structures were sought.

Cultured HeLa S3 cells grow as a monolayer and therefore divide and align their mitotic spindle within a plane parallel to the growth surface. When these cells are fixed, stained and imaged using standard microscopy, a series of images is collected at different focal positions through the three-dimensional sample, which is projected into a two-dimensional image. This projection results in the characteristic bar-like array of chromosomes centred in the middle of the ellipsoid mitotic spindle. However, rotation of the spindle results in a projection with apparently disordered, scattered chromatin despite a normal bipolar spindle architecture (Figure 2.43, page 84).

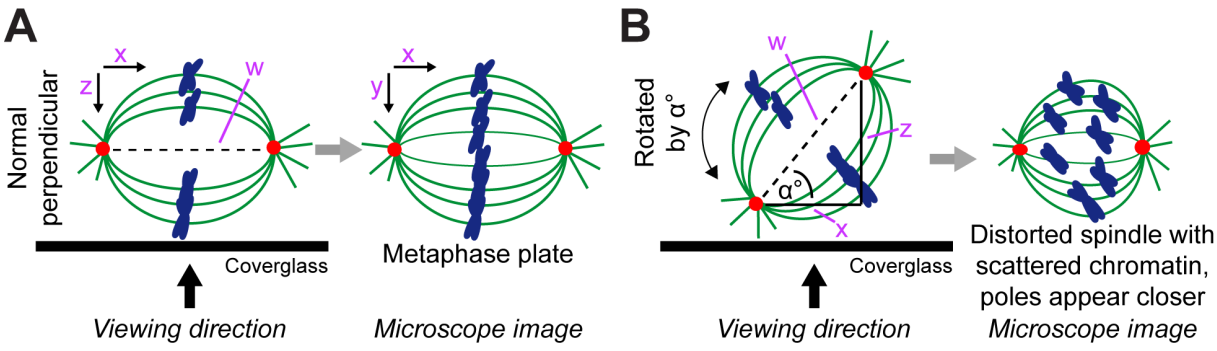


Figure 2.43: Model of projected microscope images. A schematic representing observed microscope images of normally aligned spindles (A) or rotated spindles (B) and showing the distances x and z measured from the microscope images and used to calculate α, the angle of spindle rotation.

In dividing cultured cells, both spindle poles are therefore typically equidistant from the growth surface. As expected, visualisation of these by the centriolar marker pericentrin showed that in control cells the spindle poles were found in the same focal plane causing spindles to align to within 10° of the plane of the coverglass (Figure 2.44, page 85).

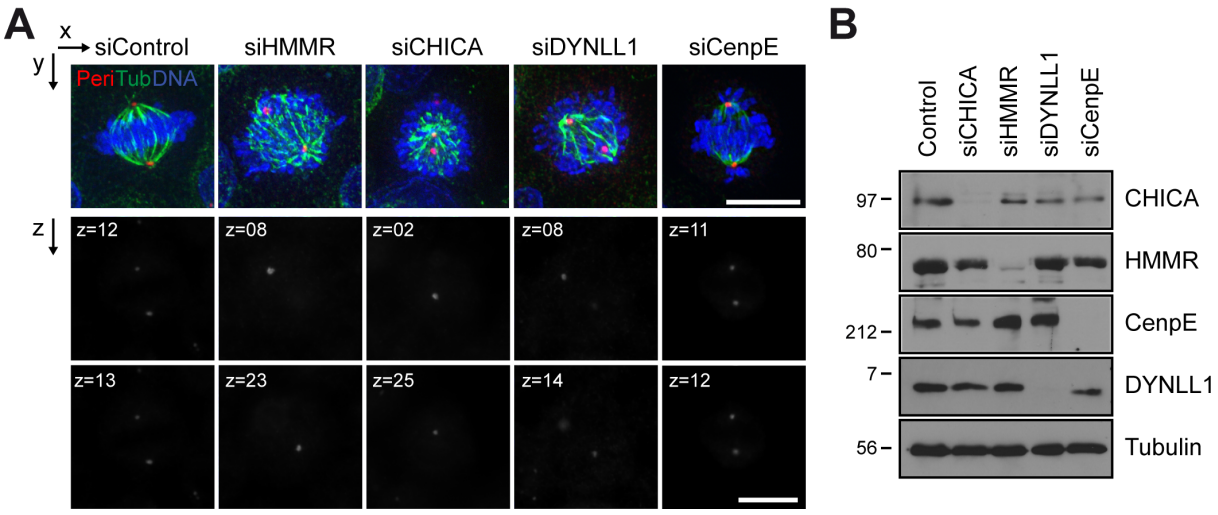


Figure 2.44: Spindles of DYNLL1-, CHICA- and HMMR-depleted cells are rotated.
(A) HeLa cells were transfected with control, CHICA, HMMR, DYNLL1, or CenpE (48 h) siRNA duplexes, fixed after 72 hours, and then stained for tubulin and pericentrin to define the position of the mitotic spindle, and DAPI to detect DNA. The full cell volume was imaged acquiring z stacks containing 26 steps, 0.4 μm apart. z indicates the focal plane. Scale bar, 10 μm (B) Samples were Western blotted to test for depletion of the respective target proteins.

However, in cells depleted of HMMR, CHICA, or DYNLL1 the spindle poles were found at different distances from the coverglass, and spindles showed widely differing angles of 0-60° to the coverglass plane (Figure 2.43 B, page 84, Figure 2.44, page 85 and Figure 2.45 A, page 86).

Up to 60% of HMMR-, CHICA-, or DYNLL1-depleted cells had spindles rotated by over 10° (Figure 2.45 B, page 86). These effects were not due to general perturbations of chromosome segregation, since depletion of the CenpE motor protein required for proper chromosome alignment caused scattered chromatin but had little effect on spindle orientation compared to the control (Figure 2.44, page 85). If spindle orientation

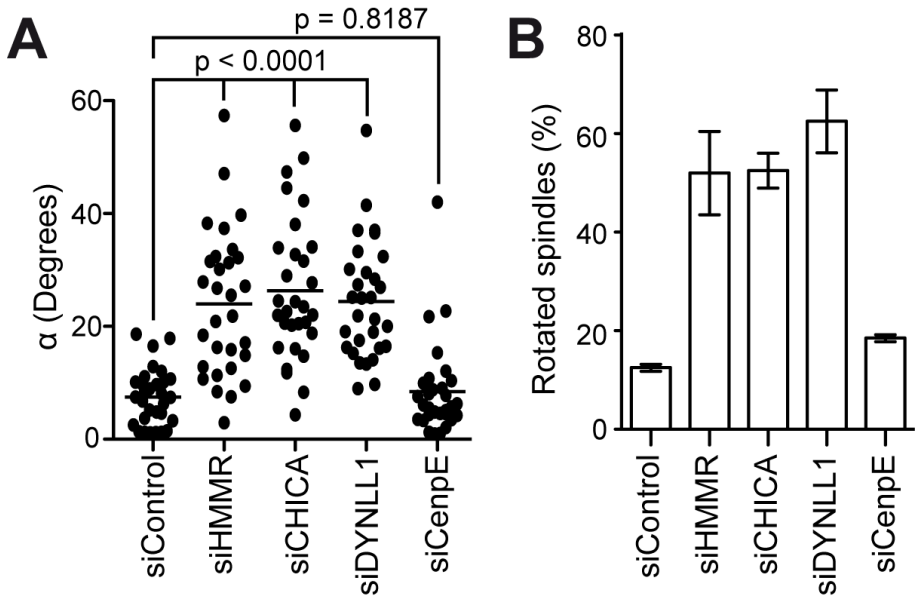


Figure 2.45: The DYNLL1-CHICA-HMMR complex is required for proper spindle orientation. (A) HeLa cells were transfected with control, CHICA, HMMR, DYNLL1, or CenpE (48 h) siRNA duplexes, fixed after 72 hours, and then stained for tubulin and pericentrin to define the position of the mitotic spindle, and DAPI to detect DNA. The angle of spindle rotation was measured and is plotted in the graph. The Mann-Whitney test was used to calculate the p values for comparisons. (B) The percentage of cells with visibly rotated spindles is plotted in the graph, errors bars show the standard error of the mean (n=100).

was completely random in the absence of HMMR, CHICA, or DYNLL1, then any rotation angle between 0° and 90° could be expected. However, none of the measurements made on fixed cell samples exceeded 60°. One possibility was that the angle of spindle rotation was underestimated in the fixed samples due to drying artefacts causing flattening of the sample. Therefore, those angles were compared to measurements of spindle rotation made from live cell imaging data. This analysis showed again that spindles in HMMR-, CHICA-, or DYNLL1-depleted cells did not align to the coverglass and the maximum angle of rotation was close to 90° (Figure 2.46 C, page 87). Interestingly, three-dimensional analysis of these cells revealed that, contrary to initial impressions, these cells exhibited robust bipolar spindles of normal size with fully aligned chromosomes (Figure 2.46 A and B, page 87 and Movie of CHICA-depleted cells).

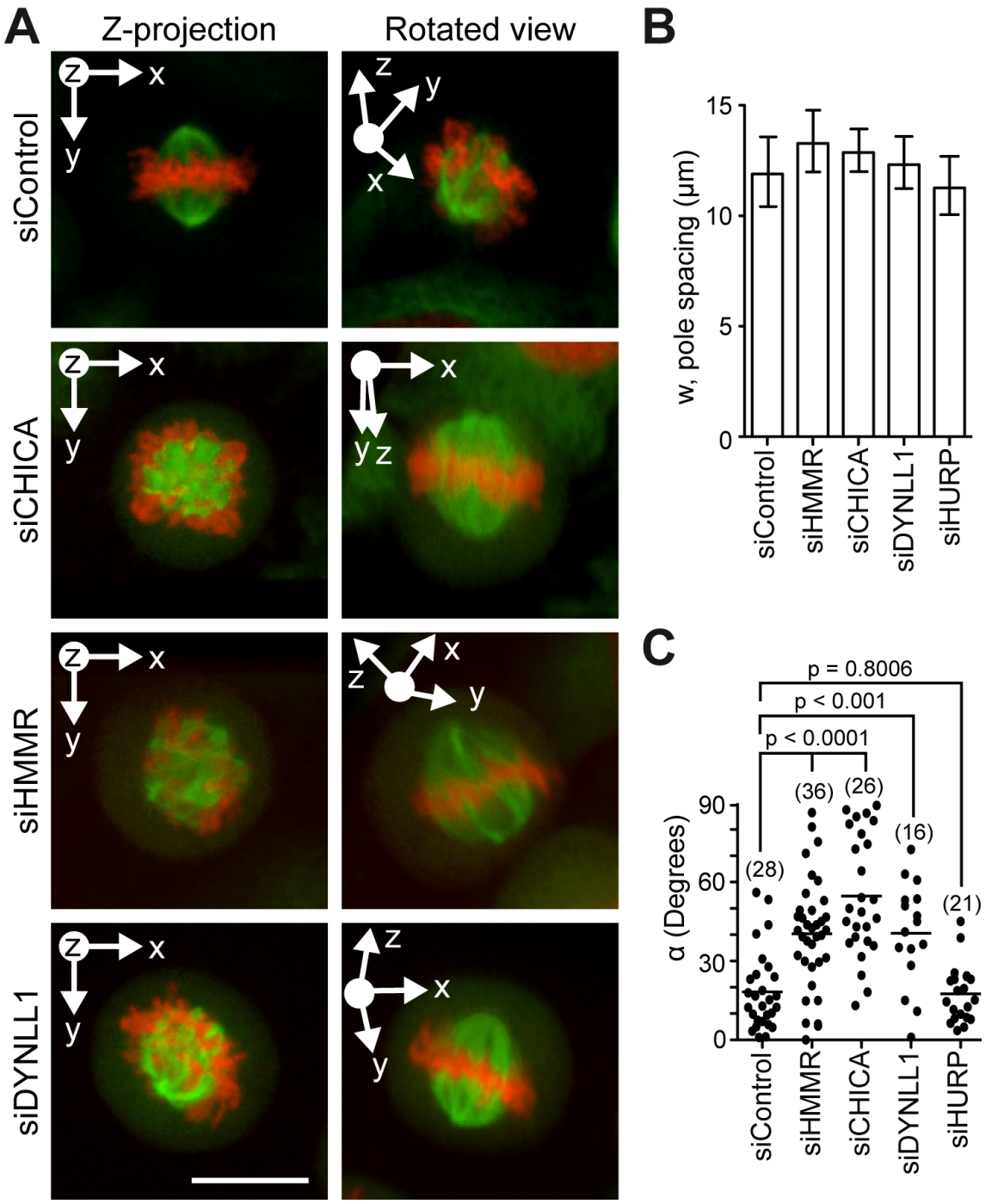


Figure 2.46: HMMR-, CHICA- or DYNLL1-depleted cells build organised bipolar spindles. (A) HeLa cells stably expressing GFP-tubulin and mCherry-histone H2B were transfected with the siRNA duplexes shown in the figure for 72 h, and the full cell volume was imaged every minute as the cells passed through mitosis. Using Volocity software, the microscopy data were rotated until both poles lay in the same focal plane and images were projected. Representative images are shown. White arrows labelled x, y, z indicate the rotation in three dimensions between projections of the same cell. Scale bar, 10 μm (B) The pole-to-pole distances of control, and HMMR-, CHICA- DYNLL1- or HURP-depleted cells were measured and plotted in the graph. (C) The angle of spindle rotation at the metaphase to anaphase transition was calculated and is plotted in the graph. The Mann-Whitney test was used to calculate the p values for comparisons.

Open file in Adobe Reader to view movie

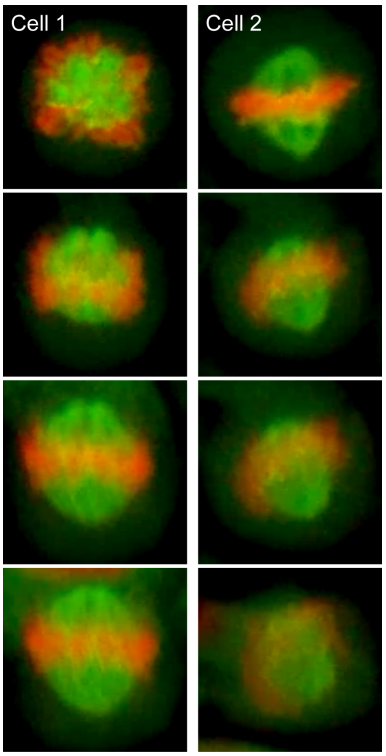


Figure 2.47: Still images of movie of CHICA-depleted cells. Still images for two cells are shown. Cell 1 appears to have an abnormal spindle structure and unaligned chromosomes, while cell 2 contains a proper bipolar spindle. However, rotation of the view point revealed that cell 1 exhibits a robust bipolar spindle with aligned chromosomes, whereas rotation of cell 2 demonstrates that the spindle now appears abnormal with misaligned chromosomes.

Next, I investigated if DYNLL1-, CHICA- and HMMR-depleted cells maintain a random spindle orientation or whether spindles rotate continuously. To this end, spindle angles were measured every five minutes as cells underwent mitosis. Detailed analysis of these live cell imaging experiments showed that HMMR-, CHICA- or DYNLL1-depleted cells acquire a random spindle rotation early in mitosis and are unable to correct this rotation angle, before cells enter anaphase, when cells gain contacts to the substrate and spread out again. Angle measurements over time revealed that the spindle orientation is maintained, typically within 10°, and the spindles did not tumble continuously (Figure 2.48, page 89).

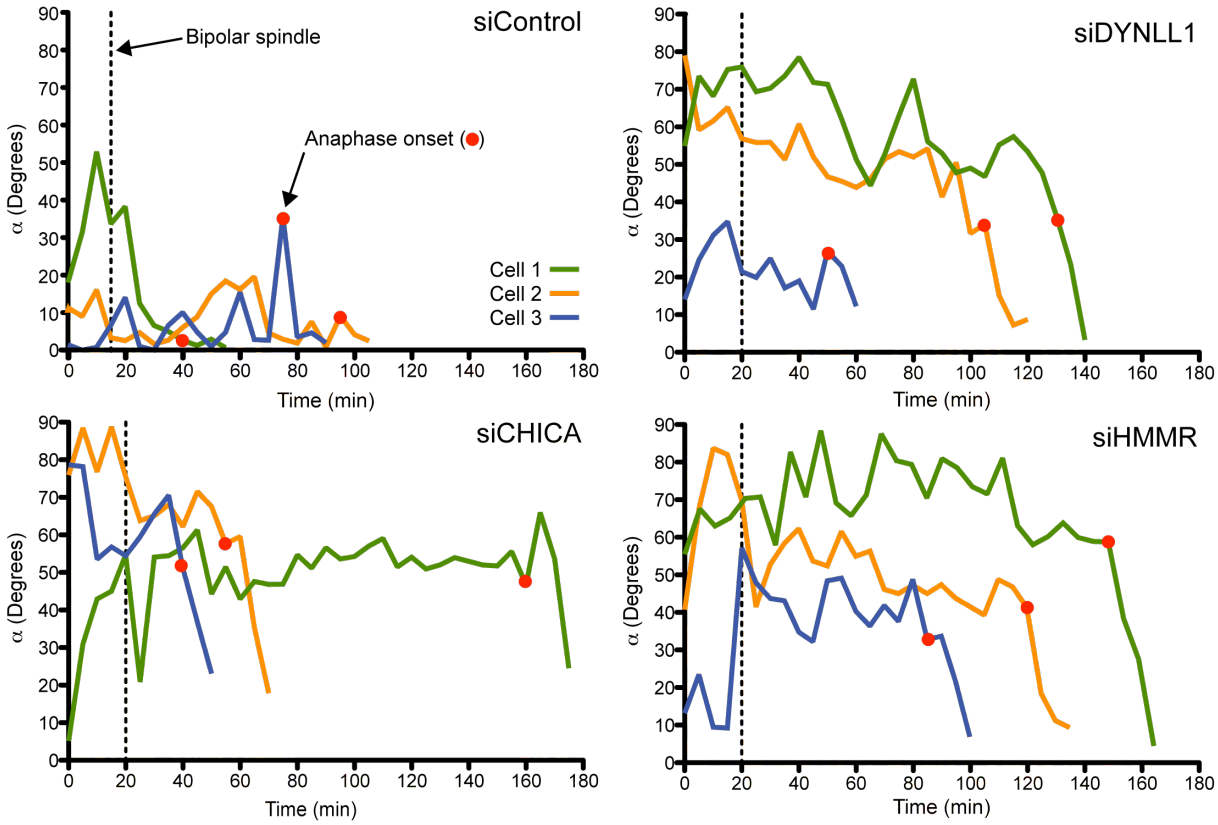


Figure 2.48: Spindles adopt a fixed but incorrect orientation angle in cells depleted of CHICA, HMMR or DYNLL1. HeLa cells stably expressing GFP-tubulin and mCherry-histone H2B were transfected with siRNA duplexes targeting CHICA, HMMR or DYNLL1 for 72 h, and the full cell volume was imaged on an Ultraview spinning disk confocal microscope every minute as the cells passed through mitosis. The angle of spindle rotation from nuclear envelope breakdown to telophase was measured and is plotted in the graph. The dotted line indicates the time point at which a bipolar spindle had been assembled and the red circle represents the timeframe when chromosome segregation was first observed, as a marker for anaphase onset. Three example curves are shown per condition.

This maintenance of a random, but fixed orientation angle requires attachment of the spindle to some point within the cell and is likely to be mediated by contacts of astral microtubules to the cortex. This suggested that astral microtubules were not grossly altered. To test this idea, cells depleted of the components of the DYNLL1-CHICA-HMMR complex were imaged on an OMX V3 BLAZE microscope using super-resolution 3D structured illumination. Reconstruction images of the whole mitotic cell volume and rotation of the viewpoint so that both spindle poles fell within the same plane showed that astral microtubules appear similar in size and thickness in CHICA-, HMMR- or

DYNLL1-depleted cells compared to control cells (Figure 2.49, page 90).

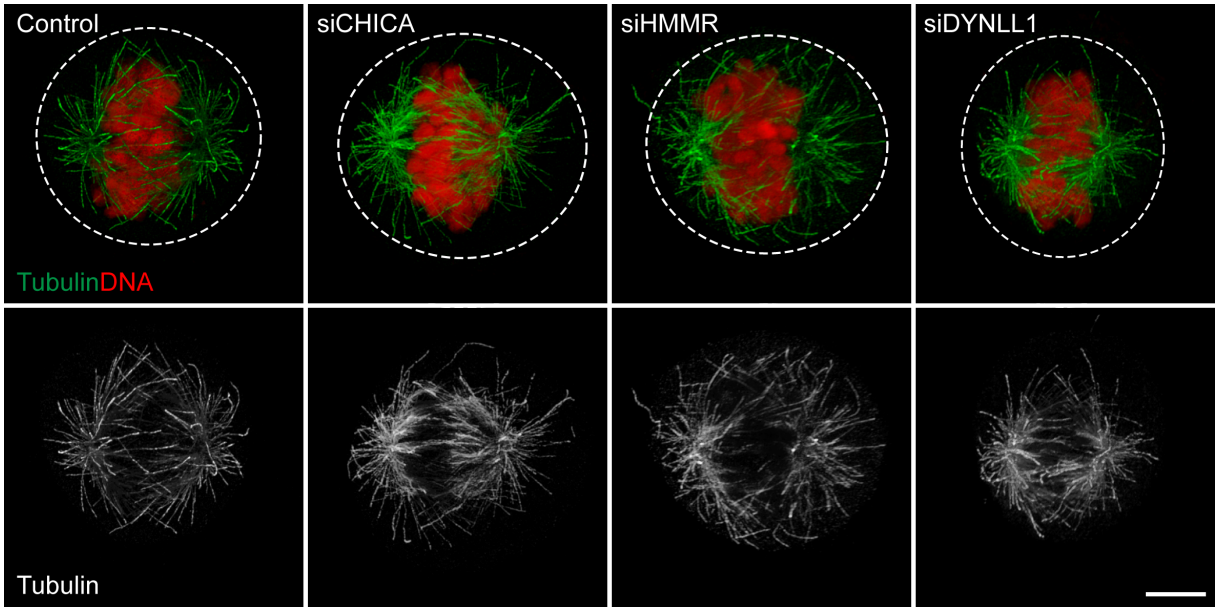


Figure 2.49: Astral microtubules appear unaltered in CHICA-, HMMR- or DYNLL1-depleted cells. HeLa S3 cells were depleted of CHICA, HMMR or DYNLL1 with specific siRNA duplexes for 72 h, cells were fixed and stained with antibodies towards tubulin. Imaging was performed using super-resolution structured illumination microscopy in collaboration with Dr. Lothar Schermelleh. DNA was visualised with DAPI. Scale bar, 5 μm.

These results suggest that the observed spindle rotation phenotype is unlikely due to impaired astral microtubules. To further strengthen this idea, spindle phenotypes caused by altered astral microtubule dynamics were investigated. It has been shown that low concentrations of the microtubule destabilising drug nocodazole specifically disrupt astral microtubule formation. Cells treated with 6.25 ng/ml nocodazole showed rotated spindles that were mainly off-center and localised close to the cell cortex (Figure 2.50 A, page 91). Due to the altered microtubule dynamics, these spindles were also smaller but they still comprised stable kinetochore fibres that captured and aligned the chromosomes. In contrast to this, loss of CHICA, HMMR or DYNLL1 caused spindles to acquire a random rotation, but the spindles were typically centred within the cell (Figure 2.50 B, page 91).

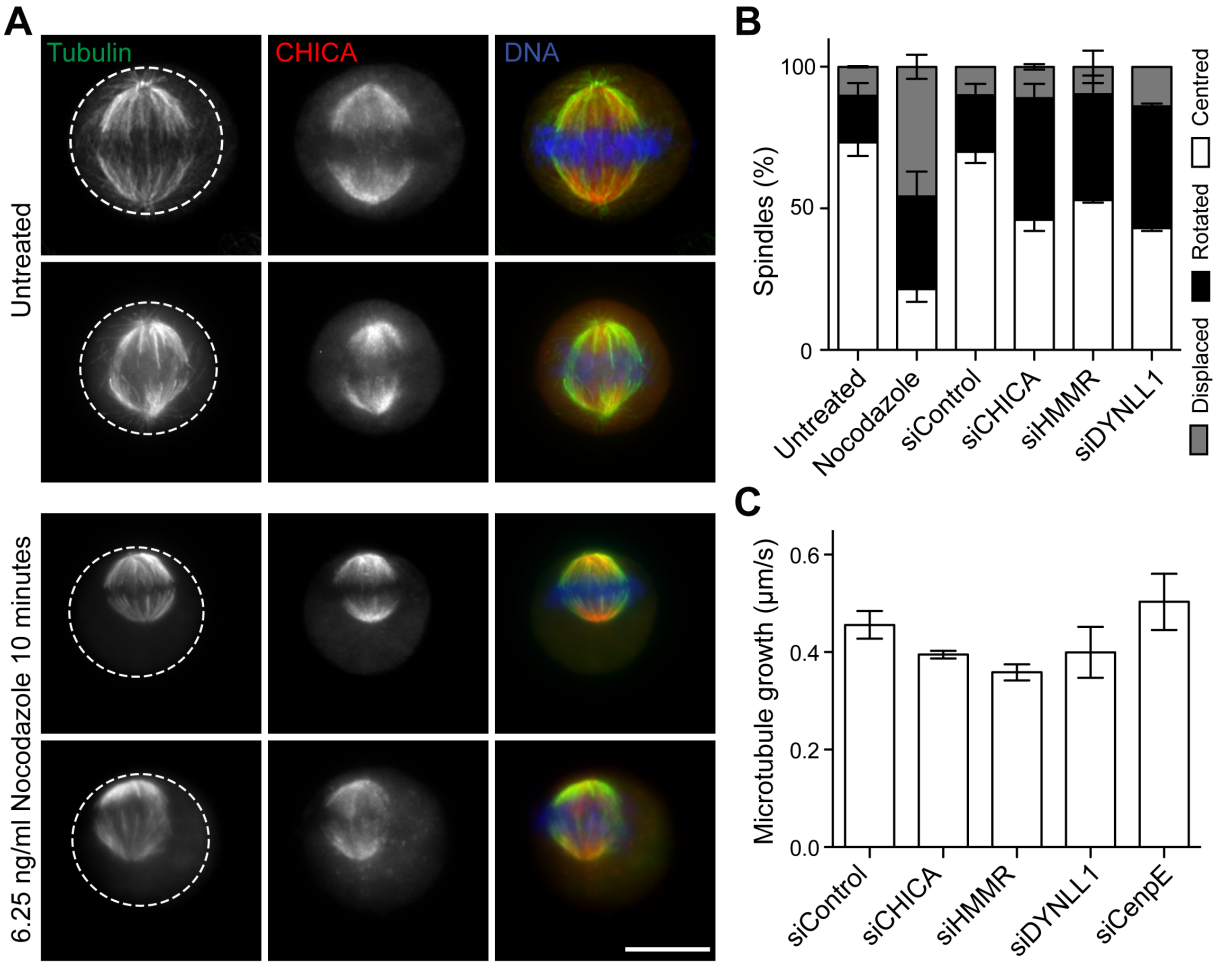


Figure 2.50: Astral microtubule dynamics seem unaltered in CHICA-, HMMR- or DYNLL1-depleted cells. (A) HeLa S3 cells were mock treated or treated with 6.25 ng/ml nocodazole for 10 min. Cells were fixed and stained for tubulin and CHICA. DNA was visualised with DAPI. Scale bar represents 10 μm. (B) Cells treated as in A) or treated with siRNA duplexes targeting CHICA, HMMR or DYNNL1 for 72 h were fixed and stained with tubulin. The spindle position in these cells was determined and is plotted in the graph. (C) HeLa cells stably expressing EB1-mCherry were transfected with control, CHICA, HMMR, DYNLL1 or CenpE (48 h) siRNA duplexes for 72 h. Cells were imaged at 0.87 frames per second at four z-planes positioned at the cell equator to cut through both poles. EB1 comets marking growing microtubule plus ends were identified and the mean distance moved per time unit was used to calculate the microtubule growth rate, which is plotted in the graph. Error bars indicate the standard error of the mean.

Moreover, astral microtubule dynamics were analysed using the microtubule plus end tracking protein EB1 as a marker for growing microtubules. This revealed that microtubules in CHICA-, HMMR- or DYNLL1-depleted cells grew at the same rate of about 0.39 ± 0.05 μm/s, which was similar to the rate observed in control cells and was consis-

tent with my previous findings on EB1 plus end tracking velocities (Figure 2.23, page 61 and 2.50 C, page 91). These findings strongly support the idea, that the spindle rotation observed upon loss of the DYNLL1-CHICA-HMMR complex was not due to altered astral microtubule stability and dynamics. Additionally, the results show that astral microtubules play two roles in spindle positioning. They position the spindle within the centre of the cell and also apply forces onto the spindle during spindle rotation. While low doses of nocodazole disrupt both functions of astral microtubules, loss of the DYNLL1-CHICA-HMMR complex has no effect on spindle centering. Therefore, the DYNLL1 complex controls spindle rotation by means different from regulating astral microtubule dynamics.

My previous results revealed that HMMR binds microtubules and targets CHICA to the mitotic spindle, where it is required to establish correct spindle orientation. Thus, the molecular function of the interaction of this CHICA-HMMR complex with DYNLL1 was analysed futher.

2.10. CHICA binds DYNLL1 via three TQT motifs in its C-terminus

A series of elegant studies identified a binding motif for the DYNLL1 protein defined by a highly conserved TQT motif (Rapali *et al.*, 2011a). Inspection of the CHICA sequence revealed the presence of three consensus TQT motifs. Western blot analysis of immunoprecipitations of CHICA fragments showed that DYNLL1 was present in pull-downs of full-length CHICA or the C-terminal fragment (aa 383-615) containing all three TQT motifs (Figure 2.51 A, page 93).

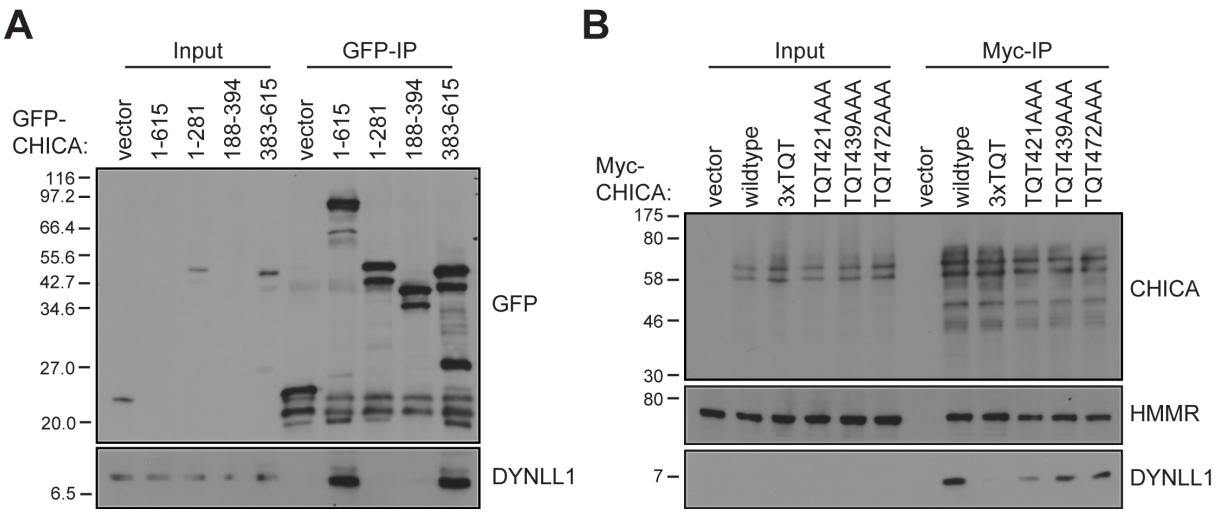


Figure 2.51: Mutation of TQT motifs in CHICA abolished interaction with DYNLL1. (A) GFP-CHICA fragments were transiently transfected into HEK 293T cells for immune precipitations. Cells were synchronised in mitosis by addition of 10 μM STLC for 14 h after 24 h of transfection. The cells were then harvested and lysed, and anti-GFP immunoprecipitations were performed. Western blots were probed as indicated. (B) Wild-type Myc-CHICA, single or triple CHICA TQT mutant constructs were transiently transfected into HEK 293T cells for immune precipitations. Cells were arrested, harvested and lysed as in A). Anti-Myc immunoprecipitations were performed. Western blots were probed as indicated.

DYNLL1 was not detected in precipitations of the other CHICA fragments tested. The TQT residues of these three motifs were then mutated to alanine, alone or in combination, to define their role in mediating the CHICA-DYNLL1 interaction. Whereas mutation of each one of the TQT motifs reduced the amount of DYNLL1 precipitated with CHICA, only mutation of all three TQT motifs completely abolished the interaction of CHICA with DYNLL1 (Figure 2.51 B, page 93). This supports the idea that CHICA interacts with DYNLL1 via all three C-terminal TQT motifs.

Next, it was tested whether this TQT-mediated interaction was required for proper spindle localisation of DYNLL1 and for function of the complex in spindle orientation. To this end, endogenous CHICA was depleted using siRNA duplexes targeting the 3' UTR of the gene, and wild-type CHICA or the 3x TQT to AAA mutant construct were transfected into these cells. While ectopical expression of wild-type CHICA could rescue

the depletion phenotype and restored DYNLL1 targeting to the mitotic spindle as well as alignment of the spindle, the triple TQT mutant was not able to target DYNLL1 onto the spindle or to correct the spindle rotation defect (Figure 2.52, page 94).

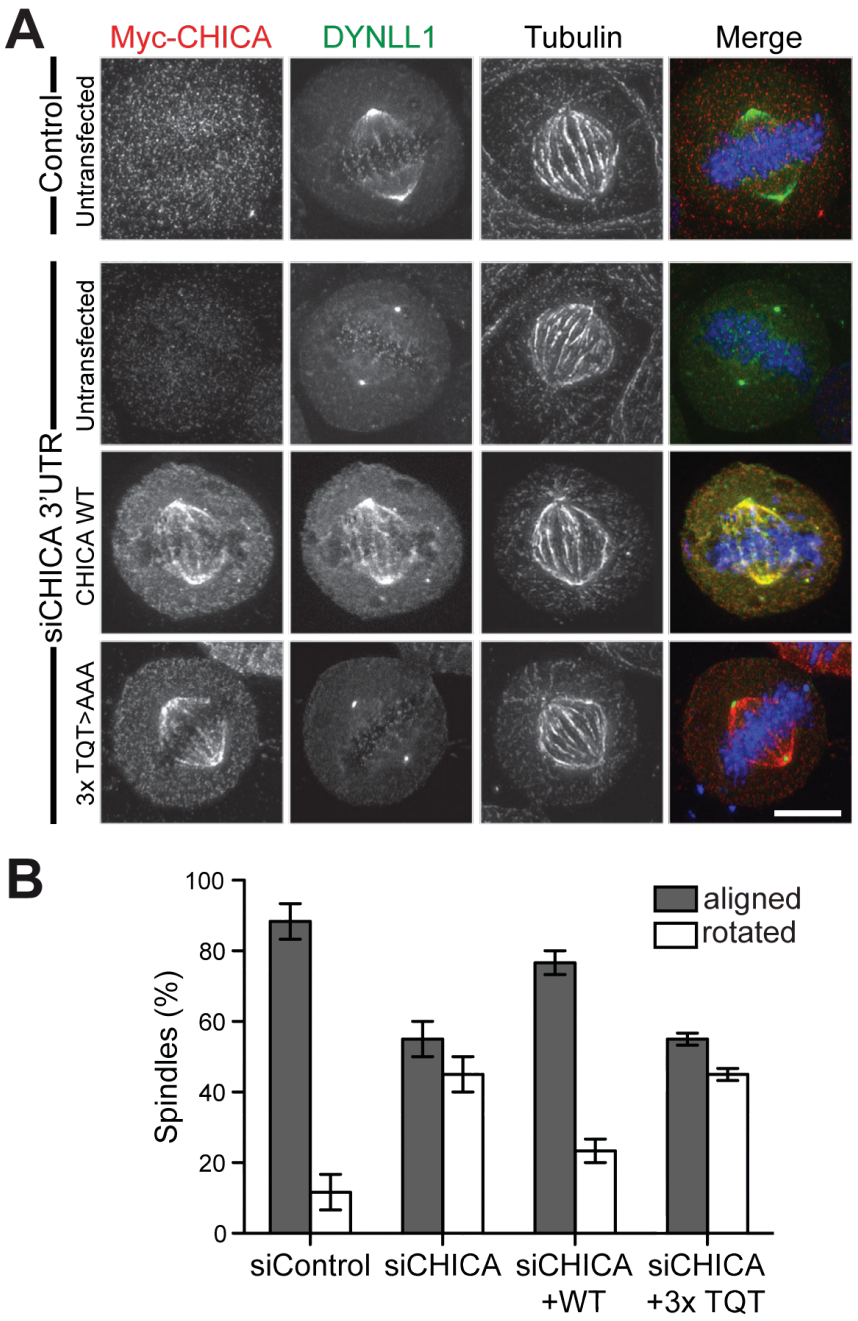


Figure 2.52: CHICA binding to DYNLL1 is required for proper spindle orientation. (A) HeLa cells stably expressing GFP-DYNLL1 were treated with control siRNA or duplexes targeting the 3' UTR of CHICA for 72 h. CHICA-depleted cells were transfected with wild-type or 3x TQT to AAA mutant Myc-CHICA for 36 h. Cells were fixed and stained with antibodies to Myc and tubulin. DYNLL1 was visualised using GFP fluorescence. DNA was stained with DAPI. Scale bar, 10 μm. (B) The percentage of cells with aligned or rotated spindles is plotted in the graph. Error bars represent the standard error of the mean.

These findings support the notion that DYNLL1 is recruited onto the spindle via TQT-mediated binding to CHICA, where it is required to establish the correct spindle orientation.

2.11. Asymmetric localisation of cortical dynein requires the DYNLL1-CHICA-HMMR complex

Spindle orientation is established by a balance of forces between growing astral microtubules pushing against the cell cortex and cortical dynein pulling on these microtubules. I have shown here that altered astral microtubules can not explain the spindle orientation defects observed in CHICA-, HMMR- or DYNLL1-depleted cells. Therefore, the involvement of cortical dynein was investigated in more detail. Kiyomitsu *et al.* have shown that an inhibitory signal emitted from spindle pole localised Plk1 disrupts the interaction between cortical NuMA and dynein, which results in dynein accumulation only at the side of the cortex that is farthest from the spindle (Kiyomitsu and Cheeseman, 2012). One possibility was that CHICA-HMMR forms part of the pathway controlling dynein asymmetry at the cell cortex.

To test this idea dynein was visualised using HeLa cells stably expressing GFP-tagged dynein heavy chain. As expected, in more than 60% of control cells dynein heavy chain was found asymmetrically localised on the one cell pole that was farthest away from the spindle (Figure 2.53, page 96). However, depletion of CHICA, HMMR or DYNLL1 resulted in a loss of this asymmetry and dynein heavy chain was found at both cell poles or in multiple smaller patches at the cell cortex (Figure 2.53, page 96). Depletion of the kinetochore fibre protein HURP did not affect the cortical localisation of dynein heavy chain confirming that the phenotype is specific for loss of the DYNLL1-CHICA-HMMR complex.

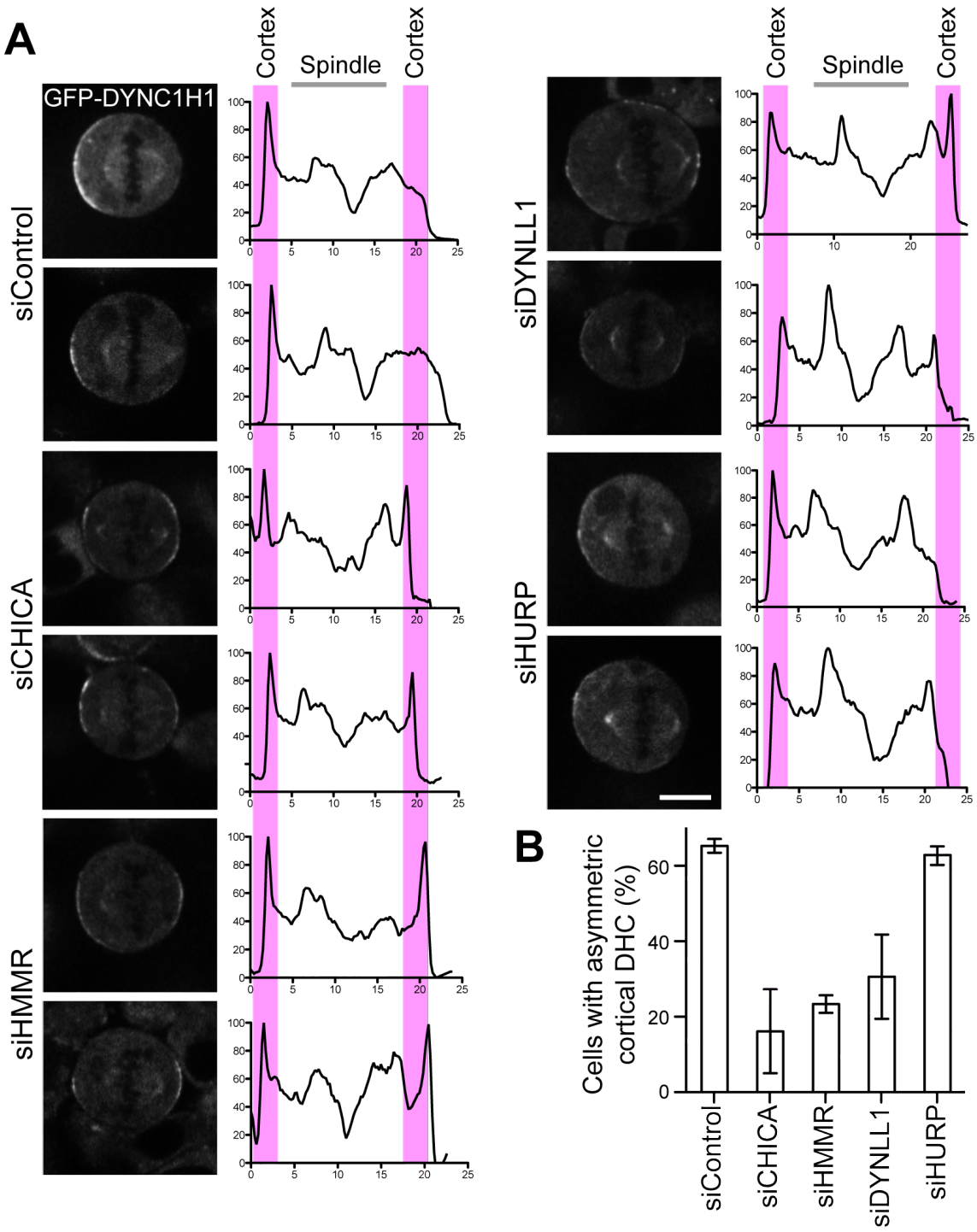


Figure 2.53: Asymmetric distribution of cortical dynein is lost in CHICA-, HMMR- or DYNLL1-depleted cells. (A) HeLa Kyoto cells stably expressing GFP-tagged dynein heavy chain were treated with control siRNA or duplexes targeting CHICA, HMMR, DYNLL1 or HURP for 72 h. Images of metaphase cells were taken at a single plane and the intensity profile from a 20 pixel-wide bar across both spindle poles was generated with ImageJ. Scale bar, 10 μm. (B) The cortical localisation of dynein heavy chain in the different conditions was scored and is plotted in the graph. Error bars represent the standard error of the mean.

Dynein is recruited to the cortex by interaction with NuMA. A spindle pole derived gradient of Plk1 inhibits this interaction at the cortical pole, which is closest to the spindle, resulting in an asymmetric localisation of dynein (Figure 1.7, page 27). This asymmetry is lost in CHICA-, HMMR- and DYNLL1-depleted cells. Therefore, NuMA accumulation at the cell cortex under the same conditions was investigated next. This analysis revealed that NuMA targeting to the cortex was unaltered in CHICA-, HMMR- or DYNLL1-depleted cells when compared to control cells (Figure 2.54, page 97).

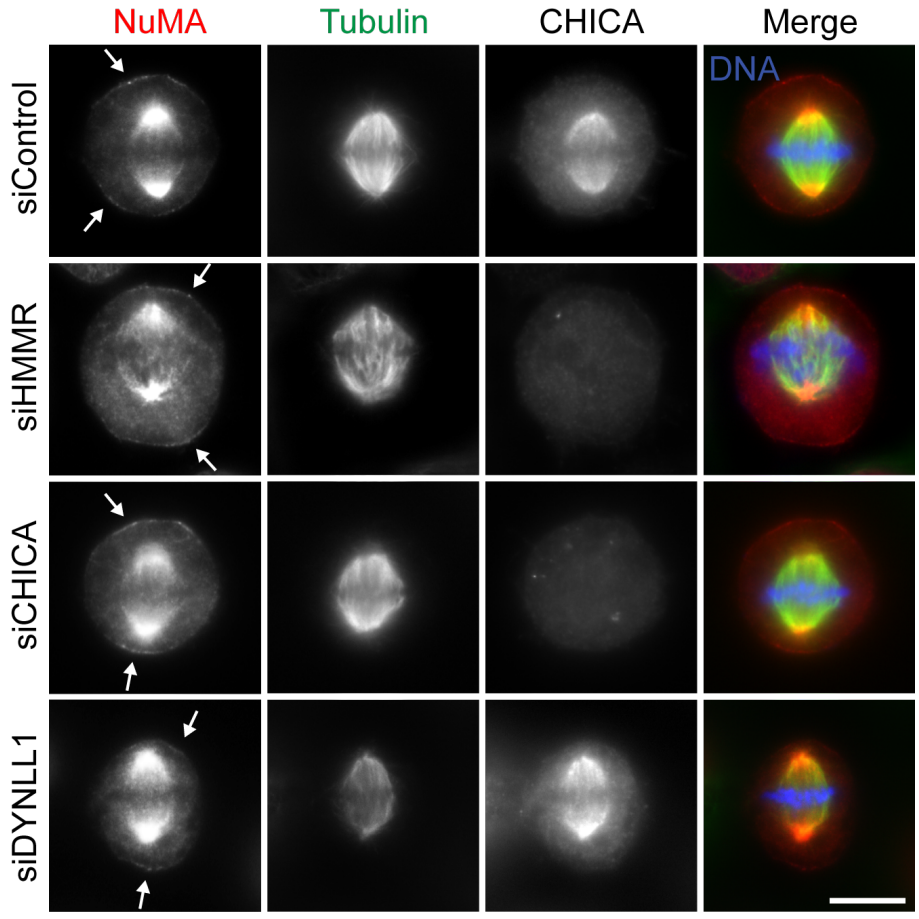


Figure 2.54: Cortical NuMA localisation is unaltered in CHICA-, HMMR- or DYNLL1-depleted cells. HeLa S3 cells were transfected with control siRNA or duplexes targeting CHICA, HMMR or DYNLL1 for 72 h, fixed and stained with antibodies against NuMA, tubulin and CHICA. DNA was visualised with DAPI. Scale bar, 10 μm.

Thus, the DYNLL1-CHICA-HMMR complex does not affect NuMA localisation but rather

negatively regulates dynein targeting to the cortex. To investigate whether the function in asymmetric dynein recruitment is mediated by the interaction of DYNLL1 with CHICA and HMMR at the spindle, dynein localisation was analysed in CHICA TQT-binding mutants. Cells expressing GFP-tagged dynein heavy chain were depleted of endogenous CHICA and transfected with either wild-type mCherry CHICA or the 3xTQT to AAA mutant construct. As observed previously, loss of CHICA impaired dynein asymmetry at the cell cortex (Figure 2.55, page 98).

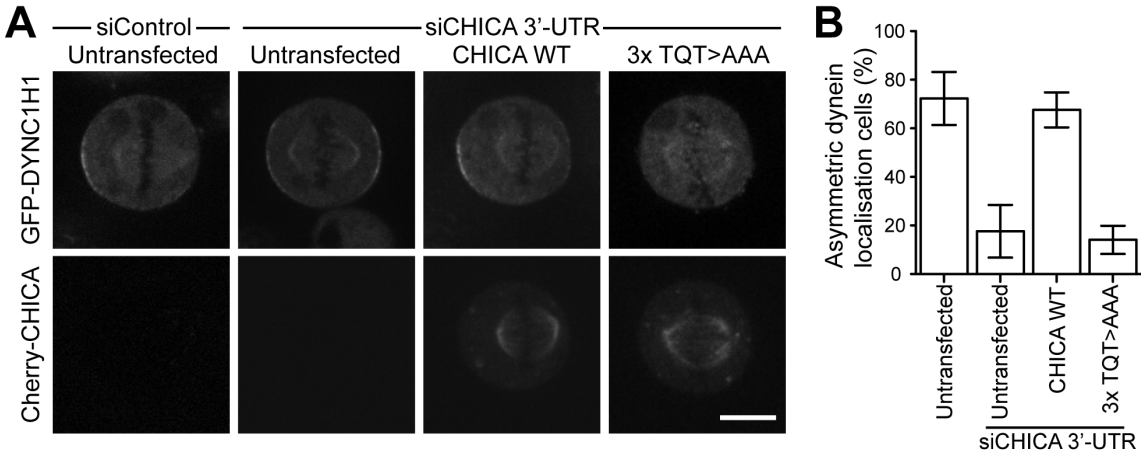


Figure 2.55: CHICA-mediated spindle targeting of DYNLL1 is required to establish cortical dynein asymmetry. (A) HeLa cells stably expressing GFP-tagged dynein heavy chain were treated with control siRNA or duplexes targeting the 3' UTR of CHICA for 72 h. CHICA-depleted cells were transfected with wild-type mCherry-CHICA or 3x TQT to AAA mutant mCherry-CHICA for 36 h. Cells were imaged using a spinning-disk confocal microscope and images were taken at a single focal plane. Scale bar, 10 μm (B) Asymmetric localisation of dynein was scored and is plotted in the graph. Error bars represent the standard error of the mean.

Expression of wild-type CHICA could restore this asymmetry. By contrast, expression of the CHICA TQT-binding mutant was not sufficient to establish asymmetric targeting of dynein. These results suggested that the CHICA-HMMR complex specifically recruits DYNLL1 via TQT-mediated binding to CHICA to the mitotic spindle, where it regulates the cortical localisation of dynein.

2.12. Loss of retraction fibres in CHICA-HMMR-depleted cells

Emerging evidence indicates that retraction fibres attaching the mitotic cell body to the growth surface play a crucial role in spindle orientation by controlling subcortical actin dynamics (Fink *et al.*, 2011). To investigate whether retraction fibres are altered in cells depleted of DYNLL1, CHICA or HMMR, actin localisation was analysed using cells expressing mCherry-tagged LifeAct. Strikingly, in about 60% of HMMR-, CHICA- or DYNLL1-depleted cells, these retraction fibres were lost (Figure 2.56, page 99).

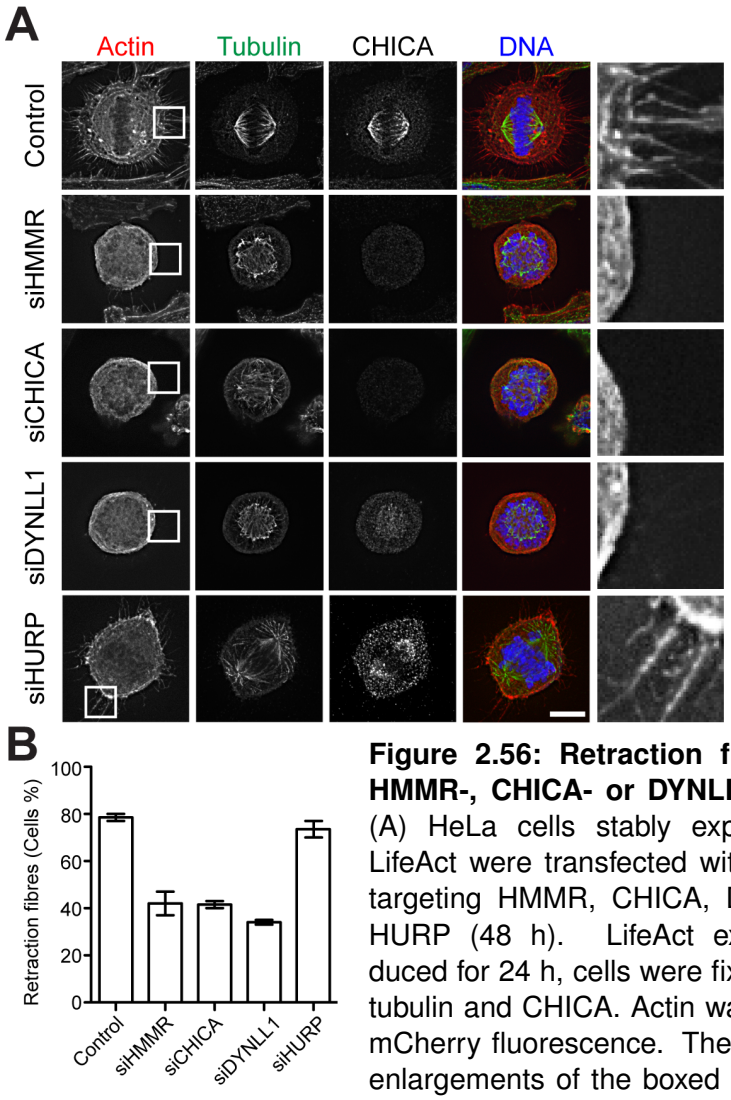


Figure 2.56: Retraction fibres are lost in HMMR-, CHICA- or DYNLL1-depleted cells. (A) HeLa cells stably expressing mCherry-LifeAct were transfected with siRNA duplexes targeting HMMR, CHICA, DYNLL1 (72 h) or HURP (48 h). LifeAct expression was induced for 24 h, cells were fixed and stained for tubulin and CHICA. Actin was visualised using mCherry fluorescence. The right panels show enlargements of the boxed area. Scale bar is 10 μm. (B) The percentage of cells with retraction fibres is plotted in the graph, error bars show the standard error of the mean (n=30).

These results suggested that CHICA-, HMMR- or DYNLL1-depleted cells are either unable to sense their growth surface or the positional information of interphase cells, which regulates actin retraction fibres, is lost when these cells enter mitosis.

I have shown here that CHICA, HMMR or DYNLL1 depletion results in a random spindle rotation accompanied by loss of retraction fibres. However, it is not fully understood how information about the spindle and cell position is communicated between spindle microtubules and membranes or the cell cortex. My results presented here suggest the hypothesis that the DYNLL1-CHICA-HMMR complex plays a major role in this signalling process. Interestingly, analysis of conserved sequences revealed that a CHICA dimer resembles the structure of a phospholipase D family member (Figure 2.57, page 100).

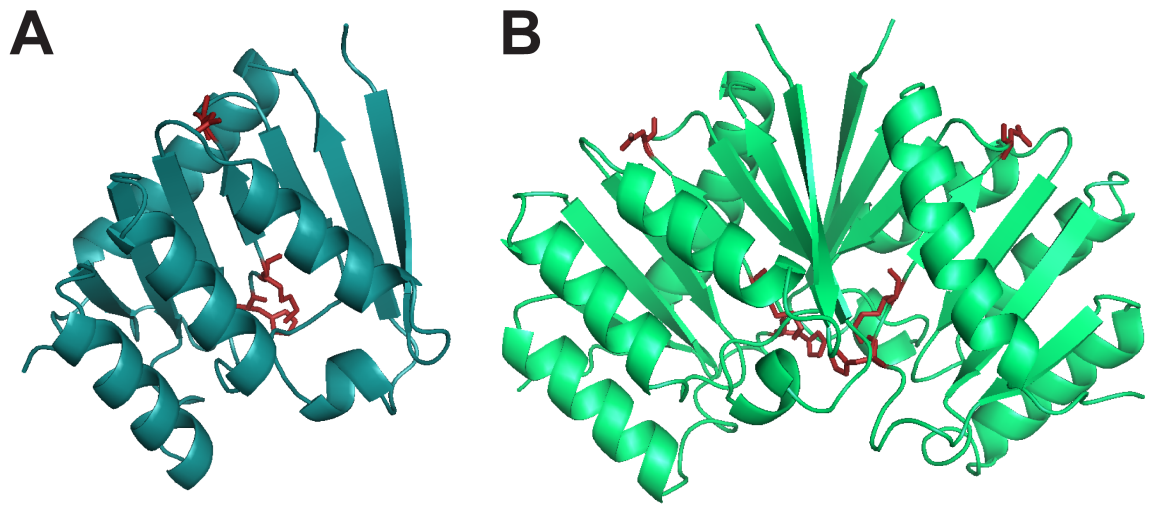


Figure 2.57: CHICA contains a phospholipase D domain. The structure of CHICA aa 165-329 (A) predicted by structure homology search software (Fugue) resembles the enzyme phospholipase D (B). The active site of the enzyme is formed by dimerisation of two phospholipase domains with the residues HxKxxxxD, represented in red, lying at the interface.

The active site of this enzyme family is formed by dimerisation of two phospholipase domains, with the common HxK$[x]_4$D$[x]_6$GSxN motifs of each monomer lying adjacent to one another. These highly conserved catalytic residues are present in CHICA sug-

gesting that CHICA may act as a phosphatase or other hydrolase with its catalytic site formed by dimerisation. To analyse this possible enzymatic function, cell lines inducibly expressing CHICA mutants were generated. Residue H272 was mutated to arginine (H272R mutant) or the histidine, lysine and asparagine residues of the common phospholipase D motif were mutated to alanines (PLD mutant). Preliminary experiments showed that CHICA localises to patches at the cell membrane in interphase cells, which is strongly increased upon mutation of the phospholipase D motif (Figure 2.58, page 101).

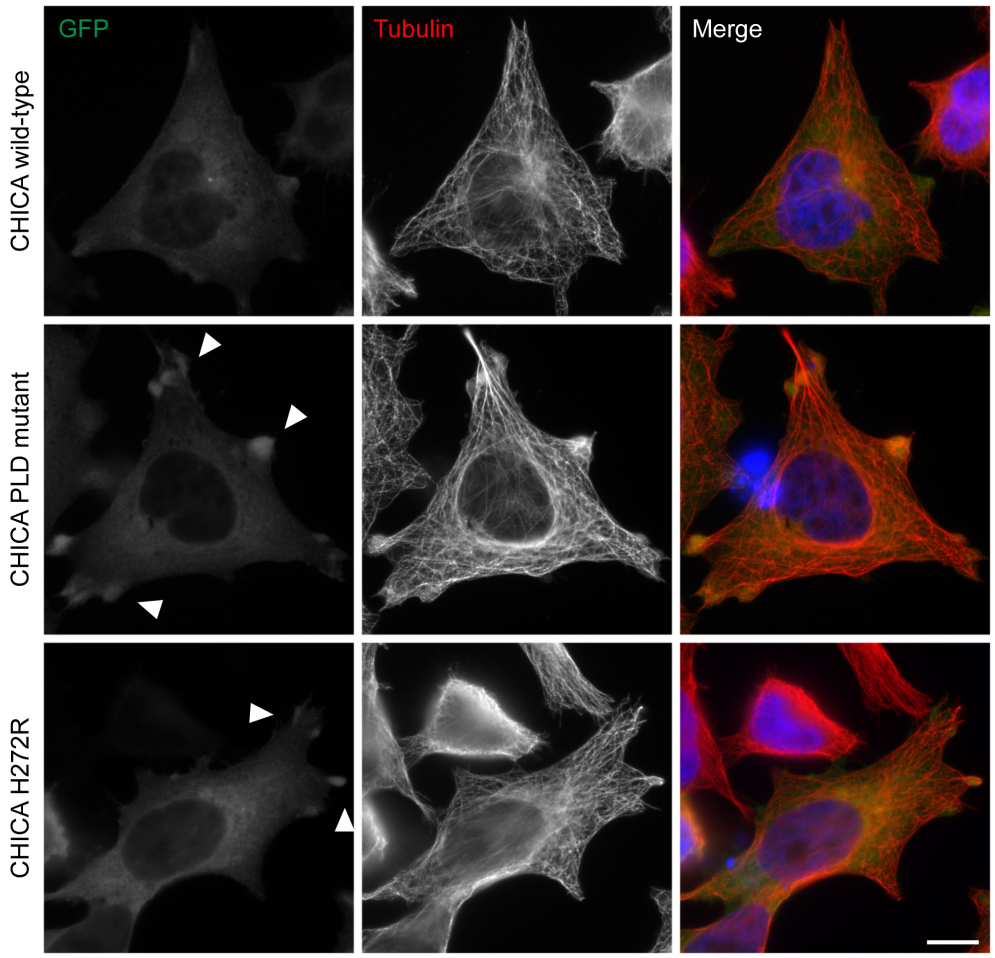


Figure 2.58: CHICA accumulates in cortical patches. HeLa cells stably expressing GFP-tagged wild-type, PLD mutant or H272R CHICA were treated with siRNA targeting the 3'UTR of CHICA for 72 h, and expression of the transgene was induced with 1 μg/ml of doxycycline for 16 h. Cells were fixed and stained with antibodies to tubulin. CHICA was visualised using GFP fluorescence. DNA was stained with DAPI. Scale bar, 10 μm.

This suggests that CHICA localises to the cell cortex, where its enzymatic activity acts on cortical structures. One possibility is that CHICA might be a phosphatase acting on phospholipids, promoting lipid signalling from the cell membrane. However, further experiments using pure preparations of CHICA, ideally in complex with HMMR, are required to investigate the possible enzymatic function of CHICA.

3. Discussion

In the present study, a combined approach of specific immunoprecipitations and mass spectrometry was used to identify DYNLL1 interaction partners in mitosis. DYNLL1 defines a subset of complexes in mitotic cells including the Astrin-Kinastrin complex and the CHICA-HMMR complex. Biochemical analysis indicates that these are discrete complexes, and immunopurification of HMMR and CHICA revealed that these proteins are associated with DYNLL1 but not Astrin or Kinastrin. Furthermore, the two complexes differ in their spatial localisation (Figure 3.1, page 103). Astrin and Kinastrin recruit DYNLL1 to the kinetochores, whereas HMMR and CHICA are required for spindle microtubule targeting of DYNLL1 (Figure 3.1, page 103).

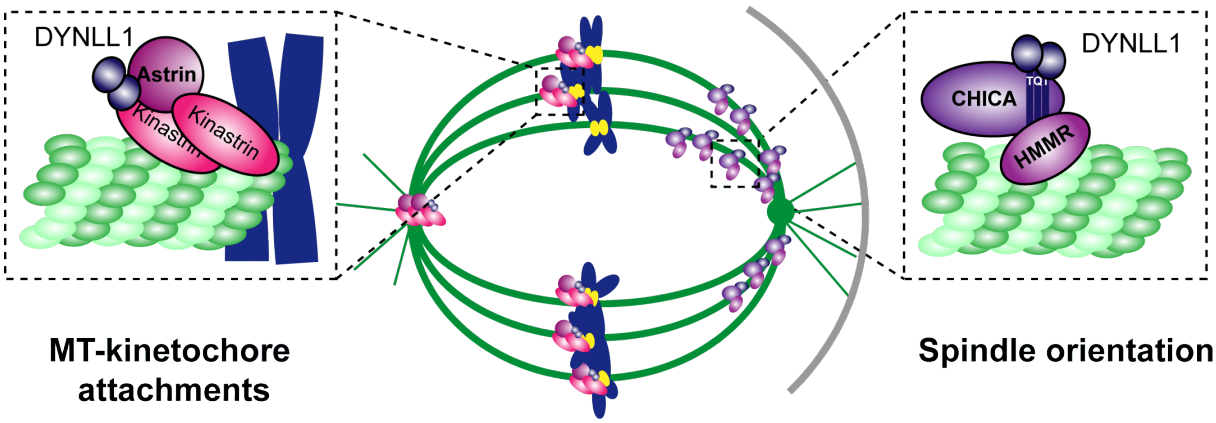


Figure 3.1: Model of DYNLL1 complexes.
DYNLL1 is recruited to the kinetochores by the Astrin-Kinastrin complex, whereas spindle localisation is dependent on TQT-mediated interaction with the CHICA-HMMR complex.

Here, Kinastrin (C15orf23) has been identified as the major interaction partner of Astrin (Dunsch *et al.*, 2011). I have shown that the spindle and kinetochore localised Astrin-Kinastrin complex tracks microtubule plus ends and is required to form stable microtubule-kinetochore attachments. Depletion of Kinastrin results in the same phenotype as loss of Astrin, namely chromosome segregation defects, untimely sister chromatid separation and multipolar spindles caused by prematurely disengaged

centrioles (Dunsch *et al.*, 2011). This untimely sister chromatid separation and centriole splitting presumably results from premature activation of separase due to a loss of inhibition by cyclin B. Interestingly, overexpression of Kinastrin displaces Astrin from the spindle, giving rise to the same defects as depletion of Astrin or Kinastrin. Thus, Kinastrin is targeting Astrin to the spindle and proper Astrin localisation is required for the function of the complex.

In the second part of this work, the novel DYNLL1-CHICA-HMMR complex was identified and characterised. The results presented here show that CHICA interacts with DYNLL1 via conserved TQT motifs in its C-terminal region. Moreover, CHICA was found to interact with HMMR, which targets the DYNLL1-CHICA complex to the mitotic spindle, where it is required for correct spindle orientation by regulating dynein accumulation at the cell cortex.

Analysis of mitotic DYNLL1 complexes by mass spectrometry has revealed that DYNLL1 forms multiple subcomplexes at the mitotic spindle, which are devoid of dynactin (Table 2.1, page 34). These findings support the notion that DYNLL1 acts as a regulatory hub protein, involved in various biological processes, independent of complex formation with dynein-dynactin (Barbar, 2008; Pfister *et al.*, 2006). This diverse network of interaction partners suggests that DYNLL1 plays a more general role than dynein itself and raises the question whether DYNLL1 represents a real dynein light chain. DYNLL1 may act similar to 14-3-3 proteins, which interact with diverse phosphorylated proteins and regulate multiple signalling networks (Bustos, 2012). Both, 14-3-3 and DYNLL1 assemble into homodimers with each monomer containing a ligand binding motif (Bustos, 2012). The dimer can therefore interact with two binding partners simultaneously and may thereby integrate signals from several complex components. Interestingly, the DYNLL1 interactors DYNC1I2, Astrin, Nek9 and CHICA are neither structurally, nor

functionally related, an aspect shared by 14-3-3 binding partners (Bustos, 2012). 14-3-3 proteins bind multiple structurally disordered and phosphorylated partners, which makes them a typical example of the 'many-to-one signalling network'. There, disordered regions with different sequences use their flexibility to bind to a common binding site on 14-3-3 proteins (Dunker *et al.*, 1998). Similarly, structurally different DYNLL1 interactors containing the TQT motif may associate with the TQT-binding site on DYNLL1.

3.1. Formation of stable microtubule-kinetochore attachments by the Astrin-Kinastrin complex

The findings presented here suggest that the microtubule plus end tracking Astrin-Kinastrin complex accumulates at the kinetochores upon attachment and then in turn stabilises the associated K fibre microtubules. In support of my findings, an independent study published while this work was conducted also described an interaction between Astrin and Kinastrin (Schmidt *et al.*, 2010). In agreement with the present and previous studies, the authors also observed chromosome alignment defects, a SAC-dependent arrest and a significant reduction in kinetochore fibre stability in prometaphase in the absence of the Astrin-Kinastrin complex (Dunsch *et al.*, 2011; Manning *et al.*, 2010; Schmidt *et al.*, 2010; Thein *et al.*, 2007). Recently, Schmidt *et al.* have shown that Aurora B inhibition promotes Astrin-Kinastrin targeting to the kinetochores, and they therefore suggested that Aurora B activity regulates kinetochore localisation of the complex (Schmidt *et al.*, 2010). However, Astrin does not appear to be a direct substrate of Aurora B and the effect is most likely indirect. Previously, Astrin was shown to exclusively localise to kinetochores of attached chromosomes (Thein *et al.*, 2007). As described in section 1.4, Aurora B senses and dissolves erroneous, syntelic attachments (Welburn *et al.*, 2010). Inhibition of Aurora B therefore will generate more attachments, simply increasing binding sites for the Astrin-Kinastrin complex. This re-

sults in an apparent recruitment of the complex to these kinetochores, independent of a direct interaction between Astrin and Aurora B.

Moreover, it has been proposed that Astrin forms a complex with CLASP1 at the kinetochore to suppress microtubule turnover (Manning *et al.*, 2010). In support of this notion, it has been shown that CLASP1 is lost from kinetochores in Astrin-depleted cells (Schmidt *et al.*, 2010). The Astrin-CLASP1 complex was suggested to stabilise attachments and thereby promote SAC silencing (Manning *et al.*, 2010). However, Astrin complexes purified in this study were devoid of CLASP1 (Table 2.2, page 38) and CLASP1 depletion did not interfere with Astrin localisation at the kinetochores (Dunsch, 2010). Therefore, the stabilising function of Astrin and CLASP1 at attached microtubules likely represents a synergistic co-operative function of two plus end tracking proteins, rather than a direct interaction.

Similar to Astrin and Kinastrin, the Ska complex comprising Ska1, Ska2 and Ska3 targets to the mitotic spindle and kinetochores and is required for stable microtubule kinetochore attachments (Hanisch *et al.*, 2006; Gaitanos *et al.*, 2009; Theis *et al.*, 2009). Interestingly, kinetochore targeting of the Ska complex is negatively regulated by Aurora B (Chan *et al.*, 2012). Aurora B-mediated phosphorylation of Ska1 and Ska3 disrupts the interaction between the Knl1, Mis12, Ndc80 (KMN) network members Mis12 and Hec1 and the Ska complex, and thus prevents Ska accumulation at the kinetochore (Chan *et al.*, 2012). Once sister chromatids are bi-oriented and tension is generated, the KMN and Ska complex are dephosphorylated and the Ska complex targets to the kinetochores, where it supports the stabilisation of attachments. Loss of Ska3, reminiscent of Astrin or Kinastrin depletion, results in a SAC-dependent mitotic arrest accompanied by premature sister chromatid separation (Daum *et al.*, 2009; Theis *et al.*, 2009). Thus, it was suggested that the Ska complex couples sensing of stable attachments with SAC silencing and timely cohesion release. Although no direct interaction between the Astrin-Kinastrin and the Ska complex has been detected (Ta-

ble 2.2, page 38), it may be interesting to analyse the potential functional interplay in stable kinetochore attachment formation between both complexes.

Recently, Kinastrin has been reported to interact with CenpE (Huang *et al.*, 2012). This interaction was proposed to aid the establishment of microtubule kinetochore attachments by linking the kinetochore component CenpE to spindle microtubules via the microtubule-binding protein Kinastrin (Huang *et al.*, 2012). However, I did not observe a direct interaction between Kinastrin and CenpE (Table 2.2, page 38). Nonetheless, my results propose that Kinastrin does stabilise microtubule kinetochore attachments independent of CenpE by directly promoting microtubule polymerisation. Several modes of action are conceivable. Kinastrin might promote polymerisation similar to TOG proteins, which associate with microtubule ends and bind free α/β-tubulin heterodimers via their TOG domains, thereby delivering tubulin subunits to growing microtubule plus ends (Al-Bassam *et al.*, 2006). On the other hand, Kinastrin could play a more indirect role in promoting microtubule polymerisation and *in vivo* additional factors are recruited to the end of microtubules, where they build a platform for polymerisation.

3.2. Plus end tracking behaviour of the Astrin-Kinastrin complex

The Astrin-Kinastrin complex was shown to track microtubule plus ends (Dunsch *et al.*, 2011), which places the complex in a good position to stabilise kinetochore fibres. However, it needs to be kept in mind that these movements do not reflect actual transport of the protein, but rather binding and dissociation at growing microtubule plus ends with a high turnover (Bieling *et al.*, 2008). An interaction with dynein, a minus-end directed motor protein, mediated by binding to the dynein light chain DYNLL1 might facilitate the transport of factors from the microtubule plus ends to the spindle poles and thereby may promote chromosome congression, attachment and spindle checkpoint regulation. Based on the plus end tracking behaviour of Astrin and Kinastrin, the complex can be

classed into the group of +TIP proteins, which are factors that form comet-like structures at the growing microtubule ends and regulate microtubule dynamics, stability or interactions (Schuyler and Pellman, 2001). The family of +TIPs is growing steadily and currently more than 20 +TIPs have been identified (Akhmanova and Steinmetz, 2010). Within the group of +TIPs, the end binding (EB) proteins are able to autonomously associate with the plus ends, whilst all other +TIPs bind to these EB proteins in order to track the microtubule tips. During microtubule polymerisation, the α- and β-tubulin monomers bind GTP. When the tubulin subunits are incorporated into the microtubule lattice, the GTP is hydrolysed to GDP. However, microtubule growth at the plus end is faster than GTP hydrolysis, resulting in a cap of GTP-tubulin at the plus end. The EB proteins recognise that plus end cap by sensing the state of the guanine nucleotide associated with the tubulin monomers (Maurer *et al.*, 2011). Since GTP is hydrolysed over time as the microtubule matures, the EBs bind to and dissociate from the microtubule tips rapidly and have a dwell time at the plus end of less than 1s (Dragestein *et al.*, 2008; Dixit *et al.*, 2009). As mentioned previously, most other +TIPs associate with the microtubule plus ends via interaction with EB proteins. Interestingly, Kinastrin contains a hydrophobic (S/T)xLP sequence motif, a common motif in EB-binding proteins, e.g. CLASPs or MCAK (Kumar and Wittmann, 2012). EB family proteins bind this motif via two hydrophobic grooves in their C-terminus and specifically associate with the growing microtubule ends by recognising a conformational change in β-tubulin after GTP hydrolysis (Kumar and Wittmann, 2012). Preliminary experiments indicate that Kinastrin interacts specifically with EB1 (Figure 2.29, page 68). Further analysis of this interaction and its effect on microtubule dynamics will be an intriguing future objective. Additionally, Kinastrin has been shown to directly bind to microtubules (Schmidt *et al.*, 2010; Huang *et al.*, 2012), which is a common feature among +TIPs. Binding to EB proteins recruits these +TIPs to the microtubule plus ends, where they establish direct lateral and end-on attachments with microtubules thereby increasing

their residence time at the plus ends, which may even exceed that of the EB proteins themselves (Galjart, 2010). Consistent with this idea, it has been observed that the targeting of many +TIPs to the plus end does not exactly correlate with EB localisation. EB1 is often found more abundant at the distal tip, whereas other +TIP proteins are localised more proximally (Slep *et al.*, 2005), which is in agreement with the observations of this study (Figure 2.24, page 62). It has been suggested that EB1 binding at the very end masks binding sites for other +TIPs. As the microtubule matures and EB1 binding decays, more binding sites will become available and +TIPs become enriched at sites proximal to EB1. Interestingly, it has been shown that the EB1-SxIP interaction is negatively regulated by phosphorylation (Honnappa *et al.*, 2009). Therefore, future studies on plus end tracking of Kinastrin could analyse whether a SxLP motif-mediated binding of Kinastrin is also phospho-regulated.

3.3. Loss of the Astrin-Kinastrin complex induces untimely separase activation

Consistent with the findings presented here, an independent study has shown that Kinastrin localises to the mitotic spindle and kinetochores and that depletion of Kinastrin causes a metaphase arrest with multipolar spindles, followed by chromosome segregation defects (Fang *et al.*, 2009). Based on BubR1 intensity measurements and analysis of separase auto-cleavage, the authors suggested that loss of Kinastrin does not activate the SAC, and delays separase activation. These reported findings contradict the results of this study. Closer examination of the data, however, supports the idea of a SAC-dependent cell arrest and premature separase activation, and the apparent discrepancies can be accounted for by the use of different points of reference. Fang *et al.* determined BubR1 and Mad2 signal intensity in control and Kinastrin-depleted cells for prometaphase and metaphase kinetochores and concluded that there is no

alteration (Fang *et al.*, 2009). In contrast, comparison with signal intensity at anaphase kinetochores showed that the SAC is still activated and BubR1 and Bub1 levels were sufficient to halt mitotic progression (Figure 2.13, page 49). Separase activation was evaluated by Western blotting of separase auto-cleavage fragments. The authors argued that separase activation is delayed compared to control cells (Fang *et al.*, 2009). However, in light of the intensity measurements regarding SAC arrest, it is feasible to suggest that Kinastrin-depleted cells are still SAC arrested and activation of separase is therefore premature, which supports the findings presented here.

In Astrin- or Kinastrin-depleted cells, a fraction of separase is activated, presumably due to the loss of inhibition by cyclin B. This results in premature sister chromatid separation and centriole disengagement generating multipolar spindles. As described previously, depletion of Ska3 also causes centriole splitting and loss of chromatid cohesion (Theis *et al.*, 2009). An involvement of separase in the development of the Ska3 depletion phenotype has not been analysed. Nevertheless, it was shown that Ska3 accumulation at the kinetochores is dependent on Sgo1, which places Ska3 downstream of Sgo1 (Daum *et al.*, 2009). In contrast, no direct interaction between the Astrin-Kinastrin complex and Sgo1 was detected (Table 2.2, page 38) and Sgo depletion appears not to interfere with Kinastrin recruitment to the kinetochore (Figure 2.19, page 57), supporting the idea that Astrin-Kinastrin targeting to the kinetochore is Sgo-independent.

In future experiments, the spatial and temporal activation of separase in Astrin- or Kinastrin-depleted cells could be analysed using a biosensor for separase activity. In budding yeast, a fusion protein containing an internal fragment of Scc1 inserted between a GFP tag and a specific chromosome locus was generated to measure separase activation as well as the kinetics and timings of cohesion cleavage (Yaakov *et al.*, 2012). Expression of a Scc1-fragment comprising the separase cleavage sites between a fluorophore and a marker protein of known localisation combined with live cell

imaging of human cells could provide a detailed picture of where and when separase gets activated in Astrin- or Kinastrin-depleted cells (Shindo *et al.*, 2012). Whilst separase is inactive, the fluorophore will be detected at the locus of the marker protein. Upon separase activation, Scc1 will be cleaved and the fluorophore will be diffusely localised in the cytoplasm. Using marker proteins with different localisations, the position of separase activation within the spindle could also be determined. Moreover, ectopic expression of non-cleavable Scc1 subunits combined with depletion of the endogenous protein is an intriguing further objective to strengthen the hypothesis that separase-mediated cleavage of cohesin causes the Astrin- or Kinastrin-depletion phenotype.

It has been reported that prolonged arrest of cells in metaphase induces uncoordinated loss of cohesion and results in sister chromatid separation, a process termed 'cohesion fatigue' (Stevens *et al.*, 2011; Daum *et al.*, 2011). Subsequently, spindle defects including centriole separation were also observed in these cells (Stevens *et al.*, 2011). This loss of cohesion was microtubule-dependent and it has been proposed that centromeric cohesin was unable to resist spindle pulling forces over a prolonged time. Daum *et al.* suggested that the loss of sister chromatid cohesion upon Ska3 depletion is an indirect consequence of metaphase arrest and does not reflect a direct function of the Ska complex in cohesion establishment or maintenance (Daum *et al.*, 2011). Astrin and Kinastrin depletion cause a SAC-dependent arrest in a metaphase-like state. Therefore, the sister chromatid separation observed in these cells could be caused by 'cohesion fatigue'. However, there are several important facts speaking against this hypothesis (Figure 3.2, page 112).

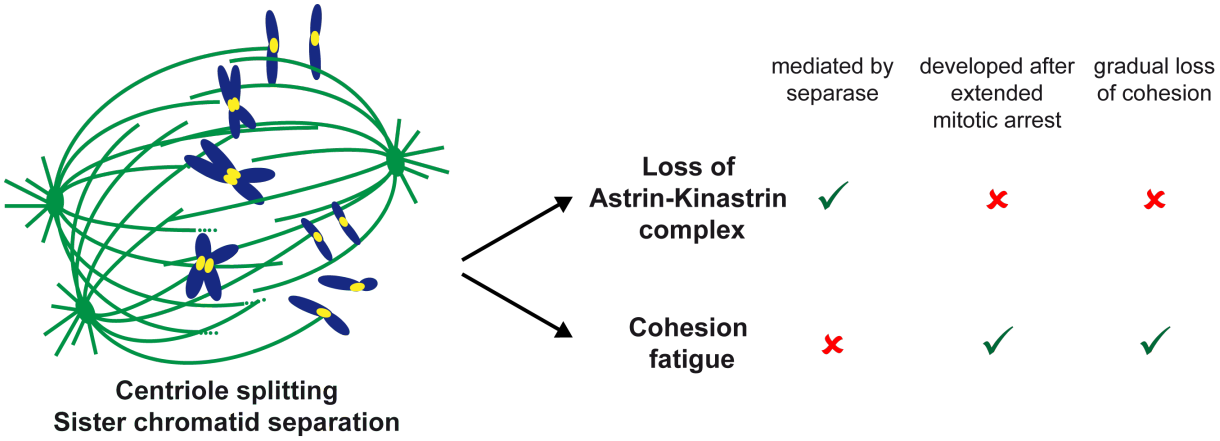


Figure 3.2: Phenotype observed upon loss of the Astrin-Kinastrin complex compared to 'cohesion fatigue'

Firstly, co-depletion of Astrin or Kinastrin and separase significantly reduced the amount of cells with separated sister chromatids suggesting that loss of cohesion in these cells is mediated by separase (Figure 2.20, page 58). In contrast, 'cohesion fatigue' is not blocked by depletion of separase (Daum *et al.*, 2011). Second, 'cohesion fatigue' is a consequence of a metaphase delay induced by drug perturbations and a time-dependent increase in the percentage of cells with single sister chromatids was observed (Daum *et al.*, 2009). Initially, cells aligned their chromosomes at the metaphase plate and the scattering of chromosomes along the mitotic spindle developed over time (Daum *et al.*, 2011; Stevens *et al.*, 2011). Moreover, spindle defects observed in these cells were a secondary consequence of chromosome scattering and altered spindle forces (Stevens *et al.*, 2011). Cells depleted of Astrin or Kinastrin, on the other hand, fail to align their chromosomes at a metaphase plate and often enter mitosis with scattered chromosomes. Additionally, cells overexpressing Myc-Kinastrin, which were not subject to long siRNA treatment, also exhibit multipolar spindle phenotypes and sister chromatid separation (Figure 2.14, page 50), indicating that both phenotypes are a direct consequence of Astrin mislocalisation rather than an indirect effect of prolonged metaphase arrest. Third, chromatid separation induced by 'cohesion fatigue' appeared

to be gradual (Daum *et al.*, 2011). Separation at the centromere precedes, followed by dissociation of chromosome arms. This caused the appearance of intermediate stages where the centromeres were distantly separated, while cohesion at chromosome arms persisted (Daum *et al.*, 2011). It is unclear whether these cells entered mitosis with chromosomes faithfully linked by the cohesin complex or if cohesin loading in S phase was already impaired. This intermediate phenotype has not been observed upon loss of Astrin or Kinastrin. In these cells, all sister chromatids were separated and were neither joined at the centromeres nor at the chromosome arms (Figure 2.16, page 52). Therefore, 'cohesion fatigue' is unlikely to explain the Astrin or Kinastrin depletion phenotypes.

I have shown here that the Astrin-Kinastrin complex associates with microtubule plus ends, participates in the establishment of microtubule kinetochore attachments and the maintenance of sister chromatid cohesion. As suggested for the Ska complex, Astrin and Kinastrin therefore play an important role in coupling stable attachments with silencing of the SAC and cohesion release. The premature sister chromatid separation and centriole splitting observed upon loss of both proteins propose the idea that the Astrin-Kinastrin complex either directly inhibits separase or protects the cohesion at the centromeres and centrosomes until anaphase onset. The localisation of the complex at the spindle poles and kinetochores supports the model of a protective function, rather than an inhibitory role of the cytoplasmic protease separase. Speaking against this is the finding that a fraction of separase is activated upon loss of the complex and that co-depletion of separase reduces the phenotype, arguing for a more direct role in separase inhibition. As explained previously, analysis of timing and localisation of separase activation as well as introduction of non-cleavable cohesin will provide important answers to the question.

3.4. DYNLL1 is recruited to the spindle by the CHICA-HMMR complex

The findings presented here reveal that DYNLL1 is recruited onto the mitotic spindle by the CHICA-HMMR complex, where it regulates mitotic spindle orientation. HMMR can directly bind to microtubules with its N-terminus and associates with CHICA via its C-terminus. CHICA contains three TQT motifs mediating interaction with DYNLL1. Cells depleted of either CHICA, HMMR or DYNLL1 require more time to progress from nuclear envelope breakdown to anaphase consistent with an increase in mitotic index (Figure 2.40, page 80 and Santamaria *et al.*, 2008). These cells exhibit stable bipolar spindles, that are randomly oriented. Emerging evidence has implicated retraction fibres, remnants of interphase cell-substratum adhesions, in spindle positioning and orientation (Théry *et al.*, 2005). In support of this notion, retraction fibres are lost in cells depleted of CHICA, HMMR or DYNLL1 (Figure 2.56, page 99). These results suggest that the position of the mitotic spindle defined by the CHICA-HMMR complex feeds back to the cell cortex in a dynein and DYNLL1 dependant pathway. This is important to stabilise the retraction fibres and allow them to transmit information about the external environment to the spindle. Although a direct interplay between the CHICA-HMMR complex and retraction fibre proteins like actin has not been observed, it is conceivable that the complex employs dynein to signal along astral microtubules to the cell cortex.

The analysis of conserved sequences of the DYNLL1-CHICA-HMMR complex suggests that CHICA might play an additional role at the cell cortex. It has been noted that CHICA dimers resemble the structure of a phospholipase D (PLD) family member (Stuckey and Dixon, 1999). The PLD superfamily includes diverse enzymes like phospholipase D, polyphosphate kinase and the nuclease Nuc. All of them share a common

catalytic mechanism in which the active site of the enzyme is formed by two copies of the signature motif HxK[x]$_4$D[x]$_6$GSxN. These motifs can lie in a single polypeptide or at the interface formed by dimerisation so that the motifs of each monomer lie adjacent to one another (Stuckey and Dixon, 1999). These highly conserved catalytic residues are present in CHICA in a single copy, which suggests that CHICA may act as a phosphatase or other hydrolase with its catalytic site formed by dimerisation. Mutation of the conserved residues and enzyme assays using purified protein will elucidate the interesting possibility of an enzymatic function in CHICA.

3.5. DYNLL1-CHICA-HMMR complexes promote correct spindle orientation

It is important to define the mechanisms controlling spindle orientation and positioning in order to understand mitosis. As outlined in the introduction, the dynein motor plays an essential role in mitosis due to its multiple functions in the formation and positioning of the mitotic spindle. It was shown here that a specific dynein light chain, DYNLL1, is required for a subset of these processes. In DYNLL1-depleted cells, spindle formation proceeds normally but the spindle fails to align with the growth surface. This raises the question how a spindle localised complex can control spindle orientation. DYNLL1, CHICA or HMMR were undetectable at the cell cortex or on astral microtubules. But, remarkably, the asymmetric distribution of dynein at the cell cortex is lost in cells depleted of the complex. It has been demonstrated recently that cortical dynein generates pulling forces on astral microtubules, which drives spindle positioning (Laan *et al.*, 2012). The findings presented here show that DYNLL1 inhibits cortical localisation of dynein and that DYNLL1 plays an important role in the intrinsic spindle positioning pathway similar to Plk1 (Figure 3.3, page 116) (Kiyomitsu and Cheeseman, 2012).

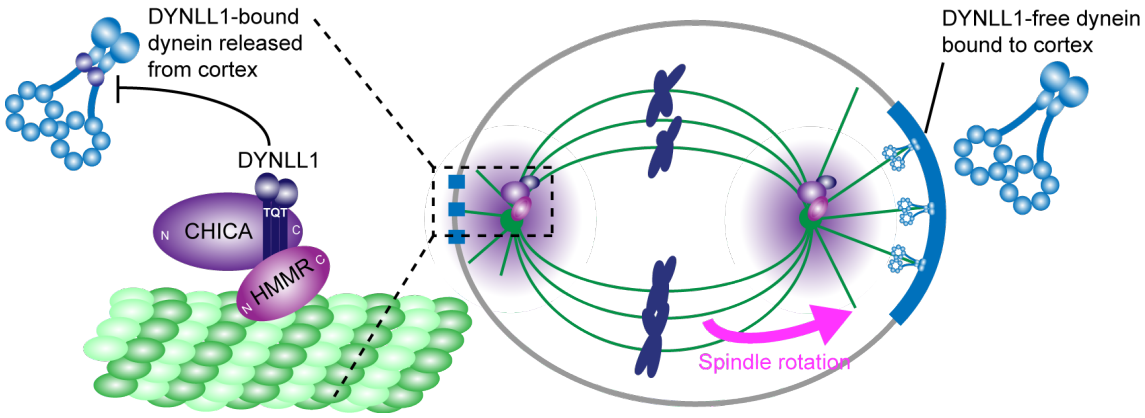


Figure 3.3: Model for DYNLL1 function in spindle positioning and orientation
DYNLL1 is recruited onto spindle microtubules via TQT-mediated interaction with the CHICA-HMMR complex. DYNLL1 has an inhibitory effect on cortical dynein accumulation. When the spindle pole-localised DYNLL1-CHICA-HMMR complex comes in close proximity to the cortex, this inhibitory signal removes dynein from the cortex.

Both, spindle alignment and the establishment or maintenance of cortical dynein asymmetry requires the microtubule-associated complex of HMMR and CHICA, and the TQT-motif mediated interaction of DYNLL1 with CHICA. Interestingly, DYNLL1 complexes at the mitotic spindle did not contain dynactin subunits suggesting a dynactin-independent role for dynein in spindle orientation. This supports the notion, that DYNLL1 acts as a regulatory hub (Rapali *et al.*, 2011b) rather than a dynein scaffolding subunit of the core dynein complex containing dynactin. The data presented here suggest that the CHICA-HMMR complex regulates dynein function by acting as a DYNLL1 loader. CHICA contains three canonical TQT motifs and therefore has the ability to bind three DYNLL1 molecules. When the mitotic spindle is in the proximity of the cell cortex, DYNLL1, which is delivered by CHICA, associates with dynein thereby releasing it from the cell cortex (Figure 3.3, page 116). This model is supported by the biochemical studies presented here. While dynein can be isolated in a complex with DYNLL1 and is seen at the mitotic spindle, DYNLL1 does not localise at the cell cortex. Therefore, a spindle-associated DYNLL1-CHICA-HMMR complex regulates forces exerted on as-

tral microtubules by inhibition of the cortical dynein motor. This provides a mechanism regulating force generation in order to control spindle positioning in the horizontal and vertical axes in symmetrically dividing cells and the present findings on the DYNLL1-CHICA-HMMR complex add to our understanding of the intrinsic spindle orientation pathway (Kiyomitsu and Cheeseman, 2012).

Recently, another component of the spindle orientation pathway in symmetrically dividing cells has been identified. The mitotic interactor and substrate of Plk1 (MISP) is an actin-binding protein localised at the cell cortex, where it interacts with the dynactin subunit p150^{Glued} thereby linking plus end microtubules to the cell cortex (Zhu *et al.*, 2013). It was suggested that phosphorylation of MISP by Plk1 reduces cortical targeting of dynactin. It is unclear whether dynein heavy chain accumulation at the cortex is also decreased upon Plk1-mediated phosphorylation. However, these findings underline the idea that spindle pole localised Plk1 regulates recruitment of cortical factors (Kiyomitsu and Cheeseman, 2012). It is conceivable that MISP acts as an additional factor transmitting the inhibitory Plk1-signal from spindle poles to cortical dynein.

Interestingly, an involvement of the dynein light chain in spindle orientation has also been observed in *Drosophila*. There, the spindle-associated complex of Ana2 (anastral spindle 2) and the DYNLL2 homologue Ctp (Cut up) direct spindle orientation by regulating the accumulation of the NuMA homologue Mud to the cell cortex (Wang *et al.*, 2011). Cortical Mud interacts with the Gα protein regulator Pins, which binds astral microtubules. Deletion of the complex resulted in similar phenotypes to depletion of the DYNLL1-CHICA-HMMR complex, namely an increased mitotic index and a random spindle orientation with angles between 0° and 90° (Wang *et al.*, 2011). However, loss of Ana2 or Ctp caused impaired astral microtubules (Wang *et al.*, 2011). Thus, although both dynein light chain complexes fulfil similar roles in spindle orientation in human and *Drosophila*, the modes of action are different. While the DYNLL1-CHICA-HMMR complex specifically regulates dynein accumulation at the cell cortex and does not interfere

with NuMA targeting, the Ana2-Ctp-Mud complex regulates spindle orientation by controlling Mud (NuMA) localisation and its interaction with astral microtubules.

A common aspect of the loss of both complexes, however, is the increase in the mitotic index caused by a mitotic arrest. I have shown here that this mitotic arrest is likely mediated by the SAC, which raises the question of why the SAC is not satisfied in DYNLL1-, CHICA- or HMMR-depleted cells. According to the current model, the SAC detects unattached kinetochores or a lack of tension across sister chromatids. Cells depleted of DYNLL1, CHICA and HMMR form proper bipolar spindles and show stable microtubule kinetochore attachments, which should not evoke a SAC response. Therefore, these results suggest that the altered pulling forces exerted on astral microtubules may delay the inactivation of the SAC and therefore cause a moderate increase in the time taken for NEBD to anaphase. As an alternative, an additional checkpoint might exist in mammalian cells, which controls spindle orientation, similar to the SPOC in budding yeast.

In summary, the findings of the present study support the view that specific dynein adaptors play a crucial role in regulating the function of dynein in different cellular processes. HMMR and CHICA form a novel adaptor specifically targeting DYNLL1 complexes to mitotic spindle microtubules, where they are required to promote correct spindle orientation. Unravelling the interplay between this intrinsic positioning pathway involving DYNLL1 and cortical cues provided by external signals is a future challenge (Théry *et al.*, 2005; Fink *et al.*, 2011).

The results presented here provide valuable insights into how the dynein light chain subunit DYNLL1 might coordinate the processes of spindle formation and orientation by assembling discrete subcomplexes. This study has shown that the Astrin-Kinastrin complex contributes to the formation of the mitotic spindle and chromosome segregation, whilst HMMR and CHICA have been identified as novel regulators of spindle

orientation in mammalian cells. The identification of components of the intrinsic spindle orientation pathway adds to our understanding of the regulation of symmetric cell divisions.

4. Materials and Methods

4.1. Reagents

All reagents were obtained from Sigma Aldrich (Dorset, UK), Fisher Scientific (Loughborough UK) or VWR (Leicestershire UK) unless stated otherwise.

4.2. Equipment

Table 4.1: Equipment

Equipment	Manufacturer and Model
Benchtop Centrifuge (Refrigerated)	Eppendorf centrifuge 5417R
Benchtop Centrifuge	Eppendorf centrifuge 5417C
Heating block and thermomixer	Eppendorf Thermomix compact
Centrifuge	Beckman Coulter
Cell culture hoods	Heraeus HeraSafe
Cell culture incubators	Heraeus HeraCell
Film developer	Kodak X-OMAT 2000 Processor
High pressure cell homogeniser	Avastin Emulsiflex C5
Incubators	Heraeus Function Line
PCR machine	Eppendorf Mastercycler Personal
Magnetic stirrer	IKA RET basic IKAMAG
Gel system	Bio-Rad Protean
Gel power pack	Bio-Rad power pack
Gel drier	Bio-Rad 583
pH meter	Beckman Coulter 350
Semi dry blotter	Bio-Rad Laboratories Trans-blot SD
	Bio-Rad Laboratories Trans-blot Turbo Transfer system
Wet transfer blotter	Premium Genie Blotter
Shakers	Infors HT multitron standard
Vortex	IKA MS3 basic
Centrifuge rotors	Beckman coulter JA17
	Beckman coulter JLA 8.1000
Waterbath	Haake DC10

Continued on next page

Equipment	Manufacturer and Model
Fixed cell microscope	Standard upright microscope (model BX61; Olympus) equipped with a CoolSNAP HQ2 camera (Roper Scientific)
Live cell microscope	Olympus IX81-ZDC with a CoolSNAP HQ2 camera (Roper Scientific)
Spinning disc live cell microscope	Ultraview Vox spinning disk confocal system (Perkin Elmer)

4.3. Solutions and buffers

The following solutions and buffers were used in this study.

Table 4.2: Solutions

Buffer	Composition
Blocking buffer (Western blot)	5% (w/v) milk powder in PBS
Cushion buffer	80 mM piperazine-bis(ethanesulphonic acid) (PIPES) pH 7.0
	1 mM $MgCl_2$
	1 M EGTA
	60% (v/v) Glycerol
DNA loading dye (6x)	0.25% (w/v) bromophenol blue
	40% (w/v) sucrose in TE
IMAC 20,50,200	20 mM Tris-HCl pH8.0
	300 mM NaCl
	20, 50, 200 mM Imidazole
Laemmli buffer (3x)	0.1875 mM Tris-HCl pH 6.8
	1% (w/v) SDS
	10% (v/v) glycerol
	0.05% (w/v) bromophenol blue
	10% (w/v) β-mercaptoethanol
LB (Agar)	10 g/l Bacto-tryptone,
	5 g/l Bacto-yeast extract

Continued on next page

Buffer	Composition
	10 g/l NaCl
	15 g/l Agar)
LB (Broth)	10 g/l Bacto-tryptone
	5 g/l Bacto-yeast extract
	10 g/l NaCl
Mitotic cell lysis buffer	20 mM Tris-HCl pH 7.4
	150 mM NaCl
	1% (v/v) Igepal
	0.1% (v/v) Sodium deoxycholate
	40 mM β-glycerophosphate
	10mM NaF
	0.3 mM Orthovanadate
	100 nM Okadaic acid
	1 : 250 Protease Inhibitor cocktail
Mowiol	2.4 g Mowiol 4-88
	6g glycerol
	6 ml ddH_2O
	12 ml Tris-HCl pH 8.5 (0.2 M)
phosphate-buffered saline (PBS)	8 g/l NaCl
	0.2 g/l KCl
	1.44 g/l Na_2HPO_4
	0.24 g/l KH_2PO_4 (pH 7.4)
Ponceau	0.2% (w/v) Ponceau red
	1% (v/v) acetic acid
PTEMF fixation solution	0.2% (v/v) Triton X-100
	20 mM PIPES, pH 6.8
	1 mM $MgCl_2$
	10 mM EGTA
	4% (v/v) Formaldehyde
SDS-PAGE separating buffer	181.72 g/l Tris base
	4 g/l SDS
SDS-PAGE stacking buffer	60.6 g/l Tris base
	4 g/l SDS
SDS-PAGE running buffer	30.2 g/l Tris base
	188 g/l glycine

Continued on next page

Buffer	Composition
	10 g/l sodium dodecyl sulphate (SDS)
TAE buffer (50x)	242.4 g/l Tris base
	57.2 ml/l glacial acetic acid
TBS	50 mM Tris base
	150 mM NaCl
	2 mM DTT
	50 mM ethylene diamine tetraacetic acid (EDTA) pH 8.0
TE buffer	10 mM Tris-HCl pH 8.0
	1 mM EDTA
Transfer buffer (Semi-dry Transfer)	20 mM Tris base
	150 mM glycine
	10% (w/v) SDS
	20% (v/v) Methanol
Tubulin buffer	80 mM PIPES pH 7.0
	2 mM $MgCl_2$
	0.5 M EGTA

4.4. Molecular cloning

The technique of molecular cloning allows the fusion of a tag onto a protein of interest. This tag enables either to visualise the protein by immunofluorescence or to express and purify the protein. The gene encoding the protein of interest is amplified and inserted into a delivery vector. After amplifying this plasmid in bacteria, the gene is inserted into a destination vector, which can be used for transfection of mammalian cells.

The plasmids used in this study (Table: A.2, page 155) were either cloned as described in the following sections or were provided by Prof. Francis Barr or Dr. Ulrike Grüneberg.

4.4.1. Gene amplification by nested PCR and cloning into pCR2.1-TOPO-vector

Full length genes or gene fragments were amplified from Marathon Human Fetus or Testis cDNA (Takara Bio, Inc.) by polymerase chain reaction (PCR) using Pfu or KOD polymerase

(Agilent Technologies or Takara Biotech). This *in vitro* DNA replication results in exponential amplification of a specific DNA sequence. Specificity is achieved by using oligonucleotides, called primers, that are complementary to the 5' and 3' end of the desired sequence.

During the first step, template deoxyribonucleic acid (DNA) is denatured at high temperature to produce single strands. Lower temperature enables the primers to anneal with the single stranded template in the second step. Subsequently, at an intermediate temperature, a polymerase adds complementary nucleotides onto the primers to produce double strands again. By repeating the cycle several times, the PCR product is amplified exponentially. A nested-PCR increases the amount of specific PCR product. After the first amplification round with primers flanking the gene (outer primers), the product is purified and used as a template for a second round with inner primers (complementary to 5' and 3' end of the gene).

The PCR components (Table 4.3, page 124 or Table 4.4, page 125) were mixed and incubated in a ThermoCycler. The temperature program used for amplification is shown in Table 4.5 (page 125).

Table 4.3: Pfu polymerase PCR reaction mixture.

Substance	Amount
Human cDNA	2.5 μl
10x Pfu buffer (Stratagene)	5 μl
10 μM Primer I	1 μl
10 μM Primer II	1 μl
40 mM dNTPs	1 μl
Pfu polymerase (Stratagene)	1 μl
ddH_2O	38.5 μl

The PCR product of the first round was purified by Column Purification using the PCR DNA Fragments Extraction Kit (RBC Bioscience) according to the manufacturer's instructions followed by the second round of nested-PCR. Primers used for the second round introduced enzyme restriction sites at the 5' and the 3' end of the sequence, respectively. The primer sequences are shown in Table A.3 on page 157. Afterwards, the PCR product was gel-purified.

Table 4.4: KOD polymerase PCR reaction mixture.

Substance	Amount
Human cDNA	2.5 μl
10x KOD buffer	5 μl
10 μM Primer I	3 μl
10 μM Primer II	3 μl
25 mM $MgSO_4$	2 μl
10 mM dNTPs	5 μl
KOD polymerase (Takara Biotech)	1 μl
ddH_2O	28.5 μl

Table 4.5: Temperature programme for both rounds of nested PCR.

Step	Temperature in °C	Time in s	Repeats
1	95	120	
2	95	30	
3	55	30	
4	72	120/kb (Pfu) 30/kb (KOD)	24 $\times$ to step 2
5	72	600	
6	4	∞	

To this end, the PCR reaction was mixed with 6x DNA Loading Dye and separated by gel electrophoresis on a 0.8% (w/v) agarose gel. DNA has a negative charge due to its phosphate groups and migrates to the anode in an electric field. The agarose acts as a sieve separating the DNA by size. The DNA was visualised by the intercalating dye ethidium bromide. DNA of the appropriate size was extracted using the HiYield Gel Extraction Kit (RBC Bioscience) as described by the manufacturer. Subsequently, 28 μl of purified DNA were incubated with 1 μl of 10 mM dNTPs, 15.5 μl of ddH_2O, 5 μl of 10x Taq buffer and 0.5 μl of Taq polymerase (NEB) for 30 min at 72°C. Adenosine phosphate nucleotides were added at the 3' end of the PCR product during this step. Afterwards, 2 μl of the A-tailed DNA were either mixed with 0.5 μl of Salt Solution and 0.5 μl of pCR2.1-TOPO-vector (Invitrogen), or with 3 μl StrataClone Cloning buffer and 1 μl StrataClone pScA vector mix (Agilent Tech.), and incubated for 5 minutes. The

vector mix contains two DNA strands of which one end is charged with Topoisomerase I and has uridine overhangs, whereas the other end comprises *loxP* recognition sequences. The PCR product is ligated to the vector arms through base-pairing between the adenosine- and uridine-overhangs and ligation by Topoisomerase I. Subsequently, One Shot Top10 competent cells (Invitrogen) were transformed with the pCR2.1-TOPO construct or StrataClone SoloPack competent cells were transformed with the pScA construct, respectively. The transformation mixture was incubated on ice for 20 minutes, the bacteria were heat-shocked for 45 seconds at 42°C and chilled on ice for another 2 minutes. 250 μl of pre-warmed Luria Bertani (LB) were added and the bacteria were allowed to recover for 1 hour at 37°C. The bacteria transiently express Cre recombinase, an enzyme that recognises and recombines the *loxP* sites of the vector arms, resulting in a circular plasmid. Transformed bacteria were plated on LB containing 30 μg/ml kanamycin. The plasmid pCR2.1-TOPO or pScA, respectively, contains an ampicillin and kanamycin resistance cassette, that enable only transformed bacteria to grow on the plates.

4.4.2. Amplification and preparation of plasmid DNA

Molecular cloning techniques take advantage of bacteria to amplify plasmid DNA. Bacteria replicate introduced plasmids as they grow and divide. After lysing the bacterial cells, the plasmid can be purified.

For plasmid preparation in a small scale, 2 ml of LB containing 100 μg/ml ampicillin were inoculated with a single colony growing on a selective plate, for large scale plasmid preparation, 200 ml LB were used respectively. The culture was incubated overnight, at 220 rpm shaking and 37°C, and plasmids were purified using a plasmid miniprep or maxiprep kit (Qiagen) according to the manufacturer's instructions. In brief, cells were harvested by centrifugation and resuspended in buffer containing RNase in order to degrade intervening ribonucleic acid (RNA). Alkaline lysis by adding sodium hydroxide and SDS and the following neutralisation with potassium acetate resulted in the precipitation of proteins and genomic DNA. After another centrifugation, the supernatant containing the plasmid DNA was applied onto a column. Plasmid

DNA was bound to the column, washed and eluted with 10 mM Tris. For large scale preparations, plasmid DNA was eluted with elution buffer (Qiagen), precipitated with isopropanol and washed with 70% ethanol. The DNA was resuspended in TE buffer. DNA concentrations were measured spectrophotometrically at 260 nm. All constructs were checked by sequencing.

4.4.3. Restriction enzyme digests

Restriction enzymes are bacterial nucleases with the ability to recognise and cut specific DNA sequences. Thereby, either blunt or cohesive ends are generated. Purified pCR2.1-TOPO or pScA plasmids, respectively, containing the insert were cut with enzymes according to the restrictions sites introduced with the inner primers (Table A.3, page A.3). The destination vector, pcDNA3.1-Myc, pcDNA5/FRT/TO-Myc or pcDNA5/FRT/TO-GFP, was digested with the same restriction enzymes to produce compatible overhangs. The restriction mixture is shown in Table 4.6 (page 127). After incubation for 2 hours at 37°C, 1 μl of Calf Intestinal phosphatase (NEB) was added to vector digests in order to remove 5'-phosphates from the ends and prevent self re-ligation. The insert- and vector-DNA were again size separated by gel-electrophoresis and extracted from the gel.

Table 4.6: Preparative digestion mixture.

Substance	Amount
pCR2.1-TOPO- or pScA-plasmid DNA	25 μl
Destination vector	2-3 μg
Enzyme I	1 μl
Enzyme II	1 μl
10x enzyme buffer (NEB)	5 μl
ddH_2O	up to 50 μl

4.4.4. Ligation and transformation

The insert was ligated into the destination vector using T4 DNA ligase (NEB). The ligation mixture (Table 4.7, page 128) was incubated for 1-3 hours at room temperature (RT). Then, the

construct was amplified by transforming chemically competent *E. coli* XL1 blue cells (50 μl) with the ligated DNA. After adding the ligation mixture to the bacteria, cells were incubated on ice for 20 minutes, followed by a heat-shock at 42°C for 90 seconds, which resulted in the uptake of the insert-vector construct. The bacteria were chilled on ice for another 2 minutes. 200 μl of LB were added and cells were incubated for 1 hour at 37°C. The bacteria were spread over LB-plates containing 100 μg/ml ampicillin. The vectors, pcDNA3.1-Myc, pcDNA5/FRT/TO-Myc or -GFP include an ampicillin-resistance cassette that enables transformed bacteria to degrade ampicillin. A control ligation without insert DNA was used to exclude re-ligation of the vector. Plasmid DNA of positive clones was prepared and verified again by restriction enzyme analysis and sequencing.

Table 4.7: Ligation mixture.

Substance	Amount
Insert DNA	3 μl
Vector DNA	1 μl
10x ligation buffer (NEB)	1 μl
T4 DNA ligase (NEB)	0.5 μl
ddH_2O	4.5 μl

4.4.5. Site-directed mutagenesis

Mutations are a change in the nucleotide sequence of a gene compared to the wild-type gene. They can occur spontaneously as a result from DNA damage, from replication errors or from insertions or deletions of mobile genetic elements.

In molecular cloning, specific mutations can be introduced to analyse the contribution of a certain amino acid residue to the function of a protein. There, the mutation is introduced by site-directed mutagenesis PCR, in which the whole plasmid is amplified with a single set of primers containing the altered nucleotide codon.

Since both primers contain the changed nucleotide, the mutant plasmid will be amplified exponentially, whereas the wild-type template is amplified only lineally. Both, Pfu and KOD poly-

merases can be used for amplification. However, while Pfu has a proof-reading activity and might therefore yield more accurate PCR products, its lower processivity might impair the amplification of a large plasmid. The PCR components (Table 4.8, page 129 or Table 4.9, page 130) were mixed and incubated in a ThermoCycler. The temperature program used for amplification is shown in Table 4.10 (page 130) and the primers used for mutagenesis are represented in Table A.4 (page 158). After the PCR, the reactions were incubated with 1μl of DpnI at 37°C for 1 hour. This restriction enzyme recognises and specifically cuts methylated DNA. Only the parental wild-type plasmid has been amplified in bacteria and received methylations, thus the DpnI digest will specifically digest the wild-type template, leaving only mutant plasmid behind. Subsequently, chemically competent *E. coli* XL1 blue cells (50 μl) were transformed with 5-10 μl of mutant plasmid, as described in section 4.4.4.

Table 4.8: Pfu polymerase mutagenesis reaction mixture.

Substance	Amount
template DNA	50 ng
10x Pfu buffer (Stratagene)	5 μl
125 ng/2.5pmol Primer I	1 μl
125 ng/2.5pmol Primer II	1 μl
10 mM dNTPs	1 μl
Pfu polymerase (Stratagene)	1 μl
ddH_2O	up to 50 μl

4.5. Recombinant protein purification from *E. coli*

Proteins were expressed in bacteria to obtain suitable amounts for antibody production or *in vitro* protein assays.

The gene encoding the protein or fragments was amplified and cloned into the bacterial expression vectors pQE32 or pGEX-5X-I as described in section 4.4. The vector pQE32 encodes a hexahistidine-tag at the N-terminus of the protein, whereas the pGEX-5X-I vector encodes

Table 4.9: KOD polymerase mutagenesis reaction mixture.

Substance	Amount
template DNA	50 ng
10x KOD buffer	5 μl
125 ng/2.5pmol Primer I	3 μl
125 ng/2.5pmol Primer II	3 μl
25 mM $MgSO_4$	2 μl
2 mM dNTPs	5 μl
KOD polymerase (Takara Biotech)	1 μl
ddH_2O	up to 50 μl

Table 4.10: Temperature programme for mutagenesis PCR.

Step	Temperature in °C	Time in s	Repeats
1	95	30	
2	95	15	
3	55	30	
4	68	120/kb (Pfu) 30/kb (KOD)	18 $\times$ to step 2
5	4	∞	

a GST-tag. Both vectors transcribe the gene under the control of a lac-repressed promoter. Therefore the gene transcription is repressed, until isopropyl-thiogalactopyranoside (IPTG), a molecular mimic of allolactose, is added to the bacteria. Allolactose or IPTG bind to the lac repressor and hinder it from binding to the promoter region thereby allowing the transcription of the gene.

For the purification of recombinant protein, *E. coli* JM109 cells were transformed with 1 μl of pQE32- or pGEX-5X-I-plasmid DNA and spread over LB-plates containing 100 μg/ml ampicillin and 34 μg/ml chloramphenicol. While the ampicillin resistance is encoded by the pQE32 or pGEX-5X-I plasmid, respectively, JM109 cells carry the pRIL plasmid, which expresses the tRNA genes for rare arginine, isoleucine, and leucine codons and conveys chloramphenicol resistance. 100 ml of LB containing 100 μg/ml ampicillin and 34 μg/ml chloramphenicol were inoculated with a single colony and grown at 37°C overnight. Subsequently, 1-2 L of LB con-

taining the same antibiotics were inoculated with the overnight culture and grown at 37°C, until the bacterial culture reached an OD_{600} of 0.5-0.6. Protein expression was then induced with 0.1 mM IPTG and the bacteria were grown either for 3 h at 37°C or overnight at 18°C. The bacteria were harvested by centrifugation in a JLA-8.100 rotor (Beckman) at 4000 g for 20 min at 4°C.

For purification of His-tagged proteins, the bacterial pellet was lysed in 20 ml of IMAC20 supplemented with 0.1 mM PMSF. The lysate was homogenised by passing it three times through a chilled high-pressure homogeniser. Subsequently, the lysate was cleared by centrifugation at 16,000 rpm for 30 min at 4°C in a JA-17 rotor (Beckman). The cleared bacterial lysate was incubated with 0.5 ml of agarose beads coupled to Nickel-nitrilotriacetic acid (NTA). The histidine residues of the tagged protein have a high affinity for nickel ions and thus the protein will bind to the Ni-NTA-agarose beads. After incubation at 4°C for 2 h, the agarose pellet was washed three times with 10 ml of IMAC50. Finally, the resin was transferred into a column and the protein was eluted with IMAC200, which competes with the His-tag for binding to the Nickel ions. The eluate was dialysed against PBS and concentrated using centrifugal filter units (Millipore).

For purification of recombinant GST-tagged protein, the bacterial pellet was lysed in 20 ml of PBS supplemented with 0.1 mM PMSF. The lysate was homogenised by passing it three times through a chilled high-pressure homogeniser. Subsequently, the lysate was cleared by centrifugation at 16,000 rpm for 30 min at 4°C in a JA-17 rotor (Beckman). The cleared bacterial lysate was incubated with 0.5 ml of sepharose beads coupled to glutathione. The glutathione-S-transferase-tag binds to glutathione beads. After incubation at 4°C for 2 h, the sepharose pellet was washed three times with PBS supplemented with 1 mM ATP and 1 mM $MgCl_2$. Finally, the resin was transferred into a column and the protein was eluted with 100 mM Tris-HCl pH 7.4, 150 mM NaCl, 15 mM reduced glutathione, which competes with the glutathione-sepharose for binding of the GST-tag. The eluted protein was dialysed against PBS and concentrated using centrifugal filter units (Millipore).

4.6. Antibody production

Antibodies against CHICA, HMMR, HURP and Kinastrin were raised in sheep (Scottish National Blood Transfusion Service). To this end, full length proteins or fragments were purified from bacteria as described in section 4.5. The CHICA peptide (CSRVNLLAVRD; aa 598-607) was obtained from PeptideSynthetics, UK. In order to be recognised as an antigen peptides were coupled to keyhole limpet hemocyanin (KLH) (Imject, Piere Chemical Co.) by incubation of equal amounts of peptide and KLH for 3-5 h at RT. Sheep were injected with an antigen-adjuvant emulsion several times. The immune system of the animal will recognise the protein or peptide as an antigen and produce antibodies against it, that are circulated in the blood. Therefore, bleeds were collected five, nine or thirteen weeks after the first injection, respectively. Antibodies raised against proteins as antigens then were affinity-purified by incubating the bleed with an antigen-coupled gel. To this end, the recombinant proteins or fragments were incubated for 2 h at 4°C with Affigel-15 or Affigel-10 (Bio-Rad Laboratories), an agarose gel matrix of N-hydroxy-succinimide esters that spontaneously binds to molecules with a free amino group. The protein-bound Affigel was then washed three times with PBS and once with 0.2 M glycine pH 2.8 to remove any unbound protein. Subsequently, 1 mg of protein coupled to the Affigel was incubated with 10-20 ml of the bleed serum overnight at 4°C. Again, the gel was washed several times with PBS and transferred to a column. The antibodies then were eluted with 0.2 M glycine pH 2.8, and 1 M Tris-HCl pH 8.0 was added immediately to neutralise the solution. The antibodies were dialysed, concentrated and stored with 10% (v/v) glycerol and 0.02% (v/v) sodium azide.

To purify antibodies that were raised against a peptide, the total IgG fractions were first isolated from the serum. To this end, 10-12 ml of the serum were incubated with 4-5 ml of Protein G sepharose. Protein G does recognise and bind any sheep-IgG. The sepharose was then washed several times with PBS, transferred to a column and washed once more with PBS supplemented with 1 M NaCl, to remove any non-specifically bound proteins. The IgG was then eluted with 0.2 M glycine pH 2.8 and neutralised by addition of 1 M Tris-HCl pH 8.0. The peptide was coupled to Sulfo-Link Coupling Gel (Pierce) by incubation of equal volumes

of peptide and gel for 15 min at RT. The iodoacetyl-group of the Sulfo-Link Gel binds to the sulfhydryl group of the cysteine residue of the peptide. The gel was then washed twice with 50 mM Tris, 5 mM EDTA pH 8.5 and then incubated with 50 mM L-cysteine for 15 min at RT. The cysteine will bind to the remaining iodoacetyl-groups of the gel and thereby block any non-specific binding sites. The gel was then washed once with 1 M NaCl and twice with 50 mM Tris, 5 mM EDTA pH 8.5. Finally the antibody was affinity-purified from the IgG fractions as described previously.

4.7. Mammalian cell culture and cell synchronisation

HeLa S3 cells and human embryonic kidney (HEK) 293T cells were cultured at 37°C in a 5% CO_2 atmosphere in Dulbecco's modified Eagle's medium (DMEM) supplemented with 10% heat-inactivated fetal-bovine serum (FBS) (Invitrogen). For cell passaging, the cells were washed with 1x PBS, trypsinised at 37°C for 5 minutes and cultured in fresh medium at the appropriate density.

For synchronisation, cells were accumulated at G_1 phase or metaphase, respectively, by blocking cell cycle progression. G_1 arrest was achieved by incubating the cells with 2.5 mM thymidine up to 20 hours. Thymidine in excess interferes with DNA synthesis by inhibiting ribonucleotide reductase, thus causing a block of G_1-to-S-phase transition. For mitotic arrest, cells were treated with nocodazole (100 ng/ml) for 10-16 h or with 10 μM S-trityl-L-cysteine (STLC) (Sigma-Aldrich) for 16 h. Nocodazole impairs microtubule dynamics thereby preventing the formation of a mitotic spindle. STLC inhibits Eg5, thereby causing monopolar spindles and an arrest at the metaphase to anaphase transition.

4.8. Transfection of mammalian cells

In order to analyse the function of proteins of interest, these proteins were overexpressed or depleted in mammalian cells. For overexpression, the gene was either stably integrated in the genome and expression was induced, or cells were transfected with the gene resulting in

transient expression. Protein expression was down regulated using small interfering (si)RNA, that binds to complementary mRNA resulting in mRNA degradation (Elbashir *et al.*, 2001).

4.8.1. Transient transfection

HeLa S3 cells were seeded onto coverslips at 50,000 cells/ml in 6-well plates 24 hours prior transfection and cultured at 37°C. 1 μg of plasmid DNA was mixed with 3 μl of Mirus-LT1 transfection reagent (Mirus Bio LLC) and 100 μl of OptiMEM medium (Invitrogen). After incubation for 15 minutes at RT, the mixture was spread over the cells followed by incubation for another 24 hours at 37°C and processing for immunofluorescence imaging.

For immunoprecipitations, HeLa S3 cells were cultured in a 15 cm diameter dish at 50-60% confluency and incubated with 8 μg of plasmid DNA, 24 μl of Mirus-LT1 transfection reagent and 800 μl of OptiMEM medium for 40 hours.

Double transfections were performed to overexpress two proteins simultaneously. Plasmid DNA 1 (8 μg) was incubated with 24 μl of Mirus-LT1 transfection reagent and 800 μl of OptiMEM medium for 15 minutes at RT. 1.6 μg of plasmid DNA 2 was incubated with 4.8 μl of Mirus-LT1 transfection reagent and 160 μl of OptiMEM medium, respectively. Both mixtures were spread over a 15 cm diameter dish of human embryonic kidney cells (transformed with SV40 large T-antigen) (HEK293T) cells at 50% confluency and incubated for 40 hours.

4.8.2. Stable transfection

Stable cell lines were generated in order to express a protein of interest after induction. The gene is integrated at a single locus within the genome and the expression levels therefore are lower than upon transient transfection. HeLa Flp-In T-REx cells (Invitrogen) were cultured in 3.5 cm diameter dishes at 500,000 cells/dish at 37°C in a 5% CO_2 atmosphere in DMEM supplemented with 10% heat-inactivated, tetracycline-free FBS, 50 μg/ml zeocin and 4 μg/ml blasticidin. This cell line comprises two stably transfected plasmids. First, the pFRT/*lac*Zeo vector containing a Flp recombination target (FRT) site downstream of a zeocin-resistance cassette. The second plasmid, pcDNA6/TR, constitutively expresses the Tet repressor and

blasticidin-resistance. In order to stably integrate the gene of interest into this cell line, 100 μl of OptiMEM medium (Invitrogen) were mixed with 3 μl of Mirus-LT1 transfection reagent (Mirus Bio LLC), 0.1 μg of pcDNA5/FRT/TO plasmid DNA and 0.9 μg of pOG44, a plasmid encoding Flp recombinase. The mixture was incubated for 15 minutes at RT and 100 μl were added per dish. Flp recombinase recognises and cuts DNA at FRT sites and mediates the integration of the pcDNA5/FRT/TO plasmid DNA into the genome of HeLa Flp-In T-REx cells. Plasmid pcDNA5/FRT/TO contains the gene of interest under a tetracycline-inducible promoter and a hygromycin resistance cassette. Upon integration in the genome at FRT sites, the zeocin resistance gene expression is disrupted, while the hygromycin resistance is introduced. Therefore, stably transfected HeLa Flp-In T-REx cells are hygromycin and blasticidin resistant, but zeocin sensitive. The cells were incubated for 24 hours at 37°C in a 5% CO_2 atmosphere. Subsequently, cells were plated into 15 cm dishes and cultured in DMEM supplemented with 10% heat-inactivated FBS, 200 μg/ml hygromycin and 4 μg/ml blasticidin. Hygromycin- and blasticidin-containing medium was replaced every second day until colonies appeared (approximately 10 days). Single colonies were picked, washed, trypsinised and cultured in 6-well plates to 70% confluency. Expression was induced with 1 μg/ml doxycycline, a semi-synthetic tetracycline, for 24-45 hours.

4.8.3. siRNA-mediated depletion

HeLa S3 cells were grown on coverslips at 50,000 cells/ml for 24 hours. For transfection in 6-well plates containing 2 ml of cell suspension, 200 μl of OptiMEM medium (Invitrogen) were mixed with 3 μl oligofectamine (Invitrogen) and 3 μg of pre-annealed siRNA duplexes. After incubation for 25 minutes at RT, the siRNA:oligofectamine complexes were added to the cells. The protein Dicer processes the double stranded RNA molecules into siRNA of about 21 nucleotides with 2 nucleotide-long 3' overhangs (He and Hannon, 2004). One strand of the duplex is assembled into the RNA-induced silencing complex (RISC), which then targets the complementary mRNA for cleavage. Incubation was carried out for 24-96 hours as indicated in the figure legends. Sequences of used siRNA oligos are listed in Table A.5 (page 159).

4.9. Immunofluorescence procedure

HeLa S3 cells were seeded onto coverslips and transfected with plasmid DNA or siRNA duplexes, as required. Cells on the coverslips were fixed with 3% paraformaldehyde (PFA) for 15 minutes. After washing twice with 1x PBS and once with 50 mM NH_4Cl solution, the cells were incubated with 50 mM NH_4Cl solution for 10 minutes. The coverslips were washed twice with 1x PBS and incubated with 0.2% Triton X-100 for 10 minutes to permeabilise the cell membranes. Subsequently, the cells were washed three times with 1x PBS and incubated with the primary antibody, diluted in 2% bovine serum albumin (BSA) solution, for one hour in a dark, humid environment. After washing again three times with 1x PBS, cells were incubated with the secondary antibody in 2% BSA for one hour. The secondary antibody is directed against the species of the first antibody and coupled to a fluorophore for detection. Finally, the coverslips were washed, dried and mounted onto microscope slides using Mowiol 4-88 medium containing 2 μg/ml DAPI.

Methanol or PTEMF (PIPES, Triton X-100, EGTA, $MgCl_2$, formaldehyde) fixations were performed to stain cytoskeleton binding proteins. Methanol or PTEMF removes the cytosol, thereby withdrawing the cytoplasmic protein pool and reducing cytoplasmic background staining. For methanol fixation, the coverslips were incubated with ice-cold methanol for 5 minutes at -20°C followed by washing three times with 1x PBS. For PTEMF fixation, the coverslips were incubated with PIPES, Triton X-100, EGTA, $MgCl_2$, formaldehyde (PTEMF) fixation solution (Table 4.2, page 121) for 12 minutes. The cells were washed twice with 1x tris-buffered saline (TBS), 0.1% Triton X-100 followed by incubation with TBS, 0.1% Triton X-100, 2% BSA for 30 minutes. Staining was performed as described above.

4.10. Mitotic chromosome spreads

HeLa S3 cells were treated with siRNA oligonucleotides as described in section 4.8.3. 100 ng/ml nocodazole was added to the cells to enrich for mitotic cells, if siRNA mediated gene depletion does not cause an mitotic arrest. Mitotic cells were collected by mitotic shake-off and incubated in pre-warmed hypotonic medium (40% FBS-free DMEM, 60% water) for 10 minutes at RT to

induce a swelling of the cells. Subsequently, the cells were slowly centrifuged (500 g, Eppendorf centrifuge 5417R) and incubated in Carnoy's fixative (75% methanol, 25% acetic acid) at 4°C overnight. The cells were centrifuged again and resuspended in fixative at a density of $2x10^6$ cells/ml. Dropping of the cell fixation mixture onto a -20°C coverslip from about 10 cm height burst the swollen cells and chromosomes were spread on the coverslip. After drying the coverslips on a wet tissue on a 60°C heating block, they were washed with PBS and incubated in PBS containing 2 μg/ml DAPI for 15 minutes in a dark, humid environment. Finally, the coverslips were washed with PBS, dried and mounted onto microscope slides using Mowiol 4-88.

4.11. Image acquisition and time-lapse microscopy

Fixed samples on glass slides were imaged using a 60x 1.35 NA oil immersion objective on a standard upright microscope system (model BX61; Olympus) with filter sets for DAPI, GFP/Alexa-488, Alexa-555, Alexa-568, and Alexa-647 (Chroma Technology Corp.), a CoolSNAP HQ2 camera (Roper Scientific), and Metamorph 7.5 imaging software (Molecular Dynamics Inc.). Image stacks were deconvolved using Metamorph software. For live cell imaging, cells were plated in 35-mm dishes with a 14-mm 1.5 thickness coverglass window on the bottom (MatTek), then placed in a 37°C, 5% CO_2 environmental chamber on the microscope stage of a spinning disc confocal system (Ultraview Vox; PerkinElmer). Imaging was performed using a 60x 1.4 NA oil immersion objective lens. Cells were typically imaged every minute for 12 h, acquiring z stacks containing 29 steps, 0.6 μm apart, with 2% laser power and 30 ms exposure. For microtubule plus end imaging, cells were imaged every 1.25 or 3.2 s for 1.5 minutes, acquiring z stacks with 6 steps, 0.4 μm apart. Maximum intensity projections of the fluorescent channels were performed using Volocity (PerkinElmer). Images were cropped in Photoshop CS4 (Adobe) or ImageJ (National Institutes of Health) and transferred into Illustrator CS4 (Adobe) to produce figures.

3D structured illumination microscopy (3D-SIM) was performed on a DeltaVision OMX V2 system (Applied Precision) equipped with a 100x 1.4 NA oil immersion objective (Olympus) and

Cascade II:512 EMCCD cameras (Roper Scientific),using the 405- and 488-nm diode laser lines. Cells for 3D-SIM were prepared as described for standard fixed cell microscopy with the following changes. The cells were grown on no. 1.5H precision glass coverslips (Marienfeld), then washed twice with 2 ml of PBS, and fixed with 2 ml of 4% [wt/vol] paraformaldehyde in PBS for 15 min. Coverslips were mounted in Vectashield mounting medium. Immersion oil with a refractive index of 1.514 was used after being empirically determined to give the most symmetric point spread function for the specific sample conditions. Image stacks (z-height of up to 18 μm, z-distance of 0.125) of the green (Alexa Fluor 488) and the blue (DAPI) fluorescence were recorded sequentially through the same emission light path. Reconstruction was performed with the SoftWoRx 3.7 image-processing software (Applied Precision) to obtain a super-resolution 3D image stack with an optical resolution of 120 nm in the lateral, and approximately 300 nm in the axial direction. These 3D image stacks were imported into Volocity, and a maximum-intensity projection performed. These 24-bit RGB TIFF format images were placed into Illustrator CS3 (Adobe Systems Inc.) to produce the figures.

4.12. SDS-polyacrylamide gel electrophoresis and Western blotting

Cells were harvested, washed once with 1x PBS and lysed in 50 μl of lysis buffer (Table 4.2, page 121) for 15 minutes at 4°C. Centrifugation at 14,000 rpm (F45-30-11 rotor, Eppendorf centrifuge 5417R) for 15 minutes at 4°C cleared the lysate and pelleted the cell debris. Lysate proteins were size-separated by SDS-polyacrylamide gel electrophoresis (PAGE). SDS (sodium dodecyl sulphate) is an anionic detergent binding to proteins at approximately every third amino acid. Therefore, the protein is denatured and gains a negative charge correlating to its size. Negative charged proteins migrate to the anode in an electric field. This migration is retained by a gel network formed by polyacrylamide resulting in separation of the proteins according to their molecular weights. Proteins were denatured by sample buffer containing SDS (Table 4.2, page 121), boiled and loaded onto a polyacrylamide gel. The gel was run at 200V for 50 minutes. Afterwards, the gel was either stained with Coomassie blue, destained and dried or a

Western blot (WB) was performed.

To this end, proteins were transferred from the gel onto a nitrocellulose membrane by semi-dry blotting at 100V for 45 minutes. Using the Bio-Rad Laboratories Trans-blot Turbo system, this could be reduced to 25V for 7 minutes. Free binding sites on the membrane were blocked by incubation with 5% (w/v) milk in PBS for one hour. Primary antibody, diluted in 5% milk, was added to the membrane and incubated for one hour at RT or overnight at 4°C. After washing the membrane four times with 1x PBS, 0.1% Tween for 10 minutes, the secondary horseradish-peroxidase (HRP)-coupled antibody was incubated for 30 minutes. The membrane was washed again four times. Proteins were visualised using the ECL detection system (GE Healthcare). The membrane was incubated with ECL solution for 1 minute. The solution contains HRP substrate, resulting in the production of chemiluminescence, which can be detected on a film. The membranes were placed in a dark cassette, the film was exposed to the membrane for 1-15 minutes and developed in the MI-5 X-ray film processor.

4.13. Isolation of protein complexes

Immunoprecipitations were performed to analyse protein-protein interactions. Proteins co-precipitating with endogenous protein of interest are potential interaction partners.

For immunoprecipitations of endogenous proteins, three 15 cm dishes of synchronised HeLa S3 cells per condition were arrested in interphase or mitosis. For immunoprecipitations from cells with intact mitotic spindles, cells were arrested with 200 μM monastrol for 12 hours, released by washing 3 times with pre-warmed PBS and twice with growth medium and incubated for a further 20 minutes. Mitotic cells were collected by shake-off. Cell pellets were resuspended in lysis buffer (Table 4.2, page 121), left for 15 minutes on ice, and then clarified by centrifugation at 20,000 gav for 15 minutes at 4°C. Protein complexes were isolated from 3 mg of cell lysate using 2.5 μg of specific antibody bound to 30 μl protein G sepharose or protein A sepharose (1:1 in lysis buffer, GE Healthcare), respectively, by incubation for 3 hours at 4°C. Isolated complexes were washed once with lysis buffer, then twice with 20 mM Tris-HCl, pH 7.4, 150 mM NaCl, 0.1% Igepal, then twice with 20 mM Tris-HCl, pH 7.4, 150 mM NaCl. Sub-

sequently, the beads were resuspended in 30 μl of Laemmli buffer (sample buffer) and proteins were analysed by mass spectrometry or Western blotting.

4.14. Co-immunoprecipitation assays

Co-immunoprecipitations of protein fragment were performed to identify binding or interaction domains within the respective proteins. After transfection of HEK293T cells for 40 hours with either one or two plasmids encoding tagged proteins or protein fragments, cells were harvested and washed with 1x PBS. Cell pellets obtained from one 15 cm diameter dish at approximately 80% confluency were lysed in 500 μl of lysis buffer (Table 4.2, page 121) for 15 minutes on ice. The supernatant was added to 30 μl of Protein G sepharose beads (1:1 in lysis buffer, GE Healthcare) and 2 μg of antibody. After rotation for 3 hours at 4°C, the beads were washed once with lysis buffer, twice with 20 mM Tris-HCl, 150 mM NaCl, 0.1% Igepal and twice with 20 mM Tris-HCl, 150 mM NaCl. Subsequently, the beads were resuspended in 30 μl of sample buffer and proteins were analysed by Western blotting.

4.15. Mass spectrometry of protein complexes

Protein samples for mass spectrometry were separated on 4-12% gradient NuPAGE gels, then stained using a colloidal coomassie blue stain. Gel lanes were cut into 8-12 slices, which were incubated twice in 50 μl of 50 mM NH_4HCO_3, 50% (v/v) CH_3CN for 15 min at 37°C to destain the gel slice. Subsequently, the proteins contained in the gel slices were reduced and alkylated by incubation in 100 μl of 100 mM NH_4HCO_3, 10 mM DTT for 30 min at 37°C followed by incubation in 100 μl of 100 mM NH_4HCO_3, 55 mM iodoacetamide for 30 min at 37°C. Then, the gel slices were incubated in 100% (v/v) CH_3CN for 15 min at 37°C in order to dehydrate the gel. Afterwards, the proteins were digested with trypsin (Wilm *et al.*, 1996). To this end, the dehydrated gel slice was incubated in 50 μl of trypsin dilution (2ng/ml) in 50 mM NH_4HCO_3 for 1 h at 37°C. Another 50 μl of 50 mM NH_4HCO_3 was added and incubated at 37°C overnight. The reaction was stopped by addition of formic acid to a final concentration

of 250 mM. The peptides were concentrated in a centrifugal evaporator and resuspended in 20 μl of 0.05% trifluoroacetic acid. The resulting tryptic peptide mixtures were then analysed by online liquid chromatography with tandem mass spectrometry with a nanoAcquity UPLC system (Waters Corporation) and a mass spectrometer (Orbitrap XL ETD; Thermo Fisher Scientific) fitted with a nanoelectrospray source (Proxeon). Peptides were loaded onto a 5-cm x 180-μm trap column (BEH-C18 Symmetry; Waters Corporation) in 0.1% formic acid at 15 μl/min and then resolved using a 25-cm x 75-μm column using a 20-min linear gradient of 0 to 37.5% (v/v) CH_3CN (acetonitrile) in 0.1% formic acid at a flow rate of 400 nl/min. The mass spectrometer was set to acquire a mass spectrometry survey scan in the Orbitrap (resolution = 30,000) and then perform tandem mass spectrometry on the top five multiply charged ions in the linear quadrupole ion trap after fragmentation using collision ionisation (30 ms at 35% energy). A 90-s rolling exclusion list with n=3 was used to limit redundant analysis. Maxquant and Mascot (Matrix Science) were then used to compile and search the raw data against the human IPI database. Protein group and peptide lists were sorted and analysed in Excel (Microsoft) and Maxquant (Cox and Mann, 2008).

4.16. *In vitro* translation

In vitro translations were performed in order to express proteins that could not be obtained in native form using cellular expression systems. The plasmid encoding the desired protein is transcribed by an isolated RNA-Polymerase and the mRNA is subsequently translated into a protein by ribosomes contained in the lysate mixture. A radioactive amino acid is incorporated for detection of the translated protein.

The TnT Coupled Reticulocyte Lysate System (Promega) was used to translate the full-length proteins. The components of the *in vitro* translation mixture (Table 4.11, page 142) were pipetted into a tube at 4°C. The reaction was incubated in a 30°C waterbath for 90 minutes. 2.5 μl of the reaction were analysed by SDS-PAGE. After staining, destaining and drying the gel, radioactivity was detected by exposing a film to the gel in a cassette overnight at -80°C and developing it in the Mi-5 X-ray film processor.

Table 4.11: *In vitro* translation mixture.

Substance	Amount
TnT-Reticulocyte Lysate	25 μl
Reaction buffer	2 μl
RNA Polymerase T7	2 μl
RNasin	1 μl
pcDNA3.1-Myc plasmid	2 μg
AA Mix -Met	1 μl
^{35}S-Methionine	2 μl
Nuclease-free water	up to 50 μl

4.17. Microtubule spin down assay

Microtubule spin down assays were performed to analyse binding of proteins onto microtubules *in vitro*.

47 μl of Tubulin buffer (Table 4.2, page 121) were mixed with 3 μl of *in vitro*-translated protein. Ultracentrifugation at 90,000 rpm for 10 minutes at RT in a TLA100 rotor (Optima MAX-XP ultracentrifuge, Beckman) pre-cleared the reaction. 0.5 μl of taxol solution (2 mM) were added. Tubulin (Cytoskeleton) was assembled to microtubules according to the manufacturer's instructions. In brief, 20 μl of tubulin (5 mg/ml) were incubated with 2 μl of Cushion buffer (Table 4.2, page 121) for 20 minutes at 35°C. 200 μl of Tubulin buffer and 2 μl of taxol solution (2 mM) were added. 20 μl of pre-cleared protein were added to 10 μl of Tubulin buffer and 20 μl of taxol-stabilised microtubules. A sedimentation test in the absence of microtubules was performed, since it is crucial that proteins used in microtubule spin down assays do not precipitate in the absence of tubulin. Reactions were incubated at RT for 10 minutes. Subsequently, 100 μl of Cushion buffer were overlaid with the mixtures. After ultracentrifugation at 80,000 rpm for 10 minutes at RT, the supernatant was collected and the pellet was resuspended in sample buffer. Proteins were detected by autoradiography.

4.18. Microtubule polymerisation assay

Tubulin polymerisation was measured by fluorescence enhancement because of the incorporation of a fluorescent dye into the tubulin polymers using a tubulin polymerisation kit (Cytoskeleton, Inc.). Per reaction, 100 μg of tubulin were mixed on ice with 28.5 μl buffer 1 (Cytoskeleton, Inc.), 12.5 μl Cushion buffer, 0.5 μl of 100 mM GTP and 0.5 μl of 0.1 mM ATP. 50 μl of this reaction mixture were added to 5 μl of the protein of interest and the reaction was transferred into a microtiter plate. Fluorescence emission at 460 nm was followed for 1 h at 37°C with one reading per minute using a fluorimeter (Berthold Technologies).

4.19. Gel filtration

A gel filtration was performed in order to separate proteins by size under native conditions. Gel filtration samples of mitotic cell extracts separated on a Superose 6 10/300 GL column (GE Healthcare) were obtained from Dr. Ricardo Nunes Bastos.

5. References

Abrieu, A., Magnaghi-Jaulin, L., Kahana, J., Peter, M., Castro, A., Vigneron, S., Lorca, T., Cleveland, D., and Labbé, J.: (2001): Mps1 is a kinetochore-associated kinase essential for the vertebrate mitotic checkpoint. *Cell*, **106**(1):83–93.

Akhmanova, A., Hoogenraad, C., Drabek, K., Stepanova, T., Dortland, B., Verkerk, T., Vermeulen, W., Burgering, B., Zeeuw, C.D., Grosveld, F., and Galjart, N.: (2001): Clasps are CLIP-115 and -170 associating proteins involved in the regional regulation of microtubule dynamics in motile fibroblasts. *Cell*, **104**(6):923–35.

Akhmanova, A. and Steinmetz, M.: (2010): Microtubule +TIPs at a glance. *J. Cell Sci.*, **123**(20):3415–9.

Al-Bassam, J., van Breugel, M., Harrison, S., and Hyman, A.: (2006): Stu2p binds tubulin and undergoes an open-to-closed conformational change. *J. Cell Biol.*, **172**(7):1009–22.

Alberts, B., Bray, D., Lewis, J., Raff, M., Roberts, K., and Watson, J.: (2004): *Molecular Biology of the Cell.* Taylor and Francis, New York.

Alushin, G., Ramey, V., Pasqualato, S., Ball, D., Grigorieff, N., Musacchio, A., and Nogales, E.: (2010): The Ndc80 kinetochore complex forms oligomeric arrays along microtubules. *Nature*, **467**:805–10.

Assmann, V., Jenkinson, D., Marshall, J., and Hart, I.: (1999): The intracellular hyaluronan receptor RHAMM/IHABP interacts with microtubules and actin filaments. *J. Cell Sci.*, **11**(22):3943–54.

Barbar, E.: (2008): Dynein light chain LC8 is a dimerization hub essential in diverse protein networks. *Biochemistry*, **47**(2):503–8.

Basto, R., Lau, J., Vinogradova, T., Gardiol, A., Woods, C., Khodjakov, A., and Raff, J.: (2006): Flies without centrioles. *Cell*, **125**(7):1375–86.

Bieling, P., Kandels-Lewis, S., Telley, I., van Dijk, J., Janke, C., and Surrey, T.: (2008): CLIP-170 tracks growing microtubule ends by dynamically recognizing composite EB1/tubulin-binding sites. *J. Cell Biol.*, **183**(7):1223–33.

Blangy, A., Lane, H., d'Hérin, P., Harper, M., Kress, M., and Nigg, E.: (1995): Phosphorylation by p34cdc2 regulates spindle association of human Eg5, a kinesin-related motor essential for bipolar spindle formation in vivo. *Cell*, **83**(7):1159–69.

Bornens, M. and Piel, M.: (2002): Centrosome inheritance: birthright or the privilege of maturity? *Curr. Biol.*, **12**(2):71–3.

Bringmann, H. and Hyman, A.: (2005): A cytokinesis furrow is positioned by two consecutive signals. *Nature*, **436**(7051):731–4.

Burke, D. and Stukenberg, P.: (2008): Linking kinetochore-microtubule binding to the spindle checkpoint. *Dev. Cell*, **4**(474-9).

Bustos, D.: (2012): The role of protein disorder in the 14-3-3 interaction network. *Mol. Biosyst.*, **8**(1):178–84.

Cao, L. and Wang, Y.: (1990): Mechanism of the formation of contractile ring in dividing cultured animal cells. I. Recruitment of preexisting actin filaments into the cleavage furrow. *J. Cell Biol.*, **110**(4):1089–95.

Carazo-Salas, R., Guarguaglini, G., Gruss, O., Segref, A., Karsenti, E., and Mattaj, I.: (1999): Generation of GTP-bound Ran by RCC1 is required for chromatin-induced mitotic spindle formation. *Nature*, **400**(6740):178–81.

Chan, Y.W., Fava, L.L., Uhlschmid, A., Schmitz, M.H., Gerlich, D.W., Nigg, E.A., and Santamaria, A.: (2009): Mitotic control of kinetochore-associated dynein and spindle orientation by human Spindly. *J. Cell Biol.*, **185**:859–874.

Chan, Y., Jeyaprakash, A., Nigg, E., and Santamaria, A.: (2012): Aurora B controls kinetochore-microtubule attachments by inhibiting Ska complex-KMN network interaction. *J. Cell Biol.*, **196**(5):563–71.

Cheeseman, I., Chappie, J., Wilson-Kubalek, E., and Desai, A.: (2006): The conserved KMN network constitutes the core microtubule-binding site of the kinetochore. *Cell*, **127**(5):983–97.

Ciosk, R., Shirayama, M., Shevchenko, A., Tanaka, T., Toth, A., Shevchenko, A., and Nasmyth, K.: (2000): Cohesin's binding to chromosomes depends on a separate complex consisting of Scc2 and Scc4 proteins. *Mol. Cell*, **5**(2):243–54.

Clarke, P.R. and Zhang, C.: (2008): Spatial and temporal coordination of mitosis by Ran GTPase. *Nat. Rev. Mol. Cell Biol.*, **9**:464–477.

Colombo, K., Grill, S., Kimple, R., Willard, F., Siderovski, D., and Gönczy, P.: (2003): Translation of polarity cues into asymmetric spindle positioning in Caenorhabditis elegans embryos. *Science*, **300**(5627):1957–61.

Compton, D.: (1998): Focusing on spindle poles. *J. Cell Sci.*, **111**(11):1477–81.

Cooper, G.: (2000): *The Cell: A Molecular Approach*. Sinauer Associates, Sunderland (MA), 2 edition.

Cox, J. and Mann, M.: (2008): MaxQuant enables high peptide identification rates, individualized p.p.b.-range mass accuracies and proteome-wide protein quantification. *Nat. Biotechnol.*, **26**(12):1367–72.

Daum, J., Potapova, T., Sivakumar, S., Daniel, J., Flynn, J., Rankin, S., and Gorbsky, G.: (2011): Cohesion fatigue induces chromatid separation in cells delayed at metaphase. *Curr. Biol.*, **21**(12):1018–24.

Daum, J., Wren, J., Daniel, J., Sivakumar, S., McAvoy, J., Potapova, T., and Gorbsky, G.: (2009): Ska3 is required for spindle checkpoint silencing and the maintenance of chromosome cohesion in mitosis. *Curr. Biol.*, **19**(17):1467–72.

DeAntoni, A., Pearson, C., Cimini, D., Canman, J., Sala, V., Nezi, L., Mapelli, M., Sironi, L., Faretta, M., Salmon, E., and Musacchio, A.: (2005): The Mad1/Mad2 complex as a template for Mad2 activation in the spindle assembly checkpoint. *Curr. Biol.*, **15**(3):214–25.

Dienstbier, M., Boehl, F., Li, X., and Bullock, S.: (2009): Egalitarian is a selective RNA-binding protein linking mRNA localization signals to the dynein motor. *Genes Dev.*, **23**(13):1546–58.

Dixit, R., Barnett, B., Lazarus, J., Tokito, M., Goldman, Y., and Holzbaur, E.: (2009): Microtubule plus-end tracking by CLIP-170 requires EB1. *Proc. Natl. Acad. Sci. USA*, **106**(2):492–7.

Dong, Y., Beldt, K.V., Meng, X., Khodjakov, A., and McEwen, B.: (2007): The outer plate in vertebrate kinetochores is a flexible network with multiple microtubule interactions. *Nat. Cell Biol.*, **9**(5):516–22.

Dragestein, K., van Cappellen, W., van Haren, J., Tsibidis, G., Akhmanova, A., Knoch, T., Grosveld, F., and Galjart, N.: (2008): Dynamic behavior of GFP-CLIP-170 reveals fast protein turnover on microtubule plus ends. *J. Cell Biol.*, **180**(4):729–37.

Dujardin, D. and Vallee, R.: (2002): Dynein at the cortex. *Curr. Opin. Cell Biol.*, **14**(1):44–9.

Dunker, A., Garner, E., Guilliot, S., Romero, P., Albrecht, K., Hart, J., Obradovic, Z., Kissinger, C., and Villafranca, J.: (1998): Protein disorder and the evolution of molecular recognition: theory, predictions and observations. *Pac. Symp. Bicomput.*, pages 473–84.

Dunsch, A.K.: (2010): A novel Astrin-complex required for mitosis. Diploma thesis, Friedrich-Schiller-Universität Jena, Germany.

Dunsch, A.K., Hammond, D., Lloyd, J., Schermelleh, L., Gruneberg, U., and Barr, F.: (2012): Dynein light chain 1 and a spindle-associated adaptor promote dynein asymmetry and spindle orientation. *J. Cell Biol.*, **198**(6):1039–54.

Dunsch, A.K., Linnane, E., Barr, F., and Gruneberg, U.: (2011): The astrin-kinastrin/SKAP complex localizes to microtubule plus ends and facilitates chromosome alignment. *J. Cell Biol.*, **192**(6):959–68.

Elbashir, S.M., Martinez, J., Patkaniowska, A., Lendeckel, W., and Tuschl, T.: (2001): Functional anatomy of siRNAs for mediating efficient RNAi in Drosophila melanogaster embryo lysate. *EMBO J*, **20**(23):6877–6888.

Fang, L., Seki, A., and Fang, G.: (2009): SKAP associates with kinetochores and promotes the metaphase-to-anaphase transition. *Cell Cycle*, **8**(17):2819–27.

Faragher, A. and Fry, A.: (2003): Nek2A kinase stimulates centrosome disjunction and is required for formation of bipolar mitotic spindles. *Mol. Biol. Cell*, **14**(7):2876–89.

Faulkner, N., Dujardin, D., Tai, C., Vaughan, K., O'Connell, C., Wang, Y., and Vallee, R.: (2000): A role for the lissencephaly gene LIS1 in mitosis and cytoplasmic dynein function. *Nat. Cell Biol.*, **2**(11):784–91.

Fink, J., Carpi, N., Betz, T., Bétard, A., Chebah, M., Azioune, A., Bornens, M., Sykes, C., Fetler, L., Cuvelier, D., and Piel, M.: (2011): External forces control mitotic spindle positioning. *Nat. Cell Biol.*, **21**(11):672–680.

Foley, E., Maldonado, M., and Kapoor, T.: (2011): Formation of stable attachments between kinetochores and microtubules depends on the B56-PP2A phosphatase. *Nat. Cell Biol.*, **13**(10):1265–71.

Fry, A., Mayor, T., Meraldi, P., Stierhof, Y., Tanaka, K., and Nigg, E.: (1998): C-Nap1, a novel centrosomal coiled-coil protein and candidate substrate of the cell cycle-regulated protein kinase Nek2. *J. Cell Biol.*, **141**(7):1563–74.

Funabiki, H., Kumada, K., and Yanagida, M.: (1996): Fission yeast Cut1 and Cut2 are essential for sister chromatid separation, concentrate along the metaphase spindle and form large complexes. *EMBO J*, **15**(23):6617–28.

Funabiki, H. and Murray, A.: (2000): The Xenopus chromokinesin Xkid is essential for metaphase chromosome alignment and must be degraded to allow anaphase chromosome movement. *Cell*, **102**(4):411–24.

Gadde, S. and Heald, R.: (2004): Mechanisms and molecules of the mitotic spindle. *Curr. Biol.*, **14**(18):797–805.

Gaglio, T., Saredi, A., Bingham, J., Hasbani, M., Gill, S., Schroer, T., and Compton, D.: (1996): Opposing motor activities are required for the organization of the mammalian mitotic spindle pole. *J. Cell Biol.*, **135**(2):399–414.

Gaitanos, T.N., Santamaria, A., Jeyaprakash, A.A., Wang, B., Conti, E., and Nigg, E.A.: (2009): Stable kinetochore-microtubule interactions depend on the Ska complex and its new component Ska3/C13Orf3. *EMBO J*, **28**(10):1442–52.

Galjart, N.: (2010): Plus-end-tracking proteins and their interactions at microtubule ends. *Curr. Biol.*, **20**(12):528–37.

Gandhi, R., Gillespie, P., and Hirano, T.: (2006): Human Wapl is a cohesin-binding protein that promotes sister-chromatid resolution in mitotic prophase. *Curr. Biol.*, **16**(24):2406–17.

Gassmann, R., Holland, A., Varma, D., Wan, X., Civril, F., Cleveland, D., Oegema, K., Salmon, E., and Desai, A.: (2010): Removal of Spindly from microtubule-attached kinetochores controls spindle checkpoint silencing in human cells. *Genes Dev.*, **24**(9):957–71.

Gavet, O., Ozon, S., Manceau, V., Lawler, S., Curmi, P., and Sobel, A.: (1998): The stathmin phosphoprotein family: intracellular localization and effects on the microtubule network. *J. Cell Sci.*, **111**(22):3333–46.

Gergely, F., Karlsson, C., Still, I., Cowell, J., Kilmartin, J., and Raff, J.: (2000): The TACC domain identifies a family of centrosomal proteins that can interact with microtubules. *Proc. Natl. Acad. Sci. USA*, **97**(26):14352–7.

Gorr, I., Boos, D., and Stemmann, O.: (2005): Mutual inhibition of separase and Cdk1 by two-step complex formation. *Mol. Cell*, **19**(1):135–41.

Goshima, G., Mayer, M., Zhang, N., Stuurman, N., and Vale, R.: (2008): Augmin: a protein complex required for centrosome-independent microtubule generation within the spindle. *J. Cell Biol.*, **181**(3):421–9.

Goshima, G., Wollman, R., Goodwin, S., Zhang, N., Scholey, J., Vale, R., and Stuurman, N.: (2007): Genes required for mitotic spindle assembly in Drosophila S2 cells. *Science*, **316**(5823):417–21.

Gotta, M., Dong, Y., Peterson, Y., Lanier, S., and Ahringer, J.: (2003): Asymmetrically distributed C. elegans homologs of AGS3/PINS control spindle position in the early embryo. *Curr. Biol.*, **13**(12):1029–37.

Griffis, E., Stuurman, N., and Vale, R.: (2007): Spindly, a novel protein essential for silencing the spindle assembly checkpoint, recruits dynein to the kinetochore. *J. Cell Biol.*, **177**(6):1005–15.

Groen, A., Cameron, L., Coughlin, M., Miyamoto, D., Mitchison, T., and Ohi, R.: (2004): XRHAMM functions in ran-dependent microtubule nucleation and pole formation during anastral spindle assembly. *Curr. Biol.*, **14**(20):1801–11.

Gruneberg, U., Neef, R., Li, X., Chan, E., Chalamalasetty, R., Nigg, E., and Barr, F.: (2006): KIF14 and citron kinase act together to promote efficient cytokinesis. *J. Cell Biol.*, **172**(3):363–72.

Gruss, O., Carazo-Salas, R., Schatz, C., Guarguaglini, G., Kast, J., Wilm, M., Bot, N.L., Vernos, I., Karsenti, E., and Mattaj, I.: (2001): Ran induces spindle assembly by reversing the inhibitory effect of importin alpha on TPX2 activity. *Cell*, **104**(1):83–93.

Gruss, O., Wittmann, M., Yokoyama, H., Pepperkok, R., Kufer, T., Silljé, H., Karsenti, E., Mattaj, I., and Vernos, I.: (2002): Chromosome-induced microtubule assembly mediated by TPX2 is required for spindle formation in HeLa cells. *Nat. Cell Biol.*, **4**(11):871–9.

Haering, C., Löwe, J., Hochwagen, A., and Nasmyth, K.: (2002): Molecular architecture of SMC proteins and the yeast cohesin complex. *Mol. Cell*, **9**(4):773–88.

Hanisch, A., Wehner, A., Nigg, E., and Silljé, H.: (2006): Different Plk1 functions show distinct dependencies on Polo-Box domain-mediated targeting. *Mol. Biol. Cell*, **17**(1):448–59.

Haren, L., Remy, M., Bazin, I., Callebaut, I., Wright, M., and Merdes, A.: (2006): NEDD1-dependent recruitment of the gamma-tubulin ring complex to the centrosome is necessary for centriole duplication and spindle assembly. *J. Cell Biol.*, **172**(4):505–15.

Hauf, S., Roitinger, E., Koch, B., Dittrich, C., Mechtler, K., and Peters, J.: (2005): Dissociation of cohesin from chromosome arms and loss of arm cohesion during early mitosis depends on phosphorylation of SA2. *PLoS Biol.*, **3**(3):e69.

He, L. and Hannon, G.J.: (2004): MicroRNAs: Small RNAs with a big role in Gene Regulation. *Nat. Rev. Genetics*, **5**(7):522–532.

Hinchcliffe, E., Miller, F., Cham, M., Khodjakov, A., and Sluder, G.: (2001): Requirement of a centrosomal activity for cell cycle progression through G1 into S phase. *Science*, **291**(5508):1547–50.

Holland, A., Böttger, F., Stemmann, O., and Taylor, S.: (2007): Protein phosphatase 2A and separase form a complex regulated by separase autocleavage. *J. Biol. Chem.*, **282**(34):24623–32.

Holland, A. and Taylor, S.: (2006): Cyclin-B1-mediated inhibition of excess separase is required for timely chromosome disjunction. *J. Cell Sci.*, **119**(16):3325–36.

Honnappa, S., Gouveia, S., Weisbrich, A., Damberger, F., Bhavesh, N., Jawhari, H., Grigoriev, I., van Rijssel, F., Buey, R., Lawera, A., Jelesarov, I., Winkler, F., Wüthrich, K., Akhmanova, A., and Steinmetz, M.: (2009): An EB1-binding motif acts as a microtubule tip localization signal. *Cell*, **138**(2):366–76.

Howell, B., McEwen, B., Canman, J., Hoffman, D., Farrar, E., Rieder, C., and Salmon, E.: (2001): Cytoplasmic dynein/dynactin drives kinetochore protein transport to the spindle poles and has a role in mitotic spindle checkpoint inactivation. *J. Cell Biol.*, **155**(7):1159–72.

Huang, H., Feng, J., Famulski, J., Rattner, J., Liu, S., Kao, G., Muschel, R., Chan, G., and Yen, T.: (2007): Tripin/hSgo2 recruits MCAK to the inner centromere to correct defective kinetochore attachments. *J. Cell Biol.*, **177**(3):413–24.

Huang, Y., Wang, W., Yao, P., Wang, X., Liu, X., Zhuang, X., Yan, F., Zhou, J., Du, J., Ward, T., Zou, H., Zhang, J., Fang, G., Ding, X., Dou, Z., and Yao, X.: (2012): CENP-E interacts with SKAP to orchestrate accurate chromosome segregation in mitosis. *J. Biol. Chem.*, **287**(2):1500–9.

Inaba, M. and Yamashita, Y.: (2012): Asymmetric stem cell division: precision for robustness. *Cell Stem Cell*, **11**(4):461–9.

Izawa, D. and Pines, J.: (2012): Mad2 and the APC/C compete for the same site on Cdc20 to ensure proper chromosome segregation. *J. Cell Biol.*, **199**(1):27–37.

Kaláb, P., Pralle, A., Isacoff, E., Heald, R., and Weis, K.: (2006): Analysis of a RanGTP-regulated gradient in mitotic somatic cells. *Nature*, **440**(7084):697–701.

Kalab, P., Weis, K., and Heald, R.: (2002): Visualization of a Ran-GTP gradient in interphase and mitotic Xenopus egg extracts. *Science*, **295**(5564):2452–6.

Kardon, J. and Vale, R.: (2009): Regulators of the cytoplasmic dynein motor. *Nat. Rev. Mol. Cell Biol.*, **10**(12):854–65.

Karki, S. and Holzbaur, E.: (1999): Cytoplasmic dynein and dynactin in cell division and intracellular transport. *Curr. Opin. Cell Biol.*, **11**(1):45–53.

Katis, V., Galova, M., Rabitsch, K., Gregan, J., and Nasmyth, K.: (2004): Maintenance of cohesin at centromeres after meiosis I in budding yeast requires a kinetochore-associated protein related to MEI-S332. *Curr. Biol.*, **14**(7):560–72.

Khodjakov, A., Cole, R., Oakley, B., and Rieder, C.: (2000): Centrosome-independent mitotic spindle formation in vertebrates. *Curr. Biol.*, **10**(2):59–67.

Kim, H., Ling, S., Rogers, G., Kural, C., Selvin, P., Rogers, S., and Gelfand, V.: (2007): Microtubule binding by dynactin is required for microtubule organization but not cargo transport. *J. Cell Biol.*, **176**(5):641–51.

Kirschner, M.W. and Mitchison, T.: (1986): Microtubule dynamics. *Nature*, **324**(18):621.

Kitajima, T., Kawashima, S., and Watanabe, Y.: (2004): The conserved kinetochore protein shugoshin protects centromeric cohesion during meiosis. *Nature*, **427**(6974):510–7.

Kitajima, T., Sakuno, T., Ishiguro, K., Iemura, S., Natsume, T., Kawashima, S., and Watanabe, Y.: (2006): Shugoshin collaborates with protein phosphatase 2A to protect cohesin. *Nature*, **441**(7089):46–52.

Kiyomitsu, T. and Cheeseman, I.: (2012): Chromosome- and spindle-pole-derived signals generate an intrinsic code for spindle position and orientation. *Nat. Cell Biol.*, **14**:311–317.

Kon, T., Oyama, T., Shimo-Kon, R., Imamula, K., Shima, T., Sutoh, K., and Kurisu, G.: (2012): The 2.8,ÄâÅcrystal structure of the dynein motor domain. *Nature*, **484**(7394):345–50.

Kops, G., Kim, Y., Weaver, B., Mao, Y., McLeod, I., Yates, J., Tagaya, M., and Cleveland, D.: (2005): ZW10 links mitotic checkpoint signaling to the structural kinetochore. *J. Cell Biol.*, **169**(1):49–60.

Kotak, S., Busso, C., and Gönczy, P.: (2012): Cortical dynein is critical for proper spindle positioning in human cells. *J. Cell Biol.*, **199**(1):97–110.

Kozlowski, C., Srayko, M., and Nedelec, F.: (2007): Cortical microtubule contacts position the spindle in C. elegans embryos. *Cell*, **129**(3):499–510.

Kruse, T., Zhang, G., Larsen, M., Lischetti, T., Streicher, W., Nielsen, T., Bjørn, S., and Nilsson, J.: (2013): Direct binding between BubR1 and B56-PP2A phosphatase complexes regulate mitotic progression. *J. Cell Sci.*

Kumagai, A. and Dunphy, W.: (1996): Purification and molecular cloning of Plx1, a Cdc25-regulatory kinase from Xenopus egg extracts. *Science*, **273**(5280):1377–80.

Kumagai, A., Yakowec, P., and Dunphy, W.: (1998): 14-3-3 proteins act as negative regulators of the mitotic inducer Cdc25 in Xenopus egg extracts. *Mol. Biol. Cell*, **9**(2):345–54.

Kumar, P. and Wittmann, T.: (2012): +TIPs: SxIPping along microtubule ends. *Trends Cell Biol.*, **22**(8):418–28.

Laan, L., Pavin, N., Husson, J., Romet-Lemonne, G., van Duijn, M., López, M., Vale, R., Jülicher, F., Reck-Peterson, S., and Dogterom, M.: (2012): Cortical dynein controls microtubule dynamics to generate pulling forces that position microtubule asters. *Cell*, **148**(3):502–14.

Lew, D. and Kornbluth, S.: (1996): Regulatory roles of cyclin dependent kinase phosphorylation in cell cycle control. *Curr. Opin. Cell Biol.*, **8**(6):795–804.

Liu, D., Vader, G., Vromans, M., Lampson, M., and Lens, S.: (2009): Sensing chromosome bi-orientation by spatial separation of aurora B kinase from kinetochore substrates. *Science*, **323**(5919):1350–3.

Liu, D., Vleugel, M., Backer, C., Hori, T., Fukagawa, T., Cheeseman, I., and Lampson, M.: (2010): Regulated targeting of protein phosphatase 1 to the outer kinetochore by KNL1 opposes Aurora B kinase. *J. Cell Biol.*, **188**(6):809–20.

Liu, J., Lewellyn, A., Chen, L., and Maller, J.: (2004): The polo box is required for multiple functions of Plx1 in mitosis. *J. Biol. Chem.*, **279**(20):21367–73.

Lüders, J. and Stearns, T.: (2007): Microtubule-organizing centres: a re-evaluation. *Nat. Rev. Mol. Cell Biol.*, **8**(2):161–7.

Luo, X., Tang, Z., Xia, G., Wassmann, K., Matsumoto, T., Rizo, J., and Yu, H.: (2004): The Mad2 spindle checkpoint protein has two distinct natively folded states. *Nat. Struct. Mol. Biol.*, **11**(4):338–45.

Mack, G.J. and Compton, D.A.: (2001): Analysis of mitotic microtubule-associated proteins using mass spectrometry identifies astrin, a spindle-associated protein. *Proc. Natl. Acad. Sci. USA*, **98**(25):14434–14439.

Maffini, S., Maia, A., Manning, A., Maliga, Z., Pereira, A., Junqueira, M., Shevchenko, A., Hyman, A., Yates, J., Galjart, N., Compton, D., and Maiato, H.: (2009): Motor-independent targeting of CLASPs to kinetochores by CENP-E promotes microtubule turnover and poleward flux. *Curr. Biol.*, **19**(18):1566–72.

Mahoney, N., Goshima, G., Douglass, A., and Vale, R.: (2006): Making microtubules and mitotic spindles in cells without functional centrosomes. *Curr. Biol.*, **16**(6):564–9.

Maiato, H., DeLuca, J., Salmon, E.D., and Earnshaw, W.C.: (2004): The dynamic kinetochore-microtubule interface. *J. Cell Sci.*, **117**:5641–5477.

Maiato, H., Fairley, E.A., Rieder, C.L., Swedlow, J.R., Sunkel, C.E., and Earnshaw, W.C.: (2003): Human CLASP1 Is an Outer Kinetochore Component that Regulates Spindle Microtubule Dynamics. *Cell*, **113**:891–904.

Manning, A., Bakhoum, S., Maffini, S., Correia-Melo, C., Maiato, H., and Compton, D.: (2010): CLASP1, astrin and Kif2b form a molecular switch that regulates kinetochore-microtubule dynamics to promote mitotic progression and fidelity. *EMBO J*, **29**:3531–3543.

Maresca, T. and Salmon, E.: (2009): Intrakinetochore stretch is associated with changes in kinetochore phosphorylation and spindle assembly checkpoint activity. *J. Cell Biol.*, **184**(3):373–81.

Margolis, S., Perry, J., Forester, C., Nutt, L., Guo, Y., Jardim, M., Thomenius, M., Freel, C., Darbandi, R., Ahn, J., Arroyo, J., Wang, X., Shenolikar, S., Nairn, A., Dunphy, W., Hahn, W., Virshup, D., and Kornbluth, S.: (2006): Role for the PP2A/B56delta phosphatase in regulating 14-3-3 release from Cdc25 to control mitosis. *Cell*, **127**(4):759–73.

Matanis, T., Akhmanova, A., Wulf, P., Nery, E.D., Weide, T., Stepanova, T., Galjart, N., Grosveld, F., Goud, B., Zeeuw, C.D., Barnekow, A., and Hoogenraad, C.: (2002): Bicaudal-D regulates COPI-independent Golgi-ER transport by recruiting the dynein-dynactin motor complex. *Nat. Cell Biol.*, **4**(12):986–92.

Maurer, S., Bieling, P., Cope, J., Hoenger, A., and Surrey, T.: (2011): GTPgammaS microtubules mimic the growing microtubule end structure recognized by end-binding proteins (EBs). *Proc. Natl. Acad. Sci. USA*, **108**(10):3988–93.

Maxwell, C., Keats, J., Crainie, M., Sun, X., Yen, T., Shibuya, E., Hendzel, M., Chan, G., and Pilarski, L.: (2003): RHAMM is a centrosomal protein that interacts with dynein and maintains spindle pole stability. *Mol. Biol. Cell*, **14**(6):2262–76.

Mayor, T., Stierhof, Y., Tanaka, K., Fry, A., and Nigg, E.: (2000): The centrosomal protein C-Nap1 is required for cell cycle-regulated centrosome cohesion. *J. Cell Biol.*, **151**(4):837–46.

McAinsh, A. and Meraldi, P.: (2011): The CCAN complex: Linking centromere specification to control of kinetochore-microtubule dynamics. *Semin. Cell Dev. Biol.*, **22**(9):946–52.

McEwen, B., Heagle, A., Cassels, G., Buttle, K., and Rieder, C.: (1997): Kinetochore fiber maturation in PtK1 cells and its implications for the mechanisms of chromosome congression and anaphase onset. *J. Cell Biol.*, **137**(7):1567–80.

McGuinness, B., Hirota, T., Kudo, N., Peters, J., and Nasmyth, K.: (2005): Shugoshin prevents dissociation of cohesin from centromeres during mitosis in vertebrate cells. *PLoS Biol.*, **3**(3).

McIntosh, J., Grishchuk, E., Morphew, M., Efremov, A., Zhudenkov, K., Volkov, V., Cheeseman, I., Desai, A., Mastronarde, D., and Ataullakhanov, F.: (2008): Fibrils connect microtubule tips with kinetochores: a mechanism to couple tubulin dynamics to chromosome motion. *Cell*, **135**(2):322–33.

McNally, F. and Thomas, S.: (1998): Katanin is responsible for the M-phase microtubule-severing activity in Xenopus eggs. *Mol. Biol. Cell*, **9**(7):1847–61.

Merdes, A., Heald, R., Samejima, K., Earnshaw, W., and Cleveland, D.: (2000): Formation of spindle poles by dynein/dynactin-dependent transport of NuMA. *J. Cell Biol.*, **149**(4):851–62.

Merdes, A., Ramyar, K., Vechio, J., and Cleveland, D.: (1996): A complex of NuMA and cytoplasmic dynein is essential for mitotic spindle assembly. *Cell*, **87**(3):447–58.

Merlini, L. and Piatti, S.: (2011): The mother-bud neck as a signaling platform for the coordination between spindle position and cytokinesis in budding yeast. *Biol. Chem.*, **392**(8-9):805–12.

Mi, J., Guo, C., Brautigan, D., and Larner, J.: (2007): Protein phosphatase-1alpha regulates centrosome splitting through Nek2. *Cancer Res.*, **67**(3):1082–9.

Mitchison, J.: (1971): *The Biology of the Cell Cycle*. Cambridge University Press.

Mitchison, T. and Kirschner, M.: (1984): Dynamic instability of microtubule growth. *Nature*, **312**:237–242.

Morgan, D.O.: (2007): *The Cell Cycle - Principles of Control*. New Science Press Ltd.

Morone, N., Fujiwara, T., Murase, K., Kasai, R., Ike, H., Yuasa, S., Usukura, J., and Kusumi, A.: (2006): Three-dimensional reconstruction of the membrane skeleton at the plasma membrane interface by electron tomography. *J. Cell Biol.*, **174**(6):851–62.

Muhua, L., Adames, N., Murphy, M., Shields, C., and Cooper, J.: (1998): A cytokinesis checkpoint requiring the yeast homologue of an APC-binding protein. *Nature*, **393**(6684):487–91.

Murray, A., Solomon, M., and Kirschner, M.: (1989): The role of cyclin synthesis and degradation in the control of maturation promoting factor activity. *Nature*, **339**(6222):280–6.

Musacchio, A. and Salmon, E.: (2007): The spindle-assembly checkpoint in space and time. *Nat. Rev. Mol. Cell Biol.*, **8**(5):379–93.

Nachury, M., Maresca, T., Salmon, W., Waterman-Storer, C., Heald, R., and Weis, K.: (2001): Importin beta is a mitotic target of the small GTPase Ran in spindle assembly. *Cell*, **104**(1):95–106.

Nakamura, A., Arai, H., and Fujita, N.: (2009): Centrosomal Aki1 and cohesin function in separase-regulated centriole disengagement. *J. Cell Biol.*, **187**:607–614.

Neef, R., Preisinger, C., Sutcliffe, J., Kopajtich, R., Nigg, E.A., Mayer, T.U., and Barr, F.A.: (2003): Phosphorylation of mitotic kinesin-like protein 2 by polo-like kinase 1 is required for cytokinesis. *J. Cell Biol.*, **162**:863–875.

Nilsson, J., Yekezare, M., Minshull, J., and Pines, J.: (2008): The APC/C maintains the spindle assembly checkpoint by targeting Cdc20 for destruction. *Nat. Cell Biol.*, **10**(12):1411–20.

Petry, S., Groen, A., Ishihara, K., Mitchison, T., and Vale, R.: (2013): Branching microtubule nucleation in Xenopus egg extracts mediated by augmin and TPX2. *Cell*, **152**(4):768–77.

Pfister, K., Shah, P., Hummerich, H., Russ, A., Cotton, J., Annuar, A., King, S., and Fisher, E.: (2006): Genetic analysis of the cytoplasmic dynein subunit families. *PLoS Genet.*, **2**(1).

Pinyol, R., Scrofani, J., and Vernos, I.: (2012): The Role of NEDD1 Phosphorylation by Aurora A in Chromosomal Microtubule Nucleation and Spindle Function. *Curr. Biol.*, **23**(2):143–9.

Raaijmakers, J., van Heesbeen, R., Meaders, J., Geers, E., Fernandez-Garcia, B., Medema, R., and Tanenbaum, M.: (2012): Nuclear envelope-associated dynein drives prophase centrosome separation and enables Eg5-independent bipolar spindle formation. *EMBO J*, **31**(21):4179–90.

Rapali, P., Radnai, L., Süveges, D., Harmat, V., Tölgyesi, F., Wahlgren, W., Katona, G., Nyitray, L., and Pál, G.: (2011a): Directed evolution reveals the binding motif preference of the LC8/DYNLL hub protein and predicts large numbers of novel binders in the human proteome. *PLoS ONE*, **6**(4):18818.

Rapali, P., Szenes, A., Radnai, L., Bakos, A., Pál, G., and Nyitray, L.: (2011b): DYNLL/LC8: A Light Chain Subunit of the Dynein Motor Complex and Beyond. *FEBS J*, **278**(17):2980–96.

Rappaport, R.: (1971): Cytokinesis in animal cells. *Int. Rev. Cytol.*, **31**:169–213.

Redemann, S., Pecreaux, J., Goehring, N., Khairy, K., Stelzer, E., Hyman, A., and Howard, J.: (2010): Membrane invaginations reveal cortical sites that pull on mitotic spindles in one-cell C. elegans embryos. *PLoS ONE*, **5**(8).

Rieder, C., Cole, R., Khodjakov, A., and Sluder, G.: (1995): The checkpoint delaying anaphase in response to chromosome monoorientation is mediated by an inhibitory signal produced by unattached kinetochores. *J. Cell Biol.*, **130**(4):941–8.

Rieder, C. and Salmon, E.: (1998): The vertebrate cell kinetochore and its roles during mitosis. *Trends Cell Biol.*, **8**(8):310–8.

Santaguida, S. and Musacchio, A.: (2009): The life and miracles of kinetochores. *EMBO J*, **28**:2511–2531.

Santamaria, A., Nagel, S., Sillje, H., and Nigg, E.: (2008): The spindle protein CHICA mediates localization of the chromokinesin Kid to the mitotic spindle. *Curr. Biol.*, **18**(10):723–9.

Sawin, K., LeGuellec, K., Philippe, M., and Mitchison, T.: (1992): Mitotic spindle organization by a plus-end-directed microtubule motor. *Nature*, **359**(6395):540–3.

Schaefer, M., Shevchenko, A., Shevchenko, A., and Knoblich, J.: (2000): A protein complex containing Inscuteable and the Galpha-binding protein Pins orients asymmetric cell divisions in Drosophila. *Curr. Biol.*, **10**(7):353–62.

Schmidt, J., Kiyomitsu, T., Hori, T., Backer, C., Fukagawa, T., and Cheeseman, I.: (2010): Aurora B kinase controls the targeting of the Astrin-SKAP complex to bioriented kinetochores. *J. Cell Biol.*, **191**:269–80.

Schöckel, L., Möckel, M., Mayer, B., Boos, D., and Stemmann, O.: (2011): Cleavage of cohesin rings coordinates the separation of centrioles and chromatids. *Nat. Cell Biol.*, **13**(8):966–72.

Schuyler, S. and Pellman, D.: (2001): Microtubule "plus-end-tracking proteins": The end is just the beginning. *Cell*, **105**(4):421–4.

Shindo, N., Kumada, K., and Hirota, T.: (2012): Separase sensor reveals dual roles for separase coordinating cohesin cleavage and cdk1 inhibition. *Dev. Cell*, **23**(1):112–23.

Shorter, J., Watson, R., Giannakou, M.E., Clarke, M., Warren, G., and Barr, F.A.: (1999): GRASP55, a second mammalian GRASP protein involved in the stacking of Golgi cisternae in a cell-free system5, a second mammalian GRASP protein involved in the stacking of Golgi cisternae in a cell-free system. *EMBO J*, **18**:4949–4960.

Shu, T., Ayala, R., Nguyen, M., Xie, Z., Gleeson, J., and Tsai, L.: (2004): Ndel1 operates in a common pathway with LIS1 and cytoplasmic dynein to regulate cortical neuronal positioning. *Neuron*, **44**(2):263–77.

Slep, K., Rogers, S., Elliott, S., Ohkura, H., Kolodziej, P., and Vale, R.: (2005): Structural determinants for EB1-mediated recruitment of APC and spectraplakins to the microtubule plus end. *J. Cell Biol.*, **168**(4):587–98.

Splinter, D., Tanenbaum, M., Lindqvist, A., Jaarsma, D., Flotho, A., Yu, K., Grigoriev, I., Engelsma, D., Haasdijk, E., Keijzer, N., Demmers, J., Fornerod, M., Melchior, F., Hoogenraad, C., Medema, R., and Akhmanova, A.: (2010): Bicaudal D2, dynein, and kinesin-1 associate with nuclear pore complexes and regulate centrosome and nuclear positioning during mitotic entry. *PLoS Biol.*, **8**(4).

Stemmann, O., Zou, H., Gerber, S., Gygi, S., and Kirschner, M.: (2001): Dual inhibition of sister chromatid separation at metaphase. *Cell*, **107**(6):715–26.

Stevens, D., Gassmann, R., Oegema, K., and Desai, A.: (2011): Uncoordinated loss of chromatid cohesion is a common outcome of extended metaphase arrest. *PLoS ONE*, **6**(8).

Stuckey, J. and Dixon, J.: (1999): Crystal structure of a phospholipase D family member. *Nat. Struct. Biol.*, **6**(3):278–84.

Sudakin, V., Chan, G., and Yen, T.: (2001): Checkpoint inhibition of the APC/C in HeLa cells is mediated by a complex of BUBR1, BUB3, CDC20, and MAD2. *J. Cell Biol.*, **154**(5):925–36.

Sumara, I., Vorlaufer, E., Stukenberg, P., Kelm, O., Redemann, N., Nigg, E., and Peters, J.: (2002): The dissociation of cohesin from chromosomes in prophase is regulated by Polo-like kinase. *Mol. Cell*, **9**(3):515–25.

Tanaka, T., Serneo, F., Higgins, C., Gambello, M., Wynshaw-Boris, A., and Gleeson, J.: (2004): Lis1 and doublecortin function with dynein to mediate coupling of the nucleus to the centrosome in neuronal migration. *J. Cell Biol.*, **165**(5):709–21.

Tanenbaum, M., Akhmanova, A., and Medema, R.: (2010): Dynein at the nuclear envelope. *EMBO Rep*, **11**(9):649.

Tanno, Y., Kitajima, T., Honda, T., Ando, Y., Ishiguro, K., and Watanabe, Y.: (2010): Phosphorylation of mammalian Sgo2 by Aurora B recruits PP2A and MCAK to centromeres. *Genes Dev.*, **24**(19):2169–79.

Thein, K.H., Kleylein-Sohn, J., Nigg, E.A., and Gruneberg, U.: (2007): Astrin is required for the maintenance of sister chromatid cohesion and centrosome integrity. *J. Cell Biol.*, **178**(3):345–354.

Theis, M., Slabicki, M., Junqueira, M., Paszkowski-Rogacz, M., Sontheimer, J., Kittler, R., Heninger, A.K., Glatter, T., Kruusmaa, K., Poser, I., Hyman, A.A., Pisabarro, M.T., Gstaiger, M., Aebersold, R., Shevchenko, A., and Buchholz, F.: (2009): Comparative profiling identifies C13orf3 as a component of the Ska complex required for mammalian cell division. *EMBO J*, **28**(10):1453–65.

Théry, M., Racine, V., Pépin, A., Piel, M., Chen, Y., Sibarita, J., and Bornens, M.: (2005): The extracellular matrix guides the orientation of the cell division axis. *Nat. Cell Biol.*, **7**(10):947–53.

Tolg, C., Hamilton, S., Morningstar, L., Zhang, J., Zhang, S., Esguerra, K., Telmer, P., Luyt, L., Harrison, R., McCarthy, J., and Turley, E.: (2010): RHAMM promotes interphase microtubule instability and mitotic spindle integrity through MEK1/ERK1/2 activity. *J. Biol. Chem.*, **285**(34):26461–74.

Tournebize, R., Popov, A., Kinoshita, K., Ashford, A., Rybina, S., Pozniakovsky, A., Mayer, T., Walczak, C., Karsenti, E., and Hyman, A.: (2000): Control of microtubule dynamics by the antagonistic activities of XMAP215 and XKCM1 in Xenopus egg extracts. *Nat. Cell Biol.*, **2**(1):13–9.

Trokter, M., Mücke, N., and Surrey, T.: (2012): Reconstitution of the human cytoplasmic dynein complex. *Proc. Natl. Acad. Sci. USA*, **109**(51):20895–900.

Tsai, J., Bremner, K., and Vallee, R.: (2007): Dual subcellular roles for LIS1 and dynein in radial neuronal migration in live brain tissue. *Nat. Neurosci.*, **10**(8):970–9.

Tsou, M. and Stearns, T.: (2006): Mechanism limiting centrosome duplication to once per cell cycle. *Nature*, **442**(7105):947–51.

Tsou, M., Wang, W., George, K., Uryu, K., Stearns, T., and Jallepalli, P.: (2009): Polo kinase and separase regulate the mitotic licensing of centriole duplication in human cells. *Dev. Cell*, **17**(3):344–54.

Turley, E., Austen, L., Vandeligt, K., and Clary, C.: (1991): Hyaluronan and a cell-associated hyaluronan binding protein regulate the locomotion of ras-transformed cells. *J. Cell Biol.*, **112**(5):1041–7.

Uchida, K., Takagaki, K., Kumada, K., Hirayama, Y., Noda, T., and Hirota, T.: (2009): Kinetochore stretching inactivates the spindle assembly checkpoint. *J. Cell Biol.*, **184**(3):383–90.

Uhlmann, F. and Nasmyth, K.: (1998): Cohesion between sister chromatids must be established during DNA replication. *Curr. Biol.*, **8**(20):1095–101.

Vaisberg, E., Koonce, M., and McIntosh, J.: (1993): Cytoplasmic dynein plays a role in mammalian mitotic spindle formation. *J. Cell Biol.*, **123**(4):849–58.

Vernos, I., Raats, J., Hirano, T., Heasman, J., Karsenti, E., and Wylie, C.: (1995): Xklp1, a chromosomal Xenopus kinesin-like protein essential for spindle organization and chromosome positioning. *Cell*, **81**(1):117–27.

Vigneron, S., Prieto, S., Bernis, C., Labbé, J., Castro, A., and Lorca, T.: (2004): Kinetochore localization of spindle checkpoint proteins: who controls whom? *Mol. Biol. Cell*, **15**(10):4584–96.

Waizenegger, I., Hauf, S., Meinke, A., and Peters, J.: (2000): Two distinct pathways remove mammalian cohesin from chromosome arms in prophase and from centromeres in anaphase. *Cell*, **103**(3):399–410.

Wang, C., Li, S., Januschke, J., Rossi, F., Izumi, Y., Garcia-Alvarez, G., Gwee, S., Soon, S., Sidhu, H., Yu, F., Matsuzaki, F., Gonzalez, C., and Wang, H.: (2011): An ana2/ctp/mud complex regulates spindle orientation in Drosophila neuroblasts. *Dev. Cell*, **21**(3):520–33.

Wang, C., Thor, A., Moore, D., Zhao, Y., Kerschmann, R., Stern, R., Watson, P., and Turley, E.: (1998): The overexpression of RHAMM, a hyaluronan-binding protein that regulates ras signaling, correlates with overexpression of mitogen-activated protein kinase and is a significant parameter in breast cancer progression. *Clin. Cancer Res.*, **4**(3):567–76.

Wang, X., Yang, Y., Duan, Q., Jiang, N., Huang, Y., Darzynkiewicz, Z., and Dai, W.: (2008): sSgo1, a major splice variant of Sgo1, functions in centriole cohesion where it is regulated by Plk1. *Dev. Cell*, **14**(3):331–41.

Weaver, B., Bonday, Z., Putkey, F., Kops, G., Silk, A., and Cleveland, D.: (2003): Centromere-associated protein-E is essential for the mammalian mitotic checkpoint to prevent aneuploidy due to single chromosome loss. *J. Cell Biol.*, **162**(4):551–63.

Welburn, J., Vleugel, M., Liu, D., Yates, J., Lampson, M., Fukagawa, T., and Cheeseman, I.: (2010): Aurora B phosphorylates spatially distinct targets to differentially regulate the kinetochore-microtubule interface. *Mol. Cell*, **38**(3):383–92.

Welburn, J.P., Grishchuk, E.L., Backer, C.B., Wilson-Kubalek, E.M., III, J.R.Y., and Cheeseman, I.M.: (2009): The Human Kinetochore Ska1 Complex Facilitates Microtubule Depolymerization-Coupled Motility. *Dev. Cell*, **16**:374–385.

Westhorpe, F., Tighe, A., Lara-Gonzalez, P., and Taylor, S.: (2011): p31comet-mediated extraction of Mad2 from the MCC promotes efficient mitotic exit. *J. Cell Sci.*, **124**(22):3905–16.

Wilde, A. and Zheng, Y.: (1999): Stimulation of microtubule aster formation and spindle assembly by the small GTPase Ran. *Science*, **284**(5418):1359–62.

Wilm, M., Shevchenko, A., Houthaeve, T., Breit, S., Schweigerer, L., Fotsis, T., and Mann, M.: (1996): Femtomole sequencing of proteins from polyacrylamide gels by nano-electrospray mass spectrometry. *Nature*, **379**(6564):466–9.

Wittmann, T. and Hyman, T.: (1999): Recombinant p50/dynamitin as a tool to examine the role of dynactin in intracellular processes. *Methods Cell Biol.*, **61**:137–43.

Wittmann, T., Wilm, M., Karsenti, E., and Vernos, I.: (2000): TPX2, A novel xenopus MAP involved in spindle pole organization. *J. Cell Biol.*, **149**(7):1405–18.

Wu, H. and King, S.: (2003): Backbone dynamics of dynein light chains. *Cell Motil. Cytoskeleton*, **54**(4):267–73.

Xia, G., Luo, X., Habu, T., Rizo, J., Matsumoto, T., and Yu, H.: (2004): Conformation-specific binding of p31(comet) antagonizes the function of Mad2 in the spindle checkpoint. *EMBO J*, **23**(15):3133–43.

Yaakov, G., Thorn, K., and Morgan, D.: (2012): Separase biosensor reveals that cohesin cleavage timing depends on phosphatase PP2A(Cdc55) regulation. *Dev. Cell*, **23**(1):124–36.

Yang, M., Li, B., Tomchick, D., Machius, M., Rizo, J., Yu, H., and Luo, X.: (2007): p31comet blocks Mad2 activation through structural mimicry. *Cell*, **131**(4):744–55.

Zeng, K., Bastos, R.N., Barr, F.A., and Gruneberg, U.: (2010): Protein phosphatase 6 regulates mitotic spindle formation by controlling the T-loop phosphorylation state of Aurora A bound to its activator TPX2. *J. Cell Biol.*, **191**(7):1315–32.

Zhao, Y. and Chen, R.: (2006): Mps1 phosphorylation by MAP kinase is required for kinetochore localization of spindle-checkpoint proteins. *Curr. Biol.*, **16**(17):1764–9.

Zhu, M., Settele, F., Kotak, S., Sanchez-Pulido, L., Ehret, L., Ponting, C., Gönczy, P., and Hoffmann, I.: (2013): MISP is a novel Plk1 substrate required for proper spindle orientation and mitotic progression. *J. Cell Biol.*, **200**(6):773–87.

A. Appendix

A.1. Cell lines

Table A.1: Cell lines used in this study.

Cell line	Selection	Expression of transgene
HeLa S3		
HEK 293T		
HeLa FlpIn	50 μg/ml zeocin, 4 μg/ml blasticidin	
HeLa S3 Astrin N-GFP	0.7 mg/ml geneticin	constitutive
HeLa FlpIn Astrin N-Myc	200 μg/ml hygromycin, 4 μg/ml blasticidin	inducible
HeLa Kyoto mouse DYNC1H1 N-GFP	0.7 mg/ml geneticin	constitutive
HeLa FlpIn DYNLL1 N-GFP	200 μg/ml hygromycin, 4 μg/ml blasticidin	inducible
HeLa S3 Histone H2B N-mCherry, Tubulin N-GFP	1 μg/ml puromycin, 4 μg/ml blasticidin	constitutive
HeLa S3 KID N-GFP	0.7 mg/ml geneticin	constitutive
HeLa FlpIn Kinastrin N-Myc	200 μg/ml hygromycin, 4 μg/ml blasticidin	inducible
HeLa FlpIn LifeAct N-mCherry	200 μg/ml hygromycin, 4 μg/ml blasticidin	inducible
HeLa FlpIn Plk1 N-GFP	200 μg/ml hygromycin, 4 μg/ml blasticidin	inducible
HeLa FlpIn Plk1 C-GFP	200 μg/ml hygromycin, 4 μg/ml blasticidin	inducible
HeLa Kyoto mouse Plk1 N-GFP	0.7 mg/ml geneticin	constitutive

A.2. Plasmids

Table A.2: Plasmids used in this study.

Plasmid	Gene	Insert	Vector	Tag
UGL5	Astrin	Full length	pcDNA3.1-FlagA	Flag
UGM276	Astrin	Full length	pcDNA3.1-3xMyc-A	Myc
KE9	Astrin	aa 1-481	pcDNA3.1-3xMyc-A	Myc
KE15	Astrin	aa 482-1193	pcDNA3.1-3xMyc-A	Myc
KR3.1	Astrin	aa 482-850	pcDNA3.1-3xMyc-A	Myc
KR4	Astrin	aa 851-1193	pcDNA3.1-3xMyc-A	Myc
pUGL17	Astrin	Full length	pcDNA5/FRT/TO Myc	Myc
KE3	Astrin	Full length	pcDNA3 eGFP	GFP
pFB5856.1	CHICA	Full length	pcDNA5/FRT/TO GFP	GFP

Continued on next page

Plasmid	Gene	Insert	Vector	Tag
pFB6308.1	CHICA	aa 1-281	pcDNA5/FRT/TO GFP	GFP
pFB6310.1	CHICA	aa 188-394	pcDNA5/FRT/TO GFP	GFP
pFB6311.1	CHICA	aa 383-615	pcDNA5/FRT/TO GFP	GFP
pFB6490	CHICA	Full length	pcDNA3.1-3xMyc-A	Myc
pAD74	CHICA	aa 1-281	pcDNA3.1-3xMyc-A	Myc
pAD75	CHICA	aa 188-394	pcDNA3.1-3xMyc-A	Myc
pAD76	CHICA	aa 383-615	pcDNA3.1-3xMyc-A	Myc
pAD92	CHICA	Full length, TQT421AAA	pcDNA3.1-3xMyc-A	Myc
pAD93	CHICA	Full length, TQT439AAA	pcDNA3.1-3xMyc-A	Myc
pAD94	CHICA	Full length, TQT472AAA	pcDNA3.1-3xMyc-A	Myc
pAD97	CHICA	Full length, 3xTQT<AAA	pcDNA3.1-3xMyc-A	Myc
pAD145	CHICA	Full length	pcDNA5/FRT/TO mCherry	mCherry
pAD147	CHICA	Full length, 3xTQT<AAA	pcDNA5/FRT/TO mCherry	mCherry
pAD46	DYNLL1	Full length	pcDNA5/FRT/TO GFP	GFP
pAD60	EB1	Full length	pcDNA4 C-mCherry	mCherry
pAD179	HMMR	Full length	pcDNA3.1-3xMyc-A	Myc
pAD182	HMMR	aa 1-189	pcDNA3.1-3xMyc-A	Myc
pAD183	HMMR	aa 183-364	pcDNA3.1-3xMyc-A	Myc
pAD184	HMMR	aa 365-546	pcDNA3.1-3xMyc-A	Myc
pAD185	HMMR	aa 547-726	pcDNA3.1-3xMyc-A	Myc
pFB6300	HMMR	Full length	pcDNA5/FRT/TO GFP	GFP
pFB6292	HMMR	aa 1-189	pcDNA5/FRT/TO GFP	GFP
pFB6293	HMMR	aa 183-364	pcDNA5/FRT/TO GFP	GFP
pFB6294	HMMR	aa 365-546	pcDNA5/FRT/TO GFP	GFP
pFB6295	HMMR	aa 547-726	pcDNA5/FRT/TO GFP	GFP
pUGL21	Kinastrin	Full length	pcDNA5/FRT/TO Myc	Myc
pUGL25	Kinastrin	Full length	pGEX-5X-1	GST
UGL32.1	Kinastrin	Full length	pcDNA3.1-FlagA	Flag
UGL20	Kinastrin	Full length	pcDNA3.1-3xMyc-A	Myc
pAD34	Kinastrin	aa 79-317	pcDNA3.1-3xMyc-A	Myc
pAD32	Kinastrin	aa 1-158	pcDNA3.1-3xMyc-A	Myc
pAD31	Kinastrin	aa 159-317	pcDNA3.1-3xMyc-A	Myc
pAD41	Plk1	Full length	pcDNA5/FRT/TO C-GFP	GFP
pFB3028	PRC1	Full length	pcDNA3.1-3xMyc-A	Myc
pFB2343	Rab4	Full length	pcDNA3.1-3xMyc-A	Myc
pOG44		Flp recombinase	company: Invitrogen	

A.3. Primers

Table A.3: Sequences of primers used for gene amplification. Capital letters indicate nucleotides complementary to gene sequence. Small letters indicate the restriction sites and additional nucleotides to maintain the open reading frame.

Gene	Primer name	Sequence
CHICA Full length	CHICA Fw	5'-ATGGCGCGGGCCTGTTTGATTC-3'
	CHICA Rv	5'-TTACTGATAGGAAGGATAAAGT-3'
	CHICA-Fw-BamHI	5'-cttggatcccgATGGCGCGGGCCTGTTTGA TTCA-3'
	CHICA-Rv-SalI	5'-ggcgtcgacTTACTGATAGGAAGGATAAAGT-3'
CHICA aa1-281	N term CHICA fwd-BamHI	5'-ggatccccATGGCGCGGGCCTGTTTGATT-3'
	N term CHICA rev-XhoI	5'-gctcgagtcAGATGCCATCAATCAACGTGAA-3'
CHICA aa188-394	Mid CHICA fwd BamHI	5'-gggatccccTCGGCGCGAGAGGTGATTGCA-3'
	Mid CHICA rev XhoI	5'-gctcgagtcACTCACAGTCATGGGGCTTGCG-3'
CHICA aa383-615	CHICA aa383 fwd	5'-CCATGGAGGGCAAGGCAGAGCGCA AGCCCC-3'
DYNLL1 Full length	DYNLL1-FWI	5'-CTGTCGCGGCCCCCACCTCAGGTAACC-3'
	DYNLL1-RVI	5'-GATCACTGGGTGTGTGGCACAGTC CATGCTT-3'
	DYNLL1-FWII-BamHI	5'-ggcggatccccATGTGCGACCGAAAGG CCGTGATCAAAAATG-3'
	DYNLL1-RVII-XhoI	5'-ggcctcgagTTAACCAGATTTGAACAG AAGAATGGCCAC-3'
EB1 Full length	EB1-FWI	5'-GACGCGGTTCTGCCGAGAGCCG AAG-3'
	EB1-RV	5'-GATGTTGCTCTGCTGGTCCAGGCTG-3'
	EB1-FWII-BamHI	5'-ggcggatccccATGGCAGTGAACGTAT ACTCAACGTC-3'
	EB1-RVII-noSTOP-XhoI	5'-ggcctcgagATACTCTTCTTGCTCC TCCTGTGGG-3'
Kinastrin Full length	C15ORF23-FWI	5'-GGCCTCTGAGCGAACCTTCCGTACAGT-3'
	C15ORF23-RVI	5'-GGGAGCCATCTGGCCACTTGCTTCTTC-3'
	C15ORF23-FWII-BamHI	5'-ggcggatcctcATGGCGGCTCCCGAA GCCCCGCCCCTG-3'
	C15ORF23-RVII-XhoI	5'-ggcctcgagTTACATTTCTAATAGCT GCTCCATTTC-3'
Kinastrin aa79-317	Kinastrin-N2-FW-BamHI	5'-ggcggatcctcATGACCAGTGTGGTTAA GACAGTGTATAG-3'
	C15ORF23-RVII-XhoI	5'-ggcctcgagTTACATTTCTAATAGCTGC TCCATTTC-3'

Continued on next page

Gene	Primer name	Sequence
Kinastrin aa1-158	C15ORF23-FWII-BamHI	5'-ggcggatcctcATGGCGGCTCCCGAAGCCCCGCCCCTG-3'
	Kina-N-Rev-XhoI	5'-ggcctcgagTTAATTCCTTCTGGTGGCAGTG-3'
Kinastrin aa159-317	Kina-C-Fw-BamHI	5'-ggcggatcctcGTCAGAAAAGGCTACAAAC-3'
Plk1 Full length	Plk1 nostop-RVII-XhoI	5'-GGCCTCGAGGGAGGCCTTGAGACGGTT-3'

Table A.4: Sequences of primers used for mutagenesis. Small letters indicate nucleotides complementary to gene sequence. Capital letters indicate non-complementary nucleotides generating mutations.

Gene	Primer name	Sequence
CHICA TQT421AAA	CHICA-TQT-417-AAA-Fw	5'-gccattgacgctgccGCTGCAGCAgagccaggagaggag-3'
	CHICA-TQT-417-AAA-Rv	5'-ctcctctcctggctcTGCTGCAGCggcagcgtcaatggc-3'
CHICA TQT439AAA	CHICA-TQT-435-AAA-Fw	5'-gtgagtgaggtgggaGCAGCAGCCagcatcaccacagc-3'
	CHICA-TQT-435-AAA-Rv	5'-gctgtggtgatgctGGCTGCTGCtcccacctcactcac-3'
CHICA TQT472AAA	CHICA-TQT-468-AAA-Fw	5'-ccagatcgaccactGCTGCGGCTgacatggatgagaac-3'
	CHICA-TQT-468-AAA-Rv	5'-gttctcatccatgtcAGCCGCAGCagtggtcgatctgg-3'
CHICA H272R	CHICA H272R Fw	5'-gattattgggaaggttAGGgaaaagttcacgttg-3'
	CHICA H272R Rv	5'-caacgtgaacttttcCCTaaccttccaataatc-3'
CHICA PLD272AAA	CHICA DUF to AAA-Fw	5'-gattattgggaaggttGCCgaaGCGttcacgttgattGCTggcatccgcgtggc-3'
	CHICA DUF to AAA-Rv	5'-gccacgcggatgccAGCaatcaacgtgaaCGCttcGGCaaccttcccaataatc-3'
Kinastrin SLLP111ALAP	Kinastrin-SLLP-111-ALAP-Fw	5'-gccacttctaagGCTctcGCAcctgttaggtccaaag-3'
	Kinastrin-SLLP-111-ALAP-Rv	5'-ctttggacctaacaggTGCgagAGCcttagaagtggc-3'

A.4. siRNA target sequences

Table A.5: List of duplexes used for siRNA-mediated depletion.

Targeted gene	Sense Sequence of siRNA duplex	Source/Company
Astrin 367	5'-CCGACAACTCACAGAGAAAdTdT-3'	Dharmacon
B56α	SmartPool L-009352-00	Dharmacon
CenpE	5'-CACGATACTGTTAACATGAAT-3'	Qiagen
CHICA	No.1 5'-CAAUUCCACUUCGCUGGUAdTdT-3'	Qiagen
	No.2 5'-GAACUAAGAUUAUUGGGAAdTdT-3'	Qiagen
CHICA 3'UTR	5'-GGTTTAAACACTATGGATA-3'	Qiagen
DYNLL1	5'-GAAGGACAUUGCGGCUCAUUU-3'	Qiagen
	SMARTpool L-005281	Dharmacon
Gl2	5'-CGTACGCGGAATACTTCGAdTdT-3'	Dharmacon
HMMR	No.1 5'-CUGAUUUGCAGAACCAACUdTdT-3'	Qiagen
	No.2 5'-GGAGAA UAUUGUUAUAUUAdTdT-3'	Qiagen
HURP	5'-TACTTTGAATTCACAAACTAA-3'	Qiagen
Kinastrin	No.1 5'-CAAACTCGGGCCACTTCTAdTdT-3'	Sigma-Aldrich
	No.2 5'-CAAATGAAAGCTACTGACAdTdT-3'	Sigma-Aldrich
	No.5 5'-AGGCTACAAACCACTGAGTAA-3'	Qiagen
	No.8 5'-TTGGATTGACCTTCTAGTCAA-3'	Qiagen
	SmartPool L-022219-00	Dharmacon
Nuf2	5'-GCATGCCGTGAAACGTATAdTdT-3'	Dharmacon
Separase	5'-GCCTCTTGGATGAGATCTTdTdT-3'	Dharmacon
Sgo1	5'-CAGTAGAACCTGCTCAGAA-3'	Qiagen
Sgo2	SMARTpool L-016154-01	Dharmacon
TACC3	5'-GTTACCGGAAGATCGTCTG-3'	Qiagen

A.5. Antibodies

Table A.6: Primary Antibodies used for the described experiments.

Antibody	Species	Source/Company	Conc. [μg/ml]
Actin	Goat	Santa Cruz Biotechnology, Inc.	1
Astrin	Rabbit	(Thein *et al.*, 2007)	0.2
B56α	Mouse	BD	1
BicD2	Rabbit	In-house	1
Bub1	Mouse	Abcam	1
BubR1	Mouse	Millipore	1
CenpE	Mouse	Abcam	4.5

Continued on next page

Antibody	Species	Source/Company	Conc. [μg/ml]
CenpE	Rabbit	Bethyl Laboratories, Inc.	1
Centrin-3	Mouse	Abcam	1
CHICA	Sheep	Jennifer Lloyd, (Dunsch *et al.*, 2012)	1
CREST (Serum)	Human	Europa Bioproducts Ltd.	1:3000 dilution
CyclinB1	Mouse	Millipore	0.5
DYNC1H1 (clone 440.4)	Mouse	Sigma Aldrich	0.5
DYNC1I2	Mouse	Sigma Aldrich	1
DYNLL1	Rabbit	Epitomics, Inc.	1
EB1	Mouse	Cell Signalling Technology	1
Eg5	Sheep	(Zeng *et al.*, 2010)	1
Flag	Rabbit	Sigma Aldrich	1
GFP	Rabbit	Abcam	1
GFP	Sheep	(Shorter *et al.*, 1999)	1
GST	Rabbit		1
HMMR	Sheep	In-house, (Dunsch *et al.*, 2012)	1
HMMR	Mouse	Abcam	1
HURP	Sheep	In-house	0.6
KID	Rabbit	Cytoskeleton, Inc.	0.25
Kinastrin	Sheep	In-house, (Dunsch *et al.*, 2011)	0.36
Kinastrin-Biotin	Sheep	In-house, (Dunsch *et al.*, 2011)	0.36
mCherry	Sheep	In-house	1
Myc (clone 9E10)	Mouse	Sigma Aldrich	2
Myc	Rabbit	Sigma Aldrich	0.5
NuMA	Rabbit	Abcam	1
$p150^{Glued}$	Mouse	BD	1
Pericentrin	Rabbit	Abcam	1
PICH	Mouse	Millipore	1
Plk1	Mouse	Santa Cruz Biotechnology, Inc.	1
Plk1	Goat	In-house, (Neef *et al.*, 2003)	1
PRC1	Rabbit	In-house, (Gruneberg *et al.*, 2006)	1
RanGAP1	Rabbit	Bethyl Laboratories, Inc.	1
RanBP2	Rabbit	Bethyl Laboratories, Inc.	0.2
Securin	Mouse	Bethyl Laboratories, Inc.	1
Separase	Mouse	Abcam	1
Separase	Rabbit	Bethyl Laboratories, Inc.	1
Sgo1	Mouse	Abcam	1-5
Sgo2	Rabbit	Bethyl Laboratories, Inc.	1
TACC3 (clone H-300)	Rabbit	Santa Cruz Biotechnology, Inc.	1
Tubulin (DM1A)	Mouse	Sigma Aldrich	1
Tubulin	Rabbit	Epitomics, Inc.	1

Table A.7: Secondary Antibodies used for the described experiments.

Antibody	Species	Source/Company	Conc. [μg/ml]
Human Cy5	Donkey	Jackson ImmunoRes. Lab., Inc.	1
Mouse AlexaFluor 488	Donkey	Invitrogen	1
Mouse AlexaFluor 555	Donkey	Invitrogen	1
Rabbit AlexaFluor 488	Donkey	Invitrogen	1
Rabbit AlexaFluor 555	Donkey	Invitrogen	1
Streptavidin		Jackson ImmunoRes. Lab., Inc.	1

A.6. Publications

A.6.1. Publication 1

The astrin-kinastrin/SKAP complex localizes to microtubule plus ends and facilitates chromosome alignment.

Anja K Dunsch, Emily Linnane, Francis A Barr, Ulrike Gruneberg.

Astrin is a mitotic spindle-associated protein required for the correct alignment of all chromosomes at the metaphase plate. Astrin depletion delays chromosome alignment and causes the loss of normal spindle architecture and sister chromatid cohesion before anaphase onset. Here we describe an astrin complex containing kinastrin/SKAP, a novel kinetochore and mitotic spindle protein, and three minor interaction partners: dynein light chain, Plk1, and Sgo2. Kinastrin is the major astrin-interacting protein in mitotic cells, and is required for astrin targeting to microtubule plus ends proximal to the plus tip tracking protein EB1. Cells overexpressing or depleted of kinastrin mislocalize astrin and show the same mitotic defects as astrin-depleted cells. Importantly, astrin fails to localize to and track microtubule plus ends in cells depleted of or overexpressing kinastrin. These findings suggest that microtubule plus end targeting of astrin is required for normal spindle architecture and chromosome alignment, and that perturbations of this pathway result in delayed mitosis and nonphysiological separase activation.
J Cell Biol (2011) vol. 192 (6) pp. 959-68

http://jcb.rupress.org/content/192/6/959.long

Published March 14, 2011

The astrin–kinastrin/SKAP complex localizes to microtubule plus ends and facilitates chromosome alignment

Anja K. Dunsch, Emily Linnane, Francis A. Barr, and Ulrike Gruneberg

Cancer Research UK Centre, University of Liverpool, Liverpool L3 9TA, England, UK

Astrin is a mitotic spindle–associated protein required for the correct alignment of all chromosomes at the metaphase plate. Astrin depletion delays chromosome alignment and causes the loss of normal spindle architecture and sister chromatid cohesion before anaphase onset. Here we describe an astrin complex containing kinastrin/SKAP, a novel kinetochore and mitotic spindle protein, and three minor interaction partners: dynein light chain, Plk1, and Sgo2. Kinastrin is the major astrin-interacting protein in mitotic cells, and is required for astrin targeting to microtubule plus ends proximal to the plus tip tracking protein EB1. Cells overexpressing or depleted of kinastrin mislocalize astrin and show the same mitotic defects as astrin-depleted cells. Importantly, astrin fails to localize to and track microtubule plus ends in cells depleted of or overexpressing kinastrin. These findings suggest that microtubule plus end targeting of astrin is required for normal spindle architecture and chromosome alignment, and that perturbations of this pathway result in delayed mitosis and nonphysiological separase activation.

Introduction

Successful cell division requires the formation of a bipolar spindle with sister chromatids stably attached to spindle microtubules (MTs) from opposite poles. Sister chromatids bind to MTs via their kinetochores, proteinaceous structures that are formed in mitosis on the centromeres (Cheeseman and Desai, 2008; Santaguida and Musacchio, 2009). Kinetochores that are not correctly attached generate a signal that activates the spindle assembly checkpoint (SAC) and thus prevents entry into anaphase. Once bipolar attachment and alignment of chromosomes at the metaphase plate are achieved, the cohesion between sister chromatids is abolished by the action of the protease separase, and chromosome segregation ensues (Uhlmann et al., 2000).

Recent studies suggest that MTs bind kinetochores via multiple weak attachments (Cheeseman and Desai, 2008; Santaguida and Musacchio, 2009; McEwen and Dong, 2010). The key MT attachment complex at the kinetochore is comprised of the KNL-1, Mis12, and Ndc80 protein subcomplexes (Cheeseman et al., 2006). Interference with these proteins abolishes MT–kinetochore attachments. Other kinetochore components, such as the motor proteins CenpE and dynein, MT plus end binding factors including EB1 and CLIP-170, the Ska complex, and CenpF also interact directly with MTs and aid the formation of stable MT–kinetochore attachments (Cheeseman and Desai, 2008; Santaguida and Musacchio, 2009). In addition, spindle-associated proteins such as astrin contribute to the fidelity of chromosome alignment and mitotic progression (Thein et al., 2007). However, both the molecular function of astrin and the basis for its targeting to the mitotic spindle remain unclear.

Results and discussion

Identification of the astrin–kinastrin/SKAP complex

To identify novel interaction partners of astrin, GFP–astrin complexes purified from mitotic HeLa cells stably expressing GFP–astrin were analyzed by SDS-PAGE and mass spectrometry (Fig. 1 A and Fig. S1, A and B). The two major Coomassie-stained bands at 160 kD and 30 kD were identified as astrin and

Correspondence to Ulrike Gruneberg: u.gruneberg@liv.ac.uk

Abbreviations used in this paper: HURP, hepatoma up-regulated protein; MT, microtubule; SAC, spindle assembly checkpoint; SKAP, small kinetochore-associated protein.

© 2011 Dunsch et al. This article is distributed under the terms of an Attribution–Noncommercial–Share Alike–No Mirror Sites license for the first six months after the publication date (see http://www.rupress.org/terms). After six months it is available under a Creative Commons License (Attribution–Noncommercial–Share Alike 3.0 Unported license, as described at http://creativecommons.org/licenses/by-nc-sa/3.0/).

Supplemental Material can be found at:
http://jcb.rupress.org/content/suppl/2011/03/14/jcb.201008023.DC1.html

The Rockefeller University Press $30.00
J. Cell Biol. Vol. 192 No. 6 959–968
www.jcb.org/cgi/doi/10.1083/jcb.201008023

THE JOURNAL OF CELL BIOLOGY

Downloaded from jcb.rupress.org on April 17, 2011

Published March 14, 2011

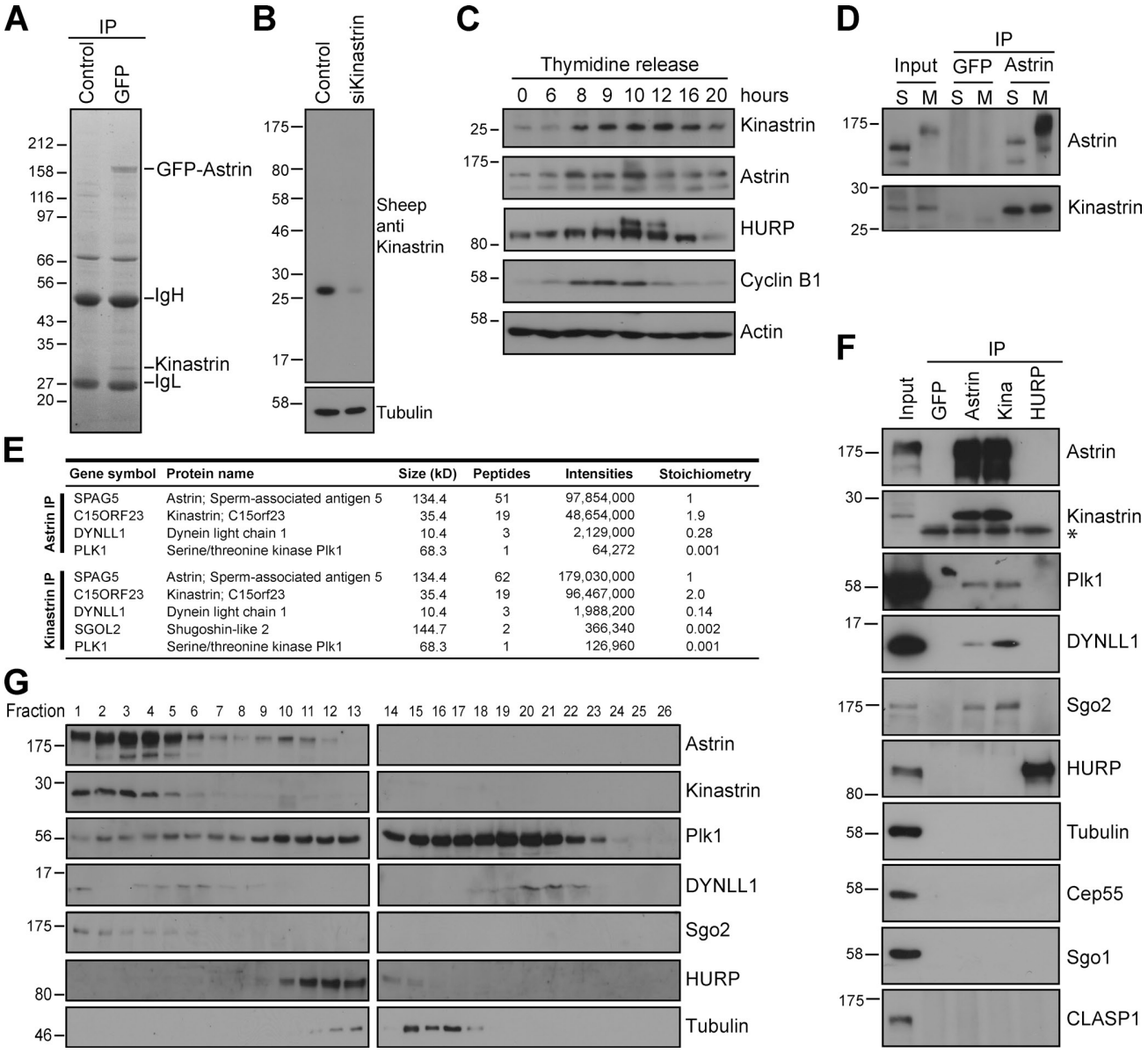


Figure 1. **Kinastrin/SKAP is a novel astrin interaction partner.** (A) Astrin complexes were immunoprecipitated from mitotic extracts of HeLa S3 GFP–astrin cells with anti-GFP or control anti-GST antibodies. The isolated complexes were separated on a 4–12% NuPAGE gel and analyzed by nano–LC-MS/MS. (B) Extracts of control or kinastrin-depleted cells were Western blotted with affinity-purified sheep anti-kinastrin antibodies. (C) HeLa S3 cells were synchronized with a double thymidine release protocol. Samples were taken at the indicated time points and Western blotted as shown. (D) Astrin immunoprecipitates from HeLa cells arrested in interphase/S phase or M phase were Western blotted with astrin and kinastrin antibodies. (E and F) Astrin, kinastrin, HURP, or GFP (control) immunoprecipitates from mitotic HeLa S3 extracts were analyzed by quantitative nano–LC-MS/MS (E) or Western blotted as indicated (F). The asterisk indicates an Ig light chain. (G) Mitotic cell extracts were separated using a Superose 6 10/300 GL column (GE Healthcare) and Western blotted as shown. Numbers next to gel blots indicate molecular mass in kilodaltons.

kinastrin/SKAP/C15orf23, respectively (Fig. 1 A). Kinastrin/SKAP/C15orf23 is present in a published total spindle proteome (Sauer et al., 2005) and *C15ORF23* was recently identified as a G2-induced gene endoding the small kinetochore-associated protein (SKAP; Whitfield et al., 2002; Fang et al., 2009), which supports the idea that it may be an important mitotic partner for astrin. For further analysis, specific antibodies to kinastrin were generated. Western blot analysis of control or kinastrin-depleted cell extracts demonstrated that a single band of the expected molecular weight was detected, the intensity of which was significantly reduced by kinastrin depletion (Fig. 1 B). Western blotting of synchronized cell extracts revealed that kinastrin protein levels increased and decreased as cells entered and exited mitosis (Fig. 1 C), which confirms that kinastrin is a mitotically regulated protein (Whitfield et al., 2002; Fang et al., 2009). Similar behavior was observed for astrin and the unrelated mitotic spindle regulator hepatoma upregulated protein (HURP; Fig. 1 C; Koffa et al., 2006; Silljé et al., 2006). To confirm that endogenous astrin and kinastrin form a complex, reciprocal immunoprecipitations were performed

Downloaded from jcb.rupress.org on April 17, 2011

Published March 14, 2011

(Fig. 1, D–F; and Fig. S1 C). Western blot analysis showed that astrin and kinastrin coprecipitated in both interphase and mitosis, whereas other spindle and kinetochore proteins such as HURP, tubulin, Cep55, and CLASP1 (Maffini et al., 2009) did not (Fig. 1, D and F). Analysis of these complexes using label-free quantitative liquid chromatography/tandem mass spectrometry (LC-MS/MS) revealed that astrin and kinastrin were the major components present, and that the apparent stoichiometry of the astrin–kinastrin complex was 1:2, which suggests that two molecules of kinastrin interact with one molecule of astrin (Fig. 1 E). This analysis also revealed minor interaction partners of the astrin–kinastrin complex, namely Polo-like kinase 1 (Plk1), Shugoshin-like protein 2 (Sgo2), and dynein light chain (DYNLL1; Fig. 1 E). In agreement with the mass spectrometry data, Western blotting revealed that Plk1, DYNLL1, and Sgo2, but not Sgo1, readily precipitated with astrin and kinastrin but not with HURP (Fig. 1 F). Gel filtration analysis of mitotic cell extracts demonstrated the presence of astrin and kinastrin, as well as Plk1, Sgo2, and DYNLL1 in the same high molecular weight fractions, which indicates that these proteins may be part of a large protein complex (Fig. 1 G). Collectively, our findings suggest that Plk1, DYNLL1, and Sgo2 may be bona fide regulators of the astrin–kinastrin complex.

Kinastrin is a mitotic spindle protein

Co-staining of HeLa cells in different stages of mitosis with antibodies against kinastrin and astrin showed that both are present at kinetochores and spindle poles (Fig. 2 A), leading us to name this novel astrin interaction partner kinastrin (kinetochore-localized astrin-binding protein). Transfection of HeLa cells for 72 h with four individual siRNA duplexes targeting C15orf23 reduced kinastrin levels measured by either Western blotting or immunofluorescence (Fig. 2 B and Fig. S1, E and F). For further analysis of kinastrin, siRNA duplex 5 was used. Strikingly, kinastrin-depleted cells often exhibited multipolar spindle structures with disorganized chromatin, which is reminiscent of astrin depletion (Fig. 2 B and Fig. S1 E). Furthermore, kinastrin and astrin depletion resulted in both loss of the respective interaction partner from the spindle and kinetochores and reduced protein levels in the extracts (Fig. 2 B). This suggests that astrin and kinastrin target to the kinetochores and spindle poles as a complex. Live cell imaging of kinastrin-depleted cells confirmed that loss of kinastrin resulted in the same phenotype as astrin depletion, specifically delayed chromosome alignment and arrest in mitosis as well as loss of both normal spindle architecture and chromatin organization (Fig. 2, C and D). Of the 51 kinastrin-depleted cells analyzed, 59% exhibited delayed chromosome congression, whereas 41% never aligned their chromosomes. The majority of cells with a congression phenotype eventually progressed into anaphase (33% of total), whereas the rest remained arrested in mitosis until the end of the experiment. Strikingly, 31% of all cells displayed strongly disorganized spindle structure and chromatin organization shortly after entering mitosis (Fig. 2 C). All mitotically arrested kinastrin-depleted cells exhibited persistent SAC signaling (Fig. 2, E and F) and were strongly positive for securin and cyclin B1 (unpublished data). In summary, our data suggest that kinastrin is an essential component of the mitotic spindle required for normal chromosome segregation and progression into anaphase.

Characterization of astrin–kinastrin complex architecture

To understand how astrin and kinastrin target to the spindle, the interaction domains in the two proteins were mapped. This revealed that the C-terminal region of astrin, comprising amino acids 482–850, is sufficient to bind kinastrin (Fig. 3 A). Interestingly, this is also the minimal MT-binding domain identified in astrin (Fig. 3 A, immunofluorescence panel), which implies that astrin localizes to MTs through kinastrin. The minimal astrin-binding site in kinastrin was mapped to amino acids 159–317, and this was also the minimal region required for kinastrin spindle localization (Fig. 3 B). Interestingly, high expression levels of kinastrin fragments capable of interacting with astrin resulted in reduced levels of astrin on the spindle and kinetochores (Fig. 3 B). These cells typically showed disturbed spindle structure and disorganized chromatin similar to the astrin depletion phenotype (Fig. 3 B). Elevated levels of kinastrin may therefore exert a dominant-negative effect on astrin, perhaps by saturating the spindle-binding sites for the astrin–kinastrin complex.

Astrin localization to the spindle poles and kinetochores is required for normal mitotic progression

Kinastrin overexpression displaces endogenous astrin–kinastrin complexes from the spindle, and therefore allowed the function of the spindle-targeted pool of astrin to be examined. Stable cell lines expressing doxycycline-inducible Myc-kinastrin were generated for this purpose. Induction of Myc-kinastrin expression for 24 h resulted in a dramatic increase in mitotic cells with multipolar spindles (Fig. 4 A and Fig. S2 A). Closer examination of these cells showed that the overexpressed Myc-kinastrin accumulated in the cytoplasm, and, as a consequence, astrin was delocalized from the spindle and kinetochores (Fig. 4 A, left immunofluorescence panel, "high"). In contrast, overexpression of Myc-astrin attracted more kinastrin to the spindle poles (Fig. 4 A, right immunofluorescence panel). The disturbed spindle architecture and highly disorganized chromatin structure observed in Myc-kinastrin–overexpressing cells was very similar to the astrin depletion phenotype, albeit with unaltered protein levels of astrin (Fig. 4 A, Western blot). Astrin-depleted cells have previously been shown to display elevated levels of prematurely separated sister chromatids and poles with single centrioles (Thein et al., 2007). This was also observed in Myc-kinastrin–overexpressing cells (Fig. 4, B and C; and Fig. S2 B). Thus, kinastrin overexpression recapitulates the key features of the astrin depletion phenotype (Thein et al., 2007). Together, these findings demonstrate that the correct localization of astrin, and not just its presence, is critical for the timely progression through mitosis and normal entry into anaphase.

Mitotically arrested cells with single centrioles at the poles of multipolar spindles and partially or fully separated sister chromatids were also observed in kinastrin-depleted cells (Fig. 4, D and E; and Fig. S2 C). Both phenotypes may be at least partially caused by aberrant separase activation

Downloaded from jcb.rupress.org on April 17, 2011

Published March 14, 2011

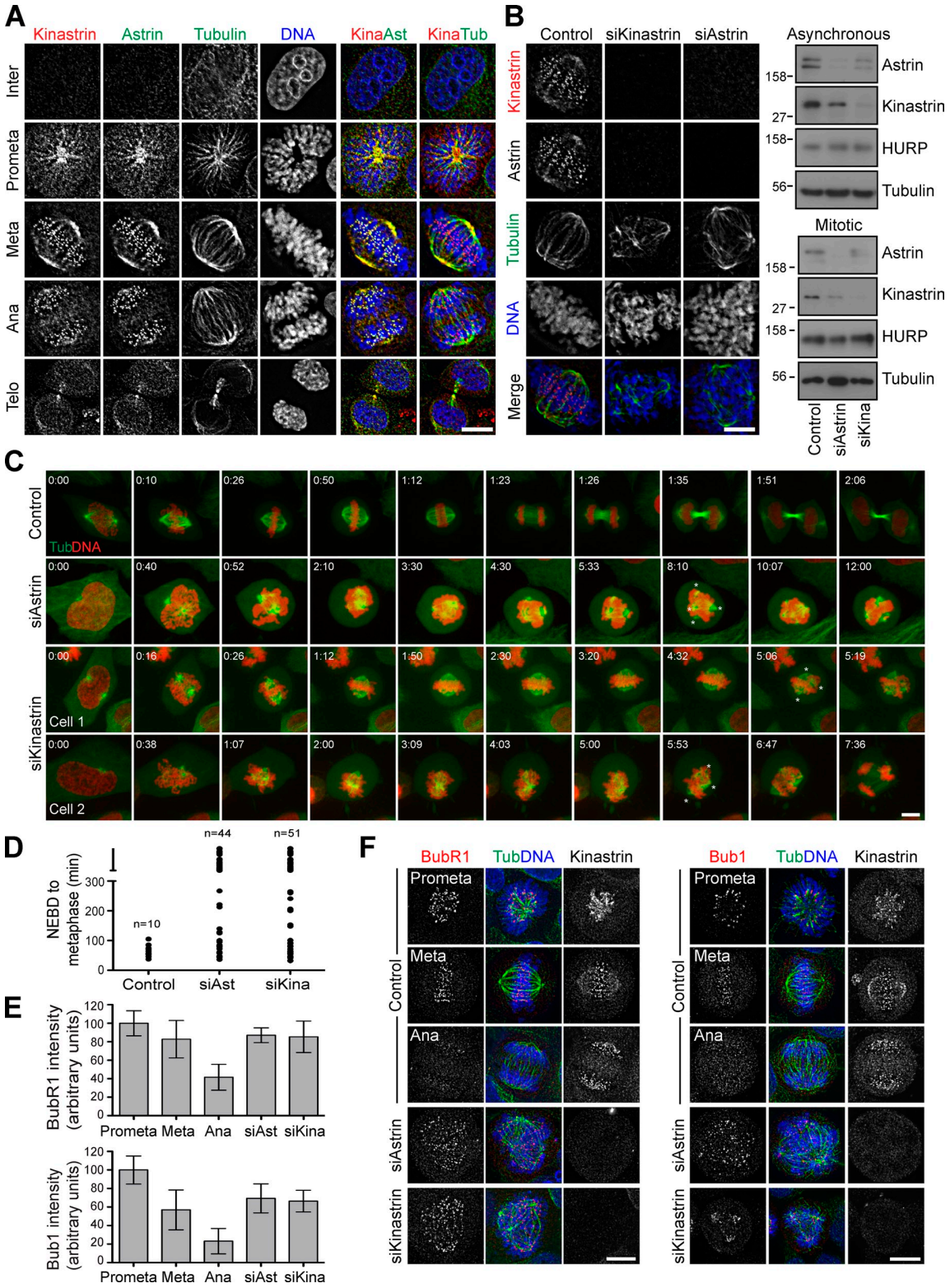


Figure 2. **The astrin–kinastrin complex is required for efficient chromosome alignment and segregation.** (A) HeLa S3 cells were stained with antibodies to kinastrin, astrin, and tubulin. DNA was stained with DAPI. (B) HeLa cells were treated with the indicated siRNAs (astrin for 48 h, kinastrin for 72 h) and stained as in A; or cell extracts were prepared from total cells or mitotic shake-offs and Western blotted with the indicated antibodies. Numbers next to gel blots indicate molecular mass in kilodaltons. Bar, 10 µm. (C and D) HeLa cells stably expressing mCherry-histone H2B and GFP–tubulin were treated with control, astrin, or kinastrin siRNA oligos and synchronized with 2.5 mM thymidine 30 h after siRNA addition. After 20 h, the cells were released, incubated for 8 h at 37°C, and then filmed for 12 h. The time required from nuclear envelope breakdown to metaphase alignment was plotted for control, astrin-depleted, and kinastrin-depleted cells (D). (E and F) Control, astrin-depleted, or kinastrin-depleted HeLa cells were fixed and stained with antibodies against kinastrin and BubR1 (left) or Bub1 (right). The staining intensity was quantified and plotted (E). Error bars indicate the standard error of the mean. Bars, 10 µm.

Downloaded from jcb.rupress.org on April 17, 2011

Published March 14, 2011

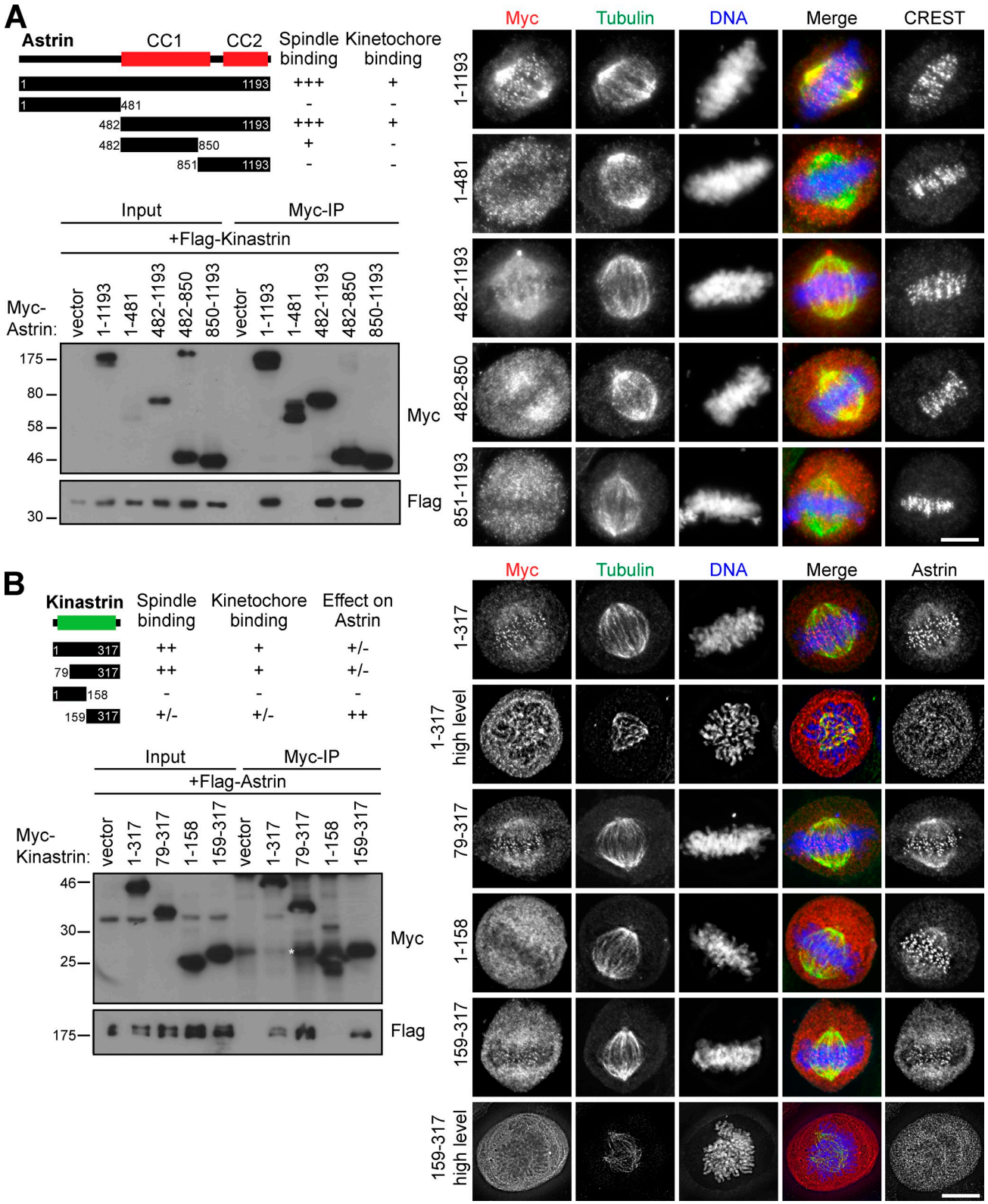


Figure 3. **Spindle targeting of astrin is mediated through the kinastrin-binding domain.** (A and B) Myc-astrin (A) or Myc-kinastrin fragments (B) alone or in conjunction with FLAG-kinastrin (A) or FLAG-astrin (B) were transiently transfected into HeLa S3 cells for immunofluorescence analysis and HEK 293T cells for immune precipitations. HEK 293T cells were synchronized in mitosis by addition of the Eg5 inhibitor S-trityl-L-cysteine (STLC; 10 µM) for 14 h after 24 h of transfection. The cells were then harvested and lysed, and anti-Myc immunoprecipitations were performed. Western blots were probed as indicated. The asterisk indicates a degradation product. For immunofluorescence analysis, fixed HeLa cells were stained with antibodies to Myc, tubulin, and CREST serum. DNA was stained with DAPI. Numbers next to gel blots indicate molecular mass in kilodaltons. Bars, 10 µm.

Downloaded from jcb.rupress.org on April 17, 2011

Published March 14, 2011

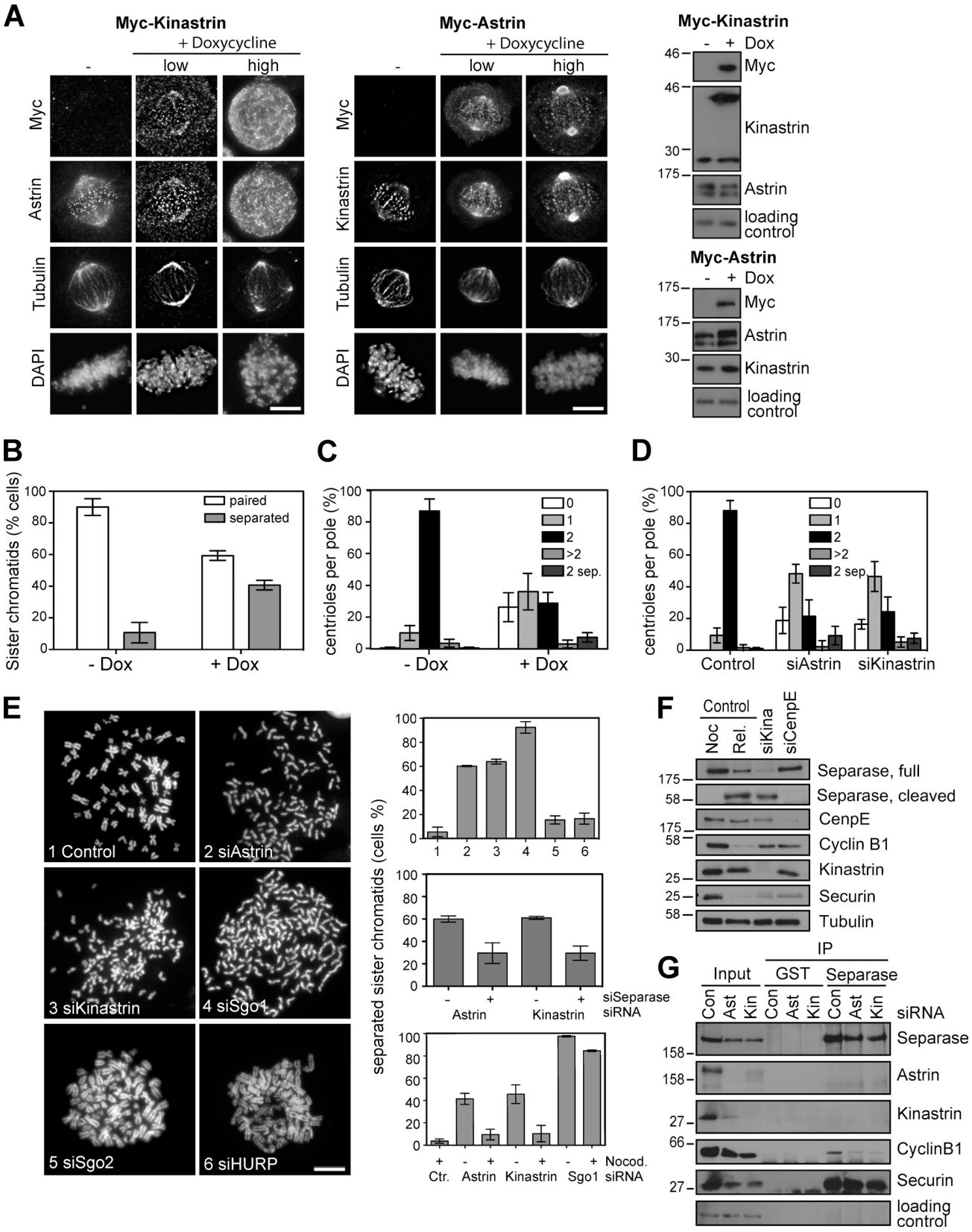


Figure 4. **Disrupted astrin function and premature loss of sister chromatid cohesion in kinastrin-depleted or overexpressing cells.** (A) HeLa Flp-in TRex Myc-kinastrin and HeLa Flp-in TRex Myc-astrin cells were mock treated or treated with 1 µg/ml doxycycline for 24 h, then stained for Myc, astrin, kinastrin, and tubulin or harvested for Western blotting with the indicated antibodies. Transfected kinastrin conforms to the longest splice variant of *C15ORF23*. DNA was stained with DAPI. Cells with different expression levels of Myc-kinastrin or Myc-astrin, respectively, are shown. Bar, 10 µm. (B) HeLa Flp-in

Downloaded from jcb.rupress.org on April 17, 2011

Published March 14, 2011

(Thein et al., 2007). Consistent with this idea, the separase autocleavage fragment of ∼60 kD could be found in kinastrin- but not CenpE-depleted cells, and there was also less separase–cyclin B1 complex in these cells (Fig. 4, F and G). Furthermore, depletion of separase in addition to astrin or kinastrin significantly reduced the amount of premature sister chromatid separation (Fig. 4 E). The addition of nocodazole to astrin- or kinastrin-depleted cells also strongly decreased the occurrence of prematurely separated sister chromatids (Fig. 4 E, bottom graph). This suggests that either spindle pulling forces are required for the separation of the sister chromatids in astrin- or kinastrin-depleted cells, or that hyperactivation of the SAC can suppress the precocious sister chromatid separation. Importantly, the shugoshin pathway for cohesin protection (Kitajima et al., 2006) was not affected by astrin or kinastrin depletion, as Sgo1, Sgo2, and PP2A-B56α were still found at centromeres (Fig. S3). Although separase is unlikely to be directly regulated by astrin or kinastrin, these data suggest that the astrin–kinastrin complex at kinetochores may be required for normal SAC function important for full separase inhibition. A related proposal has been made for the Ska proteins that have been suggested to couple the mechanical sensing of tension to SAC signaling (Daum et al., 2009). In support of this idea, a recent proteomic analysis of chromosomal proteins purified from cells depleted of the Ska complex showed that components of the anaphase-promoting complex/cyclosome were specifically lost from kinetochores (Ohta et al., 2010). Misregulated anaphase-promoting complex/cyclosome function may then follow, and a similar scenario is possible for astrin and kinastrin.

The astrin–kinastrin complex localizes to MT plus ends

To define a molecular basis for the observed phenotypes of defective chromosome congression and disturbed spindle structure, GFP–astrin cells were analyzed in more detail. Imaging of GFP–astrin cells in interphase revealed comet-like structures moving toward the periphery of the cell with a velocity of 0.43 ± 0.05 µm/s (Fig. 5 A and Video 8), which is reminiscent of EB1 MT plus end tracking comets (Akhmanova and Steinmetz, 2008). Indeed, co-staining with antibodies against EB1 as well as live cell imaging of GFP–astrin cells transiently transfected with EB1-mCherry confirmed that GFP–astrin decorated EB1-labeled MTs in both interphase and mitosis, and that the mCherry- and GFP-labeled structures moved together (Fig. 5, B and C; and Video 9). The GFP–astrin staining was always proximal to the EB1 signal at the MT plus end, which suggests that the features on the MT plus ends recognized by astrin and EB1 are not identical. Endogenous astrin and kinastrin also labeled MT plus ends in a similar manner (Fig. 5 D and not depicted). As expected for MT-associated labeling, both EB1 and GFP–astrin comet staining was lost upon nocodazole treatment (Fig. 5 E). Interphase GFP–astrin comet staining was also lost in the absence of kinastrin, which confirms the idea that astrin localizes to MTs via kinastrin in a manner independent of the cell cycle stage (Figs. 1 D and 5 F).

To test if the astrin–kinastrin complex exerts a direct effect on MT dynamics, in vitro polymerization assays using purified tubulin were performed. Titration of recombinant kinastrin into MT polymerization assays resulted in increased tubulin polymerization (Fig. 5 G), which suggests it may act to stabilize MT plus ends. Altered MT–kinetochore regulation may therefore be the underlying molecular defect resulting in impaired chromosome alignment and spindle integrity in cells with perturbed astrin–kinastrin function. Consistent with this idea, kinastrin-depleted cells were impaired in their ability to reform robust bipolar spindles after combined monastrol and cold treatment (Fig. 5 H), and kinetochore fibers formed in the absence of kinastrin were disorganized and stained less intensely for tubulin compared with control cells (Fig. 5 I).

The astrin–kinastrin complex promotes stable MT-kinetochore attachments

We have characterized kinastrin/SKAP/C15orf23, an astrin partner protein with an identical cellular localization to astrin. Like astrin, kinastrin is required for chromosome alignment, normal timing of sister chromatid segregation, and maintenance of spindle pole architecture. Furthermore, astrin and kinastrin form an MT plus end tracking complex that is required for the formation of normal kinetochore fibers (Fig. 5). While this work was under revision, two studies were published that showed that astrin depletion destabilizes kinetochore fibers and that Aurora B inhibition promotes astrin complex localization to the kinetochores (Manning et al., 2010; Schmidt et al., 2010). Our data on the plus end tracking characteristics of astrin–kinastrin provide a molecular explanation for both these findings, as such a complex would be in a good position to stabilize kinetochore fibers and would also accumulate upon the stabilization of MT–kinetochore attachments by Aurora B inhibition. Interestingly, one of the astrin–kinastrin interaction

TRex Myc-kinastrin cells were mock treated and mitotically arrested with 100 ng/ml nocodazole for 14 h or induced with 1 µg/ml doxycycline for 24 h. Chromosome spreads were prepared and the percentage of cells with separated sister chromatids was assessed. (C) HeLa Flp-in TRex Myc-kinastrin cells were treated as in A and stained for centrin-3 and tubulin. The percentages of spindle poles with zero, one, two, more than two, or markedly separated centrioles are plotted in the bar graph. (D) HeLa S3 cells treated with control, astrin, or kinastrin siRNA oligos for 48 or 72 h (kinastrin) were stained as in C. Centriole numbers at the spindle poles are plotted in the bar graph. (E) HeLa S3 cells were transfected with control, astrin, kinastrin, Sgo1, Sgo2, or HURP siRNA duplexes for 48 or 72 h (kinastrin), harvested by mitotic shake-off (control cells were treated with 100 ng/ml nocodazole for 14 h before harvest), and processed for chromosome spreads. 100 cells were counted from each condition ($n = 3$; top graph, representative images are shown on the left). Depletion of separase in addition to astrin or kinastrin significantly lowered the amount of cells with separated sister chromatids (middle graph). The addition of nocodazole to astrin- or kinastrin-depleted cells released from a thymidine block significantly reduced the amount of premature loss of sister chromatid cohesion (bottom graph). (F) HeLa cells arrested in mitosis with nocodazole, released from the nocodazole block, or treated with siRNAs targeting CenpE (48 h) or kinastrin (72 h) were harvested by mitotic shake-off (except nocodazole release), then lysed and blotted with the indicated antibodies. Note that kinastrin-depleted cells have cyclin B1 and securin levels lower than nocodazole-arrested cells but comparable to CenpE-depleted cells. The separase cleavage fragment, however, only appears in kinastrin-depleted cells. (G) Separase immunoprecipitations from HeLa cells depleted of astrin or kinasterin for 48 or 72 h were blotted as indicated. All error bars indicate the standard error of the mean. Numbers next to gel blots indicate molecular mass in kilodaltons.

Downloaded from jcb.rupress.org on April 17, 2011

Published March 14, 2011

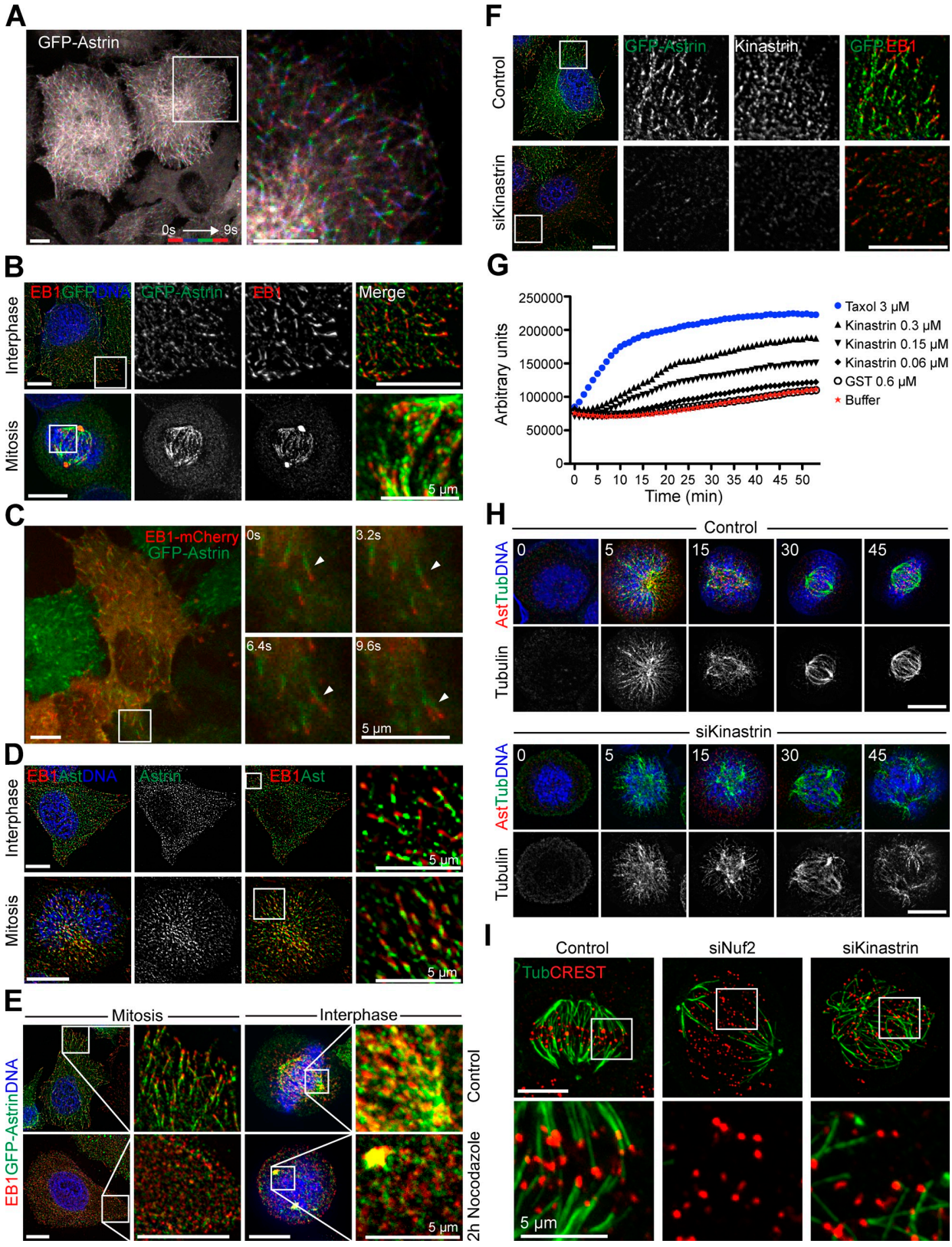


Figure 5. **The astrin-kinastrin/SKAP complex localizes to MT plus ends.** (A) GFP–astrin cells were imaged every 1.25 s. The first, third, fifth, and seventh frames were projected into one image using different colors as indicated. (B) Methanol-fixed GFP–astrin cells were stained for EB1 and GFP. (C) GFP–astrin cells transiently expressing EB1-mCherry were imaged every 3.2 s. The arrowheads indicate one growing MT plus end that can be followed through the different frames of the movies. (D) Methanol-fixed HeLa cells were stained for astrin and EB1. Single focal planes are shown. (E) GFP–astrin cells were mock-treated or treated with 100 ng/ml nocodazole for 2 h, then stained with CREST antiserum and for EB1 and GFP. (F) GFP–astrin cells were treated

Downloaded from jcb.rupress.org on April 17, 2011

Published March 14, 2011

partners that we identified is the dynein light chain DYNLL1, one of three different dynein light chains found in cytoplasmic dynein (Fig. 1, E and F; Pfister et al., 2005, 2006). Dynein has been implicated in chromosome alignment, the formation of MT–kinetochore attachments, and SAC silencing, and has also been found to localize to MT plus ends (Kobayashi and Murayama, 2009; Bader and Vaughan, 2010). Other dynein-associated complexes, such as dynactin, associate with MT plus ends, and this may be important for MT search–capture functions (Echeverri et al., 1996; Varma et al., 2008). Although the precise interplay between the astrin–kinastrin/SKAP complex and dynein is currently unclear, it is conceivable that this complex promotes dynein-mediated transport from MT plus ends toward spindle poles of factors, such as Spindly, required to promote timely chromosome congression and attachment, and spindle checkpoint regulation (Chan et al., 2009; Barisic et al., 2010; Gassmann et al., 2010).

Materials and methods

Antibodies

Hexahistidine-tagged C-astrin aa 1,014–1,193 and C15orf23/kinastrin/SKAP were expressed in and purified from bacteria. Antibodies against C-astrin and full-length kinastrin/SKAP were raised in sheep (Scottish National Blood Transfusion Service) and affinity-purified using the His-tagged proteins coupled to Affigel-15 (Bio-Rad Laboratories). For Western blotting after immunoprecipitation, biotinylated anti-kinastrin antibodies were used in some experiments. Other antibodies were as follows: mouse anti–actin-HRP (Abcam), rabbit anti-astrin (Thein et al., 2007), mouse anti-B56α (BD), mouse anti-Bub1 (Abcam), mouse anti-BubR1 (Millipore), mouse anti-centrin-3 (Abcam), sheep anti-Cep55 (Bastos and Barr, 2010), rabbit anti-CLASP1 (Bethyl Laboratories, Inc.), CREST autoimmune serum (Europa Biosciences), mouse anti-cyclin B1 (Millipore), rabbit anti-CenpE (Bethyl Laboratories, Inc.), rabbit anti-DYNLL1 (Epitomics, Inc.), mouse anti-EB1 (Cell Signaling Technology), rabbit anti-FLAG (Sigma-Aldrich), sheep anti-HURP (a kind gift of J. Harper, Cancer Research Centre, University of Liverpool, England, UK), mouse anti-Myc (clone 9E10), rabbit anti-Myc (both from Sigma-Aldrich), mouse anti-Plk1 (Santa Cruz Biotechnology, Inc.), mouse anti-PPP2CA (BD), mouse anti-Sgo1 (Abcam), rabbit anti-Sgo2 (Bethyl Laboratories, Inc.), mouse anti-securin (Bethyl Laboratories, Inc.), mouse anti-separase (Abcam), rabbit anti-separase (Bethyl Laboratories, Inc.), mouse anti–α-tubulin (clone DM1A; Sigma-Aldrich), and rabbit anti-tubulin (Epitomics, Inc.). Secondary antibodies conjugated to HRP or Cy5 were obtained from Jackson ImmunoResearch Laboratories, Inc. Secondary antibodies conjugated to Alexa Fluor 488, 555, and 647 were obtained from Invitrogen. DNA was stained with DAPI (Sigma-Aldrich).

Molecular biology

C15ORF23 transcript variant 1 and EB1 were amplified from Marathon human testis cDNA (Takara Bio, Inc.) using Pfu polymerase (Agilent Technologies). Full-length astrin constructs have been described previously (Thein et al., 2007). C15ORF23, astrin fragments, and EB1 expression constructs were generated using pcDNA3.1 and pcDNA5/FRT/TO vectors (Invitrogen) modified to encode N-Myc, N-FLAG, or C-mCherry tags, respectively. For bacterial expression, C15ORF23 was cloned into pGEX-5X-1 (GE Healthcare). GST and GST–kinastrin were purified according to the manufacturer's recommendations.

Cell lines

HeLa S3 cells stably expressing GFP–astrin were generated using standard procedures and selected with 0.7 mg/ml geneticin. Stable cell lines with single copies of the desired transgene were created using the TRex inducible Flp-In system (Invitrogen). HeLa S3 mCherry-histone H2B-tubulin GFP cells were provided by K. Zeng (Cancer Research Centre, University of Liverpool, England, UK; Zeng et al., 2010).

Gel filtration, immunoprecipitations, and protein identification

Samples of mitotic cell extracts separated on a Superose 6 10/300 GL column (GE Healthcare) were provided by R. Nunes-Bastos (Cancer Research Centre, University of Liverpool, Liverpool, England, UK). For immunoprecipitation of GFP–astrin, endogenous astrin, kinastrin/SKAP, or HURP, HeLa S3 cells were arrested in mitosis by addition of 10 µM S-trityl-L-cysteine (Sigma-Aldrich) 14 h before mitotic shake-off. Cell pellets were lysed in lysis buffer (20 mM Tris-Cl, pH 7.4, 150 mM NaCl, 1% IGEPAL, 0.1% sodium deoxycholate, 40 mM β-glycerophosphate, 10 mM NaF, 0.3 mM orthovanadate, 100 nM okadaic acid, and protease inhibitor cocktail [Sigma-Aldrich]) and cleared by centrifugation. Protein complexes were isolated using sheep antibodies against GFP, astrin, kinastrin/SKAP, and HURP bound to protein G–Sepharose and washed with lysis buffer followed by washes in 20 mM Tris-Cl, pH 7.4, 150 mM NaCl, 0.1% IGEPAL, 20 mM Tris-Cl, pH 7.4, and 150 mM NaCl. Protein samples for mass spectrometry were separated on 4–12% gradient NuPAGE gels (Invitrogen), then stained using a colloidal Coomassie blue stain. Gel lanes were cut into 12 slices and then digested with trypsin (Shevchenko et al., 1996). Tryptic peptides were resolved using a 25 cm × 75 µm BEH-C18 column in 0–37.5% acetonitrile in 0.1% formic acid at a flow rate of 400 nl/min with a nanoAcquity ultra performance liquid chromatography device (Waters). Online LC-MS/MS was performed with an Orbitrap XL ETD mass spectrometer (Thermo Fisher Scientific) fitted with a nano-electrospray source (Proxeon) set to acquire an MS survey scan in the Orbitrap (R = 30,000) and then perform MS/MS on the top five multiple-charged ions in the linear quadrupole ion trap after fragmentation using collision ionization (30 ms, 35% energy). Maxquant and Mascot (Matrix Science) were then used to compile and search the raw data against the human International Protein Index database (Cox and Mann, 2008). Protein group and peptide lists were sorted and analyzed in Excel (Microsoft) and Maxquant.

RNA interference

RNA interference using astrin, Sgo1, Gl2 (control), Nuf2 and separase siRNA oligos was performed as described previously (Thein et al., 2007). Kinastrin/SKAP oligos were: No. 1, 5′-CAAACTCGGGCCACTTCTA-dTdT-3′; No. 2, 5′-CAAATGAAAGCTACTGACAdTdT-3′ (Sigma-Aldrich); No. 5, 5′-AGGCTACAAACCACTGAGTAA-3′; No. 8, 5′-TTGGATTGACC-TTCTAGTCAA-3′ (QIAGEN), and Dharmacon SmartPool L-022219-00 (Thermo Fisher Scientific). Sgo2 and B56α were depleted using Dharmacon SmartPools L-016154-01 and L-009352-00, respectively, and HURP and CenpE were targeted with 5′-TACTTTGAATTCACAAACTAA-3′ and 5′-CACGATACTGTTAACATGAAT-3′, respectively (QIAGEN).

Mitotic chromosome spreads

HeLa S3 cells were treated with Gl2, astrin, HURP, Sgo1, or Sgo2 siRNA oligonucleotides for 48 h or kinastrin/SKAP siRNA for 72 h. 100 ng/ml nocodazole was added to the control cells 14 h before harvesting. Mitotic cells were collected by mitotic shake-off, and chromosome spreads were prepared as described previously (Thein et al., 2007).

Image acquisition and time-lapse microscopy

Cells were processed for immunofluorescence analysis as described previously (Thein et al., 2007). For MT plus end staining, cells were fixed with methanol for 5 min at −20°C. Image acquisition was performed on an upright microscope (BX61; Olympus) with Plan-Apochromat 100×/1.4 NA and 60×/1.35 NA oil immersion objective lenses and a CoolSnap HQ2 camera (Roper Industries) under the control of MetaMorph 7.5 software (Molecular Devices). Image stacks were deconvolved using MetaMorph software. For live cell imaging, cells were plated in 35-mm dishes with a 14-mm 1.5 thickness coverglass window on the bottom (MatTek), then placed in a 37°C, 5% CO_2 environmental chamber on the microscope stage of a spinning disc confocal system (Ultraview Vox; Perkin Elmer). Imaging was performed using a 60× 1.4 NA oil immersion objective lens.

with control or siKinastrin oligos for 72 h, then stained for EB1 and kinastrin. Boxed regions are shown enlarged on the right. (G) MT polymerization in the presence of buffer, taxol, GST, or GST–kinastrin at the indicated concentrations was followed in a fluorimeter. Each curve is representative of three independent experiments. (H) HeLa cells were treated overnight with 200 µM monastrol followed by 1 h cold treatment on ice. MT regrowth was initiated by the addition of fresh 37°C medium then monitored for 45 min by staining for astrin, tubulin, and DNA (DAPI). (I) HeLa cells treated with control, Nuf2, or kinastrin siRNA oligos for 72 h were cold treated for 10 min to visualize stable kinetochore fibers. The bottom row shows enlarged views of the boxed regions. Bars, 10 µm unless otherwise indicated.

Downloaded from jcb.rupress.org on April 17, 2011

Published March 14, 2011

Cells were typically imaged every minute for 12 h, acquiring z stacks containing 29 steps, 0.6 µm apart, with 2% laser power and 30 ms exposure. For MT plus end imaging, cells were imaged every 1.25 or 3.2 s for 1.5 min, acquiring z stacks with 6 steps, 0.4 µm apart. Maximum intensity projections of the fluorescent channels were performed using Volocity (PerkinElmer). Images were cropped in Photoshop CS3 (Adobe) or ImageJ (National Institutes of Health) and transferred into Illustrator CS3 (Adobe) to produce figures.

MT polymerization assay

Tubulin polymerization was measured by fluorescence enhancement because of the incorporation of a fluorescent dye into the tubulin polymers using a tubulin polymerization kit (Cytoskeleton, Inc.). Fluorescence emission at 460 nm was followed for 1 h at 37°C with one reading per minute using a fluorimeter (Berthold Technologies).

Online supplemental material

Fig. S1 describes the characterization of the GFP–astrin cell line, sheep anti-astrin antibodies, and C15orf23 siRNA duplexes. Figs. S2 and S3 show that perturbing the astrin–kinastrin complex results in loss of centrosome cohesion but does not affect the shugoshin pathway required for centromeric cohesin protection. Videos 1–7 show spindle formation and chromosome alignment in control, astrin-depleted, and kinastrin-depleted cells passing through mitosis. In Videos 8 and 9, MT plus end tracking of GFP–astrin alone and GFP–astrin and EB1-mCherry together is followed.

We thank Drs. Ricardo Nunes-Bastos and Kang Zeng for reagents and advice, Jenny Harper for HURP antibodies, and Sabine Hiltscher for excellent technical assistance.

This work was supported by a Cancer Research UK career development fellowship to U. Gruneberg (C24085/A8296), and a Cancer Research UK program grant to F.A. Barr (C20079/A9473). A.K. Dunsch is supported by a Boehringer Ingelheim Fonds Fellowship. A Cancer Research UK equipment grant and generous donation from North West Cancer Research funded the Orbitrap mass spectrometer system used in this work.

Submitted: 4 August 2010
Accepted: 15 February 2011

References

Akhmanova, A., and M.O. Steinmetz. 2008. Tracking the ends: a dynamic protein network controls the fate of microtubule tips. *Nat. Rev. Mol. Cell Biol.* 9:309–322. doi:10.1038/nrm2369

Bader, J.R., and K.T. Vaughan. 2010. Dynein at the kinetochore: timing, interactions and functions. *Semin. Cell Dev. Biol.* 21:269–275. doi:10.1016/j.semcdb.2009.12.015

Barisic, M., B. Sohm, P. Mikolcevic, C. Wandke, V. Rauch, T. Ringer, M. Hess, G. Bonn, and S. Geley. 2010. Spindly/CCDC99 is required for efficient chromosome congression and mitotic checkpoint regulation. *Mol. Biol. Cell.* 21:1968–1981. doi:10.1091/mbc.E09-04-0356

Bastos, R.N., and F.A. Barr. 2010. Plk1 negatively regulates Cep55 recruitment to the midbody to ensure orderly abscission. *J. Cell Biol.* 191:751–760. doi:10.1083/jcb.201008108

Chan, Y.W., L.L. Fava, A. Uldschmid, M.H. Schmitz, D.W. Gerlich, E.A. Nigg, and A. Santamaria. 2009. Mitotic control of kinetochore-associated dynein and spindle orientation by human Spindly. *J. Cell Biol.* 185:859–874. doi:10.1083/jcb.200812167

Cheeseman, I.M., and A. Desai. 2008. Molecular architecture of the kinetochore-microtubule interface. *Nat. Rev. Mol. Cell Biol.* 9:33–46. doi:10.1038/nrm2310

Cheeseman, I.M., J.S. Chappie, E.M. Wilson-Kubalek, and A. Desai. 2006. The conserved KMN network constitutes the core microtubule-binding site of the kinetochore. *Cell.* 127:983–997. doi:10.1016/j.cell.2006.09.039

Cox, J., and M. Mann. 2008. MaxQuant enables high peptide identification rates, individualized p.p.b.-range mass accuracies and proteome-wide protein quantification. *Nat. Biotechnol.* 26:1367–1372. doi:10.1038/nbt.1511

Daum, J.R., J.D. Wren, J.J. Daniel, S. Sivakumar, J.N. McAvoy, T.A. Potapova, and G.J. Gorbsky. 2009. Ska3 is required for spindle checkpoint silencing and the maintenance of chromosome cohesion in mitosis. *Curr. Biol.* 19:1467–1472. doi:10.1016/j.cub.2009.07.017

Echeverri, C.J., B.M. Paschal, K.T. Vaughan, and R.B. Vallee. 1996. Molecular characterization of the 50-kD subunit of dynactin reveals function for the complex in chromosome alignment and spindle organization during mitosis. *J. Cell Biol.* 132:617–633. doi:10.1083/jcb.132.4.617

Fang, L., A. Seki, and G. Fang. 2009. SKAP associates with kinetochores and promotes the metaphase-to-anaphase transition. *Cell Cycle.* 8:2819–2827. doi:10.4161/cc.8.17.9514

Gassmann, R., A.J. Holland, D. Varma, X. Wan, F. Civril, D.W. Cleveland, K. Oegema, E.D. Salmon, and A. Desai. 2010. Removal of Spindly from microtubule-attached kinetochores controls spindle checkpoint silencing in human cells. *Genes Dev.* 24:957–971. doi:10.1101/gad.1886810

Kitajima, T.S., T. Sakuno, K. Ishiguro, S. Iemura, T. Natsume, S.A. Kawashima, and Y. Watanabe. 2006. Shugoshin collaborates with protein phosphatase 2A to protect cohesin. *Nature.* 441:46–52. doi:10.1038/nature04663

Kobayashi, T., and T. Murayama. 2009. Cell cycle-dependent microtubule-based dynamic transport of cytoplasmic dynein in mammalian cells. *PLoS ONE.* 4:e7827. doi:10.1371/journal.pone.0007827

Koffa, M.D., C.M. Casanova, R. Santarella, T. Köcher, M. Wilm, and I.W. Mattaj. 2006. HURP is part of a Ran-dependent complex involved in spindle formation. *Curr. Biol.* 16:743–754. doi:10.1016/j.cub.2006.03.056

Maffini, S., A.R. Maia, A.L. Manning, Z. Maliga, A.L. Pereira, M. Junqueira, A. Shevchenko, A. Hyman, J.R. Yates III, N. Galjart, et al. 2009. Motor-independent targeting of CLASPs to kinetochores by CENP-E promotes microtubule turnover and poleward flux. *Curr. Biol.* 19:1566–1572. doi:10.1016/j.cub.2009.07.059

Manning, A.L., S.F. Bakhoum, S. Maffini, C. Correia-Melo, H. Maiato, and D.A. Compton. 2010. CLASP1, astrin and Kif2b form a molecular switch that regulates kinetochore-microtubule dynamics to promote mitotic progression and fidelity. *EMBO J.* 29:3531–3543. doi:10.1038/emboj.2010.230

McEwen, B.F., and Y. Dong. 2010. Contrasting models for kinetochore microtubule attachment in mammalian cells. *Cell. Mol. Life Sci.* 67:2163–2172. doi:10.1007/s00018-010-0322-x

Ohta, S., J.C. Bukowski-Wills, L. Sanchez-Pulido, Fde.L. Alves, L. Wood, Z.A. Chen, M. Platani, L. Fischer, D.F. Hudson, C.P. Ponting, et al. 2010. The protein composition of mitotic chromosomes determined using multiclassifier combinatorial proteomics. *Cell.* 142:810–821. doi:10.1016/j.cell.2010.07.047

Pfister, K.K., E.M. Fisher, I.R. Gibbons, T.S. Hays, E.L. Holzbaur, J.R. McIntosh, M.E. Porter, T.A. Schroer, K.T. Vaughan, G.B. Witman, et al. 2005. Cytoplasmic dynein nomenclature. *J. Cell Biol.* 171:411–413. doi:10.1083/jcb.200508078

Pfister, K.K., P.R. Shah, H. Hummerich, A. Russ, J. Cotton, A.A. Annuar, S.M. King, and E.M. Fisher. 2006. Genetic analysis of the cytoplasmic dynein subunit families. *PLoS Genet.* 2:e1. doi:10.1371/journal.pgen.0020001

Santaguida, S., and A. Musacchio. 2009. The life and miracles of kinetochores. *EMBO J.* 28:2511–2531. doi:10.1038/emboj.2009.173

Sauer, G., R. Körner, A. Hanisch, A. Ries, E.A. Nigg, and H.H. Silljé. 2005. Proteome analysis of the human mitotic spindle. *Mol. Cell. Proteomics.* 4:35–43.

Schmidt, J.C., T. Kiyomitsu, T. Hori, C.B. Backer, T. Fukagawa, and I.M. Cheeseman. 2010. Aurora B kinase controls the targeting of the Astrin-SKAP complex to bioriented kinetochores. *J. Cell Biol.* 191:269–280. doi:10.1083/jcb.201006129

Shevchenko, A., M. Wilm, O. Vorm, and M. Mann. 1996. Mass spectrometric sequencing of proteins silver-stained polyacrylamide gels. *Anal. Chem.* 68:850–858. doi:10.1021/ac950914h

Silljé, H.H., S. Nagel, R. Körner, and E.A. Nigg. 2006. HURP is a Ran-importin beta-regulated protein that stabilizes kinetochore microtubules in the vicinity of chromosomes. *Curr. Biol.* 16:731–742. doi:10.1016/j.cub.2006.02.070

Thein, K.H., J. Kleylein-Sohn, E.A. Nigg, and U. Gruneberg. 2007. Astrin is required for the maintenance of sister chromatid cohesion and centrosome integrity. *J. Cell Biol.* 178:345–354. doi:10.1083/jcb.200701163

Uhlmann, F., D. Wernic, M.A. Poupart, E.V. Koonin, and K. Nasmyth. 2000. Cleavage of cohesin by the CD clan protease separin triggers anaphase in yeast. *Cell.* 103:375–386. doi:10.1016/S0092-8674(00)00130-6

Varma, D., P. Monzo, S.A. Stehman, and R.B. Vallee. 2008. Direct role of dynein motor in stable kinetochore-microtubule attachment, orientation, and alignment. *J. Cell Biol.* 182:1045–1054. doi:10.1083/jcb.200710106

Whitfield, M.L., G. Sherlock, A.J. Saldanha, J.I. Murray, C.A. Ball, K.E. Alexander, J.C. Matese, C.M. Perou, M.M. Hurt, P.O. Brown, and D. Botstein. 2002. Identification of genes periodically expressed in the human cell cycle and their expression in tumors. *Mol. Biol. Cell.* 13:1977–2000. doi:10.1091/mbc.02-02-0030.

Zeng, K., R.N. Bastos, F.A. Barr, and U. Gruneberg. 2010. Protein phosphatase 6 regulates mitotic spindle formation by controlling the T-loop phosphorylation state of Aurora A bound to its activator TPX2. *J. Cell Biol.* 191:1315–1332. doi:10.1083/jcb.201008106

Downloaded from jcb.rupress.org on April 17, 2011

A.6.2. Publication 2

Dynein light chain 1 and a spindle-associated adaptor promote dynein asymmetry and spindle orientation.

Anja K Dunsch, Dean Hammond, Jennifer Lloyd, Lothar Schermelleh, Ulrike Gruneberg, Francis A Barr.

The cytoplasmic dynein motor generates pulling forces to center and orient the mitotic spindle within the cell. During this positioning process, dynein oscillates from one pole of the cell cortex to the other but only accumulates at the pole farthest from the spindle. Here, we show that dynein light chain 1 (DYNLL1) is required for this asymmetric cortical localization of dynein and has a specific function defining spindle orientation. DYNLL1 interacted with a spindle-microtubule-associated adaptor formed by CHICA and HMMR via TQT motifs in CHICA. In cells depleted of CHICA or HMMR, the mitotic spindle failed to orient correctly in relation to the growth surface. Furthermore, CHICA TQT motif mutants localized to the mitotic spindle but failed to recruit DYNLL1 to spindle microtubules and did not correct the spindle orientation or dynein localization defects. These findings support a model where DYNLL1 and CHICA-HMMR form part of the regulatory system feeding back spindle position to dynein at the cell cortex.
J Cell Biol (2012) pp.

http://jcb.rupress.org/content/198/6/1039.full?sid=e77441bd-030b-4928-95a2-bf6c4144c9f1

Published September 10, 2012

Dynein light chain 1 and a spindle-associated adaptor promote dynein asymmetry and spindle orientation

Anja K. Dunsch,[1] Dean Hammond,[2] Jennifer Lloyd,[2] Lothar Schermelleh,[1] Ulrike Gruneberg,[1] and Francis A. Barr[1]

[1]Department of Biochemistry, University of Oxford, Oxford OX1 3QU, England, UK
[2]Cancer Research Centre, University of Liverpool, Liverpool L3 9TA, England, UK

The cytoplasmic dynein motor generates pulling forces to center and orient the mitotic spindle within the cell. During this positioning process, dynein oscillates from one pole of the cell cortex to the other but only accumulates at the pole farthest from the spindle. Here, we show that dynein light chain 1 (DYNLL1) is required for this asymmetric cortical localization of dynein and has a specific function defining spindle orientation. DYNLL1 interacted with a spindle-microtubule–associated adaptor formed by CHICA and HMMR via TQT motifs in CHICA. In cells depleted of CHICA or HMMR, the mitotic spindle failed to orient correctly in relation to the growth surface. Furthermore, CHICA TQT motif mutants localized to the mitotic spindle but failed to recruit DYNLL1 to spindle microtubules and did not correct the spindle orientation or dynein localization defects. These findings support a model where DYNLL1 and CHICA-HMMR form part of the regulatory system feeding back spindle position to dynein at the cell cortex.

Introduction

Cytoplasmic dynein is a multisubunit force-generating AAA ATPase, or motor protein, with diverse cellular functions in both dividing and nondividing cells (Kardon and Vale, 2009). It has a complex structure comprised of a large, >400-kD heavy chain containing the ATPase domains, and a series of smaller subunits referred to as the light-intermediate, intermediate, and light chains, all associated with the N-terminal tail region of the heavy chain (Kardon and Vale, 2009). There are three different light chain (LC) subunits, LC7, LC8, and the T-complex testis-specific protein 1 (Kardon and Vale, 2009). A series of additional factors interact with dynein via these light and intermediate chains, the best characterized of which is dynactin, a multisubunit microtubule plus end–binding complex (Kardon and Vale, 2009). Dynactin acts in concert with other microtubule-associated proteins such as CLIP170, NudE, and EB1 to mediate the interaction of specific cargo with dynein at the microtubule (Kardon and Vale, 2009). Dynein can then promote the directed movement of the cargo toward the minus end of the microtubule.

In mitosis, dynein is found associated with specific regions of the cell cortex, as well as the mitotic spindle poles, spindle microtubules, and kinetochores (Pfarr et al., 1990; Steuer et al., 1990; Busson et al., 1998). Accordingly, disrupting dynein function results in defective and abnormally positioned or rotated spindles with misaligned chromosomes (Li et al., 1993; Echeverri et al., 1996; Gönczy et al., 1999; O'Connell and Wang, 2000; Sharp et al., 2000; Rebollo et al., 2007). Other evidence suggests that specific combinations of dynein adaptor proteins can independently regulate these functions. At the kinetochore, dynactin together with the Rod–ZW10–Zwilch complex, Lis1, Spindly, and NudE promotes microtubule attachment to the kinetochore, and also plays a role in mitotic checkpoint function (Starr et al., 1998; Scaërou et al., 1999; Faulkner et al., 2000; Wojcik et al., 2001; Williams et al., 2003; Cockell et al., 2004; Stehman et al., 2007; Chan et al., 2009; Gassmann et al., 2010).

Dynein is crucial for the exact positioning and rotation of the mitotic spindle in relation to extracellular cues in symmetric and asymmetric cell divisions during development (Rhyu and Knoblich, 1995; Kaltschmidt et al., 2000; Cabernard and Doe, 2009; Siller and Doe, 2009; Poulson and Lechler, 2010; Morin and Bellaïche, 2011). In part this is due to a role for dynein in a signaling pathway that relays information from a G protein–signaling module at the cell cortex to the spindle pole proteins NuMA and Aurora A in polarized cell divisions (Sanada and

D. Hammond and J. Lloyd contributed equally to this paper.

Correspondence to Francis A. Barr: francis.barr@bioch.ox.ac.uk

Abbreviation used in this paper: DYNLL1: dynein light chain 1.

© 2012 Dunsch et al. This article is distributed under the terms of an Attribution–Noncommercial–Share Alike–No Mirror Sites license for the first six months after the publication date (see http://www.rupress.org/terms). After six months it is available under a Creative Commons License (Attribution–Noncommercial–Share Alike 3.0 Unported license, as described at http://creativecommons.org/licenses/by-nc-sa/3.0/).

The Rockefeller University Press $30.00
J. Cell Biol.
www.jcb.org/cgi/doi/10.1083/jcb.201202112

THE JOURNAL OF CELL BIOLOGY

Downloaded from jcb.rupress.org on September 12, 2012

Published September 10, 2012

Tsai, 2005; Bowman et al., 2006; Siller et al., 2006; Nguyen-Ngoc et al., 2007; Johnston et al., 2009; van der Voet et al., 2009; Zheng et al., 2010; Ellefson and McNally, 2011; Kiyomitsu and Cheeseman, 2012). NuMA together with dynactin is required for targeting of dynein to the cell cortex (Johnston et al., 2009; van der Voet et al., 2009; Woodard et al., 2010; Kiyomitsu and Cheeseman, 2012). Even so-called nonpolarized cells in culture typically position the mitotic spindle such that the axis of chromosome segregation is parallel to the growth surface (Toyoshima et al., 2007; Mitsushima et al., 2009). In this case, dynein–dynactin complexes play a role in the cortical capture and sliding of astral microtubules used to position and orient the spindle (Samora et al., 2011). Emerging evidence also implicates the retraction fibers, remnants of interphase cell–substratum adhesions, in spindle positioning and orientation in classical two-dimensional cell culture models (Théry et al., 2005; Fink et al., 2011). This may reflect the role of adhesion signaling through Rho family GTPases in more physiological cell divisions in tissues and three-dimensional cell culture systems (Gotta et al., 2001; Fernández-Miñán et al., 2007; Toyoshima et al., 2007; Buttrick et al., 2008; Jaffe et al., 2008; Inaba et al., 2010; Qin et al., 2010; Rodriguez-Fraticelli et al., 2010). Although a full picture has yet to emerge, current evidence supports the idea that a combination of extrinsic and intrinsic signals imparts defined spindle position and orientation (Kiyomitsu and Cheeseman, 2012).

As already mentioned, dynein is required for multiple processes during the formation and positioning of the mitotic spindle. However, the molecular nature of the different dynein complexes involved in spindle formation, positioning, and orientation remains unclear. We have therefore investigated the role of a specific cytoplasmic dynein light chain of the LC8 family, and find that it is needed together with a spindle-associated complex of CHICA and HMMR for correct spindle orientation.

Results

Dynein light chain 1 interacts with a subset of mitotic spindle proteins

To understand the function of dynein–dynein light chain 1 (DYNLL1) complexes at the mitotic spindle, HeLa cells stably expressing GFP-DYNLL1 were created. Analysis of DYNLL1 complexes isolated from mitotic populations of these cells by SDS-PAGE and mass spectrometry revealed the presence of dynein heavy, intermediate, light-intermediate, and the specific DYNLL1 light chain (Fig. 1 A and Table S1). In addition to these dynein subunits, a subset of mitotic spindle proteins were identified. Two of these, astrin and kinastrin/SKAP, have previously been reported to form a complex that interacts with dynein–DYNLL1 (Schmidt et al., 2010; Dunsch et al., 2011). A further two, HMMR/RHAMM and CHICA/FAM83D, are novel components of DYNLL1 complexes (Maxwell et al., 2003; Evanko et al., 2004; Santamaria et al., 2008; Tolg et al., 2010). Western blotting confirmed the presence of the different dynein subunits, astrin, kinastrin, HMMR, and CHICA in DYNLL1 complexes identified by mass spectrometry (Fig. 1 B). It also showed that these complexes do not contain tubulin, or other

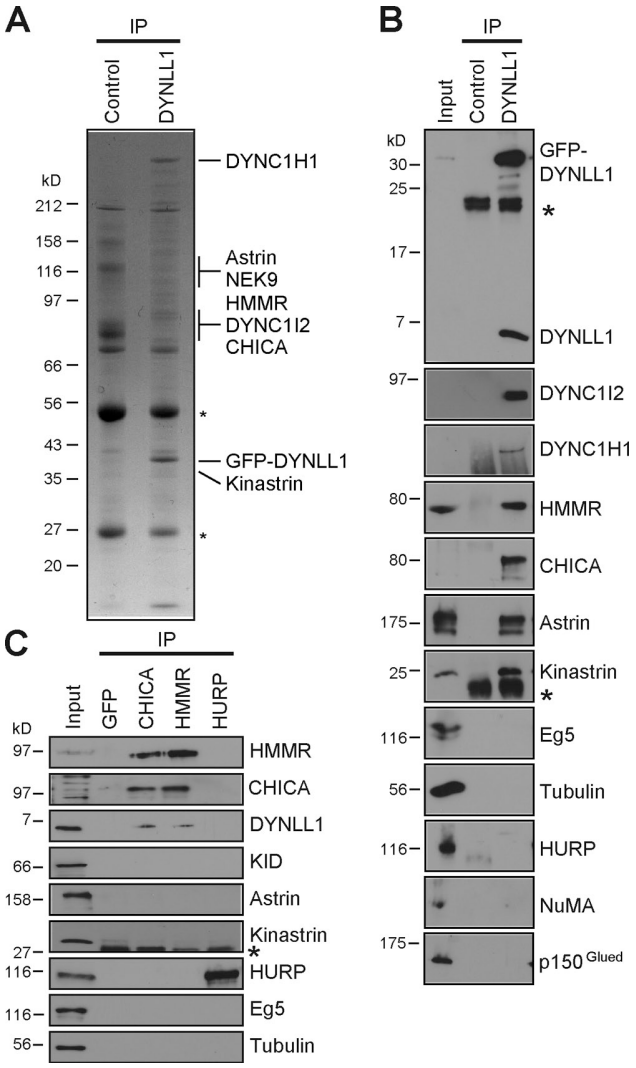


Figure 1. **DYNLL1-dynein associates with a defined subset of spindle proteins in mitosis.** (A) Control and DYNLL1 complexes were analyzed by SDS-PAGE and the major Coomassie blue–stained proteins identified by mass spectrometry are marked, or (B) by Western blotting using the specific antibodies shown in the figure. CHICA-C antibody was used for blotting. Asterisks mark the antibody heavy and light chains. (C) Complexes were immunoprecipitated using HMMR, CHICA-N, and HURP antibodies from HeLa cells arrested in mitosis using 200 ng/ml nocodazole for 18 h before cell lysis. Antibodies to GFP were used as a negative control. The immunoprecipitates were Western blotted using the antibodies shown in the figure. CHICA-C antibody was used for blotting. The asterisk marks light chain cross reactivity in the kinastrin blot.

spindle and spindle pole proteins Eg5, HURP, and NuMA, or the p150^{Glued} subunit of dynactin. DYNLL1 therefore defines specific subcomplexes of dynein in mitotically arrested cells, which are discrete from those formed by dynactin.

Specific antibodies were then raised against HMMR and CHICA, and affinity purified to permit characterization of these two proteins and their interactions with DYNLL1. Western blotting showed that HMMR antibodies detected a single protein of the expected size, and that this was depleted by two different siRNA duplexes (Fig. S1 A). Similarly, CHICA antibodies detected a single protein of the expected size, and again this was depleted by two different siRNA duplexes (Fig. S1 A). These HMMR and

Downloaded from jcb.rupress.org on September 12, 2012

Published September 10, 2012

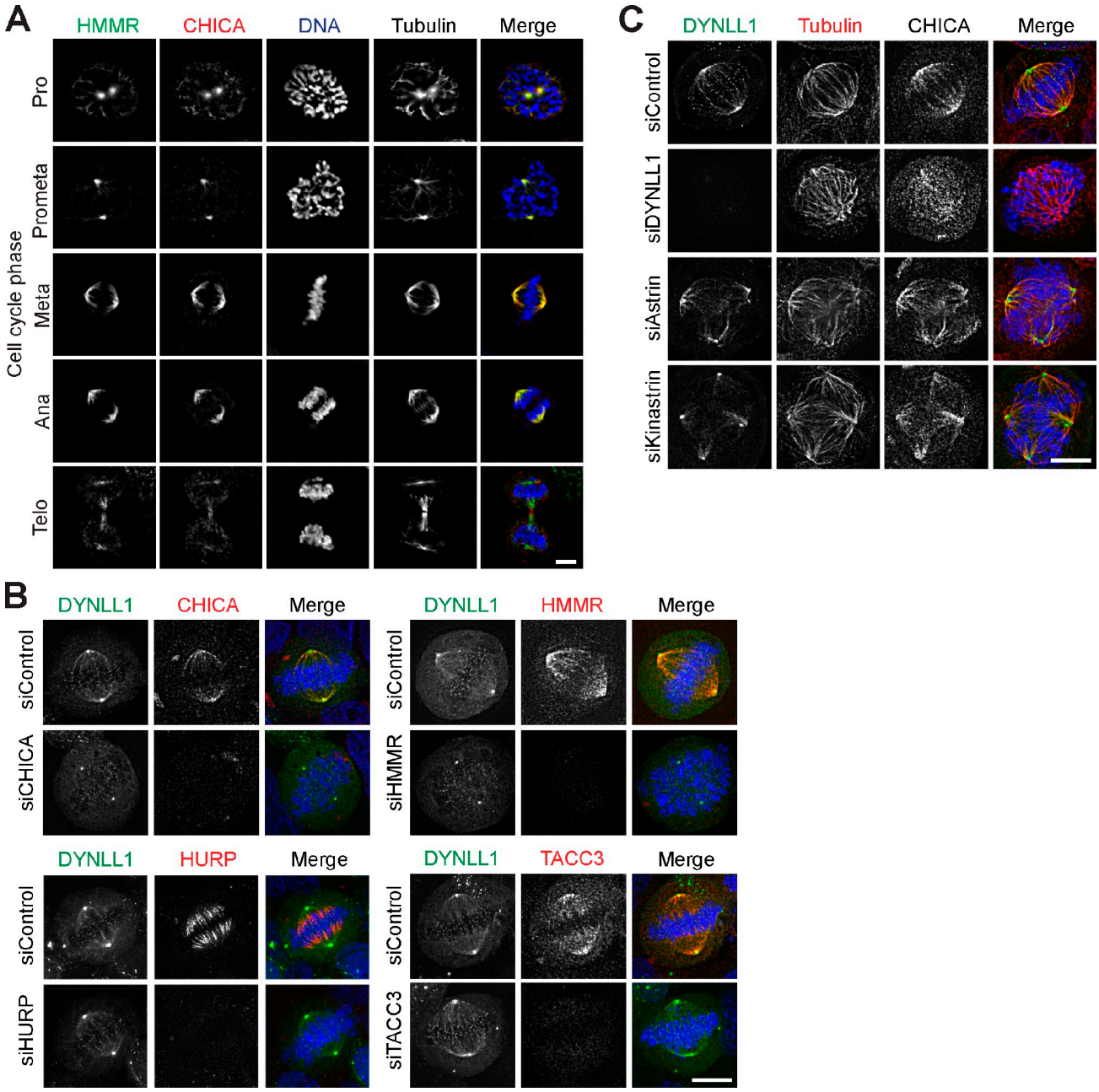


Figure 2. **HMMR and CHICA are spindle-associated factors required for DYNLL1 targeting.** (A) Asynchronous cultures of HeLa cells were fixed and then stained with mouse anti-HMMR, sheep anti-CHICA, rabbit anti-tubulin, and DAPI to detect DNA. Representative examples of the different stages of mitosis are shown. (B) HeLa cells stably expressing GFP-DYNLL1 were transfected with control, CHICA, HMMR, or HURP siRNA duplexes for 72 h, or TACC3 siRNA duplexes for 48 h. The cells were fixed and then stained for CHICA, HMMR, HURP, or TACC3 as appropriate and DAPI to detect DNA. DYNLL1 was visualized using GFP fluorescence. (C) HeLa cells stably expressing GFP-DYNLL1 were transfected with control, DYNLL1, or kinastrin, siRNA duplexes for 72 h, or astrin siRNA duplexes for 48 h. The cells were fixed and then stained for tubulin, CHICA, and DAPI to detect DNA. DYNLL1 was visualized using GFP fluorescence. CHICA-N antibodies were used for all stainings. Bars, 10 µm.

CHICA antibodies gave similar staining of the mitotic spindle, and in both cases this was lost in cells treated with specific siRNA duplexes. To test if HMMR and CHICA form a complex, these antibodies were used to immunoprecipitate the two proteins. Mass spectrometry (Table S1) and Western blotting (Fig. 1 C) revealed that CHICA and HMMR coprecipitate, consistent with the idea that the two proteins form a complex. In addition, DYNLL1 but not astrin or kinastrin were present in both CHICA and HMMR immunoprecipitates (Fig. 1 C). CHICA, HMMR, and DYNLL1 were not present in control or immunoprecipitations of the spindle and kinetochore fiber protein HURP (Fig. 1 C).

Spindle targeting of DYNLL1 requires HMMR and CHICA

The localization of HMMR and CHICA as cells passed through mitosis was then investigated (Fig. 2 A). This revealed that both

Downloaded from jcb.rupress.org on September 12, 2012

Published September 10, 2012

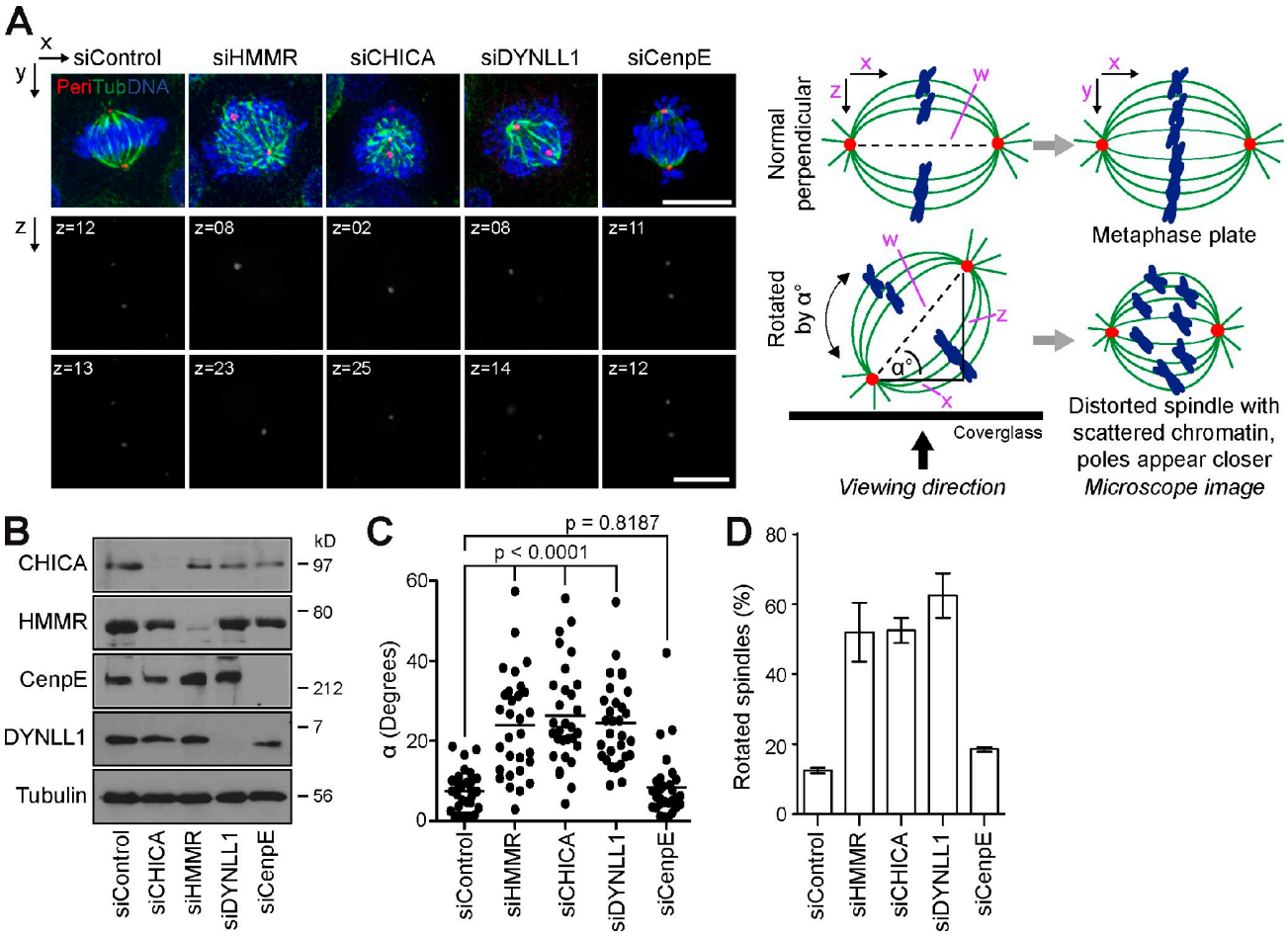


Figure 3. **Spindle orientation is perturbed in CHICA-, HMMR-, and DYNLL1-depleted cells.** (A) HeLa cells were transfected with control, CHICA, HMMR, DYNLL1 siRNA duplexes for 72 h, or CenpE siRNA duplexes for 48 h. The cells were fixed and then stained for tubulin and pericentrin to define the position of the mitotic spindle, and DAPI to detect DNA. A schematic shows the distances x and z measured from the microscope images and used to calculate α, the angle of spindle rotation and w, the pole-to-pole distance. (B) Samples were Western blotted to test for depletion of the respective target proteins. CHICA-C antibody was used for blotting. (C) Plots showing the angle of spindle rotation for cells depleted of the proteins indicated in the figure (n = 30). The Mann-Whitney test was used to calculate P-values for comparison of control and experimental samples. Median spindle angle was significantly different ($P < 0.0001$) in the DYNLL1-, HMMR-, and CHICA-depleted cells but not the CenpE-depleted cells ($P = 0.8187$) when compared with the control. (D) The percentage of cells with rotated spindles is plotted in the graph, error bars show the SEM (n = 100 in three independent experiments).

proteins localize to the spindle poles in prophase and prometaphase, and then spread out along the mitotic spindle in metaphase and then dissociate from the spindle in anaphase and telophase (Fig. 2 A). Depletion of either HMMR or CHICA, but not two other spindle proteins HURP or TACC3, resulted in a reduction of DYNLL1 at the mitotic spindle (Fig. 2 B). By contrast, depletion of the other DYNLL1-associated proteins astrin or kinastrin did not result in the loss of DYNLL1 from the spindles (Fig. 2 C), although spindles were highly disorganized as expected (Schmidt et al., 2010; Dunsch et al., 2011). Careful examination of astrin- and kinastrin-depleted cells revealed that DYNLL1 was lost from kinetochores, consistent with previous findings (Schmidt et al., 2010). Together, these findings show that DYNLL1 is present in two discrete complexes at the mitotic spindle: one containing astrin and kinastrin, the second previously uncharacterized complex containing HMMR and CHICA. The function of this latter complex and its relationship to dynein–DYNLL1 was therefore investigated further.

HMMR, CHICA, and DYNLL1 are required for normal mitotic progression

Previous studies have suggested that XRHAMM, the *Xenopus* orthologue of HMMR, has a function in the centrosome-independent pathway of spindle assembly (Groen et al., 2004). Other work suggests that HMMR promotes microtubule instability in interphase cells, and is important for mitotic spindle integrity (Tolg et al., 2010). By contrast, CHICA has been linked to the targeting of the kinesin-like motor protein KID to the mitotic spindle (Santamaria et al., 2008). HeLa cells were therefore depleted of HMMR, CHICA, or DYNLL1. Examination of these cells revealed apparently abnormal spindles with scattered chromatin (Fig. S1 B). A slight increase in mitotic index relative to the control was also observed for all CHICA, HMMR, and DYNLL1 duplexes tested (Fig. S1 C), consistent with the idea they have a function in mitosis. Live-cell imaging of cells expressing GFP-tubulin and mCherry-histone H2B showed that depletion of HMMR, CHICA, or DYNLL1 resulted

Downloaded from jcb.rupress.org on September 12, 2012

Published September 10, 2012

in an increase in the time taken from nuclear envelope breakdown (NEBD) to the onset of anaphase from 70 min in control cells to 110 min (Fig. S1 D). Although chromosomes and microtubules appeared disordered during spindle formation in each of these conditions, there was no obvious effect on chromosome segregation in anaphase (unpublished data). Other possibilities were that either kinetochore fiber function or spindle checkpoint activation were altered in the absence of the HMMR–CHICA–DYNLL1 complex. Speaking against these, cold-stable kinetochore fibers were still present in HMMR-, CHICA-, and DYNLL1-depleted cells, (Fig. S2 A), and none of these proteins localize to kinetochore fibers (Fig. S2 B). Furthermore, HMMR- and CHICA-depleted cells showed the expected localizations of the Bub1 checkpoint protein (Fig. S2 C) and a robust arrest in response to nocodazole (Fig. S2 D). These findings show that the HMMR–CHICA–DYNLL1 complex is not essential for kinetochore fiber stabilization or activation of the spindle checkpoint pathway. The role of DYNLL1 and the CHICA–HMMR complex in other dynein-dependent mitotic events was therefore investigated.

HMMR, CHICA, and DYNLL1 are required to define spindle orientation

In standard microscopy, cells are viewed through a coverglass that also acts as the growth surface, and a series of images collected at different focal positions through the sample data are projected to give a 2D image of the 3D sample (Fig. 3 A, schematic). Because cells grown in this way typically align the mitotic spindle parallel to the glass surface, this gives rise to the characteristic bar-like array of chromosomes (Fig. 3 A). Both spindle poles, defined in this case by the centriolar marker pericentrin are therefore typically equidistant from the coverglass or growth surface. This results in spindles aligning to within 10° of the plane of the coverglass. However, in cells depleted of HMMR, CHICA, or DYNLL1 (Fig. 3 B), the spindle poles are found at different distances from the coverglass (Fig. 3 A), and spindles showed widely differing angles of 0–60° to the coverglass plane (Fig. 3 C). Up to 60% of HMMR-, CHICA-, or DYNLL1-depleted cells had spindles rotated by over 10° (Fig. 3 D). These effects are not due to general perturbation of chromosome segregation because depletion of the CenpE motor protein required for proper chromosome alignment causes scattered chromatin but has little effect on spindle orientation compared with the control (Fig. 3, A–D).

Live-cell imaging was then performed to confirm these findings. As expected, cells depleted of CHICA, HMMR, or DYNLL1 showed apparently abnormal spindles (Fig. 4 A; see also Videos 1–4). Contrary to initial impressions, when the viewpoint was rotated these apparently abnormal spindles are revealed to be bipolar structures with the chromosomes aligned at a metaphase plate similar to the control cells (Fig. 4 B and Video 5). If spindle orientation was random in the absence of HMMR, CHICA, or DYNLL1, then the maximum angle observed should be 90°. However, none of the measurements made on fixed-cell samples exceeded 60°. One possibility was that the angle of spindle rotation was underestimated in the fixed samples due to drying artifacts causing flattening of the sample. Measurements of spindle rotation and pole-to-pole distance made from live-cell imaging data showed that spindles in HMMR-, CHICA-, or DYNLL1-depleted cells are of similar size (Fig. 4 C) but do not align to the coverslip, and the maximum angle of rotation is close to 90° compared with 10° in control samples (Fig. 4 D). DYNLL1, CHICA, and HMMR therefore act in a pathway required for proper mitotic spindle orientation.

Spindles orient at a fixed but incorrect angle

Inspection of the live-cell imaging data revealed that the spindles adopt a fixed but incorrect orientation with respect to the growth surface when DYNLL1, CHICA, or HMMR are depleted, and do not tumble continuously. Measurements over time for three individual cells for each condition showed that the spindle angle is rapidly established after bipolar spindle formation (Fig. 5, dotted line marks the point where a bipolar spindle is formed). Strikingly, even in cells showing prolonged time in metaphase this angle is maintained, typically within 10°, until the onset of anaphase (Fig. 5, marked by a red circle). Once in anaphase the angle of the spindle tends to zero as the cells flatten along the growth surface as they divide. The observation that spindle orientation became fixed indicated that the spindle was still contacting the cortex, suggesting that astral microtubules were not grossly altered. To clarify this, we made use of super-resolution 3D structured illumination microscopy (3D-SIM) to image the entire volume of mitotic cells under different depletion conditions. Astral microtubule organization was similar in DYNLL1-, CHICA-, or HMMR-depleted cells and control cells (Fig. 6 A). Furthermore, disruption of astral microtubules using 6.25 ng/ml nocodazole resulted in rotated but mainly off-center spindles positioned close to the cell cortex (Fig. 6, B and C). Under these conditions spindles are smaller due to altered microtubule dynamics, but kinetochore fibers still capture and align the chromosomes (Fig. 6 B). This effect is different to the consequences of depleting DYNLL1, CHICA, or HMMR. In these instances spindles are rotated but typically remain centered within the cell (Fig. 6 C). The microtubule plus end–tracking protein EB1 was then used to measure the dynamics of astral microtubules. This revealed that astral microtubule growth rates are similar in control, DYNLL1-, CHICA-, or HMMR-depleted cells (Fig. 6 D; see also Videos 6–10), and are in the range of values reported previously (Dunsch et al., 2011). These observations support the idea that astral microtubules play two roles in spindle positioning. First, they are important for centering the spindle within the cells, and second, they are used to transmit force during spindle rotation. Low doses of nocodazole disrupt the astral microtubules and interfere with both functions. However, the data presented here show that the DYNLL1 pathway is not required for astral microtubule formation, is not a major regulator of astral microtubule growth, and is not part of the NuMA–Plk1 intrinsic spindle-positioning pathway. This therefore suggests that DYNLL1, CHICA, and HMMR function during spindle rotation rather than as direct regulators of astral microtubules.

Downloaded from jcb.rupress.org on September 12, 2012

Published September 10, 2012

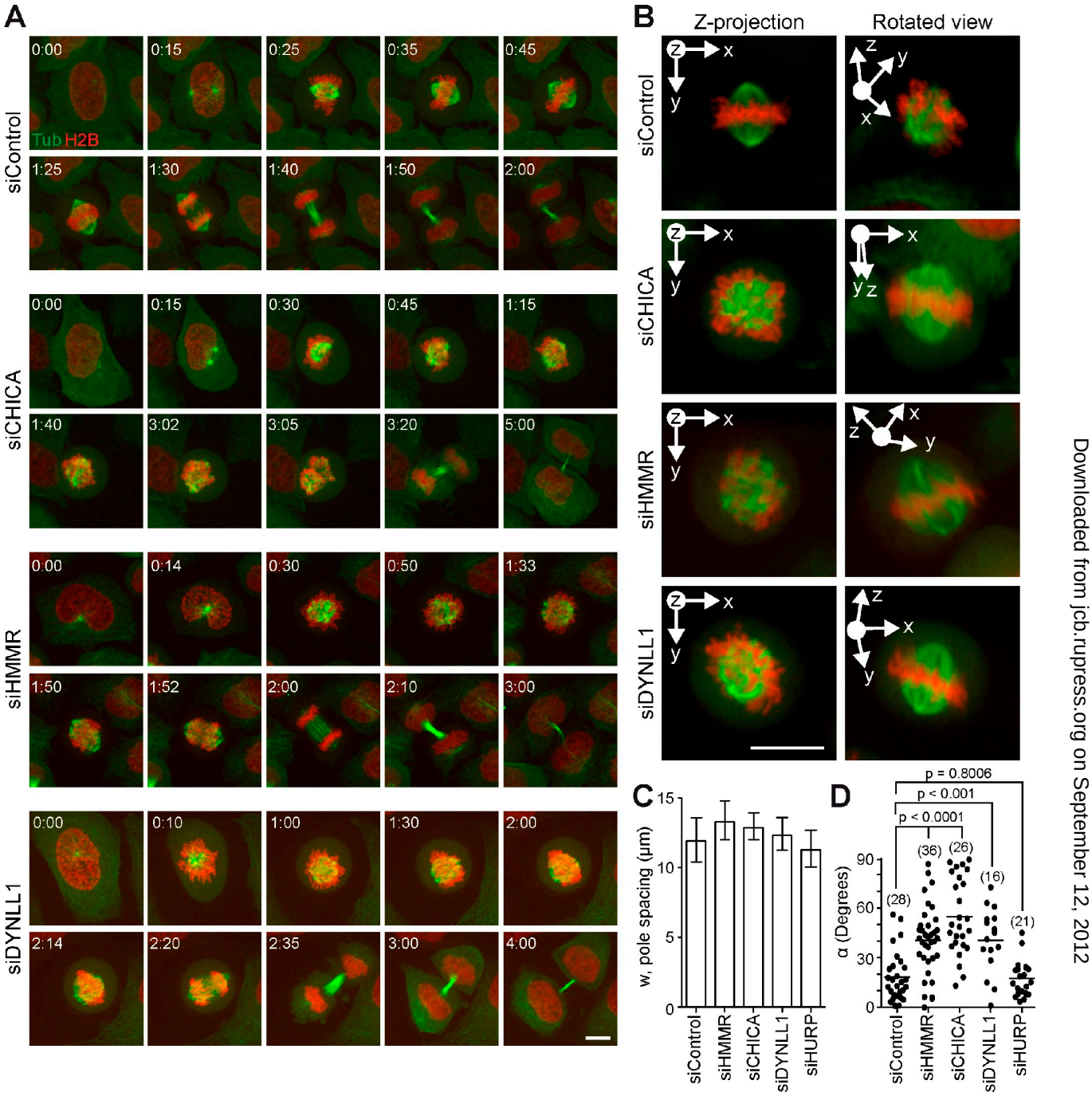


Figure 4. **HMMR, CHICA, and DYNLL1 are required for normal mitotic progression.** (A) HeLa cells stably expressing GFP-tubulin and mCherry-histone H2B were transfected with the siRNA duplexes shown in the figure for 72 h, and the full cell volume was imaged on an Ultraview spinning-disk confocal microscope every minute as the cells passed through mitosis. Maximum intensity projections of tubulin and histone H2B are shown at the times indicated in the figure. Bars, 10 µm. (B) A maximum intensity z-projection of tubulin and histone H2B are shown in the left column. The full 3D dataset was rotated to view the spindle from a plane perpendicular to the chromosomes and this is shown in the right column. (C) The pole-to-pole distance and (D) angle of spindle rotation at the metaphase-to-anaphase transition were calculated as described in Fig. 3 A and are plotted in the graphs. The Mann-Whitney test was used to calculate P-values for comparison of control and experimental samples. Median spindle angle was significantly different ($P < 0.0001$) in the HMMR- and CHICA-depleted cells, $P < 0.001$ in the DYNLL1-depleted cells, but not the HURP-depleted cells ($P = 0.8006$) when compared with the control. Numbers in brackets indicate sample size.

HMMR targets CHICA to the mitotic spindle

The functions of the different components of the HMMR–CHICA complex were then investigated to explain how it promotes proper spindle orientation. First, the localizations of a series of HMMR fragments were examined (Fig. 7 A). The first 189 amino acids of HMMR showed a strong spindle pole targeting in mitotic cells, and localized to microtubules in interphase cells

Downloaded from jcb.rupress.org on September 12, 2012

Published September 10, 2012

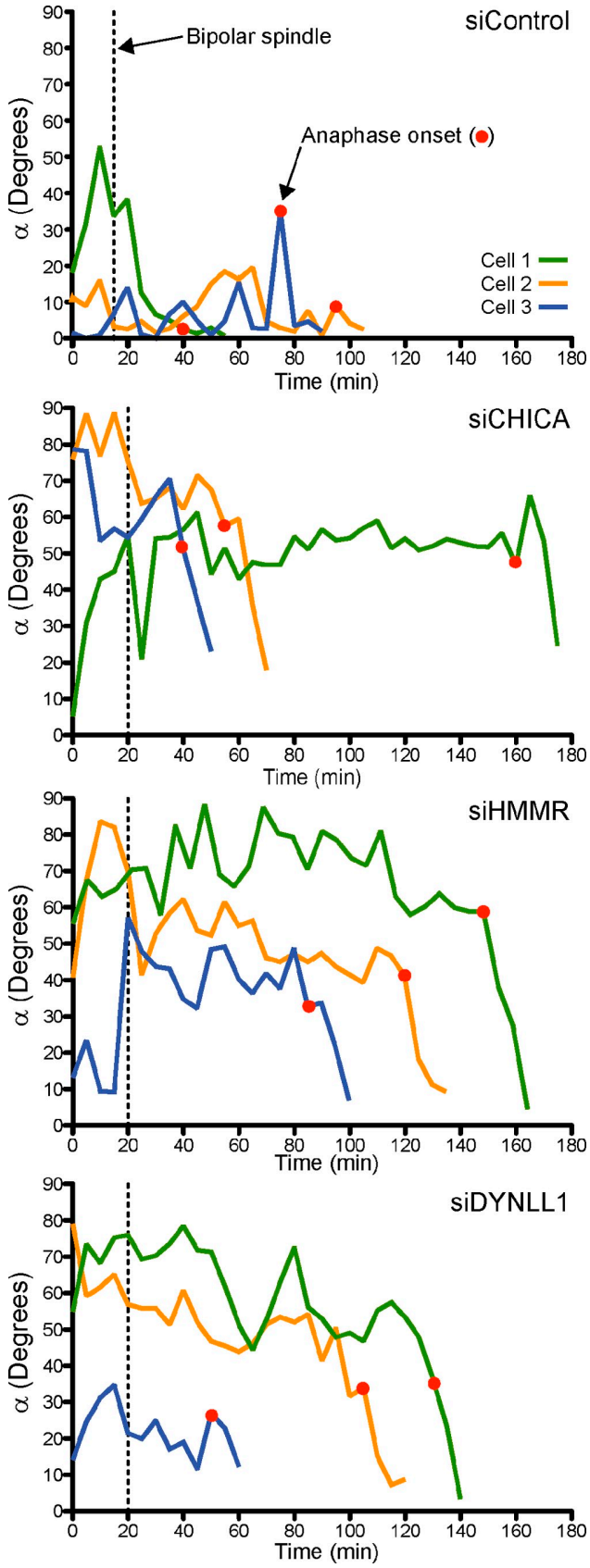


Figure 5. **Spindles adopt a fixed but incorrect orientation in CHICA-, HMMR-, or DYNLL1-depleted cells.** HeLa cells stably expressing GFP-tubulin and mCherry-histone H2B were transfected with the siRNA duplexes shown in the figure for 72 h, and the full cell volume was imaged on an Ultraview spinning-disk confocal microscope every minute as the cells passed through mitosis. The angle of spindle rotation was measured and is plotted in the graph as a function of time for three individual cells. The point at which bipolar spindle formation was complete is shown by the dotted line. A red circle marks the time point when chromosome segregation was first observed, taken as a marker for the onset of anaphase. Three example curves are shown taken from a single representative experiment of five replicates.

(Fig. 7 A). This fragment, but not the other fragments of HMMR, bound directly to microtubules when tested in in vitro pelleting assays (Fig. 7 B). A different region of HMMR, amino acids 365–546, within the predicted coiled-coil segment was required for binding to CHICA (Fig. 7 C). Reciprocal experiments with a series of CHICA fragments were then performed. This revealed that the C-terminal amino acids 383–615 localized to the mitotic spindle, and gave a weak microtubule staining in interphase cells (Fig. 7 D). However, this fragment did not show any microtubule-binding properties when tested in in vitro pelleting assays (Fig. 7 E). Mapping experiments revealed that the spindle-targeting fragment 383–615 was the binding site for HMMR (Fig. 7 F). The simplest explanation for these findings is that HMMR directly binds to microtubules and acts as an adaptor for CHICA, consistent with the requirement for HMMR in CHICA targeting to the spindle (Fig. S1 B).

Interaction of CHICA with DYNLL1 is required for spindle orientation

A series of elegant studies has identified a binding motif for the DYNLL1 protein defined by a highly conserved TQT sequence (Lo et al., 2001; Rapali et al., 2011a). Inspection of the CHICA sequence reveals the presence of three consensus TQT motifs (Fig. 8 A). Western blot analysis revealed that DYNLL1 was present in pulldowns of full-length CHICA or the 383–615 C-terminal fragment containing all three TQT motifs (Fig. 8 A). DYNLL1 was not detected in pulldowns of the other CHICA fragments tested. The three TQT motifs were then mutated to alanine, alone or in combination, to define their role in mediating the CHICA–DYNLL1 interaction. Mutation of all three TQT motifs in CHICA was necessary to abolish the interaction with DYNLL1 (Fig. 8 B). Furthermore, unlike the wild-type protein this triple TQT mutant was not able to target DYNLL1 to the spindle microtubules (Fig. 8 C), and did not correct the spindle orientation defect in CHICA-depleted cells (Fig. 8 D). DYNLL1 is therefore recruited to the mitotic spindle poles by a TQT motif–mediated interaction with CHICA, where it is required to establish the correct spindle orientation.

Asymmetric targeting of dynein to the cell cortex requires DYNLL1

During mitotic spindle positioning, dynein generates pulling forces to re-center and orient the mitotic spindle within the cell (Laan et al., 2012). In the course of this process, dynein oscillates from one pole of the cell cortex to the other but only accumulates at the pole farthest from the spindle (Kiyomitsu and Cheeseman, 2012). The cortical domains to which dynein localizes are defined by NuMA and other factors that do not show the

Downloaded from jcb.rupress.org on September 12, 2012

Published September 10, 2012

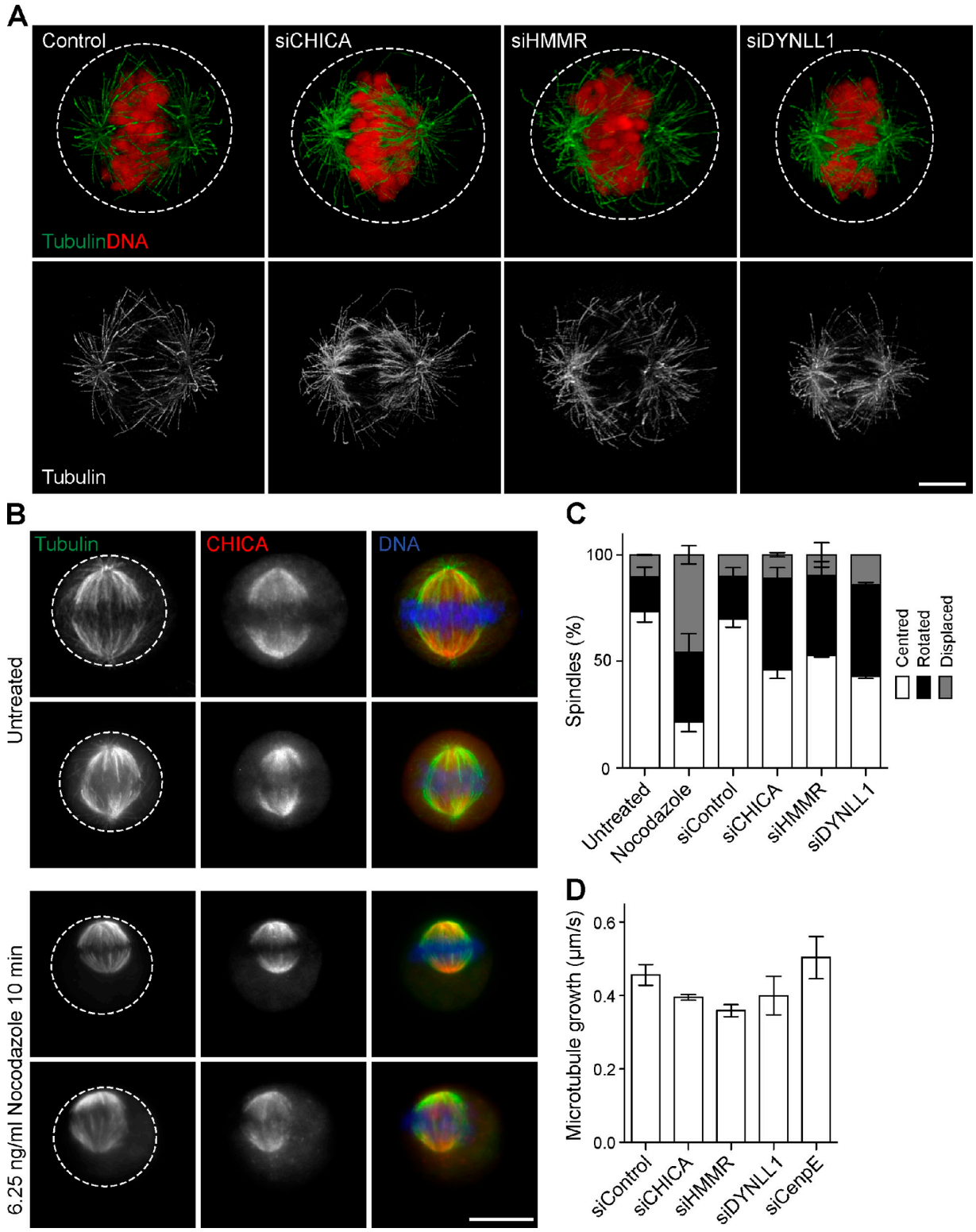


Figure 6. **Super-resolution imaging of astral microtubules in DYNLL1-, CHICA-, and HMMR-depleted cells.** (A) HeLa cells were transfected with control, HMMR, CHICA, or DYNLL1 siRNA duplexes for 72 h. The cells were fixed and then stained for CHICA, tubulin, and with DAPI to reveal DNA. Efficient depletion of CHICA and HMMR in these cells was confirmed by the loss of CHICA from the spindle microtubules (not depicted). Samples were analyzed by super-resolution imaging, and maximum intensity projections of the 3D-SIM stacks are shown from a viewpoint perpendicular to the pole-to-pole axis of the spindle. Bar, 5 µm. (B) To test the importance of astral microtubules in spindle positioning and rotation, HeLa cells were treated with a subcritical dose of nocodazole (6.25 ng/ml) for 10 min, fixed, and then stained for tubulin, CHICA, and with DAPI to reveal DNA. CHICA-C antibody was used for staining. Controls were left untreated. Example images are shown in the figure. Bar, 10 µm. (C) The number of cells with normally centered, rotated, or displaced spindles was counted and plotted in the graph. Error bars indicate the SEM (n = 50 in two independent experiments). (D) HeLa cells expressing

Downloaded from jcb.rupress.org on September 12, 2012

Published September 10, 2012

same oscillating behavior (Kiyomitsu and Cheeseman, 2012). To test if dynein function requires the DYNLL1–CHICA pathway, dynein localization was investigated using stable cell lines expressing GFP-tagged dynein heavy chain (DYNC1H1). In control cells, dynein was found asymmetrically localized to the cell cortex and to the mitotic spindle in 60% of cells (Fig. 9, A and B), as described previously (Kiyomitsu and Cheeseman, 2012). However, when DYNLL1, CHICA, or HMMR were depleted this asymmetric cortical localization was lost and dynein was found at both poles, or multiple smaller patches at the cell cortex (Fig. 9, A and B). Depletion of a kinetochore fiber protein HURP has no effect on dynein asymmetry at the cell cortex (Fig. 9, A and B). Although it was not possible to co-stain for dynein and NuMA, parallel experiments revealed that the underlying distribution of NuMA at the cell cortex was not altered by DYNLL1, CHICA, or HMMR depletion (Fig. S3). The additional dynein at the cell cortex may be relevant for the slightly increased pole-to-pole distance in these cells (Fig. 4, A and C), due to increased pulling forces on the two spindle poles. This may also delay satisfaction of the spindle assembly checkpoint due to alterations in spindle geometry, and therefore may explain the slight mitotic delays observed. Alternatively, it remains possible that DYNLL1 plays additional roles in the spindle checkpoint through other binding partners such as the astrin–kinastrin complex (Schmidt et al., 2010; Dunsch et al., 2011).

To show that the effect on dynein asymmetry is due to the pool of DYNLL1 interacting with the CHICA–HMMR complex at the mitotic spindle, rescue experiments using the CHICA TQT mutant defective in DYNLL1 binding were performed (Fig. 10). As described already, depletion of CHICA resulted in a loss of dynein asymmetry, and this could be rescued by expression of wild-type CHICA (Fig. 10, A and B). By contrast, the CHICA TQT mutant failed to support asymmetric dynein targeting to the cell cortex (Fig. 10, A and B). Together, these findings support the idea that the spindle-associated CHICA–HMMR complex acts as a regulator of dynein localization, and therefore its activity, through the DYNLL1 adaptor protein.

Discussion

A model for DYNLL1-CHICA function in spindle rotation

The findings presented here show that DYNLL1 and CHICA–HMMR form part of a regulatory system feeding back spindle position to dynein at the cell cortex. Based on this data, we propose a simple working model to explain the function of DYNLL1 and the CHICA–HMMR complex in spindle positioning (Fig. 10 C). CHICA and HMMR associate with the mitotic spindle through a spindle-microtubule–targeting region in the N terminus of HMMR. This complex can then recruit DYNLL1 via a series of canonical TQT motifs in the C-terminal region of CHICA. The model proposes that this will create a gradient of DYNLL1 activity, decreasing away from the spindle and spindle poles (Fig. 10 C, purple shaded region). During the formation of the mitotic spindle in prophase and prometaphase, or when a spindle is displaced away from the center of the cell, the spindle pole will approach the cell cortex. The resulting local increase in DYNLL1 then causes the loss of dynein from the cell cortex. This would explain why dynein can be isolated in complex with DYNLL1 and is found together with DYNLL1 at the mitotic spindle, but DYNLL1 does not localize to the cell cortex. When this inhibitory mechanism is lost, dynein localization becomes uncoupled from spindle rotation. Spindle position toward the center of the cell is relatively unaltered because astral microtubules will continue to push against the cell cortex and exert a centering effect. Providing independent support for this idea, pronounced oscillation of dynein localization and spindle position is only observed when astral microtubules are perturbed using nocodazole (Kiyomitsu and Cheeseman, 2012). A prediction of this model is that the DYNLL1-bound form of dynein cannot bind to dynein adaptors required for cortical targeting. Although not exhaustively tested, the biochemical and Western blot analysis of dynein–DYNLL1 complexes failed to reveal the presence of subunits of another major dynein adaptor dynactin or components such as NuMA required for cortical targeting of dynein.

DYNLL1-CHICA are components of the intrinsic spindle positioning pathway

Dynactin, together with NuMA and Lgn is required for targeting of dynein to the cell cortex (Johnston et al., 2009; van der Voet et al., 2009; Woodard et al., 2010; Kiyomitsu and Cheeseman, 2012). This system is controlled by extracellular cues (Théry et al., 2005, 2007; Toyoshima and Nishida, 2007; Siller and Doe, 2009), and signals intrinsic to the mitotic spindle (Kiyomitsu and Cheeseman, 2012). The spindle intrinsic signal has two components: one is the Ran-gradient system, the second is the spindle-associated mitotic kinase Plk1. Activated Ran in the vicinity of chromatin controls the interaction of importins with NuMA and modulates the interaction of the NuMA-Lgn complex with the membrane (Kiyomitsu and Cheeseman, 2012). Plk1 regulates the interaction of the NuMA-Lgn complex with dynein-dynactin, and therefore directly controls force generation (Kiyomitsu and Cheeseman, 2012). Together, these two components prevent dynein accumulation at the cell equator, and reduce dynein-dependent force generation at regions of the cell cortex close to the spindle poles. Further work will be needed to establish the relationship between these components and the DYNLL1-CHICA pathway. The most obvious possibility is that Plk1 regulates the DYNLL1-CHICA pathway through phosphorylation. Previous work has shown that CHICA is heavily phosphorylated in mitosis (Santamaria et al., 2008), but the

mCherry-tagged EB1 were transfected with control, HMMR, CHICA, or DYNLL1 siRNA duplexes for 72 h, or CenpE siRNA duplexes for 48 h. Cells were imaged at four planes positioned at the cell equator to cut through one or both spindle poles. Acquisition was with 30% laser power, 100-ms exposure time at maximum speed, equivalent to 0.87 frames per second. EB1 comets located between the spindle poles and the cell cortex, which mark growing astral microtubule ends, were identified and marked by eye in ImageJ and the mean distance moved per unit time calculated and plotted in the bar graph. Error bars indicate the SEM (n = 20).

Downloaded from jcb.rupress.org on September 12, 2012

Published September 10, 2012

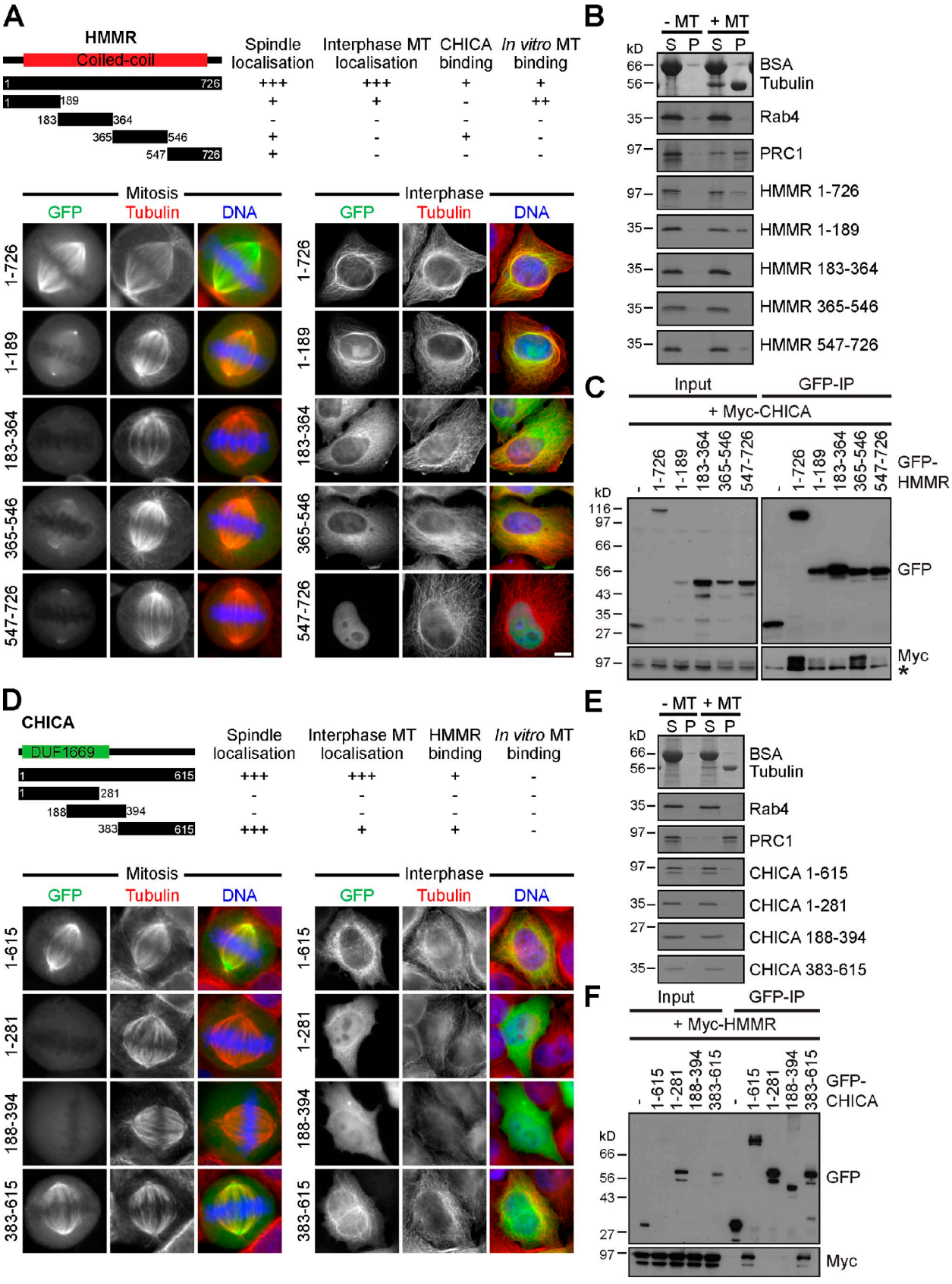


Figure 7. **HMMR is a microtubule-binding protein and partner of CHICA.** (A) HeLa cells were transfected with full-length GFP-tagged HMMR or the deletion constructs outlined in the schematic. After 24 h the cells were fixed and then stained for tubulin, and DAPI to detect DNA. HMMR was visualized using GFP fluorescence. Representative examples of the localization in mitotic or interphase cells are shown. Bar, 10 µm. (B) Microtubule-binding assays were

Downloaded from jcb.rupress.org on September 12, 2012

Published September 10, 2012

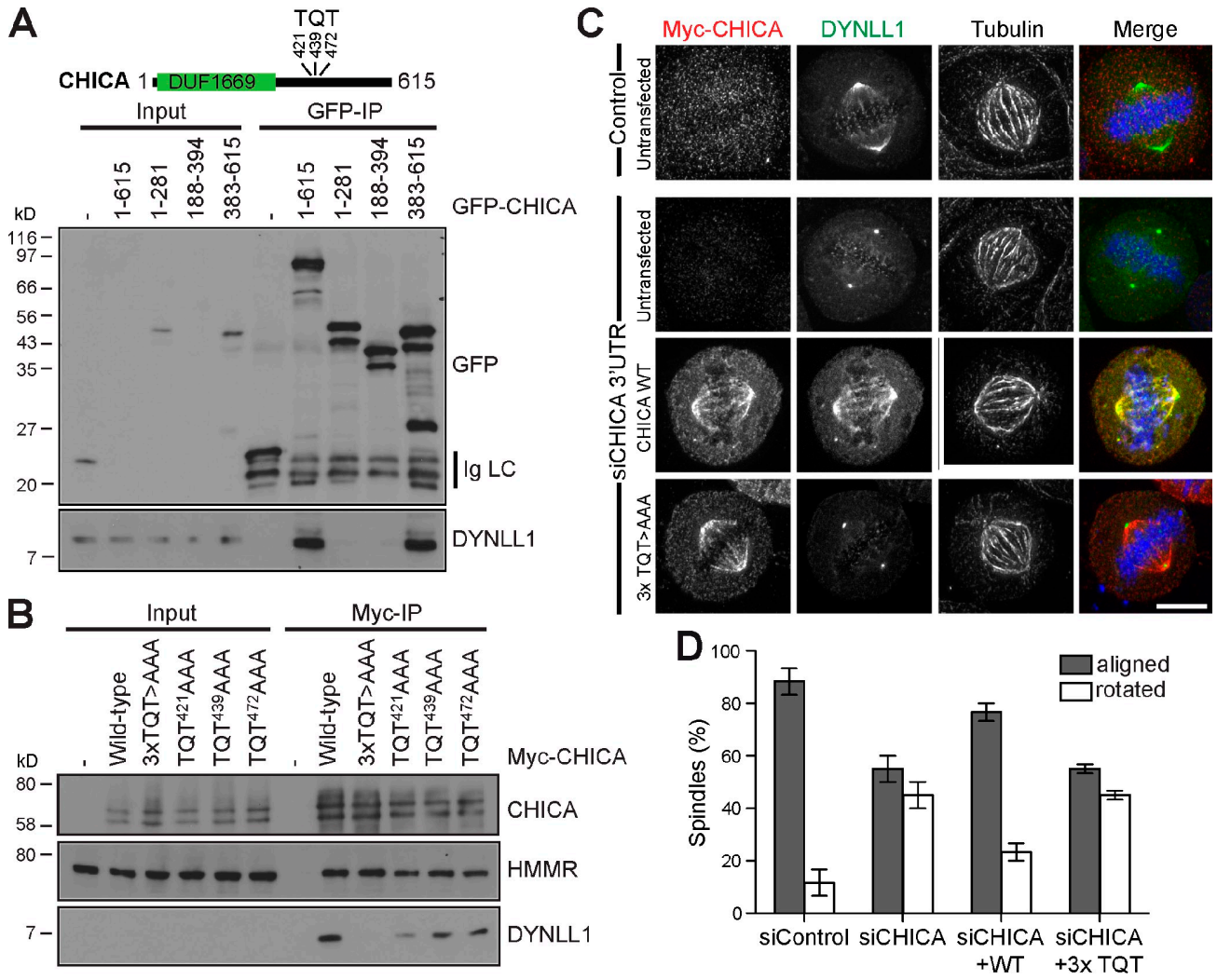


Figure 8. **CHICA binds to DYNLL1 via TQT consensus motifs.** (A) HEK293T cells were transfected with full-length and deletion constructs of GFP-CHICA for 30 h. CHICA complexes were immunoprecipitated using sheep anti-GFP antibodies, and then Western blotted using mouse anti-GFP or rabbit anti-DYNLL1 antibodies. (B) HEK293T cells were transfected with Myc-CHICA, and single or combined TQT to AAA mutants for 30 h. CHICA complexes were immunoprecipitated using mouse anti-Myc antibodies, and then Western blotted using rabbit anti-Myc, sheep anti-HMMR, or rabbit anti-DYNLL1 antibodies. (C) HeLa cells stably expressing GFP-DYNLL1 were treated with control siRNA or directed toward the 3′-UTR of CHICA for 72 h, and transfected with the wild-type or 3x TQT to AAA mutant forms of Myc-CHICA, fixed after 36 h, and then stained as indicated in the figure. DYNLL1 was directly visualized by GFP fluorescence. Bar, 10 µm. (D) The percentage of cells with aligned or rotated spindles is plotted in the bar graph. Error bars show the SEM (n = 30 in three experiments).

consequences of this modification remain unknown. Another area for future work will be the study of DYNLL1 interaction with dynein. This interaction is thought to be mediated by a TQT motif in the dynein intermediate chain (Rapali et al., 2011b), but the role this interaction plays in controlling dynein function and localization remains mysterious. Intriguingly, dynactin also binds to dynein via the dynein intermediate chain (Vaughan et al., 1995) and this interaction is mutually exclusive with another dynein regulator NudE-Lis1 (McKenney et al., 2011). Therefore, DYNLL1 may compete with dynactin for binding sites on the dynein intermediate chain, and thereby displace dynein complexes from the cell cortex.

performed using in vitro–translated full-length HMMR and the fragments shown in the figure. The anaphase spindle protein PRC1 and the small GTPase Rab4 were taken as positive and negative controls, respectively. (C) HEK293T cells were cotransfected with full-length and deletion constructs of GFP-HMMR and Myc-CHICA for 30 h. HMMR complexes were immunoprecipitated using sheep anti-GFP antibodies, and then Western blotted using mouse anti-GFP or mouse anti-Myc. An asterisk marks a nonspecific band in the Myc blots. (D) HeLa cells were transfected with full-length GFP-tagged CHICA or the deletion constructs outlined in the schematic. After 24 h, the cells were fixed and then stained for tubulin, and DAPI to detect DNA. CHICA was visualized using GFP fluorescence. Representative examples of the localization in mitotic or interphase cells are shown. Bar, 10 µm. (E) Microtubule-binding assays were performed using in vitro–translated full-length CHICA and the fragments shown in the figure. The anaphase spindle protein PRC1 and the small GTPase Rab4 were taken as positive and negative controls, respectively. (F) HEK293T cells were cotransfected with full-length and deletion constructs of GFP-CHICA and Myc-HMMR for 30 h. CHICA complexes were immunoprecipitated using sheep anti-GFP antibodies, and then Western blotted using mouse anti-GFP or mouse anti-Myc.

Downloaded from jcb.rupress.org on September 12, 2012

Published September 10, 2012

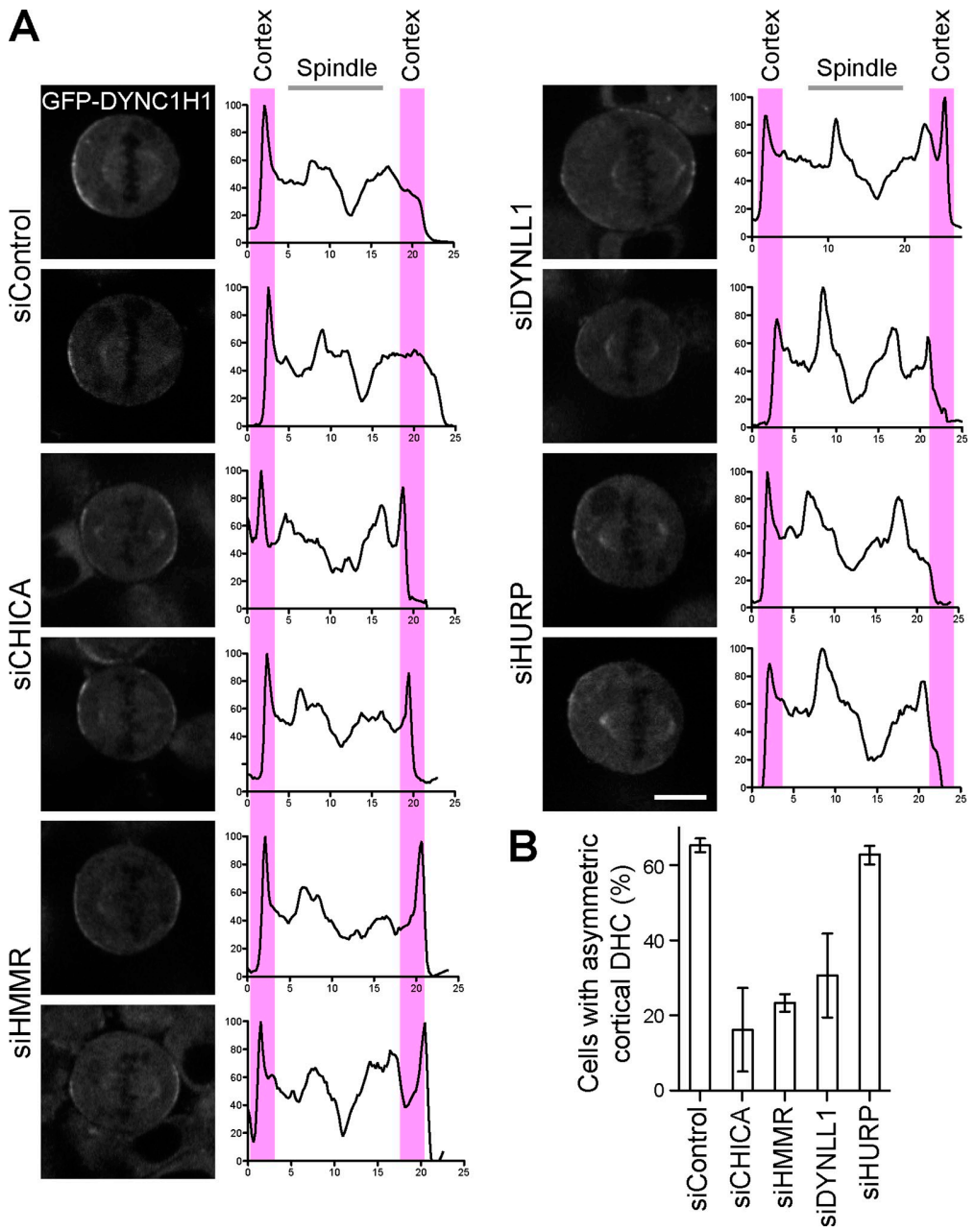


Figure 9. **Dynein heavy chain asymmetry is lost in DYNLL1-, CHICA-, and HMMR-depleted cells.** (A) GFP-dynein heavy chain (DYNC1H1) cells were transfected with control, CHICA, HMMR, DYNLL1, and HURP siRNA duplexes for 72 h. The cells were then imaged using an Ultraview Vox spinning-disk confocal system. Images of metaphase cells were taken from a single z-plane at one time point. Exposure times were 100 msec for GFP-DYNC1H1 using 50% laser power. Graphs representing the intensity profiles were generated with NIH ImageJ. A profile plot was made from a selection of 20 pixels width crossing the mitotic spindle at both spindle poles. Intensity values were extracted. An average background value was subtracted and values were normalized to the brightest point corresponding to 100%. Two representative example images and associated graphs are shown. Bar, 10 µm. (B) The cortical localization of dynein was scored in the different conditions used and is plotted in the bar graph. Error bars show the SEM (n = 25 in each of three independent experiments.

Materials and methods

Reagents and antibodies

General laboratory chemicals were obtained from Sigma-Aldrich and Thermo Fisher Scientific. Hexahistidine-tagged HMMR aa 183–364, CHICA-N aa 1–281, and HURP aa 673–890 were expressed in and purified from bacteria. Antibodies against HMMR, CHICA-N, and HURP were raised in sheep (Scottish National Blood Transfusion Service, Edinburgh, UK) and affinity purified using the His-tagged proteins coupled to Affigel-15 (Bio-Rad Laboratories). The CHICA-C antibody was raised in sheep using the CHICA peptide (CSRVNLLAVRD) as the antigen. The crude serum was affinity purified using the CHICA peptide coupled to Sulfo-link (Thermo Fisher Scientific). Commercial mouse monoclonal antibodies were used against α-tubulin (clone DM1A; Sigma-Aldrich), Bub1 (Abcam), dynein heavy chain and dynein intermediate chain (Sigma-Aldrich), HMMR (Abcam), Myc (clone 9E10; Sigma-Aldrich), and p150^{Glued} (BD); rabbit antibodies against astrin (Thein et al., 2007), CenpE (Bethyl Laboratories, Inc.), NuMA and pericentrin (Abcam), DYNLL1 (Epitomics, Inc.), KID (Cytoskeleton), Myc (Sigma-Aldrich), and TACC3 (Santa Cruz Biotechnology, Inc.); and sheep antibodies against Eg5 (Zeng et al., 2010), GFP

Downloaded from jcb.rupress.org on September 12, 2012

Published September 10, 2012

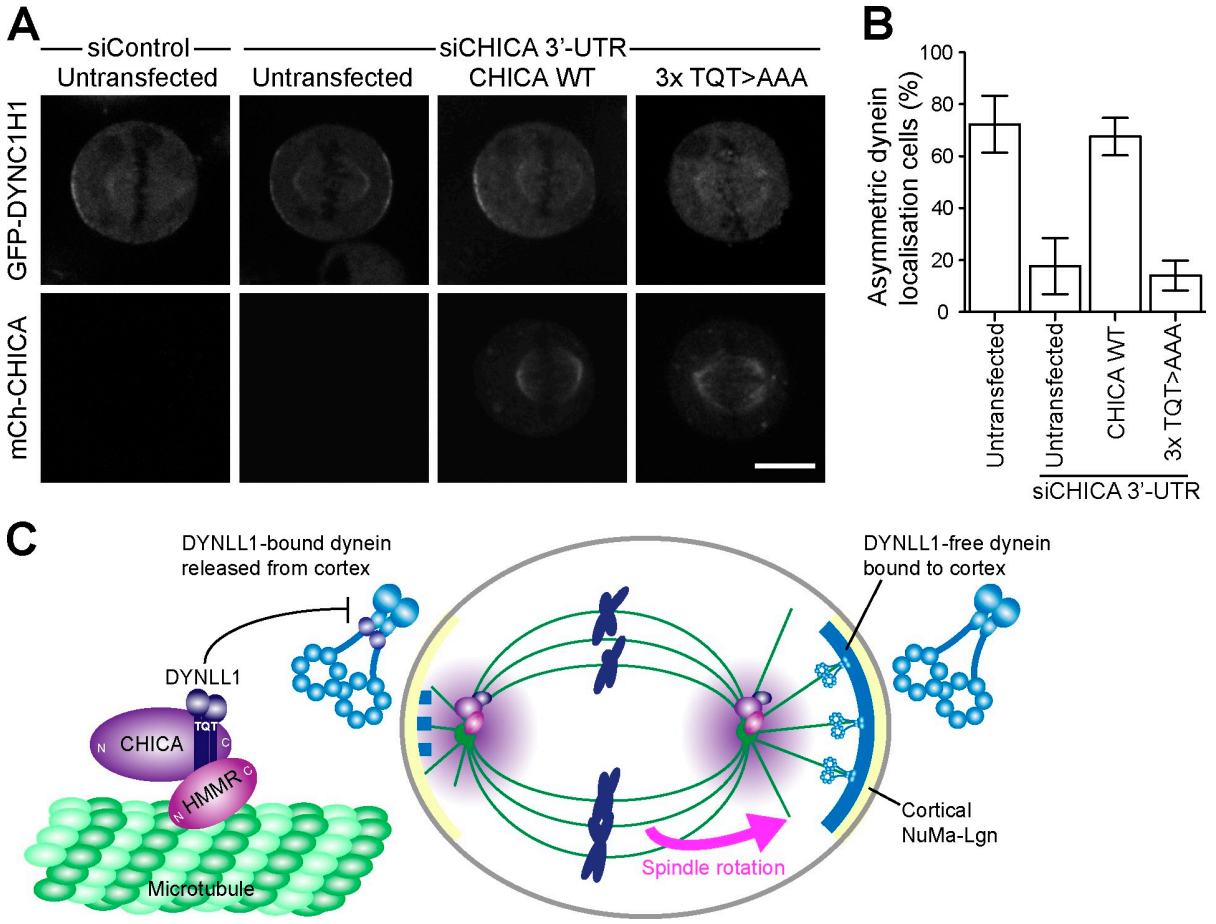


Figure 10. **Dynein heavy chain asymmetry is lost in DYNLL1-, CHICA-, and HMMR-depleted cells.** (A) GFP-dynein heavy chain (DYNC1H1) cells were transfected with control or CHICA 3′-UTR siRNA duplexes for 24 h, then left untransfected or further transfected with CHICA wild-type or the TQT mutant form for a further 48 h. The cells were then imaged using an Ultraview Vox spinning-disk confocal system. Images of metaphase cells were taken from a single z-plane at one time point. Exposure times were 100 msec for GFP-DYNC1H1 or mCherry-tagged CHICA using 50 or 30% laser power, respectively. (B) The cortical localization of dynein was scored and is plotted in the bar graph. Error bars show the SEM (n = 10 in each of two independent experiments). (C) A model or DYNLL1 function in spindle positioning and orientation. DYNLL1 is recruited to spindle poles by the triple TQT motifs in the CHICA-HMMR complex. HMMR contains an N-terminal microtubule-binding domain capable of targeting the complex to spindle microtubules. Because loss of DYNLL1 results in additional dynein at the cortex and DYNLL1 does not accumulate at the cell cortex, this model proposes that DYNLL1 is inhibitory to dynein targeting to the cortex. When a spindle pole carrying the DYNLL1–CHICA–HMMR complex approaches the cortex, this results in increased local concentration of DYNLL1 and removal of dynein from the cell cortex. Ultimately, this leads to a reduction in pulling forces on the mitotic spindle, which then fails to rotate to the correct position in response to extrinsic positioning cues.

(Shorter et al., 1999), and kinastrin (Dunsch et al., 2011). Kinetochores were visualized with CREST (human auto-antiserum; Europa Bioproducts Ltd.). Affinity-purified primary and secondary antibodies were used at 1 µg/ml final concentration; sera were used at 1:1,000 dilution. Secondary antibodies conjugated to HRP or Cy5 were obtained from Jackson ImmunoResearch Laboratories, Inc. Secondary antibodies conjugated to Alexa Fluor 488, 555, and 647 were obtained from Invitrogen. DNA was stained with DAPI (Sigma-Aldrich).

Molecular biology

Human CHICA, DYNLL1, HMMR, and EB1 were amplified from human testis cDNA (Takara Bio Inc.) using *KOD* polymerase (Takara Bio Inc.). Mammalian expression constructs for CHICA, DYNLL1, HMMR, and EB1 were made using pcDNA3.1, pcDNA4/TO, and pcDNA5/FRT/TO vectors (Invitrogen) modified to encode the Myc epitope tag, mCherry, or GFP reading frames. Bacterial expression constructs were made in pQE32 (QIAGEN). Mutagenesis was performed using the QuikChange method according to the protocol (Agilent Technologies). RNA interference for astrin, kinastrin, CenpE, GL2 luciferase (control), HURP, and Nuf2 was carried out using published (Dunsch et al., 2011) commercially available siRNA duplexes. Other siRNA duplexes were as follows: CHICA-1 5′-CAAUUCCACUUCGCUGGUAdTdT-3′; CHICA-2 5′-GAACUAAGAUUAUUGGGAAdTdT-3′; CHICA-3 5′-CCAGGATAGCAAGCTCTCAAA-3′; CHICA-4 5′-ATGGACGGATGGCAAATTAAA-3′; HMMR-1 5′-CUGAUUUGCAGAACCAACUdTdT-3′; HMMR-2 5′-GGAGAAUAUUGUUAUAUUAdTdT-3′; DYNNL1 Dharmacon SmartPool L-005281-00 (Thermo Fisher Scientific) or 5′-GAAGGACAUUGCGGCUCAUUU-3′; CHICA 3′-UTR 5′-GGTTTAAACACTATGGATA-3′; and TACC3 5′-GTTACCGGAAGATCGTCTG-3′.

Cell culture

HeLa cells and HEK293T were cultured in DME containing 10% bovine calf serum (Invitrogen) at 37°C and 5% CO_2. For synchronization, cells were treated for 18 h with 2 mM thymidine, washed three times in PBS, and twice with growth medium. For plasmid transfection and siRNA transfection, Mirus LT1 (Mirus Bio LLC) and Oligofectamine (Invitrogen), respectively, were used according to the manufacturers' instructions. Stable HeLa cell lines with single copies of the desired transgene were created using the T-Rex doxycycline-inducible Flp-In system (Invitrogen). HeLa cell lines stably expressing GFP-tagged α-tubulin selected using 0.5 µg/ml puromycin and mCherry-tagged histone H2B selected using 0.3 µg/ml blasticidin have been described previously (Zeng et al., 2010). The tagged transgenes and selection markers were under the control of the chicken β-actin promoter. Cell lines expressing GFP-tagged DYNC1H1 were obtained from the Mitocheck consortium (www.mitocheck.org).

Downloaded from jcb.rupress.org on September 12, 2012

Published September 10, 2012

Isolation of protein complexes

For immunoprecipitations of endogenous CHICA, DYNLL1, HMMR, or HURP, three 15-cm dishes of synchronized HeLa S3 cells per condition were released from the thymidine arrest for 3 h at 37°C, 100 ng/ml nocodazole was added, and the cells were incubated for a further 16 h. For HMMR or CHICA fragments, one 15-cm dish of HEK293T cells per condition was transfected with the appropriate construct for 30 h. Mitotic cells were collected by shake-off and nocodazole was removed by washing three times with prewarmed PBS and twice with growth medium. For metaphase samples, cells were collected and washed three times with ice-cold PBS. Cell pellets were resuspended in lysis buffer (20 mM Tris-HCl, pH 7.4, 150 mM NaCl, 1 mM EDTA, 1% [vol/vol] IGEPAL, 0.1% [wt/vol] sodium deoxycholate, 40 mM β-glycerophosphate, 10 mM NaF, 0.3 mM Na-vanadate, 100 nM okadaic acid, and protease inhibitor cocktail [SigmaAldrich]), left for 15 min on ice, and then clarified by centrifugation at 20,000 *g* for 15 min at 4°C. Protein complexes were isolated from 3 mg of cell lysate using 2.5 µg sheep antibodies against either mCherry, GFP, HMMR, or CHICA bound to 20 µl protein G–Sepharose by incubation for 3 h at 4°C. Isolated complexes were washed three times with lysis buffer, twice with 20 mM Tris-HCl, pH 7.4, 150 mM NaCl, 0.1% [vol/vol] IGEPAL, and then twice with 20 mM Tris-HCl, pH 7.4, 150 mM NaCl.

Mass spectrometry of protein complexes

Protein samples for mass spectrometry were separated on 4–12% gradient NuPAGE gels, then stained using a colloidal Coomassie blue stain. Gel lanes were cut into 12 slices, and then digested with trypsin (Wilm et al., 1996). The resulting tryptic peptide mixtures in 0.05% [vol/vol] trifluoracetic acid were then analyzed by online LC-MS/MS with a nanoAcquity UPLC (Waters) and an Orbitrap XL ETD mass spectrometer (Thermo Fisher Scientific) fitted with a Proxeon nano-electrospray source. Peptides were loaded on to a 5-cm × 180-µm BEH-C18 Symmetry trap column (part no. 186003514; Waters) in 0.1% [vol/vol] formic acid at 15 µl/min, and then resolved using a 25-cm × 75-µm BEH-C18 column (part no. 186003815; Waters) in 99–37.5% [vol/vol] acetonitrile in 0.1% [vol/vol] formic acid at a flow rate of 400 nl/min. The mass spectrometer was set to acquire an MS survey scan in the Orbitrap (R = 30,000) and then perform MS/MS on the top five ions in the linear quadrupole ion trap after fragmentation using collision ionization (30 msec, 35% energy). A 90-s rolling exclusion list with $n = 3$ was used to prevent redundant analysis of the same ions. Maxquant and Mascot (Matrix Science) were then used to compile and search the raw data against the human IPI database (Cox and Mann, 2008). Protein group and peptide lists were sorted and analyzed in Excel (Microsoft) and Maxquant. MS and MS/MS spectra were manually inspected using Xcalibur Qualbrowser (Thermo Fisher Scientific).

Fixed cell microscopy

Cells grown on no. 1.5 glass coverslips (Menzel-Gläser; Thermo Fisher Scientific) were washed twice with 2 ml of PBS, and fixed with 2 ml of 3% [wt/vol] paraformaldehyde in PBS for 15 min. Fixative was removed and the cells quenched with 2 ml of 50 mM NH_4Cl in PBS for 10 min. Coverslips were washed three times in 2 ml PBS before permeabilization in 0.2% [vol/vol] Triton X-100 for 10 min. In all cases primary and secondary antibody staining was performed in PBS for 60 min at room temperature. Affinity-purified antibodies were used at 1 µg/ml, whereas commercial antibodies were used as directed by the manufacturers. DAPI was added to the secondary antibody–staining solution at 1 µg/ml. Coverslips were mounted in Mowiol 4-88 mounting medium. Fixed samples on glass slides were imaged using a 60×, NA 1.35 oil immersion objective on an upright microscope (model BX61; Olympus) with filtersets for DAPI, GFP/Alexa Fluor 488, -555, -568, and -647 (Chroma Technology Corp.), a CoolSNAP HQ2 camera (Roper Scientific), and MetaMorph 7.5 imaging software (Molecular Dynamics Inc.). Illumination was provided by a Lumen 200 Watt metal halide light source (Prior Scientific Instruments Ltd.). Image stacks of 12–35 planes with a spacing of 0.2–0.4 µm through the cell volume were taken. Using MetaMorph, image stacks were maximum intensity projected and then merged to create 24-bit RGB TIFF files. Images in Figs. 2, 3, S2, and S3 were deconvolved using the nearest-neighbors method in MetaMorph. Images in 24-bit RGB format were then cropped in Photoshop CS3 and placed into Illustrator CS3 (Adobe Systems Inc.) to produce the figures.

Super-resolution imaging

3D structured illumination microscopy (3D-SIM) was performed as described previously (Schermelleh et al., 2008) on a DeltaVision OMX V2 system (Applied Precision) equipped with a 100× 1.4 NA oil immersion objective (Olympus) and Cascade II:512 EMCCD cameras (Roper Scientific), using the 405- and 488-nm diode laser lines. Cells for 3D-SIM were prepared as described for standard fixed cell microscopy with the following changes. The cells were grown on no. 1.5H precision glass coverslips (Marienfeld), then washed twice with 2 ml of PBS, and fixed with 2 ml of 4% [wt/vol] paraformaldehyde in PBS for 15 min. Coverslips were mounted in Vectashield mounting medium. Immersion oil with a refractive index of 1.514 was used after being empirically determined to give the most symmetric point spread function for the specific sample conditions. Image stacks (z-height of up to 18 µm, z-distance of 0.125) of the green (Alexa Fluor 488) and the blue (DAPI) fluorescence were recorded sequentially through the same emission light path. Exploiting the broad emission range of DAPI, this approach has the advantage to reduce additional bleaching of the green dye by otherwise interposed 405-nm excitation and avoids the need for post-acquisition channel alignment. Reconstruction was performed with the SoftWoRx 3.7 image-processing software (Applied Precision) to obtain a super-resolution 3D image stack with an optical resolution of 120 nm in the lateral, and approximately 300 nm in the axial direction. These 3D image stacks were imported into Volocity, and a maximum-intensity projection performed. These 24-bit RGB TIFF format images were placed into Illustrator CS3 (Adobe Systems Inc.) to produce the figures.

Live-cell microscopy

For live-cell imaging, cells were plated in 35-mm dishes with a 14-mm no. 1.5 thickness coverglass window in the bottom (MatTek Corporation). For imaging, the dishes were placed in a 37°C and 5% CO_2 environment chamber (Tokai Hit) on the microscope stage. Imaging was performed at 37°C in 5% CO_2 using an inverted microscope (model IX81; Olympus) with a 60× 1.42 NA oil immersion objective coupled to a spinning-disk confocal system (Ultraview Vox; PerkinElmer) fitted with an EM-CCD camera (model C9100-13; Hamamatsu Photonics). Exposure times were 30 msec for GFP-tubulin or mCherry-tagged histone H2B using 4% laser power, 100 msec and 30% laser power for mCherry-EB1, and 100 msec and 50% laser power for dynein heavy chain-GFP. For tubulin and histone double stable cells, image stacks of 29 planes spaced 0.6 µm apart were taken at 1–4 stage positions every minute for up to 12 h. For experiments analyzing EB1, 7 planes spaced 0.4 µm apart were captured at the maximum rate. Due to the low signal intensity only a single plane was captured for dynein heavy chain. Maximum intensity projection of the fluorescent channels was performed in Volocity to create 24-bit RGB TIFF files. Images in 24-bit RGB TIFF format were then placed into Adobe Illustrator CS3 to produce the figures.

Microtubule-binding assays

Full-length protein and fragments of CHICA, HMMR, Rab4, and PRC1 were in vitro translated (IVT) and labeled with ^{35}S-methionine using the TnT Coupled Reticulocyte Lysate System (Promega) according to the manufacturer's recommendations. Microtubules were prepared from bovine brain tubulin (20 µl, 5 mg/ml; Cytoskeleton) by incubation with 200 µl PEM buffer (80 mM Pipes, pH 7.0, 0.5 mM EGTA, and 2 mM $MgCl_2$), 2 µl of cushion buffer (60% [vol/vol] glycerol, 80 mM Pipes, pH 7.0, 1 mM EGTA, 1 mM MgCl), 0.22 µl 100 mM GTP, and 2 µl of 2 mM paclitaxel for 20 min at 35°C. All following procedures were performed at room temperature, ∼22–24°C. A 3-µl aliquot of the IVT mix was diluted in PEM buffer supplemented with 0.1% [vol/vol] Triton X-100, 0.5 mg/ml BSA, and 50 mM NaCl in a final volume of 50 µl. The reaction mixture was clarified by centrifugation at 90,000 rpm for 10 min in a TLA-100.3 rotor (Beckman Coulter). This clarified IVT fraction was incubated with 20 µl of taxol-stabilized microtubules for 10 min. The reactions were layered over 100 µl of cushion buffer and centrifuged at 80,000 rpm for 10 min at room temperature in the TLA-100.3 rotor.

Online supplemental material

Fig. S1 shows characterization of new CHICA and HMMR antibodies and siRNA duplexes. Fig. S2 shows the analysis of kinetochore fibers stability and checkpoint function. Fig. S3 describes the localization of NuMA and Plk1 when DYNLL1, CHICA, or HMMR are depleted. Videos 1–4 accompany Fig. 4 and show the effects of DYNLL1, CHICA, or HMMR depletion on spindle formation and position. Video 5 shows a rotation of mitotic spindles in CHICA-depleted cells. Microtubule dynamics were tracked using EB1, and these movies accompanying Fig. 6 D are shown in Videos 6–10. Table S1 shows the mass spectrometry data identifying the proteins in DYNLL1 and CHICA complexes. Online supplemental material is available at http://www.jcb.org/cgi/content/full/jcb.201202112/DC1.

We thank Ricardo Nunes Bastos and Kang Zeng for reagents and advice during the course of this work, Emily Linnane for initial help with GFP-DYNLL1 cell lines, and Ian Dobbie (Micron Advanced Bioimaging Unit) for technical help.

Downloaded from jcb.rupress.org on September 12, 2012

This work was supported by a Cancer Research UK program grant to F.A. Barr (C20079/A9473). A.K. Dunsch holds a Boehringer Ingelheim Fonds PhD fellowship. The work of L. Schermelleh and the Micron Advanced Bioimaging Unit was funded by the Wellcome Trust (067413).

Submitted: 21 February 2012
Accepted: 20 August 2012

References

Bowman, S.K., R.A. Neumüller, M. Novatchkova, Q. Du, and J.A. Knoblich. 2006. The *Drosophila* NuMA Homolog Mud regulates spindle orientation in asymmetric cell division. *Dev. Cell*. 10:731–742. http://dx.doi.org/10.1016/j.devcel.2006.05.005

Busson, S., D. Dujardin, A. Moreau, J. Dompierre, and J.R. De Mey. 1998. Dynein and dynactin are localized to astral microtubules and at cortical sites in mitotic epithelial cells. *Curr. Biol.* 8:541–544. http://dx.doi.org/10.1016/S0960-9822(98)70208-8

Buttrick, G.J., L.M. Beaumont, J. Leitch, C. Yau, J.R. Hughes, and J.G. Wakefield. 2008. Akt regulates centrosome migration and spindle orientation in the early *Drosophila melanogaster* embryo. *J. Cell Biol.* 180:537–548. http://dx.doi.org/10.1083/jcb.200705085

Cabernard, C., and C.Q. Doe. 2009. Apical/basal spindle orientation is required for neuroblast homeostasis and neuronal differentiation in *Drosophila*. *Dev. Cell*. 17:134–141. http://dx.doi.org/10.1016/j.devcel.2009.06.009

Chan, Y.W., L.L. Fava, A. Uldschmid, M.H. Schmitz, D.W. Gerlich, E.A. Nigg, and A. Santamaria. 2009. Mitotic control of kinetochore-associated dynein and spindle orientation by human Spindly. *J. Cell Biol.* 185: 859–874. http://dx.doi.org/10.1083/jcb.200812167

Cockell, M.M., K. Baumer, and P. Gönczy. 2004. lis-1 is required for dynein-dependent cell division processes in *C. elegans* embryos. *J. Cell Sci.* 117:4571–4582. http://dx.doi.org/10.1242/jcs.01344

Cox, J., and M. Mann. 2008. MaxQuant enables high peptide identification rates, individualized p.p.b.-range mass accuracies and proteome-wide protein quantification. *Nat. Biotechnol.* 26:1367–1372. http://dx.doi.org/10.1038/nbt.1511

Dunsch, A.K., E. Linnane, F.A. Barr, and U. Gruneberg. 2011. The astrin-kinastrin/SKAP complex localizes to microtubule plus ends and facilitates chromosome alignment. *J. Cell Biol.* 192:959–968. http://dx.doi.org/10.1083/jcb.201008023

Echeverri, C.J., B.M. Paschal, K.T. Vaughan, and R.B. Vallee. 1996. Molecular characterization of the 50-kD subunit of dynactin reveals function for the complex in chromosome alignment and spindle organization during mitosis. *J. Cell Biol.* 132:617–633. http://dx.doi.org/10.1083/jcb.132.4.617

Ellefson, M.L., and F.J. McNally. 2011. CDK-1 inhibits meiotic spindle shortening and dynein-dependent spindle rotation in *C. elegans*. *J. Cell Biol.* 193:1229–1244. http://dx.doi.org/10.1083/jcb.201104008

Evanko, S.P., W.T. Parks, and T.N. Wight. 2004. Intracellular hyaluronan in arterial smooth muscle cells: association with microtubules, RHAMM, and the mitotic spindle. *J. Histochem. Cytochem.* 52:1525–1535. http://dx.doi.org/10.1369/jhc.4A6356.2004

Faulkner, N.E., D.L. Dujardin, C.Y. Tai, K.T. Vaughan, C.B. O'Connell, Y. Wang, and R.B. Vallee. 2000. A role for the lissencephaly gene LIS1 in mitosis and cytoplasmic dynein function. *Nat. Cell Biol.* 2:784–791. http://dx.doi.org/10.1038/35041020

Fernández-Miñán, A., M.D. Martín-Bermudo, and A. González-Reyes. 2007. Integrin signaling regulates spindle orientation in *Drosophila* to preserve the follicular-epithelium monolayer. *Curr. Biol.* 17:683–688. http://dx.doi.org/10.1016/j.cub.2007.02.052

Fink, J., N. Carpi, T. Betz, A. Bétard, M. Chebah, A. Azioune, M. Bornens, C. Sykes, L. Fetler, D. Cuvelier, and M. Piel. 2011. External forces control mitotic spindle positioning. *Nat. Cell Biol.* 13:771–778. http://dx.doi.org/10.1038/ncb2269

Gassmann, R., A.J. Holland, D. Varma, X. Wan, F. Civril, D.W. Cleveland, K. Oegema, E.D. Salmon, and A. Desai. 2010. Removal of Spindly from microtubule-attached kinetochores controls spindle checkpoint silencing in human cells. *Genes Dev.* 24:957–971. http://dx.doi.org/10.1101/gad.1886810

Gönczy, P., S. Pichler, M. Kirkham, and A.A. Hyman. 1999. Cytoplasmic dynein is required for distinct aspects of MTOC positioning, including centrosome separation, in the one cell stage *Caenorhabditis elegans* embryo. *J. Cell Biol.* 147:135–150. http://dx.doi.org/10.1083/jcb.147.1.135

Gotta, M., M.C. Abraham, and J. Ahringer. 2001. CDC-42 controls early cell polarity and spindle orientation in *C. elegans*. *Curr. Biol.* 11:482–488. http://dx.doi.org/10.1016/S0960-9822(01)00142-7

Groen, A.C., L.A. Cameron, M. Coughlin, D.T. Miyamoto, T.J. Mitchison, and R. Ohi. 2004. XRHAMM functions in ran-dependent microtubule nucleation and pole formation during anastral spindle assembly. *Curr. Biol.* 14:1801–1811. http://dx.doi.org/10.1016/j.cub.2004.10.002

Inaba, M., H. Yuan, V. Salzmann, M.T. Fuller, and Y.M. Yamashita. 2010. E-cadherin is required for centrosome and spindle orientation in *Drosophila* male germline stem cells. *PLoS ONE*. 5:e12473. http://dx.doi.org/10.1371/journal.pone.0012473

Jaffe, A.B., N. Kaji, J. Durgan, and A. Hall. 2008. Cdc42 controls spindle orientation to position the apical surface during epithelial morphogenesis. *J. Cell Biol.* 183:625–633. http://dx.doi.org/10.1083/jcb.200807121

Johnston, C.A., K. Hirono, K.E. Prehoda, and C.Q. Doe. 2009. Identification of an Aurora-A/PinsLINKER/Dlg spindle orientation pathway using induced cell polarity in S2 cells. *Cell*. 138:1150–1163. http://dx.doi.org/10.1016/j.cell.2009.07.041

Kaltschmidt, J.A., C.M. Davidson, N.H. Brown, and A.H. Brand. 2000. Rotation and asymmetry of the mitotic spindle direct asymmetric cell division in the developing central nervous system. *Nat. Cell Biol.* 2:7–12. http://dx.doi.org/10.1038/71323

Kardon, J.R., and R.D. Vale. 2009. Regulators of the cytoplasmic dynein motor. *Nat. Rev. Mol. Cell Biol.* 10:854–865. http://dx.doi.org/10.1038/nrm2804

Kiyomitsu, T., and I.M. Cheeseman. 2012. Chromosome- and spindle-pole-derived signals generate an intrinsic code for spindle position and orientation. *Nat. Cell Biol.* 14:311–317. http://dx.doi.org/10.1038/ncb2440

Laan, L., N. Pavin, J. Husson, G. Romet-Lemonne, M. van Duijn, M.P. López, R.D. Vale, F. Jülicher, S.L. Reck-Peterson, and M. Dogterom. 2012. Cortical dynein controls microtubule dynamics to generate pulling forces that position microtubule asters. *Cell*. 148:502–514. http://dx.doi.org/10.1016/j.cell.2012.01.007

Li, Y.Y., E. Yeh, T. Hays, and K. Bloom. 1993. Disruption of mitotic spindle orientation in a yeast dynein mutant. *Proc. Natl. Acad. Sci. USA*. 90: 10096–10100. http://dx.doi.org/10.1073/pnas.90.21.10096

Lo, K.W., S. Naisbitt, J.S. Fan, M. Sheng, and M. Zhang. 2001. The 8-kDa dynein light chain binds to its targets via a conserved (K/R)XTQT motif. *J. Biol. Chem.* 276:14059–14066. http://dx.doi.org/10.1074/jbc.M104701200

Maxwell, C.A., J.J. Keats, M. Crainie, X. Sun, T. Yen, E. Shibuya, M. Hendzel, G. Chan, and L.M. Pilarski. 2003. RHAMM is a centrosomal protein that interacts with dynein and maintains spindle pole stability. *Mol. Biol. Cell*. 14:2262–2276. http://dx.doi.org/10.1091/mbc.E02-07-0377

McKenney, R.J., S.J. Weil, J. Scherer, and R.B. Vallee. 2011. Mutually exclusive cytoplasmic dynein regulation by NudE-Lis1 and dynactin. *J. Biol. Chem.* 286:39615–39622. http://dx.doi.org/10.1074/jbc.M111.289017

Mitsushima, M., F. Toyoshima, and E. Nishida. 2009. Dual role of Cdc42 in spindle orientation control of adherent cells. *Mol. Cell. Biol.* 29: 2816–2827. http://dx.doi.org/10.1128/MCB.01713-08

Morin, X., and Y. Bellaïche. 2011. Mitotic spindle orientation in asymmetric and symmetric cell divisions during animal development. *Dev. Cell*. 21: 102–119. http://dx.doi.org/10.1016/j.devcel.2011.06.012

Nguyen-Ngoc, T., K. Afshar, and P. Gönczy. 2007. Coupling of cortical dynein and G alpha proteins mediates spindle positioning in *Caenorhabditis elegans*. *Nat. Cell Biol.* 9:1294–1302. http://dx.doi.org/10.1038/ncb1649

O'Connell, C.B., and Y.L. Wang. 2000. Mammalian spindle orientation and position respond to changes in cell shape in a dynein-dependent fashion. *Mol. Biol. Cell*. 11:1765–1774.

Pfarr, C.M., M. Coue, P.M. Grissom, T.S. Hays, M.E. Porter, and J.R. McIntosh. 1990. Cytoplasmic dynein is localized to kinetochores during mitosis. *Nature*. 345:263–265. http://dx.doi.org/10.1038/345263a0

Poulson, N.D., and T. Lechler. 2010. Robust control of mitotic spindle orientation in the developing epidermis. *J. Cell Biol.* 191:915–922. http://dx.doi.org/10.1083/jcb.201008001

Qin, Y., W.H. Meisen, Y. Hao, and I.G. Macara. 2010. Tuba, a Cdc42 GEF, is required for polarized spindle orientation during epithelial cyst formation. *J. Cell Biol.* 189:661–669. http://dx.doi.org/10.1083/jcb.201002097

Rapali, P., L. Radnai, D. Süveges, V. Harmat, F. Tölgyesi, W.Y. Wahlgren, G. Katona, L. Nyitray, and G. Pál. 2011a. Directed evolution reveals the binding motif preference of the LC8/DYNLL hub protein and predicts large numbers of novel binders in the human proteome. *PLoS ONE*. 6:e18818. http://dx.doi.org/10.1371/journal.pone.0018818

Rapali, P., A. Szenes, L. Radnai, A. Bakos, G. Pál, and L. Nyitray. 2011b. DYNLL/LC8: a light chain subunit of the dynein motor complex and beyond. *FEBS J.* 278:2980–2996. http://dx.doi.org/10.1111/j.1742-4658.2011.08254.x

Rebollo, E., P. Sampaio, J. Januschke, S. Llamazares, H. Varmark, and C. González. 2007. Functionally unequal centrosomes drive spindle orientation in asymmetrically dividing *Drosophila* neural stem cells. *Dev. Cell*. 12:467–474. http://dx.doi.org/10.1016/j.devcel.2007.01.021

Downloaded from jcb.rupress.org on September 12, 2012

Rhyu, M.S., and J.A. Knoblich. 1995. Spindle orientation and asymmetric cell fate. *Cell*. 82:523–526. http://dx.doi.org/10.1016/0092-8674(95)90022-5

Rodriguez-Fraticelli, A.E., S. Vergarajauregui, D.J. Eastburn, A. Datta, M.A. Alonso, K. Mostov, and F. Martín-Belmonte. 2010. The Cdc42 GEF Intersectin 2 controls mitotic spindle orientation to form the lumen during epithelial morphogenesis. *J. Cell Biol.* 189:725–738. http://dx.doi.org/10.1083/jcb.201002047

Samora, C.P., B. Mogessie, L. Conway, J.L. Ross, A. Straube, and A.D. McAinsh. 2011. MAP4 and CLASP1 operate as a safety mechanism to maintain a stable spindle position in mitosis. *Nat. Cell Biol.* 13:1040–1050. http://dx.doi.org/10.1038/ncb2297

Sanada, K., and L.H. Tsai. 2005. G protein betagamma subunits and AGS3 control spindle orientation and asymmetric cell fate of cerebral cortical progenitors. *Cell*. 122:119–131. http://dx.doi.org/10.1016/j.cell.2005.05.009

Santamaria, A., S. Nagel, H.H. Sillje, and E.A. Nigg. 2008. The spindle protein CHICA mediates localization of the chromokinesin Kid to the mitotic spindle. *Curr. Biol.* 18:723–729. http://dx.doi.org/10.1016/j.cub.2008.04.041

Scaërou, F., I. Aguilera, R. Saunders, N. Kane, L. Blottière, and R. Karess. 1999. The rough deal protein is a new kinetochore component required for accurate chromosome segregation in *Drosophila*. *J. Cell Sci.* 112: 3757–3768.

Schermelleh, L., P.M. Carlton, S. Haase, L. Shao, L. Winoto, P. Kner, B. Burke, M.C. Cardoso, D.A. Agard, M.G.L. Gustafsson, et al. 2008. Subdiffraction multicolor imaging of the nuclear periphery with 3D structured illumination microscopy. *Science*. 320:1332–1336. http://dx.doi.org/10.1126/science.1156947

Schmidt, J.C., T. Kiyomitsu, T. Hori, C.B. Backer, T. Fukagawa, and I.M. Cheeseman. 2010. Aurora B kinase controls the targeting of the Astrin-SKAP complex to bioriented kinetochores. *J. Cell Biol.* 191:269–280. http://dx.doi.org/10.1083/jcb.201006129

Sharp, D.J., G.C. Rogers, and J.M. Scholey. 2000. Cytoplasmic dynein is required for poleward chromosome movement during mitosis in *Drosophila* embryos. *Nat. Cell Biol.* 2:922–930. http://dx.doi.org/10.1038/35046574

Shorter, J., R. Watson, M.E. Giannakou, M. Clarke, G. Warren, and F.A. Barr. 1999. GRASP55, a second mammalian GRASP protein involved in the stacking of Golgi cisternae in a cell-free system. *EMBO J.* 18:4949–4960. http://dx.doi.org/10.1093/emboj/18.18.4949

Siller, K.H., and C.Q. Doe. 2009. Spindle orientation during asymmetric cell division. *Nat. Cell Biol.* 11:365–374. http://dx.doi.org/10.1038/ncb0409-365

Siller, K.H., C. Cabernard, and C.Q. Doe. 2006. The NuMA-related Mud protein binds Pins and regulates spindle orientation in *Drosophila* neuroblasts. *Nat. Cell Biol.* 8:594–600. http://dx.doi.org/10.1038/ncb1412

Starr, D.A., B.C. Williams, T.S. Hays, and M.L. Goldberg. 1998. ZW10 helps recruit dynactin and dynein to the kinetochore. *J. Cell Biol.* 142:763–774. http://dx.doi.org/10.1083/jcb.142.3.763

Stehman, S.A., Y. Chen, R.J. McKenney, and R.B. Vallee. 2007. NudE and NudEL are required for mitotic progression and are involved in dynein recruitment to kinetochores. *J. Cell Biol.* 178:583–594. http://dx.doi.org/10.1083/jcb.200610112

Steuer, E.R., L. Wordeman, T.A. Schroer, and M.P. Sheetz. 1990. Localization of cytoplasmic dynein to mitotic spindles and kinetochores. *Nature*. 345:266–268. http://dx.doi.org/10.1038/345266a0

Thein, K.H., J. Kleylein-Sohn, E.A. Nigg, and U. Gruneberg. 2007. Astrin is required for the maintenance of sister chromatid cohesion and centrosome integrity. *J. Cell Biol.* 178:345–354. http://dx.doi.org/10.1083/jcb.200701163

Théry, M., V. Racine, A. Pépin, M. Piel, Y. Chen, J.B. Sibarita, and M. Bornens. 2005. The extracellular matrix guides the orientation of the cell division axis. *Nat. Cell Biol.* 7:947–953. http://dx.doi.org/10.1038/ncb1307

Théry, M., A. Jiménez-Dalmaroni, V. Racine, M. Bornens, and F. Jülicher. 2007. Experimental and theoretical study of mitotic spindle orientation. *Nature*. 447:493–496. http://dx.doi.org/10.1038/nature05786

Tolg, C., S.R. Hamilton, L. Morningstar, J. Zhang, S. Zhang, K.V. Esguerra, P.G. Telmer, L.G. Luyt, R. Harrison, J.B. McCarthy, and E.A. Turley. 2010. RHAMM promotes interphase microtubule instability and mitotic spindle integrity through MEK1/ERK1/2 activity. *J. Biol. Chem.* 285: 26461–26474. http://dx.doi.org/10.1074/jbc.M110.121491

Toyoshima, F., and E. Nishida. 2007. Integrin-mediated adhesion orients the spindle parallel to the substratum in an EB1- and myosin X-dependent manner. *EMBO J.* 26:1487–1498. http://dx.doi.org/10.1038/sj.emboj.7601599

Toyoshima, F., S. Matsumura, H. Morimoto, M. Mitsushima, and E. Nishida. 2007. PtdIns(3,4,5)P3 regulates spindle orientation in adherent cells. *Dev. Cell*. 13:796–811. http://dx.doi.org/10.1016/j.devcel.2007.10.014

van der Voet, M., C.W. Berends, A. Perreault, T. Nguyen-Ngoc, P. Gönczy, M. Vidal, M. Boxem, and S. van den Heuvel. 2009. NuMA-related LIN-5, ASPM-1, calmodulin and dynein promote meiotic spindle rotation independently of cortical LIN-5/GPR/Galpha. *Nat. Cell Biol.* 11:269–277. http://dx.doi.org/10.1038/ncb1834

Vaughan, K.T., E.L. Holzbaur, and R.B. Vallee. 1995. Subcellular targeting of the retrograde motor cytoplasmic dynein. *Biochem. Soc. Trans.* 23:50–54.

Williams, B.C., Z. Li, S. Liu, E.V. Williams, G. Leung, T.J. Yen, and M.L. Goldberg. 2003. Zwilch, a new component of the ZW10/ROD complex required for kinetochore functions. *Mol. Biol. Cell*. 14:1379–1391. http://dx.doi.org/10.1091/mbc.E02-09-0624

Wilm, M., A. Shevchenko, T. Houthaeve, S. Breit, L. Schweigerer, T. Fotsis, and M. Mann. 1996. Femtomole sequencing of proteins from polyacrylamide gels by nano-electrospray mass spectrometry. *Nature*. 379:466–469. http://dx.doi.org/10.1038/379466a0

Wojcik, E., R. Basto, M. Serr, F. Scaërou, R. Karess, and T. Hays. 2001. Kinetochore dynein: its dynamics and role in the transport of the Rough deal checkpoint protein. *Nat. Cell Biol.* 3:1001–1007. http://dx.doi.org/10.1038/ncb1101-1001

Woodard, G.E., N.N. Huang, H. Cho, T. Miki, G.G. Tall, and J.H. Kehrl. 2010. Ric-8A and Gi alpha recruit LGN, NuMA, and dynein to the cell cortex to help orient the mitotic spindle. *Mol. Cell. Biol.* 30:3519–3530. http://dx.doi.org/10.1128/MCB.00394-10

Zeng, K., R.N. Bastos, F.A. Barr, and U. Gruneberg. 2010. Protein phosphatase 6 regulates mitotic spindle formation by controlling the T-loop phosphorylation state of Aurora A bound to its activator TPX2. *J. Cell Biol.* 191:1315–1332. http://dx.doi.org/10.1083/jcb.201008106

Zheng, Z., H. Zhu, Q. Wan, J. Liu, Z. Xiao, D.P. Siderovski, and Q. Du. 2010. LGN regulates mitotic spindle orientation during epithelial morphogenesis. *J. Cell Biol.* 189:275–288. http://dx.doi.org/10.1083/jcb.200910021

Downloaded from jcb.rupress.org on September 12, 2012